BMI/OWTD-5

FRACFLO: Analytical Solutions for Two-Dimensional Transport of a Decaying Species in a Discrete Planar Fracture and Equidistant Multiple Parallel Fractures With Rock Matrix Diffusion

Technical Report

July 1990

A. Berge Gureghian

Office of Waste Technology Development
Battelle Energy Systems Group
7000 South Adams Street
Willowbrook, IL 60521

HYDROLOGY DOCUMENT NUMBER 693

OWTD
Office of Waste Technology Development
BATTELLE Energy Systems Group

BIBLIOGRAPHIC DATA

Gureghian, A. Berge, 1990. *FRACFLO: Analytical Solutions for Two-Dimensional Transport of a Decaying Species in a Discrete Planar Fracture and Equidistant Multiple Parallel Fractures With Rock Matrix Diffusion,* BMI/OWTD-5, Office of Waste Technology Development, Battelle, Willowbrook, IL.

NOTICE

This report was prepared as an account of work sponsored by an agency of the United States Government. Neither the United States Government nor any agency thereof, nor any of their employees, makes any warranty, expressed or implied, or assumes any legal liability or responsibility for the accuracy, completeness, or usefulness of any information, apparatus, product, or process disclosed, or represents that its use would not infringe privately owned rights. Reference herein to any specific commercial product, process, or service by trade name, trademark, manufacturer, or otherwise, does not necessarily constitute or imply its endorsement, recommendation, or favoring by the United States Government or any agency thereof. The views and opinions of authors expressed herein do not necessarily state or reflect those of the United States Government or any agency thereof.

Printed in the United States of America
Available from
National Technical Information Service
U.S. Department of Commerce
5285 Port Royal Road
Springfield, VA 22161

NTIS price codes
Printed copy: A12
Microfiche copy: A01

BMI/OWTD-5
Distribution Category UC-802

FRACFLO: Analytical Solutions for Two-Dimensional Transport of a Decaying Species in a Discrete Planar Fracture and Equidistant Multiple Parallel Fractures With Rock Matrix Diffusion

Technical Report

July 1990

A. Berge Gureghian

Office of Waste Technology Development
Battelle Energy Systems Group
7000 South Adams Street
Willowbrook, IL 60521

The content of this report was effective as of March 1989. This report was prepared by Battelle Energy Systems Group, Willowbrook, IL, under Contract No. DE-AC02-83CH10139 with the U.S. Department of Energy.

ACKNOWLEDGMENTS

Several people assisted in the preparation of this report. The authors would like to express their appreciation here for those efforts, which greatly helped the document reach its final form.

In particular, we would like to thank Dr. J. N. Ahn of the Department of Nuclear Engineering at the University of California at Berkeley, and Dr. G. Jansen, Jr., Westinghouse Hanford Company, for their review comments. L. Loebel, now with the Fermi Laboratory in Batavia, Illinois, systematically checked the data and enhanced the computer code. Finally, M. Steve assisted as Battelle Columbus Division technical editor and coordinated production of the various parts of the document with W. Young in Technical Illustrations and P. Dean and W. Veasey in Text Processing.

ABSTRACT

Analytical solutions based on the Laplace and Fourier transformation techniques are derived for the transient advective-dispersive transport of a single radionuclide through fractures (two-dimensional analysis) and rock (one-dimensional analysis). The longitudinal dispersion-free solution is also reported. The geometry considered consists of either a single planar fracture (infinite diffusion in the rock) or a system of equidistant parallel fracture planes with uniform aperture (finite diffusion in the rock). The solution assumes that the ground-water flow regime is under steady-state and isothermal conditions, and the streamlines along the direction of flow are parallel. The rock matrix is assumed to be homogeneous, isotropic, and saturated with stagnant water. The flow field is assumed to be semi-infinite in the horizontal direction normal to the source, and of either finite or infinite extent in the vertical direction orthogonal to the source. The initial concentration in both the fracture and the rock is assumed to be zero. The upstream boundary conditions exclusive to the fracture correspond to either a finite patch (single or multiple) source or a Gaussian distributed source, subject to a band or step release mode. In addition to the spatial and temporal concentration of the radionuclide in both fracture and rock, this solution also provides the mass flux and cumulative mass flux into the fracture.

The solution related to the single fracture case was verified by comparing its performance with available results from other works. Two sets of solutions were derived for the multiple parallel fracture case; the first, based on a series approximation, and the second, based on contour integration, were designed to cope efficiently with small and large Fourier numbers, respectively. Of interest in the case of the rock matrix, the solution based on contour integration is considerably simplified compared to previously reported ones. This is achieved by eliminating the infinite series summation incumbent to a convolution-based approach, which on the one hand limits its range of applicability and on the other hand undermines its computational viability. Numerical tests covering a wide range of Fourier numbers show excellent agreement between the proposed solutions. For the longitudinal dispersion-free solution, criteria are also reported for the applicability of the solution for a single fracture to the case of a multiple parallel fracture system.

The general solution requires, in both cases, the evaluation of a single integral, except in the case of the solution based on contour integration, where an additional one is required. This is performed using a Gauss-Legendre quadrature scheme.

FOREWORD

Following the passage of the Nuclear Waste Policy Act of 1982, the Civilian Radioactive Waste Management Program was organized in September 1983. The purpose of this program, managed by the U.S. Department of Energy (DOE), is to develop technology and provide facilities for safe, environmentally acceptable, permanent disposal of high-level waste (HLW). HLW includes wastes from both commercial and defense sources, such as spent (used) fuel from nuclear power reactors, accumulations of wastes from production of nuclear weapons, and solidified wastes from fuel reprocessing.

The information in this report pertains to analytical solutions based on Laplace and Fourier transformation techniques used in studying ground-water flow with the FRACFLO code for the Repository Technology Program. This work was sponsored by the DOE Repository Technology and Transportation Division.

FEDERAL INFORMATION PROCESSING STANDARD SOFTWARE SUMMARY

01. Summary date	02. Summary prepared by (Name and Phone)	03. Summary action
Yr. 90 Mo. 07 Day 10	A. B. Gureghian (708) 655-8638	New ☐ Replacement ☒ Deletion ☐
04. Software date: Yr. 90 Mo. 07 Day 10	05. Software title: FRACFLO: Analytical Solutions for Two-Dimensional Transport of a Decaying Species in a Discrete Planar Fracture and Equidistant Multiple Parallel Fractures with Rock Matrix Diffusion	Previous Internal Software ID: Version 1
06. Short title		07. Internal Software ID: Version 1.1

08. Software type
- ☐ Automated Data System
- ☒ Computer Program
- ☐ Subroutine/Module

09. Processing mode
- ☐ Interactive
- ☒ Batch
- ☐ Combination

10. Application area

General:
- ☐ Computer Systems Support/Utility
- ☒ Scientific/Engineering
- ☐ Bibliographic/Textual
- ☐ Management/Business
- ☐ Process Control
- ☐ Other

Specific: Nuclear Waste Isolation Analysis

11. Submitting organization and address

BATTELLE
Office of Waste Technology Development
7000 South Adams Street
Willowbrook IL 60521

12. Technical contact(s) and phone

Code Custodian
(708) 655-8622

13. Narrative The FRACFLO code computes the two-dimensional, space-time-dependent, convective-dispersive transport of a single radionuclide in unbounded single or multiple parallel fracture system with constant aperture. It handles the one-dimensional diffusive transport into the rock matrix, as well as the mass flux and cumulative mass flux at any point in the fracture. Steady-state isothermal ground-water flow and parallel streamlines are assumed in the fracture, and the rock matrix is assumed to be fully saturated with immobile water. The model can handle a single or multiple finite patch source or a gaussian distributed source subject to a step or band release mode. The differential equations are solved by Laplace and Fourier transforms and a Gauss-Legendre integration scheme.

14. Keywords Laplace and Fourier Transforms, Gauss-Legendre Integration, Radionuclide Transport, Analytical Solution, Convection-Dispersion, Diffusion, Radioactive Decay, Retardation, One and Two-Dimensions, Concentration, Single Fracture, Multiple Fracture, Rock Matrix, Mass Flux, Cumulative Mass, Isothermal, Parallel Streamlines, Step and Band Release Mode, Patch or Gaussian Distribution Source, Laplace & Fourier transforms, Gauss-Legendre integration scheme.

15. Computer manuf'r and model	16. Computer operating system	17. Programing language(s)	18. Number of source program statements
VAX 8700	VAX/VMS Version 4.7	FORTRAN 77	3528
19. Computer memory requirements	**20. Tape drives**	**21. Disk/Drum units**	**22. Terminals**
Actual Words			

23. Other operational requirements

24. Software availability	25. Documentation availability
Available ☒ Limited ☐ In-house only ☐	Available ☒ Inadequate ☐ In-house only ☐

26. FOR SUBMITTING ORGANIZATION USE Documentation and code are available from the National Energy Software Center, Argonne National Laboratory, 9800 S. Cass Avenue, Argonne, IL 60439

TABLE OF CONTENTS

Part 1

		Page
1.0	INTRODUCTION	1
	1.1 BACKGROUND	1
	1.2 PURPOSE	2
	1.3 APPLICATIONS	3
2.0	MASS TRANSPORT EQUATIONS FOR FRACTURE AND ROCK MATRIX	5
	2.1 INITIAL AND BOUNDARY CONDITIONS	8
	2.1.1 Fracture	8
	2.1.2 Rock Matrix	11
	2.1.3 Concentration at the Source and Band Release	11
3.0	SINGLE FRACTURE CASE WITH INFINITE DIFFUSION FIELD	13
	3.1 NON-ZERO LONGITUDINAL DISPERSION	13
	3.1.1 Rock Matrix	13
	3.1.2 Fracture	14
	3.2 NO LONGITUDINAL DISPERSION	22
	3.3 MASS FLUX	23
	3.4 CUMULATIVE MASS FLUX	27
	3.4.1 Unidimensional Flow	27
	3.4.2 No Longitudinal Dispersion	30
	3.5 RESULTS AND DISCUSSIONS	31
	3.5.1 Case 1: Concentration of Np-237 in a One-Dimensional Flow Domain	31
	3.5.2 Case 2: Spatial and Time-Dependent Concentrations, Mass Flux, and Cumulative Mass Flux Subject to a Band Release Mode in the Absence of Longitudinal Dispersion	59
	3.5.3 Case 3: Multiple Patch Source Subject to Step Release and Band Release	75
	3.5.4 Case 4: Two-Dimensional Transport of Tc-99 in Fracture and Rock Matrix	76

TABLE OF CONTENTS

Part 2

		Page
4.0	MULTIPLE PARALLEL FRACTURE CASE WITH FINITE DIFFUSION FIELD: SERIES SOLUTION	111
	4.1 NON-ZERO LONGITUDINAL DISPERSION	111
	4.1.1 Fracture	111
	4.1.2 Rock Matrix	119
	4.1.3 Mass Flux	122
	4.1.4 Cumulative Mass Flux	125
	4.2 NO LONGITUDINAL DISPERSION	127
	4.3 SOLUTION FOR BAND RELEASE	128
	4.4 CONVERGENCE OF SERIES	129
	4.5 REMARKS	129
	4.5.1 Fracture	130
	4.5.2 Rock	131
5.0	MULTIPLE PARALLEL FRACTURE CASE WITH FINITE DIFFUSION FIELD: CONTOUR INTEGRATION	133
	5.1 FRACTURE	133
	5.2 ROCK MATRIX	134
	5.3 MASS FLUX	137
	5.4 CUMULATIVE MASS FLUX	138
	5.5 NO LONGITUDINAL DISPERSION	140
6.0	DISCUSSION AND RESULTS FOR MULTIPLE PARALLEL FRACTURE CASE WITH FINITE DIFFUSION	143
	6.1 DISCUSSION OF CASE 5: SPATIAL VARIATION OF CONCENTRATION OF Np-237	143
	6.1.1 Results for Case 5A: Step Release Mode	143
	6.1.2 Results for Case 5B: Band Release Mode	154

TABLE OF CONTENTS
(Continued)

Page

6.2 DISCUSSION OF CASE 6: TEMPORAL VARIATION OF CONCENTRATION OF Np-237, INFLUENCE OF LONGITUDINAL DISPERSION 154

6.3 DISCUSSION OF CASE 7: TWO-DIMENSIONAL TRANSPORT OF Tc-99 IN FRACTURE AND ROCK MATRIX 182

7.0 SUMMARY AND CONCLUSIONS 199

8.0 REFERENCES 201

APPENDIX A. THEOREMS, LAPLACE TRANSFORMS, AND DERIVATIVES 205

APPENDIX B. QUADRATURE 211

APPENDIX C. Nth DERIVATIVE OF A PRODUCT OF TWO FUNCTIONS 223

APPENDIX D. A COMPLEX DEFINITE INTEGRAL 225

APPENDIX E. NOTATIONS 229

APPENDIX F. MODEL PARAMETERS 235

LIST OF TABLES

Table	Title	Page
3-1.	Input Parameters for Case 1	32
3-2a.	Case 1A Results: Relative Concentration, Mass Flux, and Cumulative Mass Flux in the Fracture for Np-237 With Infinite Diffusion at Time t = 10^4 yr and Rock Matrix Retardation Factor R′ = 1 (Step Release Mode)	35
3-2b.	Case 1A Results: Relative Concentration, Mass Flux, and Cumulative Mass Flux in the Fracture for Np-237 With Infinite Diffusion at Time t = 10^4 yr and Rock Matrix Retardation Factor R′ = 100 (Step Release Mode)	36
3-2c.	Case 1A Results: Relative Concentration, Mass Flux, and Cumulative Mass Flux in the Fracture for Np-237 With Infinite Diffusion at Time t = 10^4 yr and Rock Matrix Retardation Factor R′ = 10,000 (Step Release Mode)	36
3-2d.	Case 1A Results: Relative Concentration in Rock Matrix (B/A°) for Np-237 at x = 100 m (Step Release Mode)	37
3-2e.	Case 1A Results: Relative Concentration, Mass Flux, and Cumulative Mass Flux in the Fracture for Np-237 Over Time With Rock Matrix Retardation Factor R′ = 1 (Step Release Mode)	44
3-2f.	Case 1A Results: Relative Concentration, Mass Flux, and Cumulative Mass Flux in the Fracture for Np-237 Over Time With Rock Matrix Retardation Factor R′ = 100 (Step Release Mode)	45
3-2g.	Case 1A Results: Relative Concentration, Mass Flux, and Cumulative Mass Flux in the Fracture for Np-237 Over Time With Rock Matrix Retardation Factor R′ = 10,000 (Step Release Mode)	46
3-3a.	Case 1B Results: Relative Concentration, Mass Flux, and Cumulative Mass Flux in the Fracture for Np-237 With Infinite Diffusion at Time t = 10^4 yr and Rock Matrix Retardation Factor R′ = 1 (Step Release Mode)	51
3-3b.	Case 1B Results: Relative Concentration, Mass Flux, and Cumulative Mass Flux in the Fracture for Np-237 With Infinite Diffusion at Time t = 10^4 yr and Rock Matrix Retardation Factor R′ = 100 (Step Release Mode)	52
3-3c.	Case 1B Results: Relative Concentration, Mass Flux, and Cumulative Mass Flux in the Fracture for Np-237 With Infinite Diffusion at Time t = 10^4 yr and Rock Matrix Retardation Factor R′ = 10,000 (Step Release Mode)	52

LIST OF TABLES
(Continued)

Table	Title	Page
3-3d.	Case 1B Results: Relative Concentration in Rock Matrix (B/A°) for Np-237 at x = 100 m and D_{xx} = 0 (Step Release Mode)	53
3-3e.	Case 1B Results: Relative Concentration, Mass Flux, and Cumulative Mass Flux in the Fracture for Np-237 Over Time With Rock Matrix Retardation Factor R′ = 1 (Step Release Mode)	57
3-3f.	Case 1B Results: Relative Concentration, Mass Flux, and Cumulative Mass Flux in the Fracture for Np-237 Over Time With Rock Matrix Retardation Factor R′ = 100 (Step Release Mode)	58
3-3g.	Case 1B Results: Relative Concentration, Mass Flux, and Cumulative Mass Flux in the Fracture for Np-237 Over Time With Rock Matrix Retardation Factor R′ = 10,000 (Step Release Mode)	58
3-4.	Input Parameters for Case 2	60
3-5a.	Case 2 Results: Relative Concentration, Mass Flux, and Cumulative Mass Flux in the Fracture for Np-237 with Infinite Diffusion at Time t = 10^4 yr and Rock Matrix Retardation Factor R′ = 1 (Band Release Mode)	65
3-5b.	Case 2 Results: Relative Concentration, Mass Flux, and Cumulative Mass Flux in the Fracture for Np-237 at Time t = 10^4 yr and Rock Matrix Retardation Factor R′ = 100 (Band Release Mode)	66
3-5c.	Case 2 Results: Relative Concentration, Mass Flux, and Cumulative Mass Flux in the Fracture for Np-237 at Time t = 10^4 yr and Rock Matrix Retardation Factor R′ = 10,000 (Band Release Mode)	66
3-6a.	Case 2 Results: Relative Concentration in the Rock Matrix for Np-237 at Time t = 10^4 yr and Rock Matrix Retardation Factor R′ = 1 (Band Release Mode)	67
3-6b.	Case 2 Results: Relative Concentration in the Rock Matrix for Np-237 at Time t = 1 x 10^4 yr and Rock Matrix Retardation Factor R′ = 100 (Band Release Mode)	67
3-6c.	Case 2 Results: Relative Concentration in the Rock Matrix for Np-237 at Time t = 10^4 yr and Rock Matrix Retardation Factor R′ = 10,000 (Band Release Mode)	68
3-7a.	Case 2 Results: Relative Concentration, Mass Flux, and Cumulative Mass Flux in the Fracture for Np-237 Over Time with Rock Matrix Retardation Factor R′ = 1 (Band Release Mode)	72

LIST OF TABLES
(Continued)

Table	Title	Page
3-7b.	Case 2 Results: Relative Concentration, Mass Flux, and Cumulative Mass Flux in the Fracture for Np-237 Over Time With Rock Matrix Retardation Factor R′ = 100 (Band Release Mode)	73
3-7c.	Case 2 Results: Relative Concentration, Mass Flux, and Cumulative Mass Flux in the Fracture for Np-237 Over Time with Rock Matrix Retardation Factor R′ = 10,000 (Band Release Mode)	74
3-8.	Input Parameters for Case 3	75
3-9.	Case 3 Results: Relative Concentration in Fracture (A/A°) for Cm-245	76
3-10.	Input Parameters Used in Simulation of Tc-99 in Fracture and Rock Matrix for Case 4	77
3-11a.	Case 4A Results: Relative Concentration in the Fracture (A/A°) of Species Tc-99 at Time t = 5 x 10^3 yr and z = 0 m (Finite Patch Source, Step Release Mode)	84
3-11b.	Case 4A Results: Relative Concentration in the Fracture (A/A°) of Species Tc-99 at Time t = 2.5 x 10^4 yr and z = 0 m (Finite Patch Source, Band Release Mode)	84
3-11c.	Case 4A Results: Relative Concentration in the Rock Matrix (B/A°) of Species Tc-99 at Time t = 5 x 10^3 yr and z = 1 m (Finite Patch Source, Step Release Mode)	85
3-11d.	Case 4A Results: Relative Concentration in the Rock Matrix (B/A°) of Species Tc-99 at Time t = 2.5 x 10^4 yr and z = 1 m (Finite Patch Source, Band Release Mode)	85
3-11e.	Case 4A Results: Relative Concentration in the Rock Matrix (B/A°) of Species Tc-99 at Time t = 5 x 10^3 yr and z = 5 m (Finite Patch Source, Step Release Mode)	86
3-11f.	Case 4A Results: Relative Concentration in the Rock Matrix (B/A°) of Species Tc-99 at Time t = 2.5 x 10^4 yr and z = 5 m (Finite Patch Source, Band Release Mode)	86
3-12a.	Case 4B Results: Relative Concentration in the Fracture (A/A°) of Species Tc-99 at Time t = 5 x 10^4 yr (Multiple Patch Source, Step Release Mode)	92
3-12b.	Case 4B Results: X-Component of Relative Mass Flux in the Fracture (F_x/A°) (m/yr) of Species Tc-99 at Time t = 5 x 10^4 yr (Multiple Patch Source, Step Release Mode)	93

LIST OF TABLES
(Continued)

Table	Title	Page
3-12c.	Case 4B Results: Y-Component of Relative Mass Flux in the Fracture ($F_y/A°$) (m/yr) of Species Tc-99 at Time t = 5 x 10^4 yr (Multiple Patch Source, Step Release Mode)	94
3-12d.	Case 4B Results: Relative Cumulative Mass Flux in the Fracture (M/A°) of Species Tc-99 at Time t = 5 x 10^4 yr (Multiple Patch Source, Step Release Mode)	95
3-12e.	Case 4B Results: Relative Concentration in the Rock Matrix (B/A°) of Species Tc-99 at Time t = 5 x 10^4 yr and z = 1 m (Multiple Patch Source, Step Release Mode)	99
3-12f.	Case 4B Results: Relative Concentration in the Rock Matrix (B/A°) of Species Tc-99 at Time t = 5 x 10^4 yr and z = 5 m (Multiple Patch Source, Step Release Mode)	100
3-12g.	Case 4B Results: Relative Concentration in the Rock Matrix (B/A°) of Species Tc-99 at Time t = 5 x 10^4 yr and z = 10 m (Multiple Patch Source, Step Release Mode)	101
3-13a.	Case 4C Results: Relative Concentration in the Fracture (A/A°) of Species Tc-99 at Time t = 5 x 10^3 yr and z = 0 m (Gaussian Distributed Source, Step Release Mode)	108
3-13b.	Case 4C Results: Relative Concentration in the Fracture (A/A°) of Species Tc-99 at Time t = 2.5 x 10^4 yr and z = 0 m (Gaussian Distributed Source, Band Release Mode)	108
3-13c.	Case 4C Results: Relative Concentration in the Rock Matrix (B/A°) of Species Tc-99 at Time t = 5 x 10^3 yr and z = 1 m (Gaussian Distributed Source, Step Release Mode)	109
3-13d.	Case 4C Results: Relative Concentration in the Rock Matrix (B/A°) of Species Tc-99 at Time t = 2.5 x 10^4 yr and z = 1 m (Gaussian Distributed Source, Band Release Mode)	109
3-13e.	Case 4C Results: Relative Concentration in the Rock Matrix (B/A°) of Species Tc-99 at Time t = 5 x 10^3 yr and z = 5 m (Gaussian Distributed Source, Step Release Mode)	110
3-13f.	Case 4C Results: Relative Concentration in the Rock Matrix (B/A°) of Species Tc-99 at Time t = 2.5 x 10^4 yr and z = 5 m (Gaussian Distributed Source, Band Release Mode)	110
4-1.	Sets of Values for Equations 4-30a Through 4-30e	117
6-1.	Input Parameters for Case 5	144

LIST OF TABLES
(Continued)

Table	Title	Page
6-2a.	Case 5A Results: Comparison of Relative Concentration, Mass Flux, and Cumulative Mass Flux in the Fracture for Np-237 at Time t = 10^4 yr (Step Release Mode)	149
6-2b.	Case 5A Results: Comparison of Relative Concentration, Mass Flux, and Cumulative Mass Flux in the Fracture for Np-237 at Time t = 6 x 10^4 yr (Step Release Mode)	150
6-2c.	Case 5A Results: Comparison of Relative Concentration, Mass Flux, and Cumulative Mass Flux in Fracture for Np-237 at Time t = 2 x 10^5 yr (Step Release Mode)	151
6-2d.	Case 5A Results: Comparison of Relative Concentration, Mass Flux, and Cumulative Mass Flux in the Fracture for Np-237 at Time t = 10^6 yr (Step Release Mode)	152
6-2e.	Case 5A Results: Comparison of Relative Concentration in the Rock Matrix for Np-237 for Different Times at Longitudinal Distance x = 100 m (Step Release Mode)	153
6-3a.	Case 5B Results: Comparison of Relative Concentration, Mass Flux, and Cumulative Mass Flux in the Fracture for Np-237 at Time t = 6 x 10^4 yr (Band Release Mode)	159
6-3b.	Case 5B Results: Comparison of Relative Concentration, Mass Flux, and Cumulative Mass Flux in the Fracture for Np-237 at Time t = 2 x 10^5 yr (Band Release Mode)	160
6-3c.	Case 5B Results: Comparison of Relative Concentration, Mass Flux, and Cumulative Mass Flux in the Fracture for Np-237 at Time t = 10^6 yr (Band Release Mode)	161
6-3d.	Case 5B Results: Comparison of Relative Concentration in the Rock Matrix for Np-237 for Different Times at Longitudinal Distance x = 100 m (Band Release Mode)	162
6-4.	Input Parameters for Case 6	163
6-5a.	Case 6A Results: Comparison of Relative Concentration, Mass Flux, and Cumulative Mass Flux in the Fracture for Np-237 at x = 500 m, D_{xx} = 0 (Step Release Mode)	172
6-5b.	Case 6A Results: Comparison of Relative Concentration, Mass Flux, and Cumulative Mass Flux in the Fracture for Np-237 at x = 500 m, D_{xx} = 10 m^2/yr (Step Release Mode)	173

LIST OF TABLES
(Continued)

Table	Title	Page
6-5c.	Case 6A Results: Comparison of Relative Concentration, Mass Flux, and Cumulative Mass Flux in the Fracture for Np-237 at x = 500 m, D_{xx} = 100 m^2/yr (Step Release Mode)	174
6-5d.	Case 6A Results: Comparison of Relative Concentration, Mass Flux, and Cumulative Mass Flux in the Fracture for Np-237 at x = 500 m, D_{xx} = 1000 m^2/yr (Step Release Mode)	175
6-5e.	Case 6A Results: Comparison of Temporal Variation of Relative Concentration in the Rock Matrix for Np-237 for Different D_{xx} at Longitudinal Distance x = 500 m (Step Release Mode)	176
6-6a.	Case 6B Results: Comparison of Relative Concentration, Mass Flux, and Cumulative Mass Flux in the Fracture for Np-237 at x = 500 m, D_{xx} = 0 (Band Release Mode)	177
6-6b.	Case 6B Results: Comparison of Relative Concentration, Mass Flux, and Cumulative Mass Flux in the Fracture for Np-237 at x = 500 m, D_{xx} = 10 m^2/yr (Band Release Mode)	178
6-6c.	Case 6B Results: Comparison of Relative Concentration, Mass Flux, and Cumulative Mass Flux in the Fracture for Np-237 at x = 500 m, D_{xx} = 100 m^2/yr (Band Release Mode)	179
6-6d.	Case 6B Results: Comparison of Relative Concentration, Mass Flux, and Cumulative Mass Flux in the Fracture for Np-237 at x = 500 m, D_{xx} = 1,000 m^2/yr (Band Release Mode)	180
6-6e.	Case 6B Results: Comparison of Temporal Variation of Relative Concentration in the Rock Matrix for Np-237 for Different D_{xx} at Longitudinal Distance x = 500 m (Band Release Mode)	181
6-7.	Input Parameters Used in Simulation of Tc-99 in Fracture and Rock Matrix for Case 7	183
6-8a.	Case 7 Results: Relative Concentration in the Fracture (A/A°) of Species Tc-99 at Time t = 5 x 10^4 yr (Multiple Patch Source)	188
6-8b.	Case 7 Results: X-Component of Relative Mass Flux in the Fracture (F_x/A°) (m/yr) of Species Tc-99 at Time t = 5 x 10^4 yr (Multiple Patch Source)	189
6-8c.	Case 7 Results: Y-Component of Relative Mass Flux in the Fracture (F_y/A°) (m/yr) of Species Tc-99 at Time t = 5 x 10^4 (Multiple Patch Source)	190
6-8d.	Case 7 Results: Relative Cumulative Mass Flux in the Fracture (M/A°) of Species Tc-99 at Time t = 5 x 10^4 yr (Multiple Patch Source)	191

LIST OF TABLES
(Continued)

Table	Title	Page
6-8e.	Case 7 Results: Relative Concentration in the Rock Matrix (B/A°) of Species Tc-99 at Time $t = 5 \times 10^4$ yr and $z = 0.1$ m (Multiple Patch Source)	195
6-8f.	Case 7 Results: Relative Concentration in the Rock Matrix (B/A°) of Species Tc-99 at Time $t = 5 \times 10^4$ yr and $z = 0.5$ m (Multiple Patch Source)	196
6-8g.	Case 7 Results: Relative Concentration in the Rock Matrix (B/A°) of Species Tc-99 at Time $t = 5 \times 10^4$ yr and $z = 1.0$ m (Multiple Patch Source)	197
B-1.	Parameters Used to Estimate $G(\eta)$, $g_1(\eta)$, and $g_2(\eta,t)$	217
B-2.	Quadrature Points Required for Selected Range of Values of F_o and $\varepsilon/2\sqrt{t-R_\chi}$ $(D_{xx} = 0)$	220

LIST OF FIGURES

Figure	Title	Page
2-1.	Schematic of a Single Fracture Rock System	9
2-2.	Schematic of Multiple Parallel Fracture Rock System	10
3-1a.	Relative Concentrations of Np-237 in the Fracture Versus Longitudinal Distance x at y = 0 m and t = 10^4 yr for Different Rock Matrix Retardation Factors (R′ = 1, 10^2, 10^4) (Case 1A: Step Release Mode)	33
3-1b.	Relative Concentrations of Np-237 in the Rock Matrix Versus Distance in the Rock Matrix z at x = 100 m, y = 0 m, and t = 10^4 yr for Different Rock Matrix Retardation Factors (R′ = 1, 10^2, 10^4) (Case 1A: Step Release Mode)	34
3-1c.	Relative Mass Flux of Np-237 in the Fracture Versus Distance x at y = 0 m and t = 10^4 yr for Different Rock Matrix Retardation Factors (R′ = 1, 10^2, 10^4) (Case 1A: Step Release Mode)	39
3-1d.	Relative Cumulative Mass Flux of Np-237 in the Fracture Versus Longitudinal Distance x at y = 0 m and t = 10^4 yr for Different Rock Matrix Retardation Factors (R′ = 1, 10^2, 10^4) (Case 1A: Step Release Mode)	40
3-1e.	Breakthrough Curves Showing Relative Concentrations of Np-237 in the Fracture Versus Time at x = 100 m and y = 0 m for Different Rock Matrix Retardation Factors (R′ = 1, 10^2, 10^4) (Case 1A: Step Release Mode)	41
3-1f.	Relative Mass Flux of Np-237 in the Fracture Versus Time at x = 100 m and y = 0 m for Different Rock Matrix Retardation Factors (R′ = 1, 10^2, 10^4) (Case 1A: Step Release Mode)	42
3-1g.	Relative Cumulative Mass Flux of Np-237 in the Fracture Versus Time at x = 100 m and y = 0 m for Different Rock Matrix Retardation Factors (R′ = 1, 10^2, 10^4) (Case 1A: Step Release Mode)	43
3-2a.	Relative Concentrations of Np-237 in the Fracture Versus Longitudinal Distance x at y = 0 m, t = 10^4 yr, and D_{xx} = 0 for Different Rock Matrix Retardation Factors (R′ = 1, 10^2, 10^4) (Case 1B: Step Release Mode)	47
3-2b.	Relative Concentrations of Np-237 in the Rock Matrix Versus Distance in the Rock Matrix at x = 100 m, y = 0 m, t = 10^4 yr, and D_{xx} = 0 for Different Rock Matrix Retardation Factors (R′ = 1, 10^2, 10^4) (Case 1B: Step Release Mode)	48

LIST OF FIGURES
(Continued)

Figure	Title	Page
3-2c.	Relative Mass Flux of Np-237 in the Fracture Versus Distance x at y = 0 m, t = 10^4 yr, and D_{xx} = 0 for Different Rock Matrix Retardation Factors (R′ = 1, 10^2, 10^4) (Case 1B: Step Release Mode)	49
3-2d.	Relative Cumulative Mass Flux of Np-237 in the Fracture Versus Longitudinal Distance x at y = 0 m, t = 10^4 yr, and D_{xx} = 0 for Different Rock Matrix Retardation Factors (R′ = 1, 10^2, 10^4) (Case 1B: Step Release Mode)	50
3-2e.	Breakthrough Curves Showing the Relative Concentration of Np-237 in the Fracture Versus Time at x = 100 m, y = 0 m, and D_{xx} = 0 for Different Rock Matrix Retardation Factors (R′ = 1, 10^2, 10^4) (Case 1B: Step Release Mode)	54
3-2f.	Relative Mass Flux of Np-237 in the Fracture Versus Time at x = 100 m, y = 0 m, and D_{xx} = 0 for Different Rock Matrix Retardation Factors (R′ = 1, 10^2, 10^4) (Case 1B: Step Release Mode)	55
3-2g.	Relative Cumulative Mass Flux of Np-237 in the Fracture Versus Time at x = 100 m, y = 0 m, and D_{xx} = 0 for Different Rock Matrix Retardation Factors (R′ = 1, 10^2, 10^4) (Case 1B: Step Release Mode)	56
3-3a.	Relative Concentrations of Np-237 in the Fracture Versus Longitudinal Distance x at y = 0 m, t = 10^4 yr, and D_{xx} = 0 for Different Rock Matrix Retardation Factors (R′ = 1, 10^2, 10^4) (Case 2: Band Release Mode)	61
3-3b.	Relative Mass Flux in the Fracture Versus Distance x at y = 0 m, t = 10^4 yr, and D_{xx} = 0 for Different Rock Matrix Retardation Factors (R′ = 1, 10^2, 10^4) (Case 2: Band Release Mode)	62
3-3c.	Relative Cumulative Mass Flux of Np-237 in the Fracture Versus Longitudinal Distance x at y = 0 m, t = 10^4 yr, and D_{xx} = 0 for Different Rock Retardation Matrix Factors (R′ = 1, 10^2, 10^4) (Case 2: Band Release Mode)	63
3-3d.	Relative Concentrations of Np-237 in the Rock Matrix Versus Distance in the Rock Matrix at x = 100 m, y = 0 m, t = 10^4 yr, and D_{xx} = 0 for Different Rock Matrix Retardation Factors (R′ = 1, 10^2, 10^4) (Case 2: Band Release Mode)	64
3-4a.	Breakthrough Curves Showing the Relative Concentration of Np-237 in the Fracture Versus Time at x = 100 m, y = 0 m, and D_{xx} = 0 for Different Rock Matrix Retardation Factors (R′ = 1, 10^2, 10^4) (Case 2: Band Release Mode)	69

LIST OF FIGURES
(Continued)

Figure	Title	Page
3-4b.	Relative Mass Flux of Np-237 in the Fracture Versus Time at $x = 100$ m, $y = 0$ m, and $D_{xx} = 0$ for Different Rock Matrix Retardation Factors ($R' = 1, 10^2, 10^4$) (Case 2: Band Release Mode)	70
3-4c.	Relative Cumulative Mass Flux of Np-237 in the Fracture Versus Time at $x = 100$ m, $y = 0$ m, and $D_{xx} = 0$ for Different Rock Matrix Retardation Factors ($R' = 1, 10^2, 10^4$) (Case 2: Band Release Mode)	71
3-5a.	Relative Concentration Isopleths for Tc-99 in the Fracture at $z = 0$ m and $t = 5 \times 10^3$ yr, Step Release Mode (Case 4A: Finite Patch Source)	78
3-5b.	Relative Concentration Isopleths for Tc-99 in the Fracture at $z = 0$ m and $t = 2.5 \times 10^4$ yr, Band Release Mode (Case 4A: Finite Patch Source)	79
3-5c.	Relative Concentration Isopleths for Tc-99 in the Rock Matrix at $z = 1$ m and $t = 5 \times 10^3$ yr, Step Release Mode (Case 4A: Finite Patch Source)	80
3-5d.	Relative Concentration Isopleths for Tc-99 in the Rock Matrix at $z = 1$ m and $t = 2.5 \times 10^4$ yr, Band Release Mode (Case 4A: Finite Patch Source)	81
3-5e.	Relative Concentration Isopleths for Tc-99 in the Rock Matrix at $z = 5$ m and $t = 5 \times 10^3$ yr, Step Release Mode (Case 4A: Finite Patch Source)	82
3-5f.	Relative Concentration Isopleths for Tc-99 in the Rock Matrix at $z = 5$ m and $t = 2.5 \times 10^4$ yr, Band Release Mode (Case 4A: Finite Patch Source)	83
3-6a.	Relative Concentration Profiles for Tc-99 in the Fracture at $z = 0$ m and $t = 5 \times 10^4$ yr (Case 4B: Multiple Patch Source)	88
3-6b.	Relative Mass Flux Profiles for Tc-99 in the Fracture at $z = 0$ m and $t = 5 \times 10^4$ yr (Case 4B: Multiple Patch Source)	89
3-6c.	Mass Flux Vector of Tc-99 at Discrete Points in the Fracture at $z = 0$ m and $t = 5 \times 10^4$ yr (Case 4B: Multiple Patch Source)	90
3-6d.	Relative Cumulative Mass Flux Profiles for Tc-99 in the Fracture at $z = 0$ m and $t = 5 \times 10^4$ yr (Case 4B: Multiple Patch Source)	91
3-6e.	Relative Concentration Profiles for Tc-99 in the Rock Matrix at $z = 1$ m and $t = 5 \times 10^4$ yr (Case 4B: Multiple Patch Source)	96
3-6f.	Relative Concentration Profiles for Tc-99 in the Rock Matrix at $z = 5$ m and $t = 5 \times 10^4$ yr (Case 4B: Multiple Patch Source)	97
3-6g.	Relative Concentration Profiles for Tc-99 in the Rock Matrix at $z = 10$ m and $t = 5 \times 10^4$ yr (Case 4B: Multiple Patch Source)	98

LIST OF FIGURES
(Continued)

Figure	Title	Page
3-7a.	Relative Concentration Isopleths for Tc-99 in the Fracture at $z = 0$ m and $t = 5 \times 10^3$ yr (Case 4C: Gaussian Distributed Source)	102
3-7b.	Relative Concentration Isopleths for Tc-99 in the Fracture at $z = 0$ m and $t = 2.5 \times 10^4$ yr, Band Release Mode (Case 4C: Gaussian Distributed Source)	103
3-7c.	Relative Concentration Isopleths for Tc-99 in the Rock Matrix at $z = 1$ m and $t = 5 \times 10^3$ yr, Step Release Mode (Case 4C: Gaussian Distributed Source)	104
3-7d.	Relative Concentration Isopleths for Tc-99 in the Rock Matrix at $z = 1$ m and $t = 2.5 \times 10^4$ yr, Band Release Mode (Case 4C: Gaussian Distributed Source)	105
3-7e.	Relative Concentration Isopleths for Tc-99 in the Rock Matrix at $z = 5$ m and $t = 5 \times 10^3$ yr, Step Release Mode (Case 4C: Gaussian Distributed Source)	106
3-7f.	Relative Concentration Isopleths for Tc-99 in the Rock Matrix at $z = 5$ m and $t = 2.5 \times 10^4$ yr, Band Release Mode (Case 4C: Gaussian Distributed Source)	107
6-1a.	Comparison of Spatial Variation of Relative Concentration of Np-237 in the Fracture for Different Times (Case 5A: Multiple Parallel Fractures, Step Release Mode, No Longitudinal Dispersion)	145
6-1b.	Comparison of Spatial Variation of Relative Mass Flux of Np-237 in the Fracture for Different Times (Case 5A: Multiple Parallel Fractures, Step Release Mode, No Longitudinal Dispersion)	146
6-1c.	Comparison of Spatial Variation of Relative Cumulative Mass Flux of Np-237 in the Fracture for Different Times (Case 5A: Multiple Parallel Fractures, Step Release Mode, No Longitudinal Dispersion)	147
6-1d.	Comparison of Spatial Variation of Relative Concentration of Np-237 in the Rock Matrix for Different Times (Case 5A: Multiple Parallel Fractures, Step Release Mode, No Longitudinal Dispersion)	148
6-2a.	Comparison of Spatial Variation of Relative Concentration of Np-237 in the Fracture for Different Times (Case 5B: Multiple Parallel Fractures, Band Release Mode, No Longitudinal Dispersion)	155

LIST OF FIGURES
(Continued)

Figure	Title	Page
6-2b.	Comparison of Spatial Variation of Relative Mass Flux of Np-237 in the Fracture for Different Times (Case 5B: Multiple Parallel Fractures, Band Release Mode, No Longitudinal Dispersion)	156
6-2c.	Comparison of Spatial Variation of Relative Cumulative Mass Flux of Np-237 in the Fracture for Different Times (Case 5B: Multiple Parallel Fractures, Band Release Mode, No Longitudinal Dispersion)	157
6-2d.	Comparison of Spatial Variation of Relative Concentration of Np-237 in the Rock Matrix for Different Times (Case 5B: Multiple Parallel Fractures, Band Release Mode, No Longitudinal Dispersion)	158
6-3a.	Comparison of Temporal Variation of Relative Concentration of Np-237 in the Fracture for D_{xx} = 0, 10, 100, 1000 m^2/yr (Case 6A: Multiple Parallel Fractures, Step Release Mode)	164
6-3b.	Comparison of Temporal Variation of Relative Mass Flux of Np-237 in the Fracture for D_{xx} = 0, 10, 100, 1000 m^2/yr (Case 6A: Multiple Parallel Fractures, Step Release Mode)	165
6-3c.	Comparison of Temporal Variation of Relative Cumulative Mass Flux of Np-237 in the Fracture for D_{xx} = 0, 10, 100, 1000 m^2/yr (Case 6A: Multiple Parallel Fractures, Step Release Mode)	166
6-3d.	Comparison of Temporal Variation of Relative Concentration of Np-237 in the Rock Matrix at Elevation z = 0.3 m for D_{xx} = 0, 10, 100, 1000 m^2/yr (Case 6A: Multiple Parallel Fractures, Step Release Mode)	167
6-4a.	Comparison of Temporal Variation of Relative Concentration of Np-237 in the Fracture for D_{xx} = 0, 10, 100, 1000 m^2/yr (Case 6B: Multiple Parallel Fractures, Band Release Mode)	168
6-4b.	Comparison of Temporal Variation of Relative Mass Flux of Np-237 in the Fracture for D_{xx} = 0, 10, 100, 1000 m^2/yr (Case 6B: Multiple Parallel Fractures, Band Release Mode)	169
6-4c.	Comparison of Temporal Variation of Relative Cumulative Mass Flux of Np-237 in the Fracture for D_{xx} = 0, 10, 100, 1000 m^2/yr (Case 6B: Multiple Parallel Fractures, Band Release Mode)	170
6-4d.	Comparison of Temporal Variation of Relative Concentration of Np-237 in the Rock Matrix at Elevation z = 0.3 m for D_{xx} = 0, 10, 100, 1000 m^2/yr (Case 6B: Multiple Parallel Fractures, Band Release Mode)	171

LIST OF FIGURES
(Continued)

Figure	Title	Page
6-5a.	Relative Concentration Profiles for Tc-99 in the Fracture at $z = 0$ m and $t = 5 \times 10^4$ yr (Case 7: Multiple Patch Source)	184
6-5b.	Relative Mass Flux Profiles for Tc-99 in the Fracture at $z = 0$ m and $t = 5 \times 10^4$ yr (Case 7: Multiple Patch Source)	185
6-5c.	Mass Flux Vector of Tc-99 at Discrete Points in the Fracture at $z = 0$ m and $t = 5 \times 10^4$ yr (Case 7: Multiple Patch Source)	186
6-5d.	Relative Cumulative Mass Flux Profiles for Tc-99 in the Fracture at $z = 0$ m and $t = 5 \times 10^4$ yr (Case 7: Multiple Patch Source)	187
6-5e.	Relative Concentration Profiles for Tc-99 in the Rock Matrix at $z = 0.1$ m and $t = 5 \times 10^4$ yr (Case 7: Multiple Patch Source)	192
6-5f.	Relative Concentration Profiles for Tc-99 in the Rock Matrix at $z = 0.5$ m and $t = 5 \times 10^4$ yr (Case 7: Multiple Patch Source)	193
6-5g.	Relative Concentration Profiles for Tc-99 in the Rock Matrix at $z = 1.0$ m and $t = 5 \times 10^4$ yr (Case 7: Multiple Patch Source)	194
B-1.	Variations of Function $G(\eta)$, $g_1(\eta)$, and $g_2(\eta,t)$ for $x = 1$ m	214
B-2.	Variations of Function $G(\eta)$, $g_1(\eta)$, and $g_2(\eta,t)$ for $x = 100$ m	215
B-3.	Variations of Function $G(\eta)$, $g_1(\eta)$, and $g_2(\eta,t)$ for $x = 10{,}000$ m	216

PART 1

1.0 INTRODUCTION

1.1 BACKGROUND

In recent years increased interest has been registered in the U.S. and Western Europe for considering rock that may contain fractures as a viable candidate geologic medium for permanent disposal of high-level nuclear waste. The key elements prompting investigations in this area are the low porosity of hard rock coupled with its diffusive (Neretnieks, 1980) and adsorptive properties (Rickert et al., 1979).

Analytical solutions for solute transport in planar fractures reported to date are for the most part unidimensional; they neglect in some cases the dispersion phenomena as well as decay reaction at the source, and they are based on the Laplace transformation technique. The first recursive one-dimensional solution for dispersion-free transport of a decay chain of arbitrary length is a single fracture with diffusion into the rock matrix was presented by Kanki et al. (1981) (see also Chambré et al., 1982). Subsequently a nonrecursive solution for a three-member decay chain neglecting dispersion in the fracture and radioactive decay in the rock matrix was reported by the same authors (see Chambré et al., 1982). Neretnieks (1980) reported a solution for the nondispersive transport of a decaying species along a discrete fracture and rock matrix of infinite thickness, and demonstrated the overall impact of the matrix diffusion mechanism on the transport process. Rasmuson and Neretnieks (1980) presented a solution for the radial diffusion problem and longitudinal dispersion in spherical porous particles; their work is an extension of the Rosen (1952) solution, which neglected the dispersion effects, and apparently an improvement of the Babcock et al. (1966) solution of the same problem. Grisak and Pickens (1981), discounting the dispersive effects, presented a solution for a nondecaying solute. Tang et al. (1981) extended the solution presented by Neretnieks (1980) after considering the dispersive component in the governing equation; however in their case the concentration at the source is assumed constant. Chambré et al. (1982) presented a set of analytical solutions related to radionuclide decay chain transport in fractured media; these solutions neglect for the most part the effects of longitudinal dispersion. Sudicky and Frind (1982) presented the transient and steady-state solution for the dispersive and nondispersive transport of a single decaying solute in a system of parallel fractures where the concentration at the source is held constant. This solution was first revised by Davis and Johnston (1984) and the correct form was subsequently given by Ahn et al. (1986). Barker (1982) and Hodgkinson and Maul (1985), utilizing a numerical inversion of the Laplace transform, presented solutions for unidirectional and radial transport of a single decaying species in a system of parallel fractures where the initial concentration was assumed to be a function of position. Van Genuchten

et al. (1984) presented some exact solutions for transport of a single conservative species through large cylindrical macropores with simultaneous radial diffusion into the rock matrix. Rasmuson (1984) presented a solution for the transport of a radionuclide diffusing into a rock matrix simulated by spheres where the inlet concentration is kept constant; this work is an extension of an earlier paper by Rasmuson and Neretnieks (1981).

Sudicky and Frind (1984) presented a solution for the nondispersive transport of a two-member decay chain in a single fracture subjected to a nondecaying boundary condition at the source. An improved form of this solution approach was recently reported by Ahn et al. (1986). Moreno and Rasmuson (1986) examined the impact of two types of inlet boundary conditions on the concentration in the rock matrix for a conservative solute.

Chen (1986) presented solutions for a number of cases dealing with radionuclide transport from an injection well into a fractured porous formation of infinite extent; this approach includes a decaying and a nondecaying source and accounts for the diffusion process in the rock matrix.

1.2 PURPOSE

This report presents a set of analytical solutions based on the Laplace and Fourier transforms for the two-dimensional isothermal transport of a radionuclide in an idealized discrete planar fracture of constant aperture and a system of parallel fractures of infinite extent. The approach considers simultaneous infinite or finite diffusion in the rock matrix. The transport phenomena in the fracture include processes such as advection, hydrodynamic dispersion, linear equilibrium adsorption, and radioactive decay (the last two processes and rock matrix diffusion are also applicable to the rock matrix). The rock matrix is assumed to be homogeneous, isotropic, and fully saturated with stagnant water; the flowing water in the fractures, assumed to be under steady-state conditions, has a parallel streamline configuration. The solutions for the mass flux and the cumulative mass flux at any given point in the fracture as well as the longitudinal dispersion-free solution are also presented.

This report is divided into two parts. Part 1 (through Chapter 3) focuses on the derivation and verification of the two-dimensional solution for the single fracture case. Part 2 (Chapter 4 to the end) covers a similar endeavor focused on the multiple parallel fracture case where two solutions are reported: the first based on a series approximation and the second on contour integration.

The verification of the associated computer code (i.e., FRACFLO) is performed in the single fracture case by means of available one- and two-dimensional analytical solutions. The one-dimensional solution of Ahn et al. (1985) will be used for benchmarking the performance of the reported solutions, restricted however to unidimensional flow. The two-dimensional solution of Gureghian (1987) will enable a verification of the solution pertaining to the fracture in the absence of rock matrix diffusion.

In the parallel fracture case the verification will be undertaken by way of a comparison of the performance of one solution against the other.

1.3 APPLICATIONS

These solutions are designed to cope with a realistic number of idealized fracture patterns, concentration distributions (i.e., single or multiple patch, or a Gaussian distributed source) decaying with time, and release modes (i.e., step and band release) associated with the geometry of a high-level nuclear waste repository in deep geologic rock media with fractures. Applications of these solutions are also reported. The reader should note the limitations of the solutions for the cumulative mass flux, which is restricted to the one-dimensional form of this code, and for the case where the velocity vector is orthogonal to the inlet or source.

The model FRACFLO was written in VAX FORTRAN Version 4.8 using the G floating point option (REAL * 16). Auxiliary graphics programs were written using DISSPLA Version 10.5. The computation was executed on a VAX 8700 under VMS Version 4.7.

2.0 MASS TRANSPORT EQUATIONS FOR FRACTURE AND ROCK MATRIX

From the mass conservation requirement, the concentration of a nuclide flowing in a discrete fracture plane with uniform aperture while undergoing sorption and diffusion in the surrounding rock matrix under isothermal and laminar flow conditions is given by

$$\frac{\partial}{\partial t}\left(A + \frac{S}{b}\right) - \nabla \cdot (\overline{D} \cdot \nabla A - AV) - Q + \frac{J}{b} = 0 \tag{2-1}$$

$$\frac{\partial}{\partial t}(\phi B + \phi_r \rho_r S') + \frac{\partial J}{\partial z} - Q' = 0 \tag{2-2}$$

where

$\nabla\cdot$	is the divergence operator $\partial/\partial x + \partial/\partial y$ L^{-1})
∇	is the gradient operator $\partial/\partial x$, $\partial/\partial y$ (L^{-1})
x and y	are the horizontal cartesian coordinates (L)
z	is the vertical cartesian coordinate (L)
A	is the concentration in the fracture (ML^{-3})
B	is the concentration in the rock matrix (ML^{-3})
V	is the average fluid velocity vector (components v_x, v_y) in the fracture (LT^{-1})
$\overline{D}$	is the hydrodynamic dispersion tensor (L^2T^{-1})
S	is the concentration of sorbed contaminant on fracture surface (ML^{-2})
S'	is the concentration in the adsorbed phase in the rock matrix (MM^{-1})
ρ_r	is the rock density (ML^{-3})
ϕ_r	is the volumetric fraction of the solid phase in the rock matrix ($1 - \phi$)
ϕ	is the rock porosity
2b	is the fracture aperture (L)
J	is the diffusive rate of the nuclide at the surface of the fracture per unit area of fracture surface ($ML^{-2}T^{-1}$)
Q and Q'	are the rate of production or removal of solute due to radioactive decay in the fracture and rock matrix, respectively ($ML^{-3}T^{-1}$)
t	is time (T).

The diffusive rate of a nuclide into the rock matrix is assumed to obey Fick's law of diffusion written as

$$J = -D_e \frac{\partial B}{\partial z}\Big|_{z=b} \tag{2-3}$$

where D_e is the effective diffusivity in the rock matrix (Neretnieks, 1980) defined as

$$D_e = \phi D_p \tag{2-4a}$$

$$D_p = D_d \frac{\delta_d}{\tau^2} \tag{2-4b}$$

where

- D_p is the pore diffusivity (L^2T^{-1})
- D_d is the molecular diffusion of nuclide in water (L^2T^{-1})
- δ_d is the constrictivity for diffusion (L^0)
- τ is the tortuosity (L^0).

The hydrodynamic dispersion tensor (Bear, 1972) may be written as

$$D_{ij} = a_T V \delta_{ij} + (a_L - a_T) \frac{v_i v_j}{V} + \tau D_d, \quad i,j = x,y \tag{2-5}$$

where

- a_L and a_T are the dispersivities in the longitudinal and transverse direction of the flow (L)
- δ_{ij} is the Kronecker delta (L^0).

When one of the axes of the cartesian coordinate system, say x, coincides with the direction of the average velocity vector V, the hydrodynamic dispersion tensor reduces to

$$D_{xx} = a_L V + \tau D_d \tag{2-6a}$$

$$D_{yy} = a_T V + \tau D_d \tag{2-6b}$$

The following assumptions are made in this work:

(i) Fluid movement in the fracture is assumed under steady-state conditions where the streamlines are parallel.

(ii) The fracture is assumed to be analogous to an isotropic porous medium.

(iii) The rock matrix is assumed to be homogeneous, isotropic, and saturated with stagnant water.

With the assumption that the dissolved radionuclides are in adsorption equilibrium with the fissure wall and the filling material where the prevailing concentration is A, the mechanism of adsorption may be adequately described by a linear equilibrium isotherm (Neretnieks, 1982):

$$S = K_f A \tag{2-7a}$$

where K_f is the surface distribution coefficient (L) in the fracture. Similarly, in the rock the adsorption isotherm is given by

$$S' = K_r B \tag{2-7b}$$

where K_r is the distribution coefficient in the rock matrix (L^3M^{-1}).

The instantaneous rate of removal of a nuclide by radioactive decay in the fracture (Q) and the rock matrix (Q') may then be written as

$$Q = -\lambda \left[A + \frac{S}{b} \right] \tag{2-8}$$

$$Q' = -\lambda [\phi B + \phi_r \rho_r S'] \tag{2-9}$$

where λ is the first-order rate constant for decay (T^{-1}) (i.e., $\lambda = \ln 2/T_{1/2}$).

With the above considerations, the set of differential equations describing the movement of a typical nuclide in the fracture and rock matrix, respectively, is given by the following equation in which the parameters u and v replace previously used symbols v_x and v_y.

$$R \frac{\partial A}{\partial t} - D_{xx} \frac{\partial^2 A}{\partial x^2} - D_{yy} \frac{\partial^2 A}{\partial y^2} - 2D_{yx} \frac{\partial^2 A}{\partial y \partial x} + u \frac{\partial A}{\partial x} + v \frac{\partial A}{\partial y} + \lambda RA + \frac{J}{b} = 0 \tag{2-10}$$

$$R' \frac{\partial B}{\partial t} - D_p \frac{\partial^2 B}{\partial z^2} + \lambda R'B = 0 \tag{2-11}$$

where

$$R = 1 + K_f/b \tag{2-12}$$

and

$$R' = 1 + [(1-\phi)/\phi]\rho_r K_r \tag{2-13}$$

are the retardation factors of a typical nuclide embodying the overall effect of the sorption and desorption reactions in the fissure and rock matrix, respectively.

Two models of idealized fractured rock systems are investigated, namely the single fracture and the multiple parallel fracture cases, where the diffusion field of the rock matrix is assumed infinite in the former case, and finite in the latter case (see Figures 2-1 and 2-2).

2.1 INITIAL AND BOUNDARY CONDITIONS

The set of differential equations, Equations 2-10 and 2-11, are subject to the initial conditions:

$$A(x,y,0) = 0\,,\ x > 0\,,\ -\infty < y < +\infty \tag{2-14}$$

$$B(x,y,z,0) = 0\,,\ x > 0\,,\ -\infty < y < +\infty\,,\ |z| \geq b \tag{2-15}$$

and boundary conditions as follows.

2.1.1 Fracture

Finite Patch Source

$$\tilde{A}(0,y,t) = A(t)\,U(t)\left[U\left(y-y_1+\frac{d}{2}\right) - U\left(y-y_1-\frac{d}{2}\right)\right],\ t > 0\,,\ -\infty < y < +\infty \tag{2-16a}$$

$$A(\infty,y,t) = 0\,,\ t > 0\,,\ -\infty < y < +\infty \tag{2-16b}$$

$$\frac{\partial A\,(x,\pm\infty,t)}{\partial y} = 0\,,\ t > 0\,,\ x > 0 \tag{2-16c}$$

where

y_1 is the location of the source center along the Y-axis

$\tilde{A}(t)$ is the concentration at the source

d is the width of the finite patch source at the origin along the Y-axis.

Gaussian Source

In a high-level nuclear waste repository, the concentration at the source depends to a large extent on the release rate of the waste from its canister into the ground water. A boundary condition such as a finite patch source, which implies a uniform concentration across its area (2b x d), may not adequately duplicate in situ conditions. Consequently, to circumvent the uncertainty inherent in the

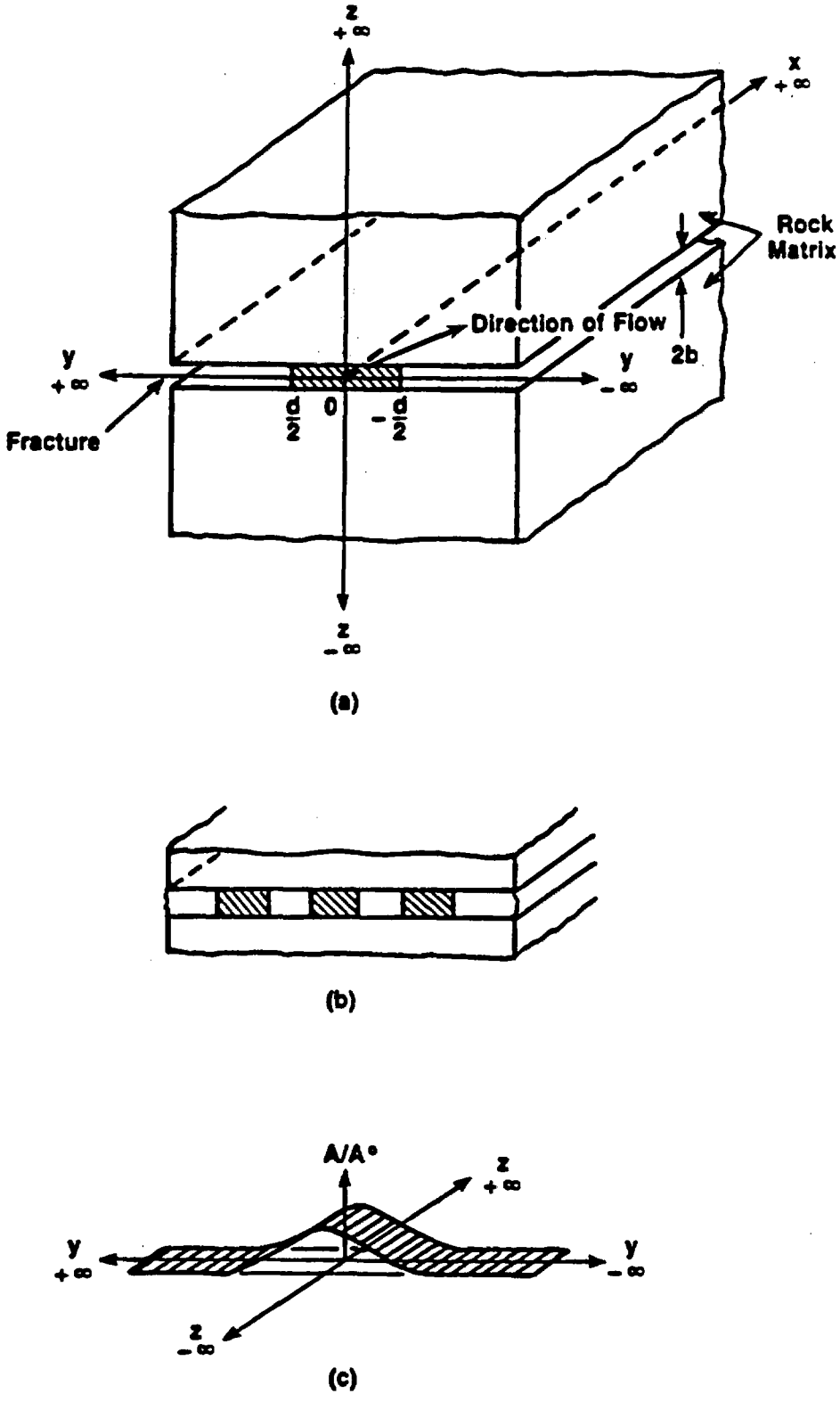

Figure 2-1. Schematic of a Single Fracture Rock System
(a) Patch Source; (b) Multiple Patch Source;
(c) Gaussian Distribution Source

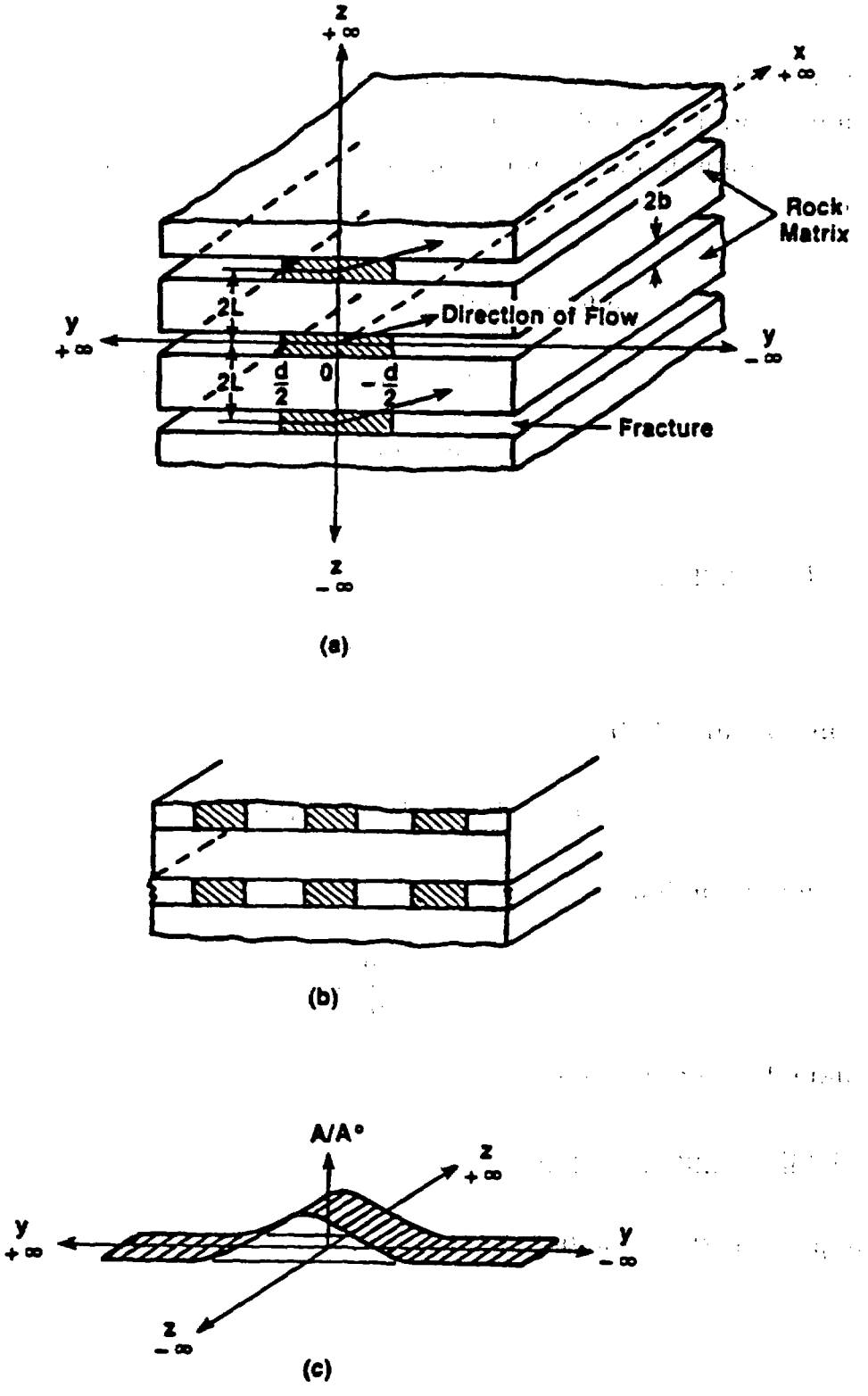

Figure 2-2. Schematic of Multiple Parallel Fracture Rock System
(a) Patch Source; (b) Multiple Patch Source;
(c) Gaussian Distributed Source

source term, a probabilistic interpretation of the concentration distribution at the source may be deemed appropriate. In this instance, a source model based on Gaussian distribution is adopted.

The boundary condition for the Gaussian source located at y_0 with standard deviation σ_y may be written as

$$A(0,y,t) = \tilde{A}(t)\,U(t)e^{-(y-y_0)^2/2\sigma_y^2}\,,\ t > 0\ ,\ -\infty < y < +\infty \tag{2-17a}$$

$$A(\infty,y,t) = 0\ ,\ t > 0\ ,\ -\infty < y < +\infty \tag{2-17b}$$

$$\frac{\partial A(x,\pm\infty,t)}{\partial y} = 0\,,\ t > 0\,,\ x > 0\ . \tag{2-17c}$$

2.1.2 Rock Matrix

$$B(x,y,b,t) = A(x,y,t)\ ,\ x > 0\ ,\ -\infty < y < +\infty \tag{2-18a}$$

Infinite Diffusion Field

$$B(x,y,\pm\infty,t) = 0\ ,\ x > 0\ ;\ -\infty < y < +\infty,\ t > 0 \tag{2-18b}$$

Finite Diffusion Field

$$\frac{\partial B}{\partial z}(x,y,L,t) = 0 \tag{2-18c}$$

where 2L is the fracture spacing.

2.1.3 Concentration at the Source and Band Release

Step Release (Continuous Decaying Source)

The concentration at the source for a typical nuclide may be written as

$$\tilde{A}(t) = A^0 e^{-\lambda t} \tag{2-19}$$

where A^0 is the concentration of the species at time equals zero.

Band Release

The boundary condition for the band release may be written as

$$A(0,y,t) = A(t)[U(t) - U(t-T)]\phi(y)\ ,\ t > 0\ ,\ -\infty < y < +\infty \tag{2-20}$$

where

$\phi(y) = U(y - y_1 + d/2) - U(y - y_1 - d/2)$ for a finite line source

$\phi(y) = \exp[-(y - y_0)^2/2\sigma_y^2]$ for a Gaussian source

T is the leaching time.

U (t − T) is the Heaviside unit function defined as

$$U(t-T) = \begin{Bmatrix} 1, t > T \\ \frac{1}{2}, t = T \\ 0, t < T \end{Bmatrix} \tag{2-21}$$

The general form of the solution for the band release mode based on a boundary condition given by Equation 2-20 and which uses the superposition technique (see Foglia et al., 1979) may be written as

$$^{b}A(x,y,t) = [A(x,y,t; A^{o}) - A(x,y,t-T; A^{o}e^{-\lambda T})]U(t-T) \tag{2-22}$$

where T corresponds to the leach duration and superscript b indicates the band release solution.

3.0 SINGLE FRACTURE CASE WITH INFINITE DIFFUSION FIELD

3.1 NON-ZERO LONGITUDINAL DISPERSION

3.1.1 Rock Matrix

The Laplace transformation of Equation 2-11 with its associated boundary condition Equation 2-18a may be written as

$$\frac{d^2\overline{B}}{dz^2} - \frac{R'}{D_p}(s+\lambda)\,\overline{B} = 0 \tag{3-1}$$

$$\overline{B}\,(x,y,b,s) = \overline{A}\,(x,y,s) \tag{3-2}$$

where

$$\overline{B} = \int_0^\infty B e^{-st}\,dt\ . \tag{3-3}$$

The solution of Equation 3-1 subject to its initial and boundary conditions Equations 2-15, 2-18b, and 3-2 is given by

$$\overline{B}\,(x,y,z,s) = \overline{A}\,e^{r_b(z-b)} \tag{3-4}$$

with

$$r_b = -c_r(s+\lambda)^{1/2} \tag{3-5a}$$

and

$$c_r = \left(R'/D_p\right)^{1/2} \tag{3-5b}$$

Note that the inverse Laplace transform of $\overline{B}$ might be sought once $\overline{A}$ is identified as shown in the subsequent section.

The transformed diffusive flux (Equation 2-3) at the interface of the fracture and rock matrix is given by

$$\bar{J} = -\phi D_p \frac{\partial \bar{B}}{\partial z}(x,y,b,s) = -\phi D_p r_b \bar{A}(x,y,s) \quad . \tag{3-6}$$

Note that r_b in the above equation is given by Equation 3-5a.

3.1.2 Fracture

After proper substitution of the transform of the diffusive flux given by Equation 3-6 into the Laplace transformation of Equation 2-10,

$$D_{xx}\frac{\partial^2 \bar{A}}{\partial x^2} + D_{yy}\frac{\partial^2 \bar{A}}{\partial y^2} + 2D_{yx}\frac{\partial^2 \bar{A}}{\partial y \partial x} - u\frac{\partial \bar{A}}{\partial x} - v\frac{\partial \bar{A}}{\partial y} - \left[R\left(s+\lambda\right) + c_f\left(s+\lambda\right)^{1/2}\right]\bar{A} = 0 \tag{3-7}$$

with

$$c_f = \frac{\phi}{b}\left(R'D_p\right)^{1/2} \quad . \tag{3-8}$$

The Laplace transforms of the boundary conditions (Equations 2-16 or 2-17 and 2-19) associated with Equation 2-10 are given by:

Finite Patch Source

$$\bar{A}(0,y,s) = A^o\theta(s)\left[U\left(y - y_1 + \frac{d}{2}\right) - U\left(y - y_1 - \frac{d}{2}\right)\right], \; -\infty < y < \infty \tag{3-9a}$$

Gaussian Source

$$\bar{A}(0,y,s) = A^o\theta(s)e^{-(y-y_0)^2/2\sigma_y^2} \tag{3-9b}$$

where

$$\theta(s) = \frac{1}{s+\lambda} \quad . \tag{3-9c}$$

Applying the following Fourier integral transform and inversion formula for an infinite region ($-\infty < y < +\infty$) (Sneddon, 1951) written as

Integral Transform

$$\bar{\bar{A}}(x,\beta,s) = \int_{-\infty}^{+\infty} e^{i\beta y'} \bar{A}(x,y',s)\,dy' \tag{3-10a}$$

Inversion Formula

$$\bar{A}(x,y,s) = \frac{1}{2\pi} \int_{-\infty}^{+\infty} e^{-i\beta y} \bar{\bar{A}}(x,\beta,s)\,d\beta \tag{3-10b}$$

the y-variation of Equation 3-7 is removed as a result of an integration by parts using Equation 3-10a to get

$$D_{xx} \frac{d^2\bar{\bar{A}}}{dx^2} - \left(u + 2D_{yx} i\beta\right) \frac{d\bar{\bar{A}}}{dx} + \left[iv\beta - D_{yy}\beta^2 - R(s+\lambda) - c_f(s+\lambda)^{1/2}\right] \bar{\bar{A}} = 0 \ . \tag{3-11}$$

The solution of the above equation subject to its initial and boundary conditions given by Equations 2-14 and 2-16 or 2-17 may be written as

$$\bar{\bar{A}}(x,\beta,s) = \bar{\bar{F}}(\beta,s) e^{a_n x} \tag{3-12}$$

where

$$a_n x = \frac{1}{2D_{xx}} \left[(u + 2D_{yx} i\beta) - \left((u + 2D_{yx} i\beta)^2 - 4D_{xx}\left[iv\beta - D_{yy}\beta^2 - R(s+\lambda) - c_f(s+\lambda)^{1/2}\right]\right)^{1/2}\right] x \tag{3-13}$$

and $\bar{\bar{F}}(\beta,s)$ is the Fourier transform corresponding to either type of boundary condition considered herein:

$$\bar{\bar{F}}(\beta,s) = \int_{-\infty}^{+\infty} \bar{A}(0,y',s) e^{i\beta y'}\,dy' \ . \tag{3-14}$$

Finite Patch Source

Using Equation 3-9a, we have

$$\bar{\bar{F}}(\beta,s) = A^{o}\theta(s)\,\frac{e^{i\beta y'}}{i\beta}\Bigg|_{y_1-\frac{d}{2}}^{y_1+\frac{d}{2}} = A^{o}\theta(s)\,\frac{e^{i\beta Y'}}{\beta}\,2\sin\left(\beta\frac{d}{2}\right) \tag{3-15a}$$

Gaussian Source

Using Equation 3-9b, we have

$$\bar{\bar{F}}(\beta,s) = A^{o}\theta(s)\int_{-\infty}^{+\infty}\exp\left[-\frac{\left(y'-y_o\right)^2}{2\sigma_y^2} + i\beta y'\right]dy' \ . \tag{3-15b}$$

Putting

$$Y = y'-y_o \tag{3-16}$$

we have

$$\bar{\bar{F}}(\beta,s) = e^{i\beta y_o}A^{o}\theta(s)\int_{-\infty}^{+\infty}\exp\left(\frac{-Y^2}{2\sigma_y^2} + i\beta Y\right)dY \tag{3-17}$$

and recognizing the following integral (see Gradshteyn and Ryzhik, 1980, p. 307)

$$\int_{-\infty}^{+\infty}\exp\left(-p^2Y^2 + iqY\right)dY = \frac{\sqrt{\pi}}{p}\exp\left(-q^2/4p^2\right) \tag{3-18}$$

Equation 3-14 becomes

$$\bar{\bar{F}}(\beta,s) = A^{o}\theta(s)\left(2\pi\sigma_y^2\right)^{1/2}\exp\left[-\beta^2\frac{\sigma_y^2}{2} + i\beta y_o\right] \ . \tag{3-19}$$

Recognizing the following integral (see Appendix D)

$$\int_0^\infty \exp\left(-\sigma^2 - \frac{\gamma^2}{\sigma^2}\right) d\sigma = \frac{\sqrt{\pi}}{2} \exp(-2\gamma) \tag{3-20}$$

Equation 3-12 may now be written in the form

$$\overline{\overline{A}}(x,\beta,s) = \int_0^\infty \psi(x,\sigma)\, \overline{\overline{F}}(\beta,s)\, \overline{\overline{G}}(\beta,\chi) e^{r_a \chi}\, d\sigma \tag{3-21}$$

where

$$\psi(x,\sigma) = \frac{2}{\sqrt{\pi}} \exp\left[-\left(\sigma - \frac{ux}{4D_{xx}\sigma}\right)^2\right] \tag{3-22a}$$

$$\overline{\overline{G}}(\beta,x,\chi) = \exp\left[-\left(D_{yy} - \frac{D_{yx}^2}{D_{xx}}\right)\chi\beta^2 + \left(\left(v - u\frac{D_{yx}}{D_{xx}}\right)\chi + \frac{D_{yx}}{D_{xx}}x\right) i\beta\right] \tag{3-22b}$$

$$r_a = -R(s+\lambda) - c_f(s+\lambda)^{1/2} \tag{3-22c}$$

and

$$\chi = \frac{x^2}{4D_{xx}\sigma^2} \quad . \tag{3-22d}$$

Note that c_f in Equation 3-22c is given by Equation 3-8. Whence by the inversion formula (Equation 3-10b), we have

$$\overline{F}(y,s) = \frac{1}{2\pi} \int_{-\infty}^{+\infty} e^{-i\beta y}\, \overline{\overline{F}}(\beta,s) d\beta \quad . \tag{3-23}$$

Finite Patch Source

Referring to Equation 3-15a, this becomes

$$\overline{F}(y,s) = A^o\theta(s)\left[U\left(y - y_1 + \frac{d}{2}\right) - U\left(y - y_1 - \frac{d}{2}\right)\right] \quad . \tag{3-24a}$$

Gaussian Source

Referring to Equation 3-19, this becomes

$$\overline{F}(y,s) = A^{o}\theta(s)\left(\frac{\sigma_y^2}{2\pi}\right)^{1/2}\int_{-\infty}^{+\infty}\exp\left[-\frac{\sigma_y^2}{2}\beta^2 - i\left(y-y_o\right)\beta\right]d\beta \quad . \tag{3-24b}$$

Hence making use of Equation 3-18, we have

$$\overline{F}(y,s) = A^{o}\theta(s)\exp\left[-\frac{\left(y-y_o\right)^2}{2\sigma_y^2}\right] \quad . \tag{3-25}$$

Similarly, applying Equation 3-18 to the inverse transform of Equation 3-22b, we have

$$\overline{G}(\beta,x,\chi) = \frac{1}{2\pi}\int_{-\infty}^{+\infty} e^{-i\beta y}\,\overline{\overline{G}}(\beta,x,\chi)d\beta = \frac{1}{2p\sqrt{\pi}}\exp\left[\frac{-\left(y-g\right)^2}{4p^2}\right] \tag{3-26}$$

where

$$g = \left(v - u\frac{D_{yx}}{D_{xx}}\right)\chi + \left(\frac{D_{yx}}{D_{xx}}\right)x \tag{3-27a}$$

$$p = \left(\left(D_{yy} - \frac{D_{yx}^2}{D_{xx}}\right)\chi\right)^{1/2} \tag{3-27b}$$

If we define

$$\overline{\overline{H}}(x,\beta,s) = \overline{\overline{F}}(\beta,s)\,\overline{\overline{G}}(\beta,x,\chi) \tag{3-28}$$

then the convolution theorem applied to this equation will yield its inverse Fourier transform, which may be written as

$$\overline{H}(x,y,s) = \int_{-\infty}^{+\infty}\overline{\overline{G}}(\beta,x,\chi)\cdot\overline{\overline{F}}(\beta,s)e^{-i\beta y}d\beta = \int_{-\infty}^{+\infty}\overline{F}(\eta,s)\cdot\overline{G}(y-\eta,x,\chi)d\eta \tag{3-29}$$

and with proper substitution, we obtain appropriate equations for the finite source and Gaussian source.

Finite Patch Source

From Equations 3-24a, 3-26, and 3-29, we obtain

$$\overline{H} = \frac{A^{o}\theta(s)}{2p\sqrt{\pi}} \int_{-\infty}^{+\infty} \exp\left[\frac{-\left(y-\eta-g\right)^{2}}{4p^{2}}\right] \left[U\left(\eta-y_{1}+\frac{d}{2}\right) - U\left(\eta-y_{1}-\frac{d}{2}\right)\right] d\eta \ . \tag{3-30}$$

Putting

$$\Gamma = \frac{y-\eta-g}{2p} \tag{3-31}$$

Equation 3-30 becomes

$$\overline{H} = A^{o}\theta(s)\frac{1}{\sqrt{\pi}} \int_{-\infty}^{+\infty} e^{-\Gamma^{2}} \left[U\left(y-y_{1}+\frac{d}{2}-g-2p\Gamma\right) - U\left(y-y_{1}-\frac{d}{2}-g-2p\Gamma\right)\right] d\Gamma \ . \tag{3-32}$$

Hence,

$$\overline{H} = A^{o}\theta(s)\, E_{f}\left[\frac{d}{2} \pm \left(y-y_{1}-g\right), p\right] \tag{3-33}$$

where

$$E_{f}\left[\frac{d}{2} + \left(y-y_{1}-g\right), p\right] = \frac{1}{2}\left[\mathrm{erf}\left(\frac{\frac{d}{2}+y-y_{1}-g}{2p}\right) + \mathrm{erf}\left(\frac{\frac{d}{2}-y+y_{1}+g}{2p}\right)\right] \tag{3-34}$$

where "erf" represents the error function.

Multiple Patch Source

Note that when an array of plane sources is encountered at $x = 0$ (see Figure 2-1b), radionuclides released from one source will influence the concentration from the remaining ones. In this case, E_{Ω} may be written as:

$$E_{\Omega} = \sum_{k=1}^{n} E_{f}\left[\frac{d}{2} + \left(y-y_{k}-g\right), p\right] \tag{3-35}$$

where n is the number of finite sources. The concentration in this case is said to be obtained after superimposing the solution of all such sources assumed to have the same width and initial concentration.

Gaussian Source

From Equations 3-25 and 3-26, we obtain

$$\overline{H} = A^0\theta(s)\frac{1}{2p\sqrt{\pi}}\int_{-\infty}^{+\infty}\exp\left[\frac{-\left(y-\eta-g\right)^2}{4p^2}\right]\exp\left[\frac{-\left(\eta-y_0\right)^2}{2\sigma_y^2}\right]d\eta \quad . \tag{3-36}$$

The above equation may also be written as

$$\overline{H} = A^0\theta(s)\frac{1}{2p\sqrt{\pi}}\int_{-\infty}^{+\infty}\exp\left[-\left(a_1\eta^2+2a_2\eta+a_3\right)\right]d\eta \tag{3-37}$$

where

$$a_1 = \frac{\sigma_y^2 + 2p^2}{4p^2\sigma_y^2} \tag{3-38a}$$

$$a_2 = -\frac{\left(y-g\right)\sigma_y^2 + 2y_0p^2}{4p^2\sigma_y^2} \tag{3-38b}$$

$$a_3 = \frac{\left(y-g\right)^2\sigma_y^2 + 2y_0^2p^2}{4p^2\sigma_y^2} \quad . \tag{3-38c}$$

Note that parameters g and p in Equations 3-36 and 3-38 are given by Equations 3-27a and 3-27b, respectively. Recognizing the following integral (see Abramowitz and Stegun, 1972)

$$\int_0^{\infty}\exp\left[-\left(at^2+2bt+c\right)\right]dt = \frac{1}{2}\sqrt{\frac{\pi}{a}}\exp\left[\frac{b^2-ac}{a}\right]\operatorname{erfc}\left(\frac{b}{\sqrt{a}}\right) \tag{3-39}$$

Equation 3-37 becomes

$$\overline{H} = A^{o}\theta(s)E_{g}\left[g,\left(y-y_{o}\right),\sigma_{y},p\right] \tag{3-40}$$

where, after substitution,

$$E_{g} = \frac{\sigma_{y}}{\sqrt{\sigma_{y}^{2}+2p^{2}}}\exp\left[-\frac{\left(y-y_{o}-g\right)^{2}}{2\left(\sigma_{y}^{2}+2p^{2}\right)}\right] \quad . \tag{3-41}$$

With the above results, the inverse Fourier transform of Equation 3-21 may now be written as

$$\overline{A}(x,y,s) = A^{o}\int_{0}^{\infty}\psi(x,\sigma)E_{\Omega}\,\theta(s)e^{r_{a}X}d\sigma \tag{3-42}$$

where subscript Ω set to f would refer to the finite or multiple patch source boundary condition, and when set to g to the Gaussian source. Substitution from Equations 3-9c and 3-22c into the above equation and using the Laplace inversion formulae (Appendix A), the final solution of the concentration in the fracture may be written as

$$A(x,y,t) = A^{o}e^{-\lambda t}\int_{0}^{\infty}\psi(x,\sigma)E_{\Omega}\,\mathrm{erfc}\left[\frac{c_{f}X}{2(t-R\chi)^{1/2}}\right]U(t-R\chi)d\sigma \quad . \tag{3-43}$$

Substitution of Equation 3-42 in Equation 3-4 gives

$$\overline{B}(x,y,z,s) = A^{o}\int_{0}^{\infty}\psi(x,\sigma)E_{\Omega}\theta(s)\exp\left[r_{b}(z-b)+r_{a}X\right]d\sigma \tag{3-44}$$

and the final solution of the concentration in the rock matrix may be written as

$$B(x,y,z,t) = A^{o}e^{-\lambda t}\int_{0}^{\infty}\psi(x,\sigma)E_{\Omega}\,\mathrm{erfc}\left[\frac{c_{f}X+c_{r}(z-b)}{2(t-R\chi)^{1/2}}\right]U(t-R\chi)d\sigma \quad . \tag{3-45}$$

Note that c_r, c_f, $\psi(x,\sigma)$, and χ in Equations 3-43 and 3-45 are given by Equations 3-5b, 3-8, 3-22a, and 3-22d, respectively.

After setting appropriate finite integration limits (see Appendix B), the integration of Equations 3-43 and 3-45 is then performed using a Gauss-Legendre quadrature scheme.

3.2 NO LONGITUDINAL DISPERSION (Case where v = 0)

When the direction of the flow is normal to the source (i.e., v = 0) and the longitudinal dispersion effects are neglected, Equation 3-11 becomes

$$u \frac{d\bar{\bar{A}}}{dx} + \left[D_{yy}\beta^2 + R(s+\lambda) + c_f(s+\lambda)^{1/2} \right] \bar{\bar{A}} = 0 \quad . \tag{3-46}$$

The solution of the above equation subject to its initial and boundary conditions given by Equations 2-14 and 2-16 or 2-17 may be written as

$$\bar{\bar{A}}(x,\beta,s) = \bar{\bar{F}}(\beta,s) e^{a_n \chi'} \tag{3-47}$$

where

$$a_n = - D_{yy}\beta^2 - R(s+\lambda) - c_f(s+\lambda)^{1/2} \tag{3-48a}$$

and

$$\chi' = \frac{x}{u} \tag{3-48b}$$

The Fourier transforms corresponding to either type of boundary conditions are obtained from Equations 3-14 to 3-21. Hence, Equation 3-21 becomes

$$\bar{\bar{A}}(x,\beta,s) = \bar{\bar{F}}(\beta,s)\, \bar{\bar{G}}(\beta,x) e^{r_a \chi'} \tag{3-49}$$

where $\bar{\bar{F}}(\beta,s)$ is given either by Equation 3-15a or 3-19 and $\bar{\bar{G}}(\beta,x)$ is given by Equation 3-22 with χ' substituting for χ. Note that Equation 3-49 is equivalent to Equation 3-21 after setting

$$\int_0^\infty \psi(x,\sigma) d\sigma = 1 \quad . \tag{3-50}$$

The inverse Fourier transforms of $\bar{\bar{A}}(x,\beta,s)$ may be obtained in the same fashion as outlined by Equations 3-24 through 3-42. Subsequently, the inverse Laplace transforms of the resulting equations yielding the solution in the fracture and the rock matrix are given by

$$A(x,y,t) = A^{o}E_{\Omega}e^{-\lambda t}\,\mathrm{erfc}\left[\frac{c_f X'}{2(t-RX')^{1/2}}\right]U(t-RX') \tag{3-51}$$

and

$$B(x,y,z,t) = A^{o}E_{\Omega}e^{-\lambda t}\,\mathrm{erfc}\left[\frac{c_f X' + c_r(z-b)}{2(t-RX')^{1/2}}\right]U(t-RX') \tag{3-52}$$

respectively. Note that p and g in E_f (Equation 3-34) or E_g (Equation 3-41) should be replaced by $(D_{yy}X')^{1/2}$ and zero; c_r and c_f are given by Equations 3-5b and 3-8, respectively.

3.3 MASS FLUX

The mass flux at any point in the fracture may be written as

$$F(t) = \left[F_x^2 + F_y^2\right]^{1/2} \tag{3-53}$$

where F_x and F_y refer to the mass fluxes in the x and y directions, respectively, given by

$$F_x = uA - D_{xx}\frac{\partial A}{\partial x} - D_{xy}\frac{\partial A}{\partial y} \tag{3-54a}$$

$$F_y = vA - D_{yx}\frac{\partial A}{\partial x} - D_{yy}\frac{\partial A}{\partial y} \tag{3-54b}$$

The evaluation of F_x and F_y is carried out after using the inverse Fourier transform of A (that is, in the Laplace domain) to estimate the spatial derivatives for the two types of source geometry considered here (i.e., finite line source and Gaussian distributed source, respectively).

Referring to Equation 3-42 the derivatives of $\bar{A}$ (x,y,s) with respect to x and y may be obtained after applying Leibniz's differentiation rule. Using the notation $E_\Omega^x = \partial E_\Omega/\partial x$, $E_\Omega^y = \partial E_\Omega/\partial y$,

$$\frac{\partial \bar{A}}{\partial x} = A^o \int_0^\infty \theta(s) \left\{ \left[\psi'(x,\sigma)E_\Omega + \psi(x,\sigma)E_\Omega^x \right] e^{r_a X} + \psi(x,\sigma)E_\Omega \frac{\partial}{\partial x}\left(e^{r_a X}\right) \right\} d\sigma \tag{3-55}$$

$$\frac{\partial \bar{A}}{\partial y} = A^o \int_0^\infty \psi(x,\sigma)E_\Omega^y \, \theta(s) \, e^{r_a X} d\sigma \ . \tag{3-56}$$

Using Equation 3-22a, we have

$$\psi'(x,\sigma) = \psi(x,\sigma)\, 2\alpha_1(\sigma - \alpha_1 x) \tag{3-57a}$$

with

$$\alpha_1 = \frac{u}{4D_{xx}\sigma} \ . \tag{3-57b}$$

Using Equations 3-22c and 3-22d, we have

$$\frac{\partial}{\partial x}\left(e^{r_a X}\right) = -\bar{\beta}\left[R(s+\lambda) + c_f(s+\lambda)^{1/2}\right] e^{r_a X} \tag{3-58}$$

with

$$\bar{\beta} = \frac{x}{2D_{xx}\sigma^2} \tag{3-59a}$$

and in the absence of longitudinal dispersion

$$\bar{\beta} = \frac{1}{u} \ . \tag{3-59b}$$

With the error function defined either as

$$\mathrm{erf}(\alpha) = \frac{2}{\sqrt{\pi}} \int_0^{\alpha(x)} e^{-\tau^2} d\tau \tag{3-60a}$$

or the integrand expanded in a power series convergent everywhere and integrated term by term to yield

$$\mathrm{erf}(a) = \frac{2}{\sqrt{\pi}}\left[a - \frac{a^3}{3} + \frac{a^5}{5.2!} - \frac{a^7}{7.3!} + \ldots\right] \tag{3-60b}$$

its derivative with respect to the variable x may be then obtained after making use of Leibnitz's differentiation rule. This is written as

$$\frac{\partial}{\partial x}(\mathrm{erf}(a)) = \frac{2}{\sqrt{\pi}}\exp(-a^2)\frac{\partial a}{\partial x} \quad . \tag{3-61}$$

Hence, for the two types of geometry of the source considered here, E_Ω^x and E_Ω^y will be handled as follows:

Finite Patch Source

Applying the above equation to Equation 3-34, we obtain

$$E_f^x = \frac{1}{2px\sqrt{\pi}}\left[\exp\left(-\left[\frac{\frac{d}{2}+y-y_1-g}{2p}\right]^2\right)\left(-\frac{d}{2}-y+y_1-\left(v-u\frac{D_{yx}}{D_{xx}}\right)x\right)\right]$$

$$+\exp\left(-\left[\frac{\frac{d}{2}-y+y_1+g}{2p}\right]^2\right)\left(-\frac{d}{2}+y-y_1+\left(v-u\frac{D_{yx}}{D_{xx}}\right)x\right)\Bigg] \tag{3-62}$$

$$E_f^y = \frac{1}{2p\sqrt{\pi}}\left[\exp\left(-\left[\frac{\frac{d}{2}+y-y_1-g}{2p}\right]^2\right)-\exp\left(-\left[\frac{\frac{d}{2}-y+y_1+g}{2p}\right]^2\right)\right] \quad . \tag{3-63}$$

Gaussian Source

Using Equation 3-41, we obtain

$$E_g^x = E_g\left[\frac{2}{x\left(\sigma_y^2+2p^2\right)}\right]\left\{(y-y_o-g)\left(g-\left(\frac{D_{yx}}{D_{xx}}\right)\frac{x}{2}\right)-p^2\left[1-\frac{(y-y_o-g)^2}{\left(\sigma_y^2+2p^2\right)}\right]\right\} \tag{3-64}$$

$$E_g^y = E_g \left[- \frac{(y - y_o - g)}{\left(\sigma_y^2 + 2p^2\right)} \right] . \tag{3-65}$$

Equation 3-55 may now be written as

$$\frac{\partial \overline{A}}{\partial x} = A^o \int_0^\infty \psi(x,\sigma) \left[\left[\frac{2a_1(\sigma - a_1 x)}{s+\lambda} - \overline{\beta}\left(R + \frac{c_f}{(s+\lambda)^{1/2}}\right) \right] E_\Omega + \frac{E_\Omega^x}{s+\lambda} \right] e^{r_a X} d\sigma . \tag{3-66}$$

Definitions are given now,

$$_xF_1 = u\,E_\Omega - D_{xx}\left[2a_1(\sigma - a_1 x)E_\Omega + E_\Omega^x\right] - D_{xy}\,E_\Omega^y \tag{3-67a}$$

$$_iF_2 = \frac{\overline{\beta}\,c_f D_{ix}}{\sqrt{\pi}}\,E_\Omega \quad , \quad (i = x,y) \tag{3-67b}$$

$$_yF_1 = v\,E_\Omega - D_{yx}\left[2a_1(\sigma - a_1 x)E_\Omega + E_\Omega^x\right] - D_{yy}\,E_\Omega^y \tag{3-67c}$$

$$F_1^* = u\,E_\Omega \tag{3-67d}$$

$$\bar{\varepsilon} = \frac{c_f X}{2} \tag{3-67e}$$

$$\bar{\bar{\varepsilon}} = \frac{c_f X'}{2} = \frac{c_f x}{2u} . \tag{3-67f}$$

Substitution of Equation 3-43 and the inverse Laplace transform of Equations 3-56 and3-66 into Equations 3-54a and 3-54b gives

$$F_i = A^o e^{-\lambda t} \int_0^\infty \psi(x,\sigma) \left[{}_iF_1 \operatorname{erfc}\left(\frac{\bar{\varepsilon}}{(t - R_X)^{1/2}} \right) \right.$$

$$\left. + {}_iF_2 \left[\frac{R_X}{2(t - R_X)^{3/2}} + \frac{1}{(t - R_X)^{1/2}} \right] \exp\left[\frac{-\bar{\varepsilon}^2}{(t - R_X)} \right] \right] U(t - R_X)\,d\sigma \ , \ (i = x,y) \tag{3-68}$$

Note that when the streamlines are normal to the source (i.e., $v = 0$) and with $D_{xx} = D_{xy} = 0$, and in view of Equation 3-50, Equation 3-68 becomes

$$F_x = A^o e^{-\lambda t} F_1^* \operatorname{erfc}\left[\frac{\bar{\bar{\varepsilon}}}{(t - R_X')^{1/2}}\right] U(t - R_X') \tag{3-69a}$$

$$F_y = -A^o e^{-\lambda t} D_{yy} E_\Omega^y \operatorname{erfc}\left[\frac{\bar{\bar{\varepsilon}}}{(t - R_X')^{1/2}}\right] U(t - R_X') \tag{3-69b}$$

3.4 CUMULATIVE MASS FLUX

The cumulative mass flux is given by

$$M(t) = \int_0^t F(\tau) d\tau \tag{3-70a}$$

where the integrand given by Equation 3-53 may be written as

$$F(\tau) = F_x(\tau)\left[1 + \left(\frac{F_y(\tau)}{F_x(\tau)}\right)^2\right]^{1/2} \tag{3-70b}$$

Because of the complex nature of Equation 3-70a, a closed form solution of this may be obtained only at the expense of some simplifications of the hydrodynamic dispersion phenomena inherent to the transport process. Two solutions dealing with the case of streamlines parallel to the x axis will be reported. The first will assume that the source is of uniform strength and extends to infinity (i.e., unidimensional flow, $F_y = 0$). The second will assume the type of source considered in this work where the streamlines are normal to the source (i.e., $v = 0$), which accounts for both F_x and F_y, but which ignores the longitudinal dispersion effects (i.e., $D_{xx} = D_{xy} = 0$).

3.4.1 Unidimensional Flow ($F_y = 0$)

In the case of unidimensional flow, the y-component of velocity and transverse dispersion in the fracture are both zero (i.e., $v = 0$; $D_{xy} = D_{yy} = 0$), p in Equation 3-27 becomes zero also. In such a situation, the width of the patch source is said to extend to infinity; hence, functions E_f and E_f given by Equations 3-34 and 3-62 will take the value of one and zero, respectively.

With $F_y(\tau)$ in Equation 3-70b set to zero, Equation 3-70a becomes

$$M(t) = \int_0^t \left[u\,A(\tau) - D_{xx} \frac{\partial A(\tau)}{\partial x} \right] d\tau \ . \tag{3-71}$$

In the presence of longitudinal dispersion, this integral is of the form

$$M(t) = \int_0^t \int_0^\infty g(\sigma,\tau)\, U(\tau - R\chi) d\sigma\, d\tau \tag{3-72a}$$

$$= \int_0^t \int_{f(\tau)}^\infty g(\sigma,\tau)\, d\sigma\, d\tau \tag{3-72b}$$

where

$$f(\tau) = \frac{x}{2} \left(\frac{R}{D_{xx}\tau} \right)^{1/2} \ . \tag{3-72c}$$

We may interchange the order of integration to yield

$$M(t) = \int_{f(t)}^\infty \int_{f(\sigma)}^t g(\sigma,\tau)\, d\tau\, d\sigma \tag{3-72d}$$

where

$$f(\tau) = \frac{x}{2} \left(\frac{R}{D_{xx}\tau} \right)^{1/2} , f(\sigma) = R\chi \ . \tag{3-72e}$$

In the absence of longitudinal dispersion,

$$M(t) = \int_{R\chi}^t g(\tau)\, d\tau \ . \tag{3-73}$$

Referring to Equations 3-67a, 3-67b, and 3-67d, these become

$${}_x\overline{F}_1 = u - 2D_{xx}\alpha_1(\sigma - \alpha_1 x) \tag{3-74a}$$

$${}_x\overline{F}_2 = \frac{\overline{\beta}\, c_f D_{xx}}{\sqrt{\pi}} \tag{3-74b}$$

$$F_1^* = u \tag{3-74c}$$

using the definitions

$$I_1 = \int_{R_X}^{t} e^{-\lambda\tau} \operatorname{erfc}\left[\frac{\bar{\varepsilon}}{\sqrt{\tau - R_X}}\right] d\tau \tag{3-75a}$$

$$I_2 = \int_{R_X}^{t} e^{-\lambda\tau - \frac{\bar{\varepsilon}^2}{\tau - R_X}} \left[\frac{R_X}{2\sqrt{(\tau - R_X)^3}} + \frac{1}{\sqrt{\tau - R_X}}\right] d\tau \tag{3-75b}$$

where $\bar{\varepsilon}$ is given by Equation 3-67e, we may then express the cumulative mass flux as

$$M(t) = A^o \int_{f(t)}^{\infty} \psi(x,\sigma)[{}_x\bar{F}_1 \cdot I_1 + {}_x\bar{F}_2 \cdot I_2] d\sigma \tag{3-76}$$

in the presence of longitudinal dispersion, and as

$$M(t) = A^o (F_1^* \cdot I_1) \tag{3-77}$$

when $D_x = 0$. Integrating Equation 3-75a by parts gives

$$I_1 = -\frac{e^{-\lambda t}}{\lambda} \operatorname{erfc}\left[\frac{\bar{\varepsilon}}{\sqrt{t - R_X}}\right] + \frac{\bar{\varepsilon}\, e^{-\lambda R_X}}{\lambda\sqrt{\pi}} \int_0^{t-R_X} \frac{1}{\sqrt{\tau^3}} \exp\left[-\lambda\tau - \frac{\bar{\varepsilon}^2}{\tau}\right] d\tau \,. \tag{3-78}$$

We further define

$$K_0(a) = -\frac{e^{-\lambda t}}{\lambda} \operatorname{erfc}\left[\frac{a}{\sqrt{t - R_X}}\right] \tag{3-79a}$$

$$K_1(a) = \int_0^{t-R_X} \frac{1}{\sqrt{\tau}} \exp\left[-\lambda\tau - \frac{a^2}{\tau}\right] d\tau \tag{3-79b}$$

$$K_2(a) = \int_0^{t-R_X} \frac{1}{\sqrt{\tau^3}} \exp\left[-\lambda\tau - \frac{a^2}{\tau}\right] d\tau \tag{3-79c}$$

Recognizing the following integral (Abramowitz and Stegun, 1972, p. 304)

$$\int e^{-p^2\gamma^2 - q^2/\gamma^2} d\gamma = \frac{\sqrt{\pi}}{4p}\left[e^{2pq} \operatorname{erf}\left(p\gamma + \frac{q}{\gamma}\right) + e^{-2pq} \operatorname{erf}\left(p\gamma - \frac{q}{\gamma}\right)\right] \tag{3-80}$$

we may evaluate K_1 and K_2 after substituting $\gamma = \sqrt{\tau}$ (for K_1) and $\gamma = 1/\sqrt{\tau}$ (for K_2). This yields

$$K_1(a) = -\frac{1}{2}\ \frac{\pi}{\lambda}\left\{e^{2a\sqrt{\lambda}}\operatorname{erfc}\left(\frac{a}{\sqrt{t-R_X}} + \sqrt{\lambda(t-R_X)}\right) - e^{-2a\sqrt{\lambda}}\operatorname{erfc}\left(\frac{a}{\sqrt{t-R_X}} - \sqrt{\lambda(t-R_X)}\right)\right\} \tag{3-81}$$

$$K_2(a) = \frac{\sqrt{\pi}}{2a}\left\{e^{2a\sqrt{\lambda}}\operatorname{erfc}\left(\frac{a}{\sqrt{t-R_X}} + \sqrt{\lambda(t-R_X)}\right) + e^{-2a\sqrt{\lambda}}\operatorname{erfc}\left(\frac{a}{\sqrt{t-R_X}} - \sqrt{\lambda(t-R_X)}\right)\right\} \tag{3-82}$$

so that we may express I_1 and I_2 (see Equations 3-75a and 3-75b) as

$$I_1 = K_0(\bar{\varepsilon}) + \frac{\bar{\varepsilon}\, e^{-\lambda R_X}}{\lambda\sqrt{\pi}}\, K_2(\bar{\varepsilon}) \tag{3-83}$$

$$I_2 = e^{-\lambda R_X}\left[\frac{R_X}{2}\, K_2(\bar{\varepsilon}) + K_1(\bar{\varepsilon})\right] . \tag{3-84}$$

We may then express the cumulative mass flux given by Equation 3-76 as

$$M(t) = A^o \int_{f(t)}^{\infty} \psi(x,\sigma)\left\{{}_x\bar{F}_1 \cdot \left(K_0(\bar{\varepsilon}) + \frac{\bar{\varepsilon}\, e^{-\lambda R_X}}{\lambda\sqrt{\pi}}\, K_2(\bar{\varepsilon})\right) + e^{-\lambda R_X}\, {}_x\bar{F}_2 \cdot \left(\frac{R_X}{2}\, K_2(\bar{\varepsilon}) + K_1(\bar{\varepsilon})\right)\right\} d\sigma \tag{3-85}$$

in the presence of longitudinal dispersion, and as

$$M(t) = A^o F_1^* \left(K_0(\bar{\bar{\varepsilon}}) + \frac{\bar{\bar{\varepsilon}}\, e^{-\lambda R_X'}}{\lambda\sqrt{\pi}}\, K_2(\bar{\bar{\varepsilon}})\right) U(t - R_X') \tag{3-86}$$

when $D_{xx} = 0$, where $\bar{\bar{\varepsilon}}$ is given by Equation 3-67f.

Note that Equation 3-85 is equivalent to

$$M(t) = A^o \int_0^{\infty} \psi(x,\sigma)\left\{{}_x\bar{F}_1 \cdot I_1 + e^{-\lambda R_X}\, {}_x\bar{F}_2 \cdot I_2\right\} U(t - R_X) d\sigma \tag{3-87}$$

where ${}_x\bar{F}_1$, ${}_x\bar{F}_2$, K_0, K_1, and K_2 are given by Equations 3-74a, 3-74b, 3-79a, 3-81, and 3-82.

3.4.2 <u>No Longitudinal Dispersion</u> (Case where $v = 0$)

After proper substitution of Equations 3-69a and 3-69b in Equations 3-54a and 3-54b and using the following definition

$$F_3 = \left[(u\, E_\Omega)^2 + (D_{yy}\, E_\Omega^y)^2\right]^{1/2} \tag{3-88}$$

Equation 3-70a becomes

$$M(t) = \frac{F_3}{E_\Omega} \int_0^t A(x,y,\tau)\, d\tau \quad . \tag{3-89}$$

Based on the derivations presented in the previous section, it may be shown that the cumulative mass flux in this case is given by an expression identical to Equation 3-86 with F_3 substituting for F_1^* .

3.5 RESULTS AND DISCUSSIONS

The analytical solutions presented in this section of the report were verified by comparison with the available one- and two-dimensional analytical solutions. The one-dimensional solution of Ahn et al. (1985) enabled a check of the performance of the reported solutions related to the concentrations in the fracture and rock matrix, as well as the mass and cumulative mass fluxes in the fracture; the two-dimensional solution of Gureghian (1987) enabled a check of the predictive capability of the model with reference to the various boundary conditions at the source and in the absence of rock matrix diffusion.

Note that the adequacy of the transformation technique of the integral (see Appendix B) as well as the quadrature scheme (Gauss-Legendre) adopted in this work have been thoroughly examined in a previous report (see Gureghian, 1987). It might be of interest to the reader to note that in practically all the test cases reported in this investigation, 60 quadrature points proved to yield a converging quadrature.

3.5.1 Case 1: Concentration of Np-237 in a One-Dimensional Flow Domain

This test case deals with the migration of Np-237 in a one-dimensional flow domain, where the concentration at the source is subjected to a step release mode. The influence of the retardation factor of the rock matrix on the concentration in the fracture and rock matrix was investigated. To this effect the flow field was assumed unidimensional (i.e., $v = 0$, $D_{yy} = 0$), and the concentration at the source was simulated by means of a plane source of infinite width. The input data pertaining to this test case are presented in Table 3-1. Results reported for Cases 1A and 1B are obtained through the general solution and the nondispersive form, respectively.

Case 1A - Influence of Retardation Factor in the Rock Matrix

Figures 3-1a and 3-1b show the relative concentrations of Np-237 in the fracture and rock matrix (i.e., at a distance of 100 m downstream from the source) corresponding to three values of rock matrix retardation factor ($R' = 1, 10^2$, and 10^4). Results reported in Tables 3-2a through 3-2c and 3-2d) are in excellent agreement with those reported by Ahn et al. (1985). The influence of the retardation factor of the rock matrix on the movement of the solute front in both fracture and rock is quite noticeable. In both cases increasing values of R′ seem to retard the movement of the solute front in both media. The explanation for these results is that the retardation factor of the rock matrix is reducing the magnitude of the apparent diffusion coefficient; the key parameter gearing the migration process of Np-237 in this medium exerts in turn a marked influence on the mass transfer process between the rock matrix and the fracture respectively (see Equation 2-10). For example, a large value of the retardation factor in the rock will increase the magnitude of the diffusive flux which may be interpreted as a sink in the equation governing solute transport in the fracture and, conversely, as a source. Referring to Figure 3-1a it may be observed that the concentration at a given point (say 100 m) decreases with increasing values of R′. To gain further insight into the diffusion processes in the rock matrix and the importance of the retardation phenomenon the reader is referred to the work of Neretnieks (1980).

Table 3-1. Input Parameters for Case 1

Species	Np-237
Initial Concentration A°	
(arbitrary units of activity/L^3)	1
Type of Release Mode	Step
Boundary Condition	Infinite Plane Source
x	100.0 m
y	0.0 m
d	∞
u	10.0 m/yr
v	0.0 m/yr
D_{xx}	Case 1A: 1.0 m^2/yr
	Case 1B: 0.0 m^2/yr
D_{yy}	0.0 m^2/yr
D_{yx}	0.0 m^2/yr
D_p	0.01 m^2/yr
$T_{1/2}$	2.14 x 10^6 yr
b	0.005 m
ϕ	10^{-2}
R	1
R′	1, 10^2, 10^4

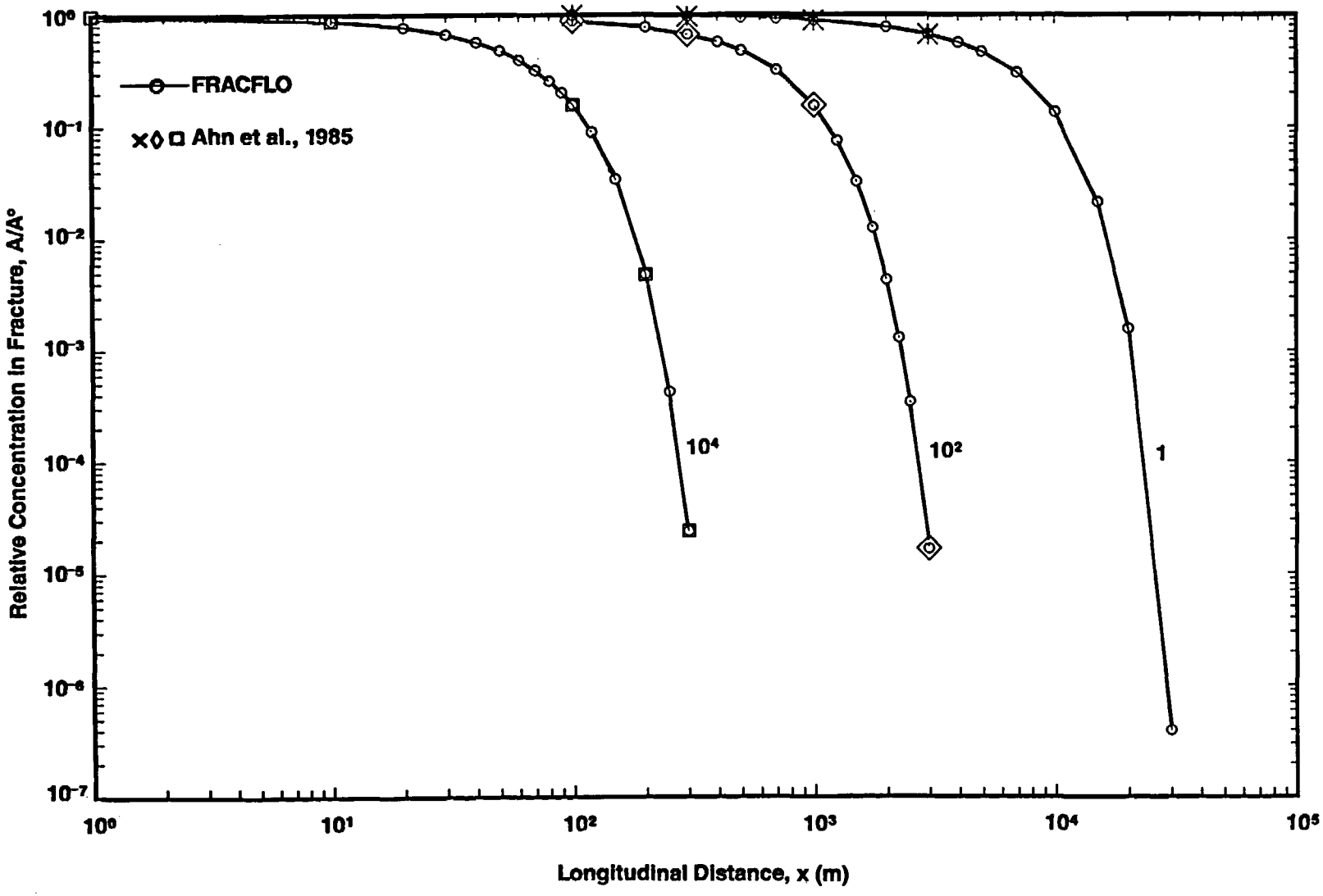

Figure 3-1a. Relative Concentrations of Np-237 in the Fracture Versus Longitudinal Distance x at y = 0 m and t = 10^4 yr for Different Rock Matrix Retardation Factors (R′ = 1, 10^2, 10^4) (Case 1A: Step Release Mode)

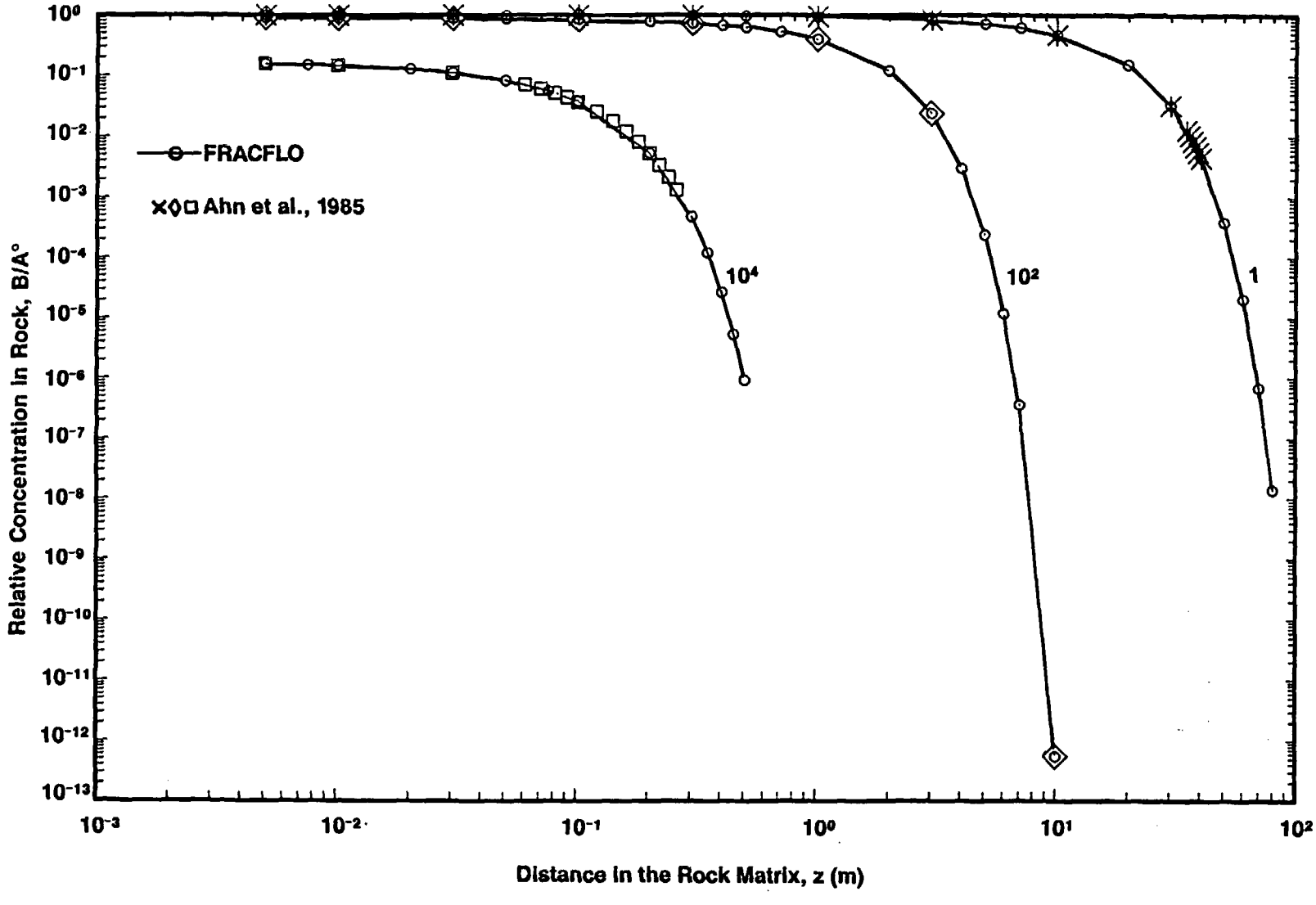

Figure 3-1b. Relative Concentrations of Np-237 in the Rock Matrix Versus Distance in the Rock Matrix z at x = 100 m, y = 0 m, and t = 10^4 yr for Different Rock Matrix Retardation Factors (R′ = 1, 10^2, 10^4) (Case 1A: Step Release Mode)

Table 3-2a. Case 1A Results: Relative Concentration, Mass Flux, and Cumulative Mass Flux in the Fracture for Np-237 With Infinite Diffusion at Time t = 10^4 yr and Rock Matrix Retardation Factor R′ = 1 (Step Release Mode)

Longitudinal Distance x (m)	Concentration A/A^o	Mass Flux F/A^o (m/yr)	Cumulative Mass Flux M/A^o (m)
1.000E+01	9.956E-01	9.957E+00	9.961E+04
1.000E+02	9.855E-01	9.855E+00	9.751E+04
1.200E+02	9.833E-01	9.833E+00	9.705E+04
1.500E+02	9.799E-01	9.799E+00	9.636E+04
2.000E+02	9.743E-01	9.743E+00	9.522E+04
2.500E+02	9.686E-01	9.686E+00	9.409E+04
3.000E+02	9.630E-01	9.630E+00	9.297E+04
4.000E+02	9.517E-01	9.517E+00	9.076E+04
5.000E+02	9.404E-01	9.404E+00	8.859E+04
7.000E+02	9.179E-01	9.179E+00	8.437E+04
1.000E+03	8.841E-01	8.841E+00	7.834E+04
1.250E+03	8.560E-01	8.560E+00	7.357E+04
1.500E+03	8.281E-01	8.281E+00	6.903E+04
1.750E+03	8.002E-01	8.002E+00	6.471E+04
2.000E+03	7.726E-01	7.726E+00	6.060E+04
2.250E+03	7.452E-01	7.452E+00	5.670E+04
2.500E+03	7.180E-01	7.180E+00	5.301E+04
3.000E+03	6.645E-01	6.645E+00	4.619E+04
4.000E+03	5.619E-01	5.619E+00	3.465E+04
5.000E+03	4.667E-01	4.667E+00	2.556E+04
7.000E+03	3.037E-01	3.037E+00	1.318E+04
1.000E+04	1.356E-01	1.356E+00	4.202E+03
1.500E+04	2.133E-02	2.133E-01	3.894E+02
2.000E+04	1.561E-03	1.561E-02	1.745E+01
3.000E+04	3.959E-07	3.960E-06	1.827E-03

Table 3-2b. Case 1A Results: Relative Concentration, Mass Flux, and Cumulative Mass Flux in the Fracture for Np-237 With Infinite Diffusion at Time t = 10^4 yr and Rock Matrix Retardation Factor R′ = 100 (Step Release Mode)

Longitudinal Distance x (m)	Concentration A/A^o	Mass Flux F/A^o (m/yr)	Cumulative Mass Flux M/A^o (m)
1.000E+01	9.855E-01	9.858E+00	9.782E+04
1.000E+02	8.848E-01	8.847E+00	7.915E+04
1.200E+02	8.624E-01	8.625E+00	7.545E+04
1.500E+02	8.292E-01	8.293E+00	7.017E+04
2.000E+02	7.746E-01	7.747E+00	6.202E+04
2.500E+02	7.210E-01	7.211E+00	5.465E+04
3.000E+02	6.688E-01	6.689E+00	4.801E+04
4.000E+02	5.690E-01	5.691E+00	3.671E+04
5.000E+02	4.769E-01	4.770E+00	2.771E+04
7.000E+02	3.195E-01	3.196E+00	1.516E+04
1.000E+03	1.548E-01	1.548E+00	5.517E+03
1.250E+03	7.508E-02	7.511E-01	2.142E+03
1.500E+03	3.251E-02	3.252E-01	7.531E+02
1.750E+03	1.252E-02	1.253E-01	2.385E+02
2.000E+03	4.277E-03	4.279E-02	6.781E+01
2.250E+03	1.292E-03	1.292E-02	1.724E+01
2.500E+03	3.442E-04	3.444E-03	3.905E+00
3.000E+03	1.664E-05	1.665E-04	1.402E-01

Table 3-2c. Case 1A Results: Relative Concentration, Mass Flux, and Cumulative Mass Flux in the Fracture for Np-237 With Infinite Diffusion at Time t = 10^4 yr and Rock Matrix Retardation Factor R′ = 10,000 (Step Release Mode)

Longitudinal Distance x (m)	Concentration A/A^o	Mass Flux F/A^o (m/yr)	Cumulative Mass Flux M/A^o (m)
1.000E+00	9.855E-01	9.868E+00	9.783E+04
1.000E+01	8.847E-01	8.858E+00	7.943E+04
2.000E+01	7.748E-01	7.759E+00	6.235E+04
3.000E+01	6.693E-01	6.704E+00	4.838E+04
4.000E+01	5.700E-01	5.709E+00	3.708E+04
5.000E+01	4.783E-01	4.792E+00	2.808E+04
6.000E+01	3.953E-01	3.961E+00	2.099E+04
7.000E+01	3.217E-01	3.224E+00	1.549E+04
8.000E+01	2.576E-01	2.582E+00	1.127E+04
9.000E+01	2.030E-01	2.035E+00	8.095E+03
1.000E+02	1.574E-01	1.578E+00	5.732E+03
1.200E+02	8.997E-02	9.024E-01	2.753E+03
1.500E+02	3.418E-02	3.430E-01	8.192E+02
2.000E+02	4.786E-03	4.807E-02	7.956E+01
2.500E+02	4.262E-04	4.284E-03	5.139E+00
3.000E+02	2.393E-05	2.408E-04	2.173E-01
4.000E+02	1.863E-08	1.878E-07	1.047E-04
5.000E+02	2.218E-12	2.240E-11	8.409E-09

Table 3-2d. Case 1A Results: Relative Concentration in Rock Matrix (B/A°) for Np-237 at x = 100 m (Step Release Mode)

Elevation z (m)	R′ = 1	R′ = 100	R′ = 10,000
5.000E-03	9.855E-01	8.848E-01	1.574E-01
7.500E-03	9.854E-01	8.832E-01	1.523E-01
1.000E-02	9.852E-01	8.818E-01	1.473E-01
2.000E-02	9.847E-01	8.763E-01	1.286E-01
3.000E-02	9.841E-01	8.707E-01	1.118E-01
5.000E-02	9.830E-01	8.596E-01	8.339E-02
6.000E-02	9.824E-01	8.541E-01	7.156E-02
7.000E-02	9.819E-01	8.485E-01	6.114E-02
7.500E-02	9.816E-01	8.458E-01	5.642E-02
8.000E-02	9.813E-01	8.430E-01	5.201E-02
9.000E-02	9.807E-01	8.375E-01	4.405E-02
1.000E-01	9.802E-01	8.320E-01	3.714E-02
1.200E-01	9.790E-01	8.210E-01	2.606E-02
1.400E-01	9.779E-01	8.100E-01	1.796E-02
1.600E-01	9.768E-01	7.991E-01	1.215E-02
1.800E-01	9.757E-01	7.882E-01	8.078E-03
2.000E-01	9.745E-01	7.774E-01	5.271E-03
2.200E-01	9.734E-01	7.666E-01	3.377E-03
2.400E-01	9.723E-01	7.558E-01	2.124E-03
2.600E-01	9.712E-01	7.451E-01	1.311E-03
3.000E-01	9.689E-01	7.239E-01	4.726E-04
3.500E-01	9.661E-01	6.976E-01	1.187E-04
4.000E-01	9.633E-01	6.716E-01	2.648E-05
4.500E-01	9.605E-01	6.461E-01	5.244E-06
5.000E-01	9.577E-01	6.209E-01	9.212E-07
7.000E-01	9.464E-01	5.249E-01	
1.000E+00	9.296E-01	3.966E-01	
2.000E+00	8.738E-01	1.201E-01	
3.000E+00	8.185E-01	2.373E-02	
4.000E+00	7.642E-01	2.990E-03	
5.000E+00	7.109E-01	2.369E-04	
6.000E+00	6.591E-01	1.169E-05	
7.000E+00	6.088E-01	3.568E-07	
1.000E+01	4.692E-01	5.479E-13	
2.000E+01	1.526E-01		
3.000E+01	3.256E-02		
3.500E+01	1.274E-02		
3.600E+01	1.041E-02		
3.700E+01	8.476E-03		
3.800E+01	6.867E-03		
3.900E+01	5.538E-03		
4.000E+01	4.446E-03		
5.000E+01	3.824E-04		
6.000E+01	2.051E-05		
7.000E+01	6.812E-07		
8.000E+01	1.395E-08		

Figures 3-1c and 3-1d show the relative mass flux and cumulative mass flux in the fracture as a function of distance for a leaching time of 10^4 years for the three values of the retardation factor. Results reported in Tables 3-2a through 3-2c agree very well with those reported by Ahn et al. (1985). In both cases the influence of an increasing retardation factor of the rock matrix seems to manifest itself by a decreasing mass accumulation at a given point, a consequence of the decreasing concentrations registered in such a situation.

Case 1A - Time-Dependent Concentrations, Mass Flux, and Cumulative Mass Flux

Figures 3-1e, 3-1f, and 3-1g show the breakthrough curves of Np-237 in the fracture, the temporal variations of the relative mass flux, and cumulative mass flux at an observation point located 100 m downstream from the source. These results were obtained through the solution of the general form of the transport equation. Tabulated results given in Tables 3-2e, 3-2f, and 3-2g indicate excellent agreement with those of Ahn et al. (1985).

Case 1B - Influence of Retardation in the Rock Matrix (No Longitudinal Dispersion)

Using the same set of data as for Case 1A (see Table 3-1), a similar investigation was subsequently carried out, ignoring the longitudinal dispersion effects (i.e., $D_{xx} = 0$) in order to verify this particular solution method (see Section 3.2).

Figures 3-2a, 3-2b, 3-2c, and 3-2d show the concentration in the fracture, the concentration in the rock matrix, the relative mass flux, and cumulative mass flux (at a distance 100 m downstream from the source). Tabulated results indicate excellent agreement with those of Ahn et al. (1985) (see also Tables 3-3a, 3-3b, 3-3c, and 3-3d). Note that because of the small magnitude in the value of the longitudinal dispersion considered in the former case (i.e., $D_{xx} = 1.0\ m^2/yr$), the results yielded by their respective solutions are practically undistinguishable.

Case 1B - Time-Dependent Concentrations, Mass Flux, and Cumulative Mass Flux

Figures 3-2e, 3-2f, and 3-2g show the breakthrough curves of Np-237 in the fracture, the variations of the relative mass flux, and cumulative mass flux at 100 m downstream from the source, respectively. Tabulated results given in Tables 3-3e, 3-3f, and 3-3g, indicate excellent agreement with those of Ahn et al. (1985).

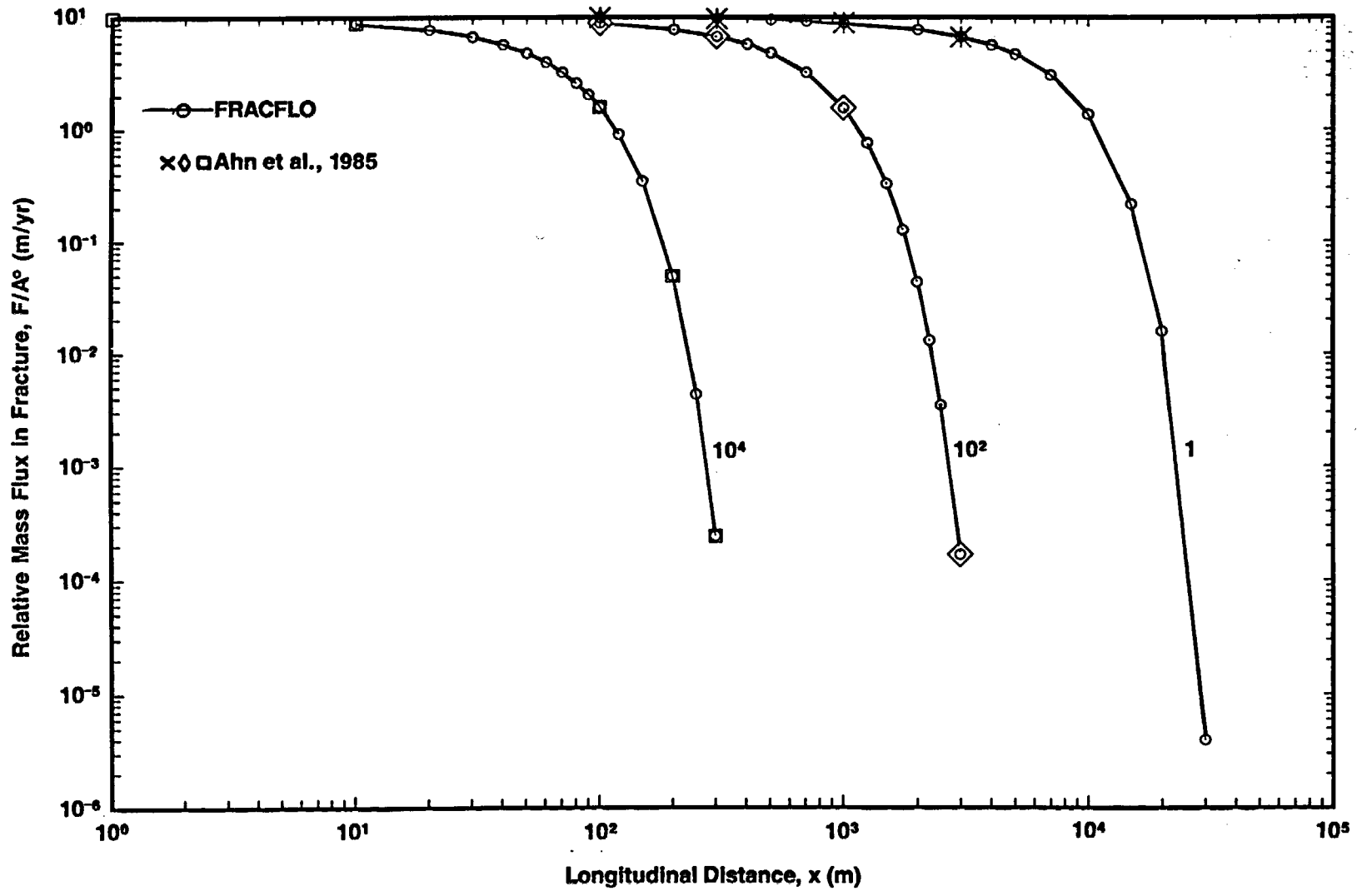

Figure 3-1c. Relative Mass Flux of Np-237 in the Fracture Versus Distance x at y = 0 m and t = 10^4 yr for Different Rock Matrix Retardation Factors (R′ = 1, 10^2, 10^4) (Case 1A: Step Release Mode)

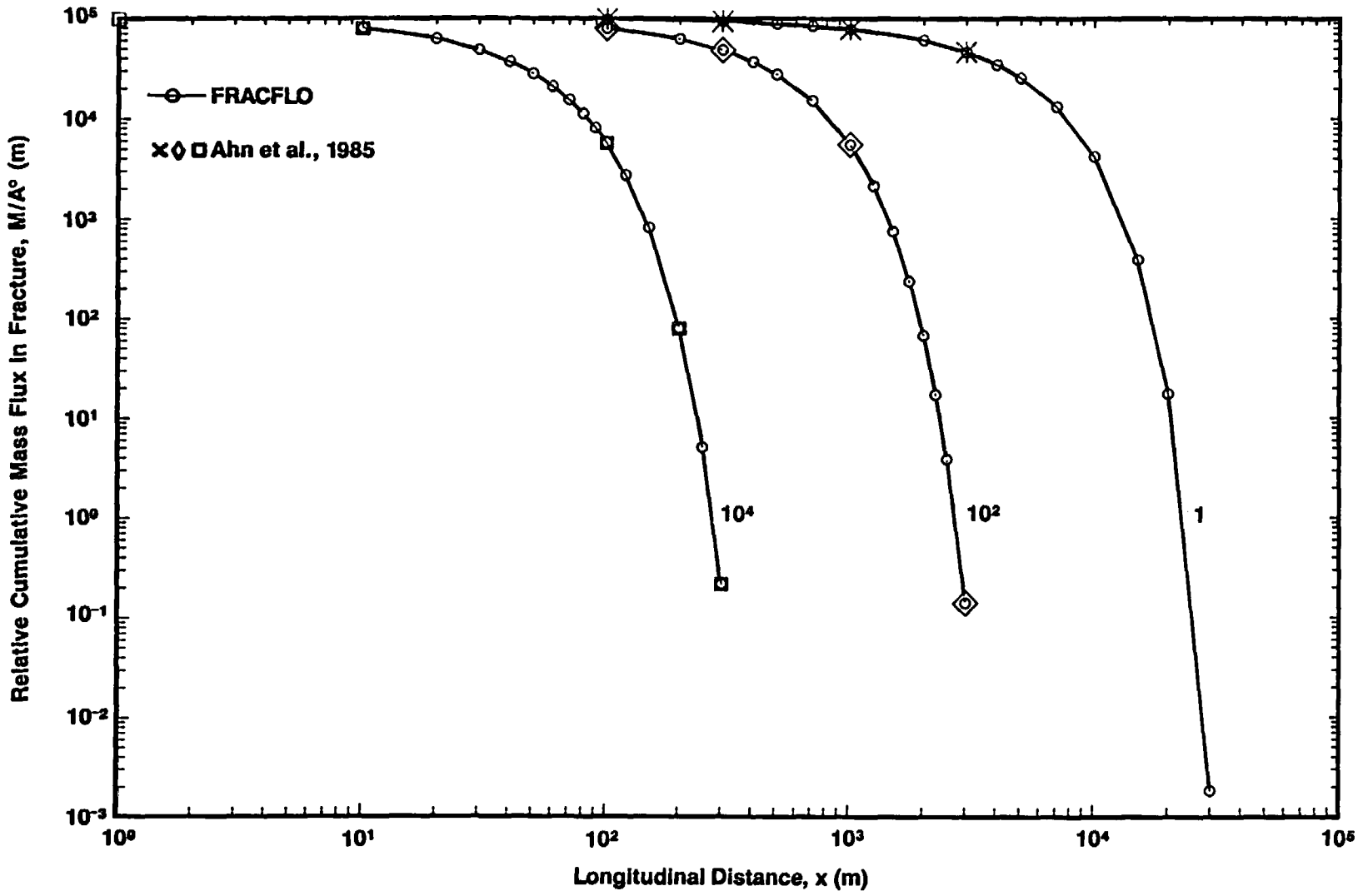

Figure 3-1d. Relative Cumulative Mass Flux of Np-237 in the Fracture Versus Longitudinal Distance x at y = 0 m and t = 10^4 yr for Different Rock Matrix Retardation Factors (R′ = 1, 10^2, 10^4) (Case 1A: Step Release Mode)

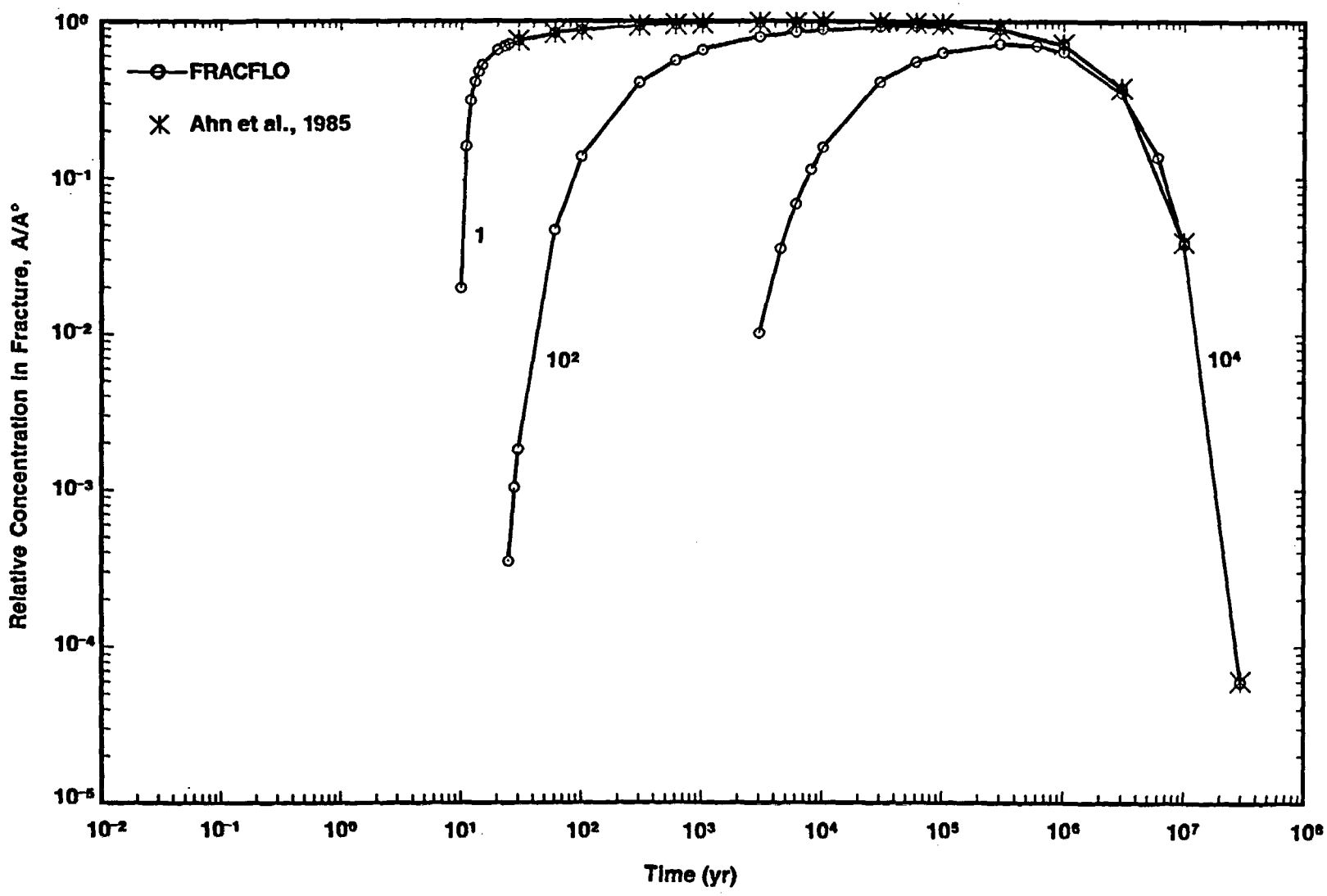

Figure 3-1e. Breakthrough Curves Showing Relative Concentrations of Np-237 in the Fracture Versus Time at x = 100 m and y = 0 m for Different Rock Matrix Retardation Factors ($R' = 1, 10^2, 10^4$) (Case 1A: Step Release Mode)

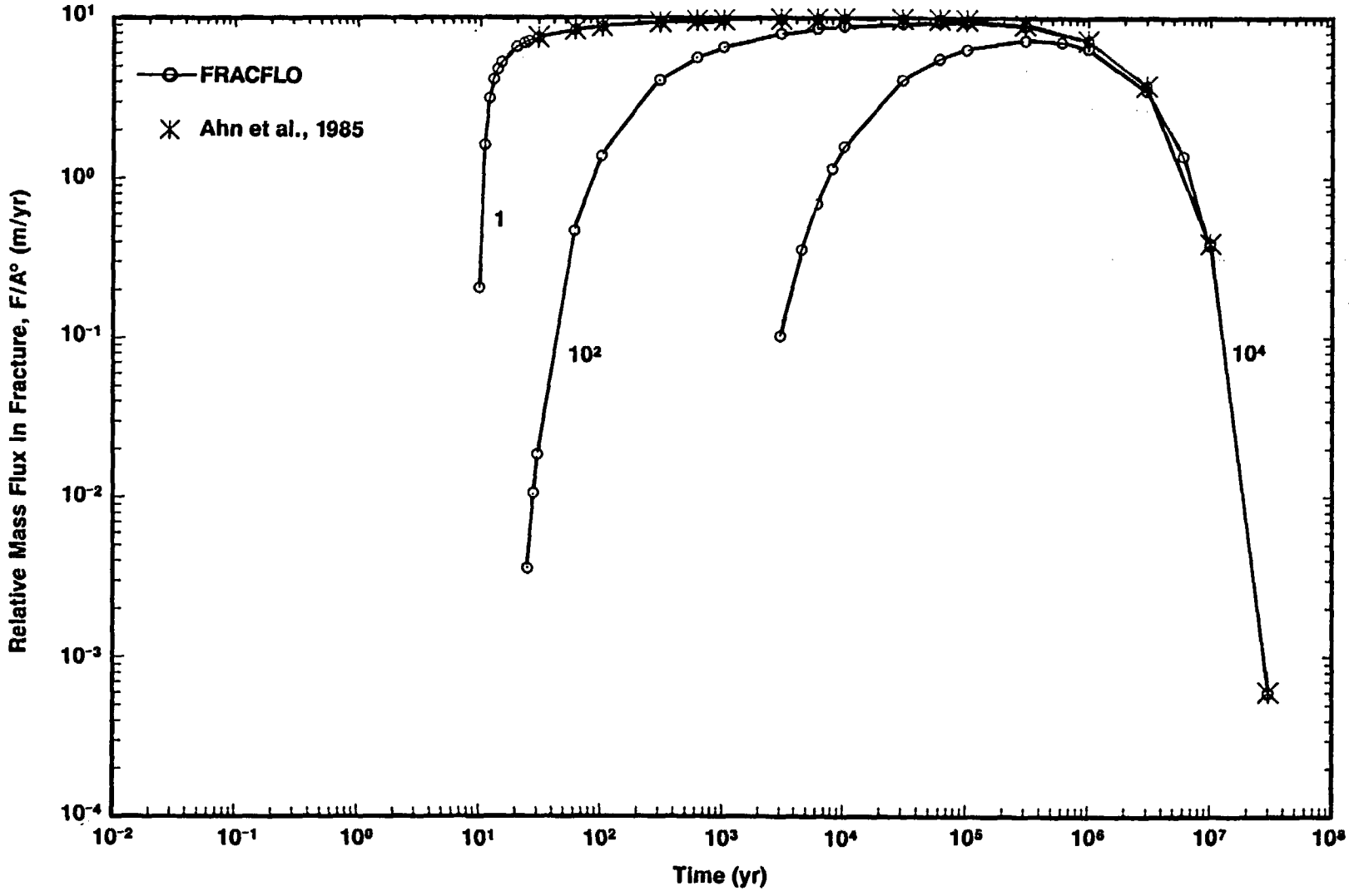

Figure 3-1f. Relative Mass Flux of Np-237 in the Fracture Versus Time at x = 100 m, and y = 0 m for Different Rock Matrix Retardation Factors (R′ = 1, 10^2, 10^4) (Case 1A: Step Release Mode)

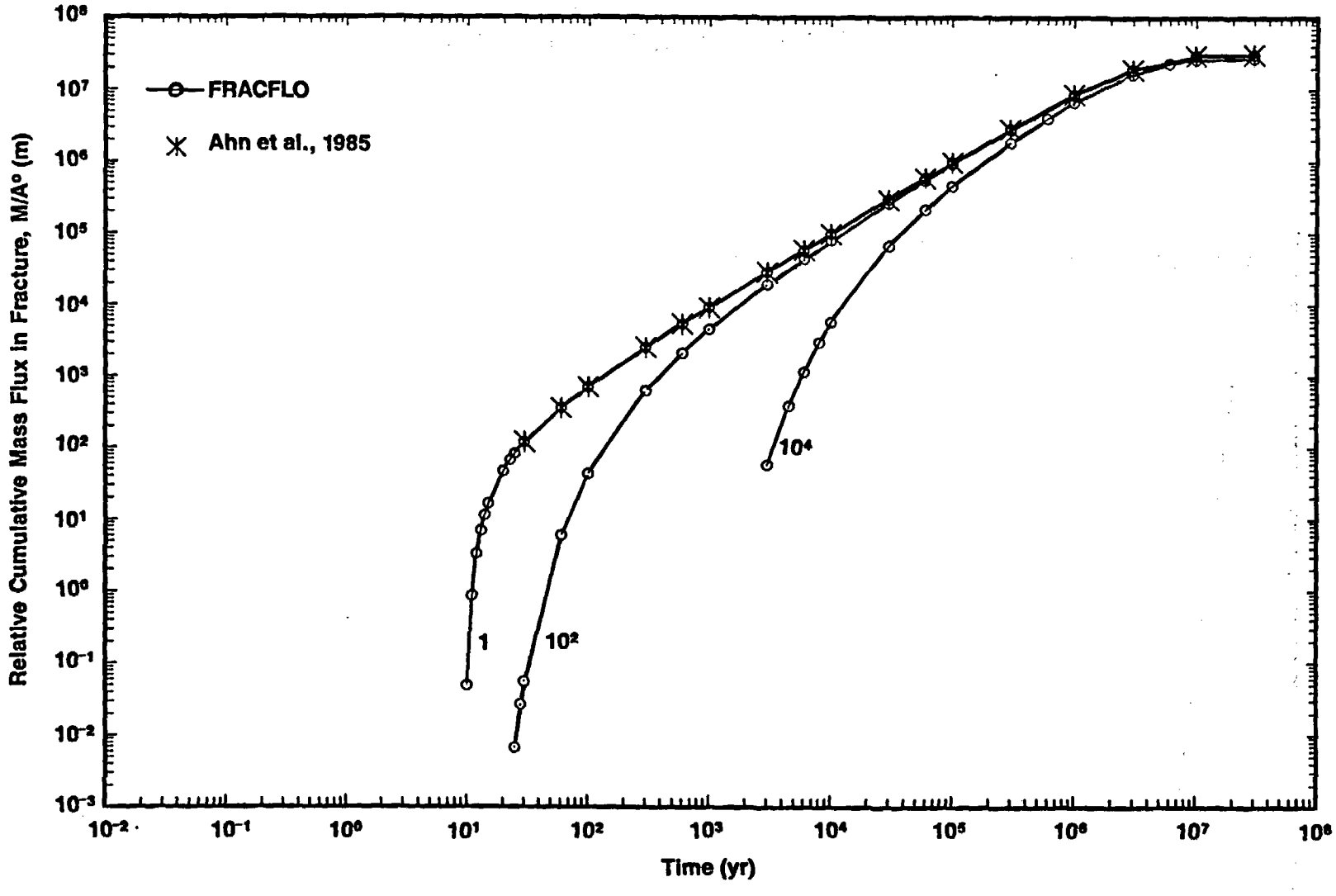

Figure 3-1g. Relative Cumulative Mass Flux of Np-237 in the Fracture Versus Time at x = 100 m and y = 0 m for Different Rock Matrix Retardation Factors (R′ = 1, 10^2, 10^4) (Case 1A: Step Release Mode)

Table 3-2e. Case 1A Results: Relative Concentration, Mass Flux, and Cumulative Mass Flux in the Fracture for Np-237 Over Time With Rock Matrix Retardation Factor R' = 1 (Step Release Mode)

Time (yr)	Concentration A/A^o	Mass Flux F/A^o (m/yr)	Cumulative Mass Flux M/A^o (m)
1.000E+01	1.981E-02	2.054E-01	4.921E-02
1.100E+01	1.587E-01	1.609E+00	8.813E-01
1.200E+01	3.120E-01	3.137E+00	3.283E+00
1.300E+01	4.109E-01	4.122E+00	6.948E+00
1.400E+01	4.774E-01	4.784E+00	1.142E+01
1.500E+01	5.257E-01	5.265E+00	1.646E+01
2.000E+01	6.543E-01	6.548E+00	4.849E+01
2.300E+01	6.946E-01	6.950E+00	6.677E+01
2.500E+01	7.148E-01	7.152E+00	8.088E+01
2.800E+01	7.387E-01	7.390E+00	1.027E+02
3.000E+01	7.517E-01	7.520E+00	1.176E+02
6.000E+01	8.414E-01	8.416E+00	3.596E+02
1.000E+02	8.815E-01	8.816E+00	7.054E+02
3.000E+02	9.337E-01	9.338E+00	2.536E+03
6.000E+02	9.534E-01	9.534E+00	5.372E+03
1.000E+03	9.638E-01	9.639E+00	9.209E+03
3.000E+03	9.784E-01	9.784E+00	2.867E+04
4.500E+03	9.817E-01	9.817E+00	4.338E+04
6.000E+03	9.835E-01	9.835E+00	5.812E+04
8.000E+03	9.848E-01	9.848E+00	7.780E+04
1.000E+04	9.855E-01	9.855E+00	9.751E+04
3.000E+04	9.839E-01	9.839E+00	2.946E+05
6.000E+04	9.762E-01	9.762E+00	5.886E+05
1.000E+05	9.647E-01	9.647E+00	9.768E+05
3.000E+05	9.055E-01	9.055E+00	2.847E+06
6.000E+05	8.222E-01	8.222E+00	5.437E+06
1.000E+06	7.225E-01	7.225E+00	8.522E+06
3.000E+06	3.782E-01	3.782E+00	1.916E+07
6.000E+06	1.431E-01	1.431E+00	2.642E+07
1.000E+07	3.919E-02	3.919E-01	2.963E+07
3.000E+07	6.024E-05	6.024E-04	3.084E+07

Table 3-2f. Case 1A Results: Relative Concentration, Mass Flux, and Cumulative Mass Flux in the Fracture for Np-237 Over Time With Rock Matrix Retardation Factor R′ = 100 (Step Release Mode)

Time (yr)	Concentration A/A^{o}	Mass Flux F/A^{o} (m/yr)	Cumulative Mass Flux M/A^{o} (m)
2.500E+01	3.501E-04	3.562E-03	6.655E-03
2.800E+01	1.042E-03	1.057E-02	2.655E-02
3.000E+01	1.824E-03	1.848E-02	5.512E-02
6.000E+01	4.649E-02	4.673E-01	6.035E+00
1.000E+02	1.370E-01	1.374E+00	4.291E+01
3.000E+02	4.066E-01	4.070E+00	6.325E+02
6.000E+02	5.604E-01	5.608E+00	2.118E+03
1.000E+03	6.529E-01	6.533E+00	4.568E+03
3.000E+03	7.952E-01	7.954E+00	1.942E+04
4.500E+03	8.316E-01	8.318E+00	3.166E+04
6.000E+03	8.53[illegible]E-01	8.535E+00	4.431E+04
8.000E+03	8.720E-01	8.722E+00	6.158E+04
1.000E+04	8.846E-01	8.847E+00	7.915E+04
3.000E+04	9.259E-01	9.259E+00	2.615E+05
6.000E+04	9.356E-01	9.356E+00	5.412E+05
1.000E+05	9.336E-01	9.336E+00	9.153E+05
3.000E+05	8.887E-01	8.887E+00	2.741E+06
6.000E+05	8.114E-01	8.114E+00	5.291E+06
1.000E+06	7.152E-01	7.152E+00	8.341E+06
3.000E+06	3.760E-01	3.760E+00	1.890E+07
6.000E+06	1.426E-01	1.426E+00	2.612E+07
1.000E+07	3.906E-02	3.906E-01	2.932E+07
3.000E+07	6.013E-05	6.013E-04	3.052E+07

Table 3-2g. Case 1A Results: Relative Concentration, Mass Flux, and Cumulative Mass Flux in the Fracture for Np-237 Over Time With Rock Matrix Retardation Factor R′ = 10,000 (Step Release Mode)

Time (yr)	Concentration A/A^{o}	Mass Flux F/A^{o} (m/yr)	Cumulative Mass Flux M/A^{o} (m)
3.000E+03	1.018E-02	1.026E-01	5.797E+01
4.500E+03	3.557E-02	3.575E-01	3.883E+02
6.000E+03	6.844E-02	6.872E-01	1.187E+03
8.000E+03	1.142E-01	1.146E+00	3.002E+03
1.000E+04	1.574E-01	1.578E+00	5.732E+03
3.000E+04	4.104E-01	4.109E+00	6.887E+04
6.000E+04	5.529E-01	5.533E+00	2.148E+05
1.000E+05	6.339E-01	6.342E+00	4.544E+05
3.000E+05	7.225E-01	7.227E+00	1.848E+06
6.000E+05	7.041E-01	7.042E+00	4.002E+06
1.000E+06	6.420E-01	6.421E+00	6.899E+06
3.000E+06	3.538E-01	3.538E+00	1.644E+07
6.000E+06	1.366E-01	1.368E+00	2.330E+07
1.000E+07	3.780E-02	3.781E-01	2.638E+07
3.000E+07	5.901E-05	5.901E-04	2.755E+07

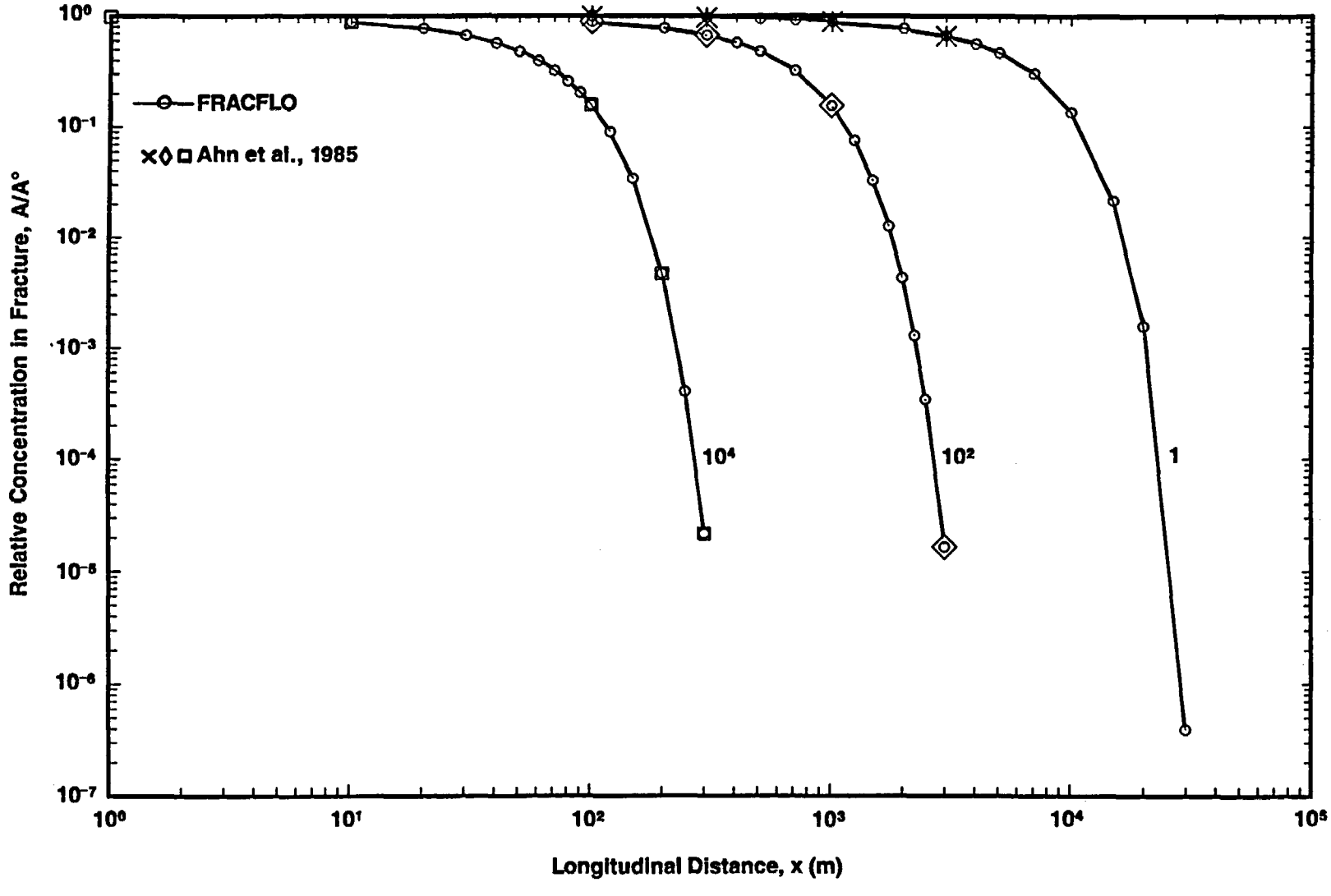

Figure 3-2a. Relative Concentrations of Np-237 in the Fracture Versus Longitudinal Distance x at y = 0 m, t = 10^4 yr, and D_{xx} = 0 for Different Rock Matrix Retardation Factors (R′ = 1, 10^2, 10^4) (Case 1B: Step Release Mode)

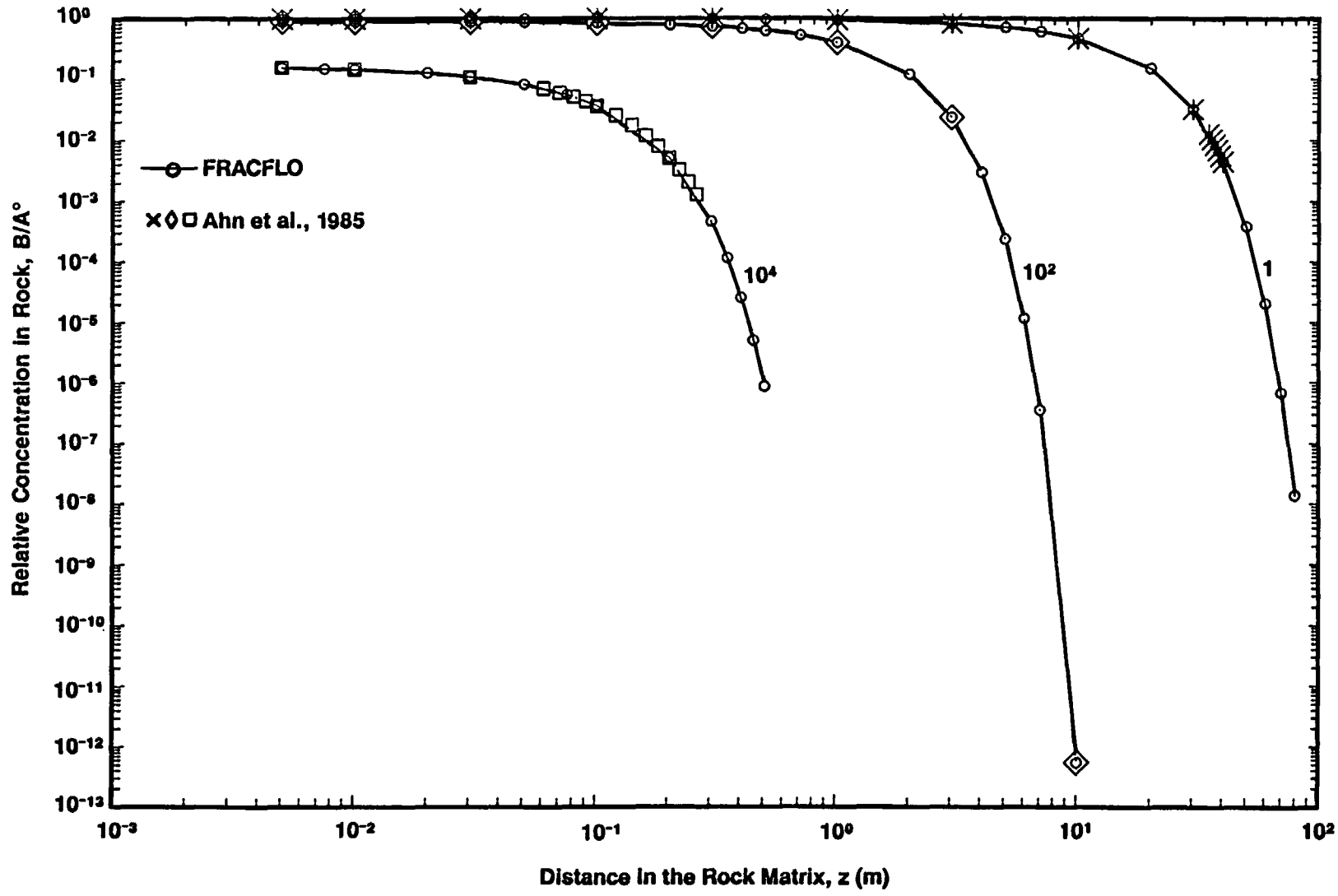

Figure 3-2b. Relative Concentrations of Np-237 in the Rock Matrix Versus Distance in the Rock Matrix at x = 100 m, y = 0 m, t = 10^4 yr, and D_{xx} = 0 for Different Rock Matrix Retardation Factors (R′ = 1, 10^2, 10^4) (Case 1B: Step Release Mode)

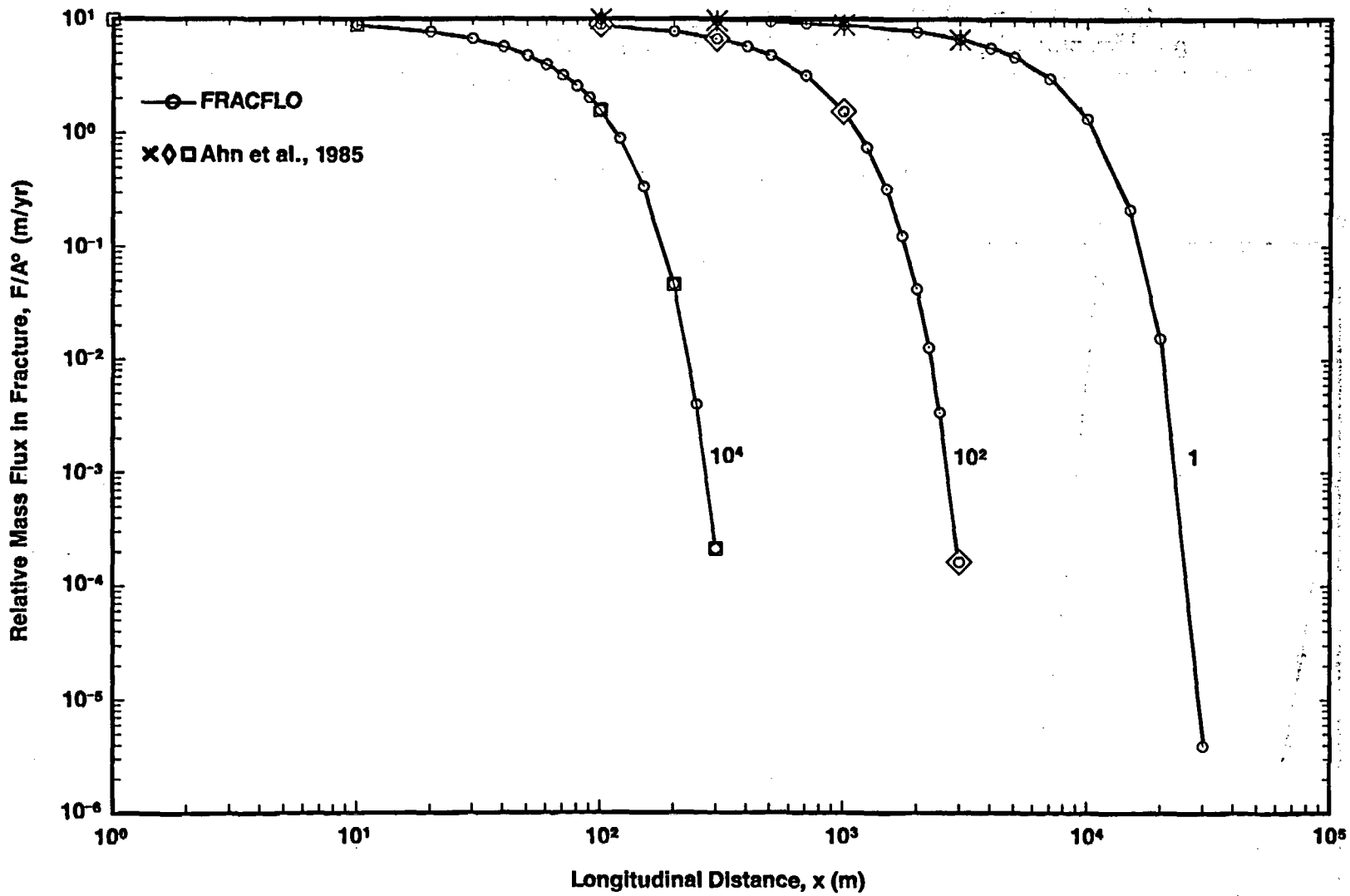

Figure 3-2c. Relative Mass Flux of Np-237 in the Fracture Versus Distance x at $y = 0$ m, $t = 10^4$ yr, and $D_{xx} = 0$ for Different Rock Matrix Retardation Factors ($R' = 1, 10^2, 10^4$)
(Case 1B: Step Release Mode)

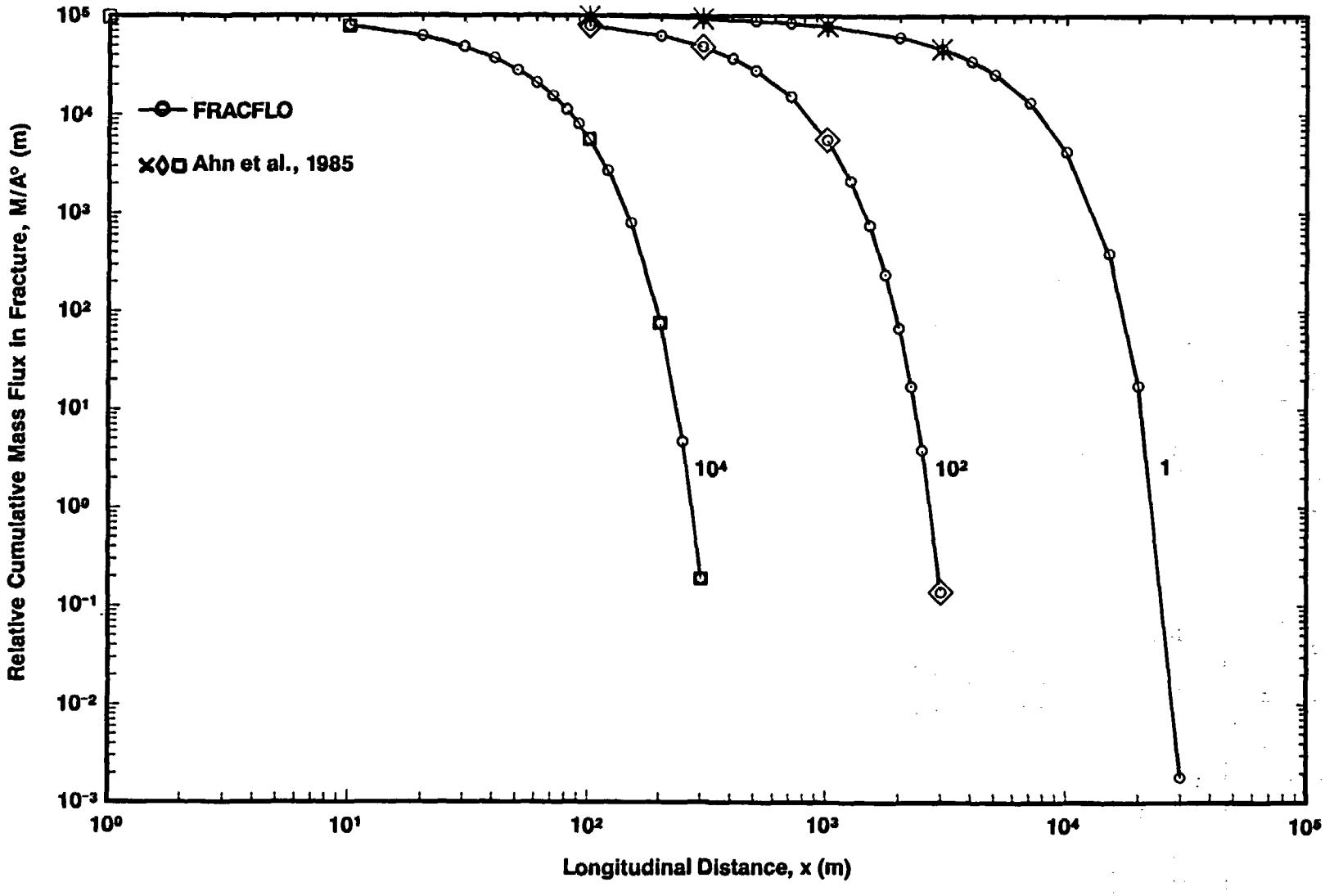

Figure 3-2d. Relative Cumulative Mass Flux of Np-237 in the Fracture Versus Longitudinal Distance x at y = 0 m, t = 10^4 yr, and D_{xx} = 0 for Different Rock Matrix Retardation Factors (R′ = 1, 10^2, 10^4) (Case 1B: Step Release Mode)

Table 3-3a. Case 1B Results: Relative Concentration, Mass Flux, and Cumulative Mass Flux in the Fracture for Np-237 With Infinite Diffusion at Time t = 10^4 yr and Rock Matrix Retardation Factor R′ = 1 (Step Release Mode)

Longitudinal Distance x (m)	Concentration A/A^o	Mass Flux F/A^o (m/yr)	Cumulative Mass Flux M/A^o (m)
1.000E+01	9.956E-01	9.956E+00	9.960E+04
1.000E+02	9.855E-01	9.855E+00	9.750E+04
1.200E+02	9.833E-01	9.833E+00	9.704E+04
1.500E+02	9.799E-01	9.799E+00	9.635E+04
2.000E+02	9.743E-01	9.743E+00	9.521E+04
2.500E+02	9.686E-01	9.686E+00	9.408E+04
3.000E+02	9.630E-01	9.630E+00	9.296E+04
4.000E+02	9.517E-01	9.517E+00	9.075E+04
5.000E+02	9.404E-01	9.404E+00	8.859E+04
7.000E+02	9.179E-01	9.179E+00	8.437E+04
1.000E+03	8.841E-01	8.841E+00	7.833E+04
1.250E+03	8.560E-01	8.560E+00	7.356E+04
1.500E+03	8.281E-01	8.281E+00	6.902E+04
1.750E+03	8.002E-01	8.002E+00	6.470E+04
2.000E+03	7.726E-01	7.726E+00	6.060E+04
2.250E+03	7.452E-01	7.452E+00	5.670E+04
2.500E+03	7.180E-01	7.180E+00	5.301E+04
3.000E+03	6.645E-01	6.645E+00	4.618E+04
4.000E+03	5.619E-01	5.619E+00	3.465E+04
5.000E+03	4.666E-01	4.666E+00	2.556E+04
7.000E+03	3.037E-01	3.037E+00	1.318E+04
1.000E+04	1.356E-01	1.356E+00	4.201E+03
1.500E+04	2.133E-02	2.133E-01	3.892E+02
2.000E+04	1.560E-03	1.560E-02	1.744E+01
3.000E+04	3.945E-07	3.945E-06	1.820E-03

Table 3-3b. Case 1B Results: Relative Concentration, Mass Flux, and Cumulative Mass Flux in the Fracture for Np-237 With Infinite Diffusion at Time t = 10^4 yr and Rock Matrix Retardation Factor R′ = 100 (Step Release Mode)

Longitudinal Distance x (m)	Concentration A/A^o	Mass Flux F/A^o (m/yr)	Cumulative Mass Flux M/A^o (m)
1.000E+01	9.855E-01	9.855E+00	9.759E+04
1.000E+02	8.846E-01	8.846E+00	7.913E+04
1.200E+02	8.624E-01	8.624E+00	7.543E+04
1.500E+02	8.292E-01	8.292E+00	7.014E+04
2.000E+02	7.746E-01	7.746E+00	6.200E+04
2.500E+02	7.210E-01	7.210E+00	5.453E+04
3.000E+02	6.687E-01	6.687E+00	4.799E+04
4.000E+02	5.690E-01	5.690E+00	3.669E+04
5.000E+02	4.769E-01	4.769E+00	2.769E+04
7.000E+02	3.195E-01	3.195E+00	1.515E+04
1.000E+03	1.547E-01	1.547E+00	5.509E+03
1.250E+03	7.501E-02	7.501E-01	2.138E+03
1.500E+03	3.246E-02	3.246E-01	7.508E+02
1.750E+03	1.249E-02	1.249E-01	2.375E+02
2.000E+03	4.261E-03	4.261E-02	6.742E+01
2.250E+03	1.285E-03	1.285E-02	1.711E+01
2.500E+03	3.417E-04	3.417E-03	3.867E+00
3.000E+03	1.844E-05	1.844E-04	1.381E-01

Table 3-3c. Case 1B Results: Relative Concentration, Mass Flux, and Cumulative Mass Flux in the Fracture for Np-237 With Infinite Diffusion at Time t = 10^4 yr and Rock Matrix Retardation Factor R′ = 10,000 (Step Release Mode)

Longitudinal Distance x (m)	Concentration A/A^o	Mass Flux F/A^o (m/yr)	Cumulative Mass Flux M/A^o (m)
1.000E+00	9.855E-01	9.855E+00	9.780E+04
1.000E+01	8.847E-01	8.847E+00	7.921E+04
2.000E+01	7.748E-01	7.748E+00	6.214E+04
3.000E+01	6.692E-01	6.692E+00	4.817E+04
4.000E+01	5.697E-01	5.697E+00	3.689E+04
5.000E+01	4.778E-01	4.778E+00	2.790E+04
6.000E+01	3.947E-01	3.947E+00	2.083E+04
7.000E+01	3.210E-01	3.210E+00	1.535E+04
8.000E+01	2.569E-01	2.569E+00	1.116E+04
9.000E+01	2.022E-01	2.022E+00	7.995E+03
1.000E+02	1.566E-01	1.566E+00	5.649E+03
1.200E+02	8.920E-02	8.920E-01	2.699E+03
1.500E+02	3.365E-02	3.365E-01	7.954E+02
2.000E+02	4.622E-03	4.622E-02	7.542E+01
2.500E+02	3.989E-04	3.989E-03	4.700E+00
3.000E+02	2.140E-05	2.140E-04	1.889E-01
4.000E+02	1.438E-08	1.438E-07	7.780E-05
5.000E+02	1.348E-12	1.348E-11	4.875E-09

Table 3-3d. Case 1B Results: Relative Concentration in Rock Matrix (B/A°) for Np-237 at $x = 100$ m and $D_{xx} = 0$ (Step Release Mode)

Elevation z (m)	R′ = 1	R′ = 100	R′ = 10,000
5.000E-03	9.855E-01	8.846E-01	1.566E-01
7.500E-03	9.854E-01	8.832E-01	1.515E-01
1.000E-02	9.852E-01	8.818E-01	1.465E-01
2.000E-02	9.847E-01	8.763E-01	1.278E-01
3.000E-02	9.841E-01	8.707E-01	1.111E-01
5.000E-02	9.830E-01	8.596E-01	8.278E-02
6.000E-02	9.824E-01	8.541E-01	7.100E-02
7.000E-02	9.819E-01	8.485E-01	6.063E-02
7.500E-02	9.816E-01	8.458E-01	5.593E-02
8.000E-02	9.813E-01	8.430E-01	5.155E-02
9.000E-02	9.807E-01	8.375E-01	4.363E-02
1.000E-01	9.802E-01	8.320E-01	3.677E-02
1.200E-01	9.790E-01	8.210E-01	2.576E-02
1.400E-01	9.779E-01	8.100E-01	1.773E-02
1.600E-01	9.768E-01	7.991E-01	1.198E-02
1.800E-01	9.757E-01	7.882E-01	7.953E-03
2.000E-01	9.745E-01	7.774E-01	5.182E-03
2.200E-01	9.734E-01	7.666E-01	3.314E-03
2.400E-01	9.723E-01	7.558E-01	2.081E-03
2.600E-01	9.712E-01	7.451E-01	1.282E-03
3.000E-01	9.689E-01	7.238E-01	4.604E-04
3.500E-01	9.661E-01	6.976E-01	1.150E-04
4.000E-01	9.633E-01	6.716E-01	2.552E-05
4.500E-01	9.605E-01	6.461E-01	5.024E-06
5.000E-01	9.577E-01	6.209E-01	8.766E-07
7.000E-01	9.464E-01	5.249E-01	
1.000E+00	9.296E-01	3.966E-01	
2.000E+00	8.738E-01	1.201E-01	
3.000E+00	8.185E-01	2.372E-02	
4.000E+00	7.642E-01	2.990E-03	
5.000E+00	7.109E-01	2.368E-04	
6.000E+00	6.591E-01	1.168E-05	
7.000E+00	6.088E-01	3.566E-07	
1.000E+01	4.692E-01	5.473E-13	
2.000E+01	1.526E-01		
3.000E+01	3.256E-02		
3.500E+01	1.274E-02		
3.600E+01	1.041E-02		
3.700E+01	8.476E-03		
3.800E+01	6.867E-03		
3.900E+01	5.538E-03		
4.000E+01	4.446E-03		
5.000E+01	3.824E-04		
6.000E+01	2.051E-05		
7.000E+01	6.812E-07		
8.000E+01	1.395E-08		

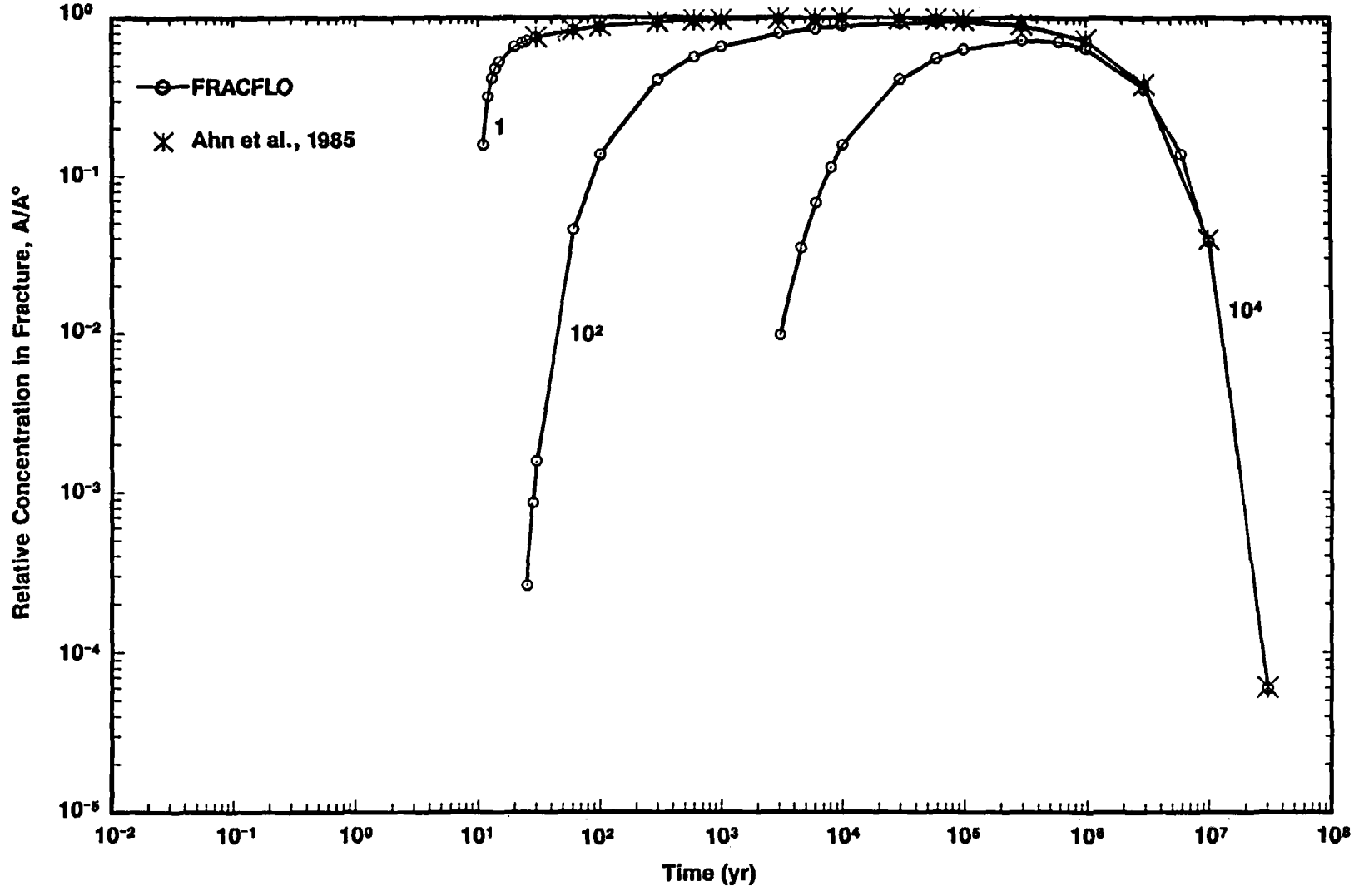

Figure 3-2e. Breakthrough Curves Showing the Relative Concentration of Np-237 in the Fracture Versus Time at x = 100 m, y = 0 m, and D_{xx} = 0 for Different Rock Matrix Retardation Factors (R′ = 1, 10^2, 10^4) (Case 1B: Step Release Mode)

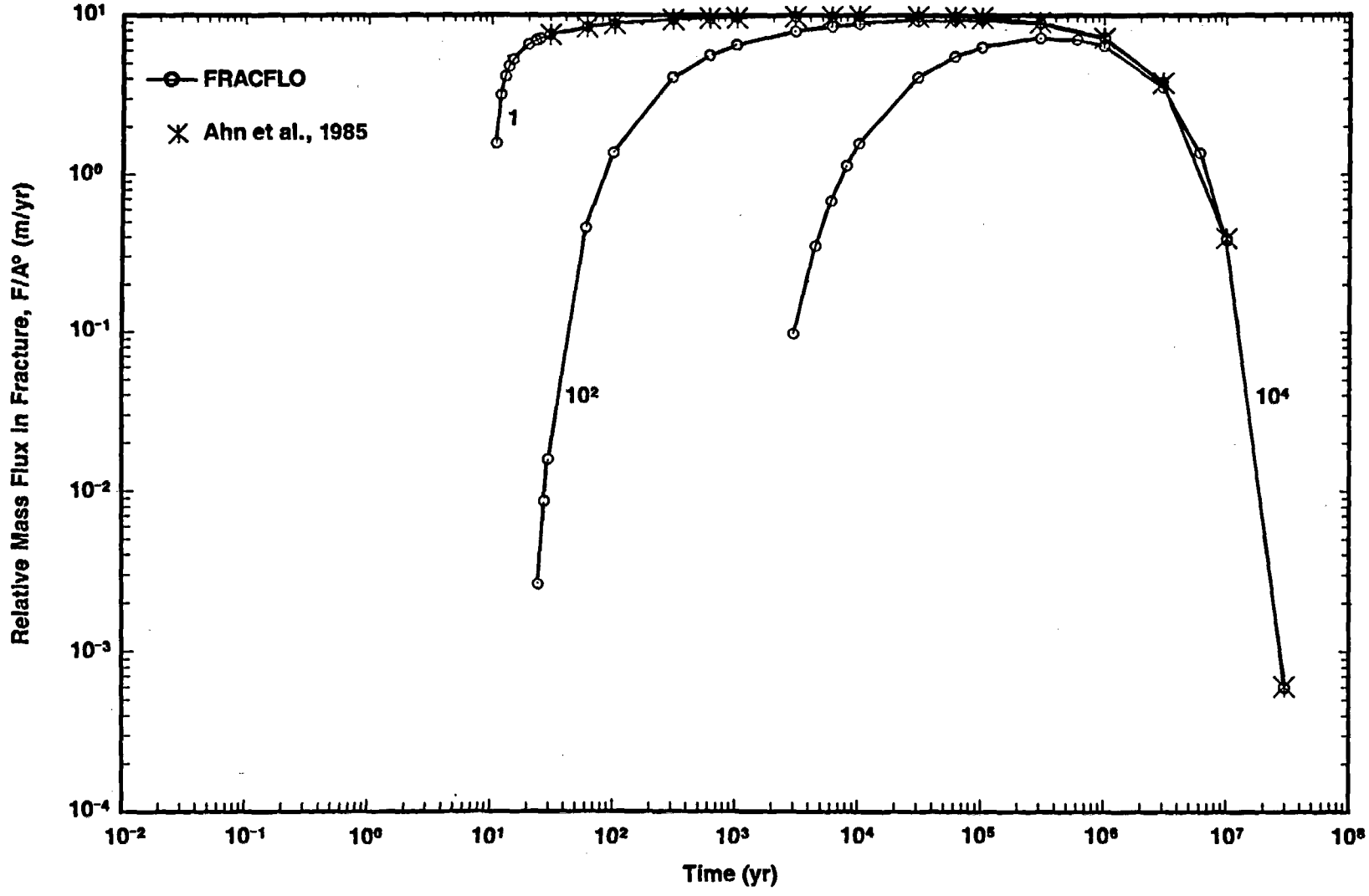

Figure 3-2f. Relative Mass Flux of Np-237 in the Fracture Versus Time at $x = 100$ m, $y = 0$ m, and $D_{xx} = 0$ for Different Rock Matrix Retardation Factors ($R' = 1, 10^2, 10^4$) (Case 1B: Step Release Mode)

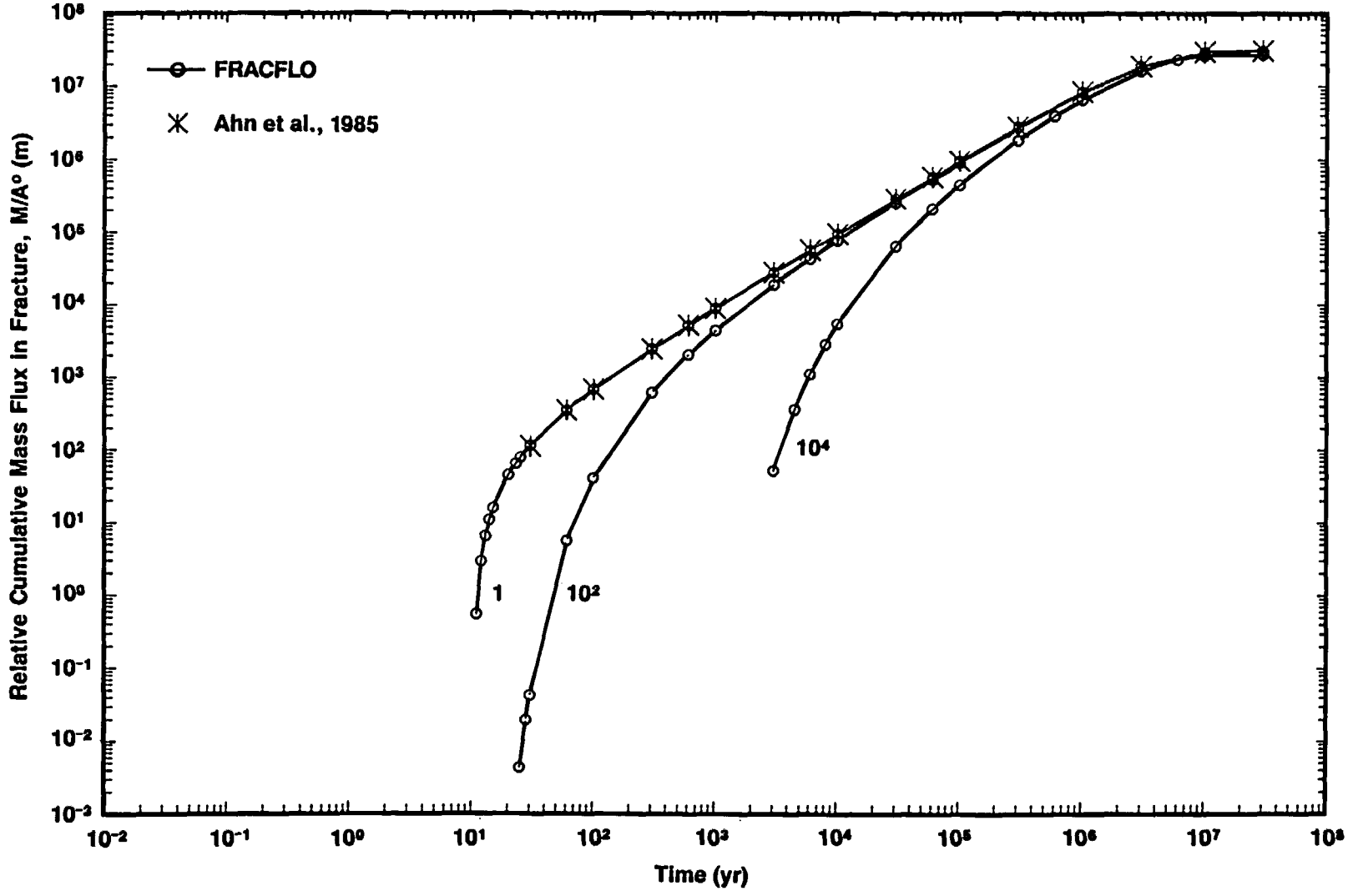

Figure 3-2g. Relative Cumulative Mass Flux of Np-237 in the Fracture Versus Time at x = 100 m, y = 0 m, and D_{xx} = 0 for Different Rock Matrix Retardation Factors (R′ = 1, 10^2, 10^4) (Case 1B: Step Release Mode)

Table 3-3e. Case 1B Results: Relative Concentration, Mass Flux, and Cumulative Mass Flux in the Fracture for Np-237 Over Time With Rock Matrix Retardation Factor R′ = 1 (Step Release Mode)

Time (yr)	Concentration A/A^o	Mass Flux F/A^o (m/yr)	Cumulative Mass Flux M/A^o (m)
1.000E+01	0.000E+00	0.000E+00	0.000E+00
1.100E+01	1.573E-01	1.573E+00	5.679E-01
1.200E+01	3.173E-01	3.173E+00	3.014E+00
1.300E+01	4.142E-01	4.142E+00	6.707E+00
1.400E+01	4.795E-01	4.795E+00	1.119E+01
1.500E+01	5.271E-01	5.271E+00	1.624E+01
2.000E+01	6.547E-01	6.547E+00	4.628E+01
2.300E+01	6.949E-01	6.949E+00	6.656E+01
2.500E+01	7.150E-01	7.150E+00	8.067E+01
2.800E+01	7.389E-01	7.389E+00	1.025E+02
3.000E+01	7.518E-01	7.518E+00	1.174E+02
6.000E+01	8.415E-01	8.415E+00	3.594E+02
1.000E+02	8.815E-01	8.815E+00	7.051E+02
3.000E+02	9.337E-01	9.337E+00	2.535E+03
6.000E+02	9.534E-01	9.534E+00	5.371E+03
1.000E+03	9.638E-01	9.638E+00	9.208E+03
3.000E+03	9.784E-01	9.784E+00	2.867E+04
4.500E+03	9.817E-01	9.817E+00	4.338E+04
6.000E+03	9.835E-01	9.835E+00	5.812E+04
8.000E+03	9.848E-01	9.848E+00	7.780E+04
1.000E+04	9.855E-01	9.855E+00	9.750E+04
3.000E+04	9.839E-01	9.839E+00	2.946E+05
6.000E+04	9.762E-01	9.762E+00	5.886E+05
1.000E+05	9.647E-01	9.647E+00	9.768E+05
3.000E+05	9.055E-01	9.055E+00	2.847E+06
6.000E+05	8.222E-01	8.222E+00	5.436E+06
1.000E+06	7.225E-01	7.225E+00	8.522E+06
3.000E+06	3.782E-01	3.782E+00	1.916E+07
6.000E+06	1.431E-01	1.431E+00	2.642E+07
1.000E+07	3.919E-02	3.919E-01	2.963E+07
3.000E+07	6.024E-05	6.024E-04	3.084E+07

Table 3-3f. Case 1B Results: Relative Concentration, Mass Flux, and Cumulative Mass Flux in the Fracture for Np-237 Over Time With Rock Matrix Retardation Factor R′ = 100 (Step Release Mode)

Time (yr)	Concentration A/A^o	Mass Flux F/A^o (m/yr)	Cumulative Mass Flux M/A^o (m)
2.500E+01	2.807E-04	2.807E-03	4.403E-03
2.800E+01	8.581E-04	8.581E-03	1.997E-02
3.000E+01	1.565E-03	1.565E-02	4.374E-02
6.000E+01	4.550E-02	4.550E-01	5.769E+00
1.000E+02	1.360E-01	1.360E+00	4.211E+01
3.000E+02	4.082E-01	4.082E+00	6.296E+02
6.000E+02	5.603E-01	5.603E+00	2.114E+03
1.000E+03	6.529E-01	6.529E+00	4.562E+03
3.000E+03	7.951E-01	7.951E+00	1.941E+04
4.500E+03	8.316E-01	8.316E+00	3.164E+04
6.000E+03	8.534E-01	8.534E+00	4.429E+04
8.000E+03	8.720E-01	8.720E+00	6.156E+04
1.000E+04	8.846E-01	8.846E+00	7.913E+04
3.000E+04	9.259E-01	9.259E+00	2.614E+05
6.000E+04	9.356E-01	9.356E+00	5.412E+05
1.000E+05	9.336E-01	9.336E+00	9.153E+05
3.000E+05	8.887E-01	8.887E+00	2.741E+06
6.000E+05	8.114E-01	8.114E+00	5.291E+06
1.000E+06	7.152E-01	7.152E+00	8.340E+06
3.000E+06	3.760E-01	3.760E+00	1.890E+07
6.000E+06	1.426E-01	1.426E+00	2.612E+07
1.000E+07	3.906E-02	3.906E-01	2.932E+07
3.000E+07	6.013E-05	6.013E-04	3.052E+07

Table 3-3g. Case 1B Results: Relative Concentration, Mass Flux, and Cumulative Mass Flux in the Fracture for Np-237 Over Time With Rock Matrix Retardation Factor R′ = 10,000 (Step Release Mode)

Time (yr)	Concentration A/A^o	Mass Flux F/A^o (m/yr)	Cumulative Mass Flux M/A^o (m)
3.000E+03	9.692E-03	9.692E-02	5.354E+01
4.500E+03	3.476E-02	3.476E-01	3.719E+02
6.000E+03	6.753E-02	6.753E-01	1.134E+03
8.000E+03	1.133E-01	1.133E+00	2.944E+03
1.000E+04	1.566E-01	1.566E+00	5.649E+03
3.000E+04	4.101E-01	4.101E+00	6.659E+04
6.000E+04	5.528E-01	5.528E+00	2.143E+05
1.000E+05	6.338E-01	6.338E+00	4.538E+05
3.000E+05	7.225E-01	7.225E+00	1.847E+06
6.000E+05	7.041E-01	7.041E+00	4.000E+06
1.000E+06	6.420E-01	6.420E+00	6.697E+06
3.000E+06	3.536E-01	3.536E+00	1.644E+07
6.000E+06	1.366E-01	1.366E+00	2.330E+07
1.000E+07	3.780E-02	3.780E-01	2.638E+07
3.000E+07	5.901E-05	5.901E-04	2.755E+07

3.5.2 Case 2: Spatial and Time-Dependent Concentrations, Mass Flux, and Cumulative Mass Flux Subject to a Band Release Mode in the Absence of Longitudinal Dispersion

This test case deals with the migration of Np-237 in a one-dimensional flow domain in the absence of longitudinal dispersion. The concentration at the source is subjected to a band release mode with a leach time corresponding to 5,000 years, and the retardation factor of the fracture is taken as unity. Similar to the previous case, the influence of the rock matrix retardation factor on the concentration in the fracture and rock matrix was investigated. The input data pertaining to this case are presented in Table 3-4. The reported results are obtained through the nondispersive form of the general solution.

Figures 3-3a, 3-3b, 3-3c show the relative concentration, the mass flux, and cumulative mass flux of Np-237 in the fracture; Figure 3-3d shows the relative concentration in the rock matrix at a distance of 100 m downstream from the source. Three values of rock matrix retardation factor ($R' = 1$, 100, and 10,000) are examined. Tabulated results in Tables 3-5 and 3-6 show excellent agreement with those reported by Ahn et al. (1985).

Figures 3-4a, 3-4b, and 3-4c show the time-dependent relative concentration, mass flux, and cumulative mass flux in the fracture at a distance of 100 m from the source. Again, three values of rock matrix retardation are examined. The peak of the curves shown in Figures 3-4a and 3-4b denotes the marked influence of the rock matrix retardation factor. The rate of concentration decrease of Np-237 at this monitoring station past the leaching time is influenced to a large extent by the prevailing concentration gradient at the fracture wall, which gears the (reversed) diffusion process (i.e., rock matrix to fracture; the higher the retardation factor the higher the gradient). The time lapse for the concentration to reach a zero value at this point will depend on the mass of Np-237 accumulated in the rock matrix; the lower the retardation factor the longer the time lapse. Tabulated results in Table 3-7 show excellent agreement with those reported by Ahn et al. (1985) for $R' = 1$.

Table 3-4. Input Parameters for Case 2

Species	Np-237
Initial Concentration A° (arbitrary units of activity/L^3)	1
Type of Release Mode	Band
Boundary Condition	Infinite Plane Source
x	100.0 m
y	0.0 m
d	∞
u	10.0 m/yr
v	0.0 m/yr
D_{xx}	0.0 m^2/yr
D_{yy}	0.0 m^2/yr
D_{yx}	0.0 m^2/yr
D_p	0.01 m^2/yr
$T_{1/2}$	2.14×10^6 yr
T	5×10^3 yr
b	0.005 m
ϕ	10^{-2}
R	1
R′	1, 10^2, 10^4

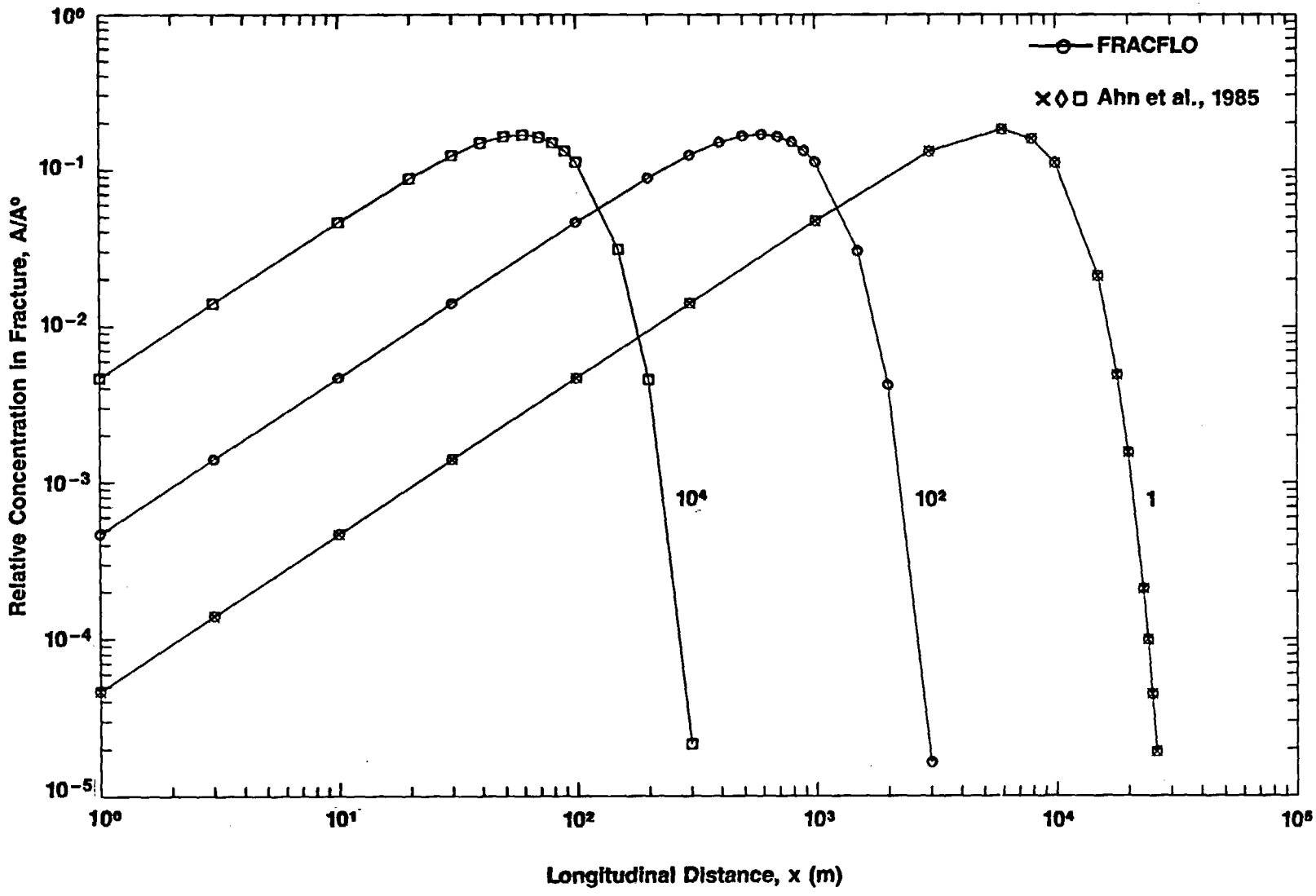

Figure 3-3a. Relative Concentrations of Np-237 in the Fracture Versus Longitudinal Distance x at y = 0 m, t = 10^4 yr, and D_{xx} = 0 for Different Rock Matrix Retardation Factors (R′ = 1, 10^2, 10^4) (Case 2: Band Release Mode)

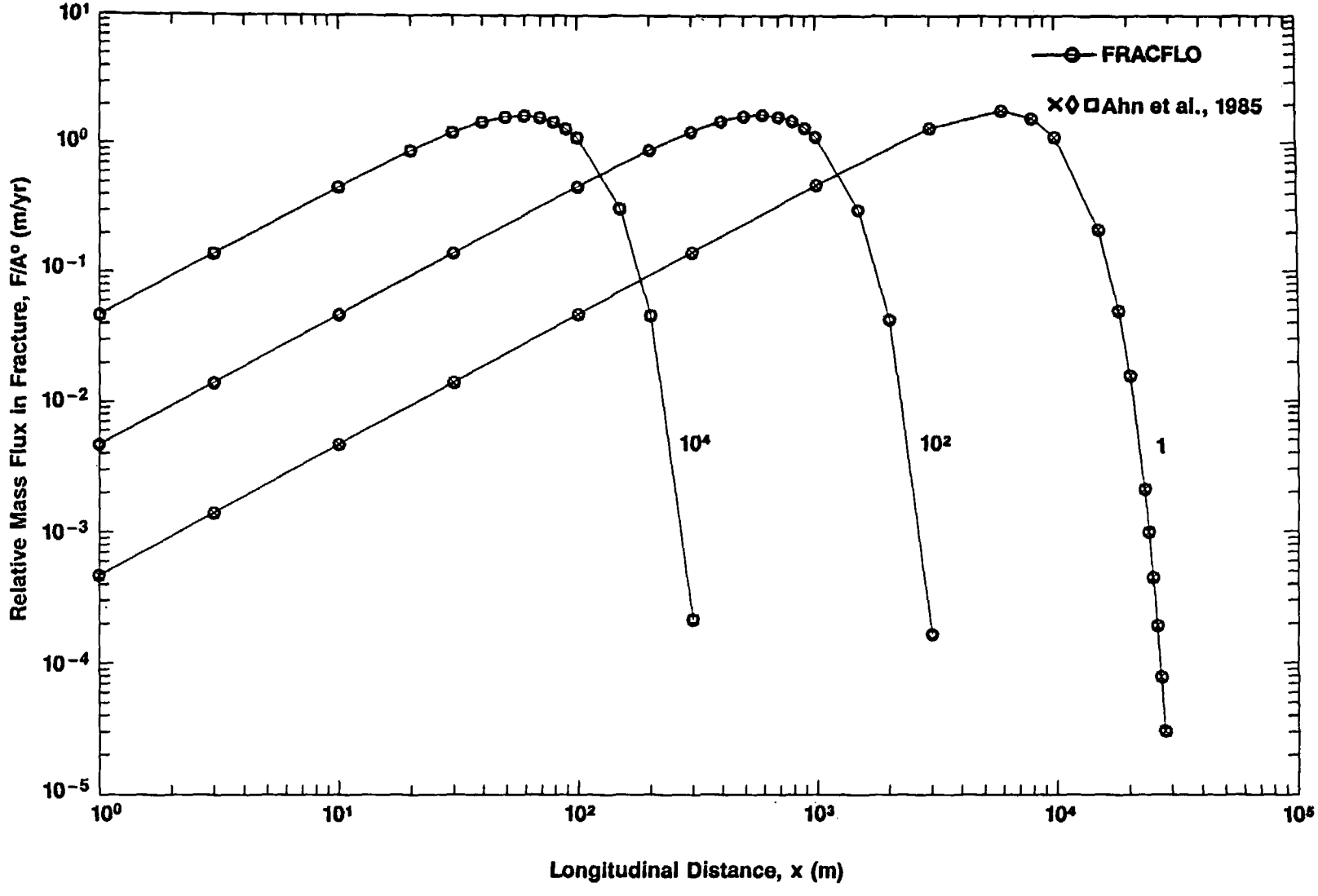

Figure 3-3b. Relative Mass Flux in the Fracture Versus Distance x at y = 0 m, t = 10^4 yr, and D_{xx} = 0 for Different Rock Matrix Retardation Factors (R′ = 1, 10^2, 10^4) (Case 2: Band Release Mode)

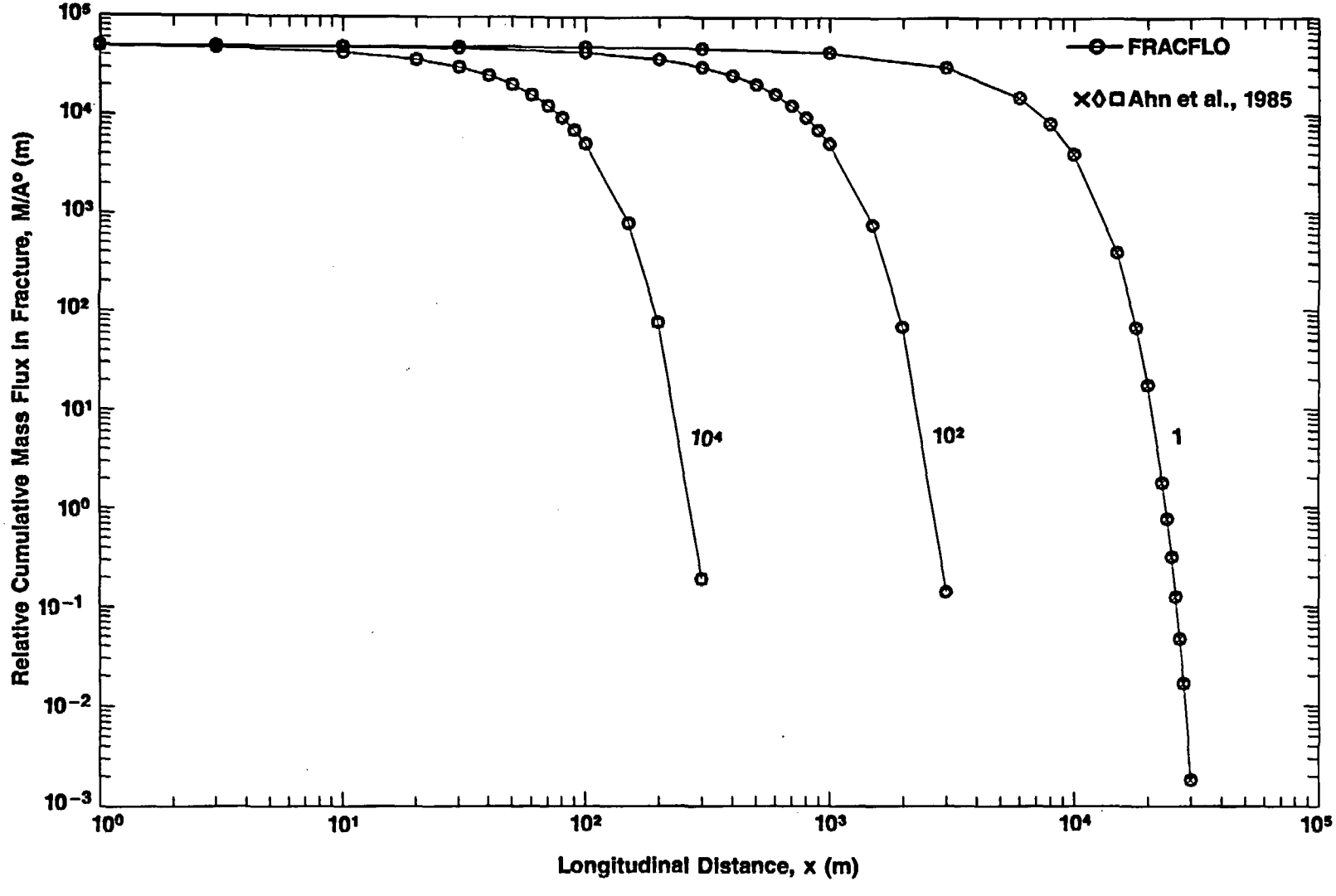

Figure 3-3c. Relative Cumulative Mass Flux of Np-237 in the Fracture Versus Longitudinal Distance x at y = 0 m, t = 10^4 yr, and D_{xx} = 0 for Different Rock Matrix Retardation Factors (R′ = 1, 10^2, 10^4) (Case 2: Band Release Mode)

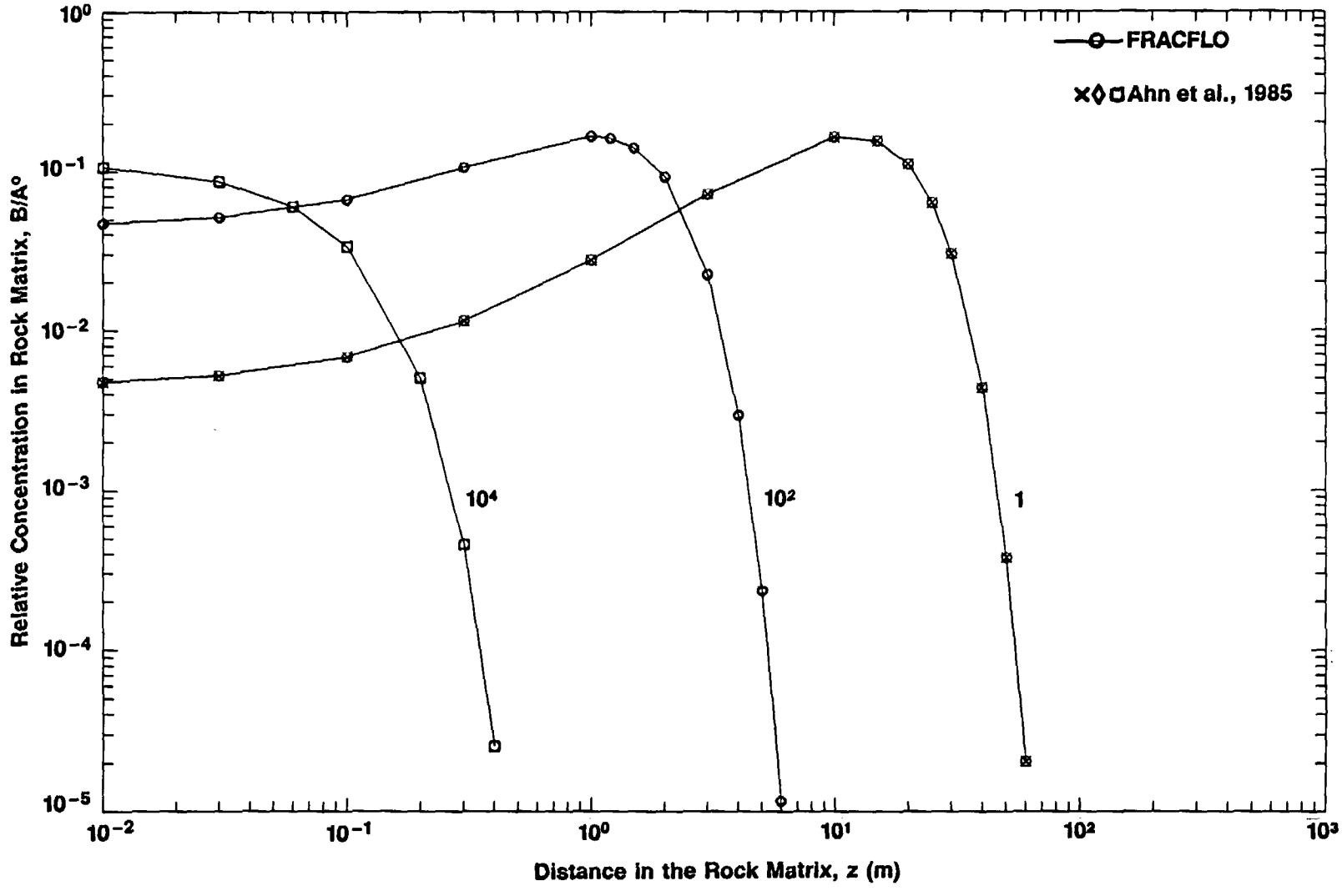

Figure 3-3d. Relative Concentrations of Np-237 in the Rock Matrix Versus Distance in the Rock Matrix at x = 100 m, y = 0 m, t = 10^4 yr, and D_{xx} = 0 for Different Rock Matrix Retardation Factors (R′ = 1, 10^2, 10^4) (Case 2: Band Release Mode)

Table 3-5a. Case 2 Results: Relative Concentration, Mass Flux, and Cumulative Mass Flux in the Fracture for Np-237 with Infinite Diffusion at Time t = 10^4 yr and Rock Matrix Retardation Factor R′ = 1 (Band Release Mode)

Longitudinal Distance x (m)	Concentration A/A^o	Mass Flux F/A^o (m/yr)	Cumulative Mass Flux M/A^o (m)
1.000E+00	4.659E-05	4.659E-04	4.995E+04
3.000E+00	1.398E-04	1.398E-03	4.994E+04
1.000E+01	4.660E-04	4.660E-03	4.989E+04
3.000E+01	1.399E-03	1.399E-02	4.976E+04
1.000E+02	4.668E-03	4.668E-02	4.930E+04
3.000E+02	1.405E-02	1.405E-01	4.797E+04
1.000E+03	4.693E-02	4.693E-01	4.333E+04
3.000E+03	1.302E-01	1.302E+00	3.055E+04
6.000E+03	1.801E-01	1.801E+00	1.506E+04
8.000E+03	1.568E-01	1.568E+00	8.198E+03
1.000E+04	1.103E-01	1.103E+00	3.976E+03
1.500E+04	2.099E-02	2.099E-01	3.879E+02
1.800E+04	4.914E-03	4.914E-02	6.661E+01
2.000E+04	1.560E-03	1.560E-02	1.744E+01
2.300E+04	2.092E-04	2.092E-03	1.772E+00
2.400E+04	9.856E-05	9.856E-04	7.631E-01
2.500E+04	4.441E-05	4.441E-04	3.146E-01
2.600E+04	1.911E-05	1.911E-04	1.240E-01
2.700E+04	7.831E-06	7.831E-05	4.659E-02
2.800E+04	3.051E-06	3.051E-05	1.666E-02
3.000E+04	3.946E-07	3.946E-06	1.820E-03
4.000E+04	2.806E-13	2.806E-12	5.792E-10

Table 3-5b. Case 2 Results: Relative Concentration, Mass Flux, and Cumulative Mass Flux in the Fracture for Np-237 at Time t = 10^4 yr and Rock Matrix Retardation Factor R′ = 100 (Band Release Mode)

Longitudinal Distance x (m)	Concentration A/A^o	Mass Flux F/A^o (m/yr)	Cumulative Mass Flux M/A^o (m)
1.000E+00	4.659E-04	4.659E-03	4.989E+04
3.000E+00	1.398E-03	1.398E-02	4.976E+04
1.000E+01	4.659E-03	4.659E-02	4.930E+04
3.000E+01	1.397E-02	1.397E-01	4.797E+04
1.000E+02	4.601E-02	4.601E-01	4.337E+04
2.000E+02	8.823E-02	8.823E-01	3.696E+04
3.000E+02	1.232E-01	1.232E+00	3.089E+04
4.000E+02	1.485E-01	1.485E+00	2.532E+04
5.000E+02	1.630E-01	1.630E+00	2.033E+04
6.000E+02	1.669E-01	1.669E+00	1.599E+04
7.000E+02	1.614E-01	1.614E+00	1.232E+04
8.000E+02	1.488E-01	1.488E+00	9.301E+03
9.000E+02	1.313E-01	1.313E+00	6.875E+03
1.000E+03	1.115E-01	1.115E+00	4.978E+03
1.500E+03	3.015E-02	3.015E-01	7.342E+02
2.000E+03	4.216E-03	4.216E-02	6.722E+01
3.000E+03	1.644E-05	1.644E-04	1.381E-01
4.000E+03	7.739E-09	7.739E-08	3.906E-05

Table 3-5c. Case 2 Results: Relative Concentration, Mass Flux, and Cumulative Mass Flux in the Fracture for Np-237 at Time t = 10^4 yr and Rock Matrix Retardation Factor R′ = 10,000 (Band Release Mode)

Longitudinal Distance x (m)	Concentration A/A^o	Mass Flux F/A^o (m/yr)	Cumulative Mass Flux M/A^o (m)
1.000E+00	4.658E-03	4.658E-02	4.930E+04
3.000E+00	1.396E-02	1.396E-01	4.797E+04
1.000E+01	4.592E-02	4.592E-01	4.337E+04
2.000E+01	8.789E-02	8.789E-01	3.697E+04
3.000E+01	1.225E-01	1.225E+00	3.093E+04
4.000E+01	1.475E-01	1.475E+00	2.537E+04
5.000E+01	1.618E-01	1.618E+00	2.041E+04
6.000E+01	1.656E-01	1.656E+00	1.608E+04
7.000E+01	1.603E-01	1.603E+00	1.243E+04
8.000E+01	1.479E-01	1.479E+00	9.408E+03
9.000E+01	1.309E-01	1.309E+00	6.981E+03
1.000E+02	1.114E-01	1.114E+00	5.079E+03
1.500E+02	3.100E-02	3.100E-01	7.755E+02
2.000E+02	4.560E-03	4.560E-02	7.512E+01
3.000E+02	2.140E-05	2.140E-04	1.889E-01
4.000E+02	1.438E-08	1.438E-07	7.780E-05

Table 3-6a. Case 2 Results: Relative Concentration in the Rock Matrix for Np-237 at Time t = 10^4 yr and Rock Matrix Retardation Factor R′ = 1 (Band Release Mode)

Vertical Distance z (m)	Concentration B/A^{o}
1.000E-02	4.785E-03
3.000E-02	5.252E-03
1.000E-01	6.885E-03
3.000E-01	1.155E-02
1.000E+00	2.775E-02
3.000E+00	7.184E-02
1.000E+01	1.627E-01
1.500E+01	1.536E-01
2.000E+01	1.095E-01
2.500E+01	6.280E-02
3.000E+01	3.006E-02
4.000E+01	4.389E-03
5.000E+01	3.819E-04
6.000E+01	2.051E-05

Table 3-6b. Case 2 Results: Relative Concentration in the Rock Matrix for Np-237 at Time t = 1 x 10^4 yr and Rock Matrix Retardation Factor R′ = 100 (Band Release Mode)

Vertical Distance z (m)	Concentration B/A^{o}
1.000E-02	4.712E-02
3.000E-02	5.156E-02
1.000E-01	6.670E-02
3.000E-01	1.056E-01
1.000E+00	1.657E-01
1.200E+00	1.606E-01
1.500E+00	1.403E-01
2.000E+00	9.215E-02
3.000E+00	2.234E-02
4.000E+00	2.963E-03
5.000E+00	2.366E-04
6.000E+00	1.168E-05
7.000E+00	3.566E-07
8.000E+00	6.704E-09
9.000E+00	7.739E-11
1.000E+01	5.473E-13

Table 3-6c. Case 2 Results: Relative Concentration in the Rock Matrix for Np-237 at Time t = 10^4 yr and Rock Matrix Retardation Factor R' = 10,000 (Band Release Mode)

Vertical Distance z (m)	Concentration B/A^{o}
1.000E-02	1.085E-01
3.000E-02	8.884E-02
5.000E-02	8.034E-02
1.000E-01	3.383E-02
2.000E-01	5.105E-03
3.000E-01	4.597E-04
4.000E-01	2.552E-05
5.000E-01	8.768E-07
8.000E-01	1.858E-08
1.000E+00	2.802E-17

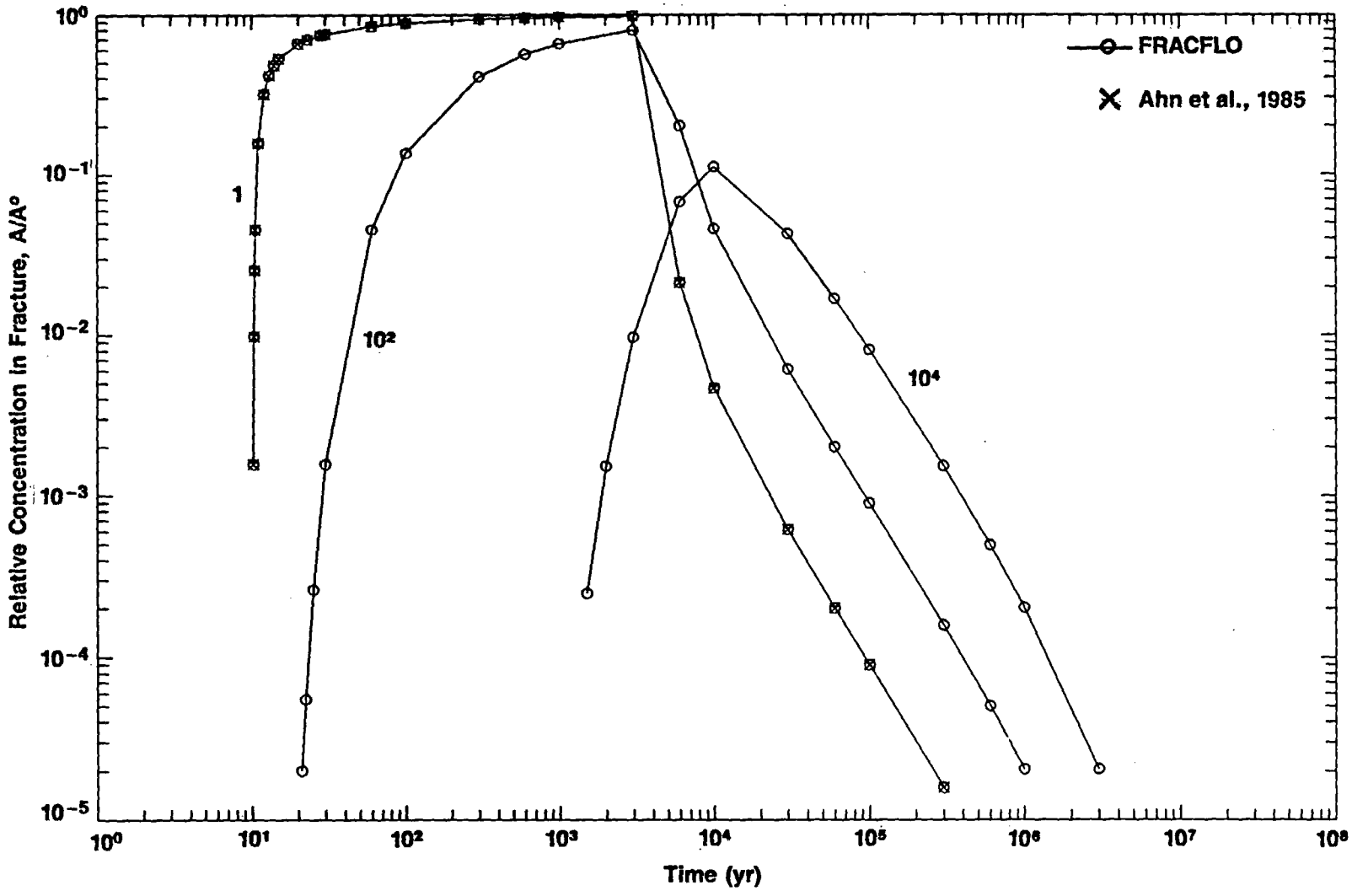

Figure 3-4a. Breakthrough Curves Showing the Relative Concentration of Np-237 in the Fracture Versus Time at x = 100 m, y = 0 m, and D_{xx} = 0 for Different Rock Matrix Retardation Factors (R′ = 1, 10^2, 10^4) (Case 2: Band Release Mode)

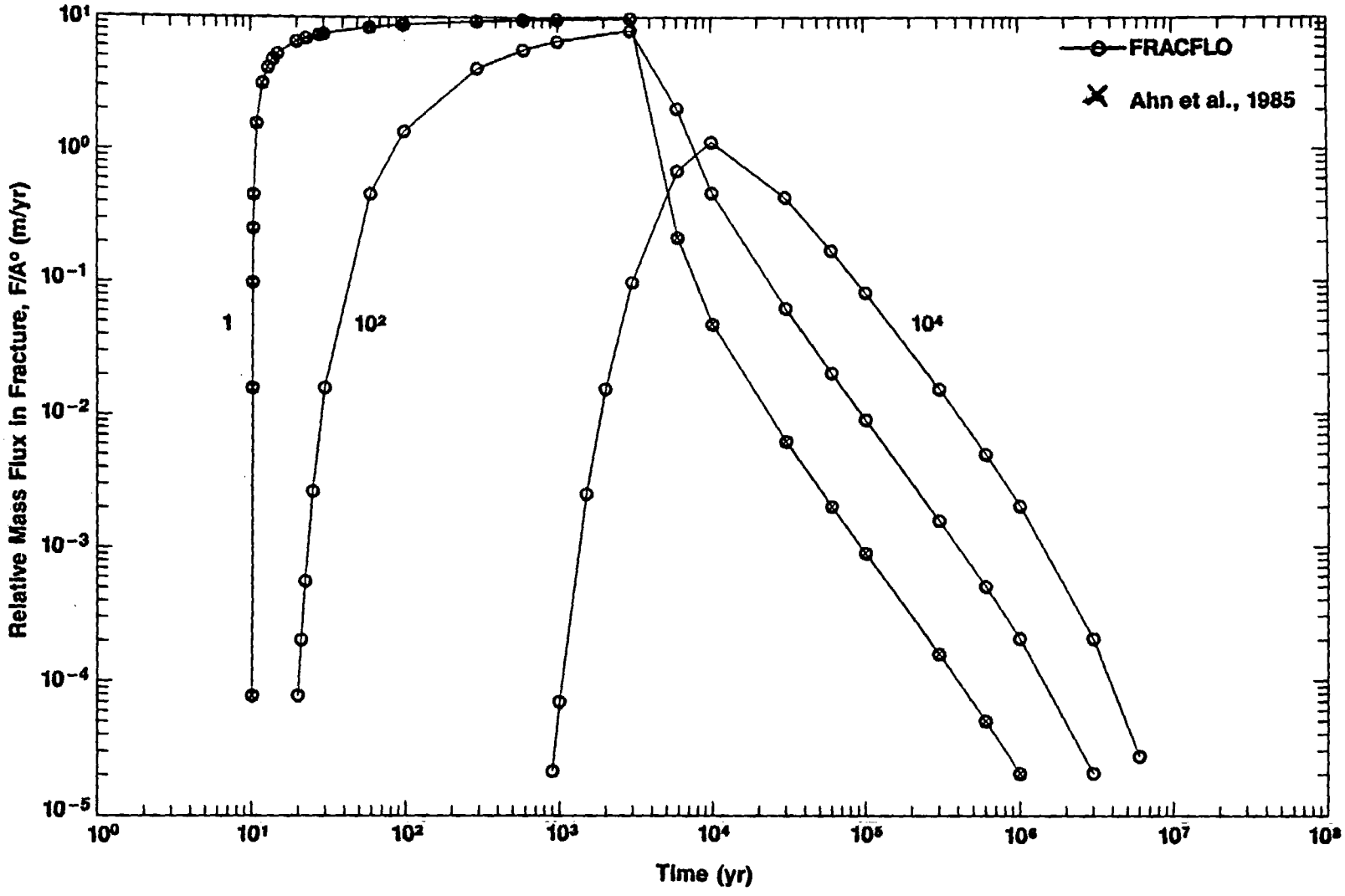

Figure 3-4b. Relative Mass Flux of Np-237 in the Fracture Versus Time at x = 100 m, y = 0 m, and D_{xx} = 0 for Different Rock Matrix Retardation Factors (R′ = 1, 10^2, 10^4) (Case 2: Band Release Mode)

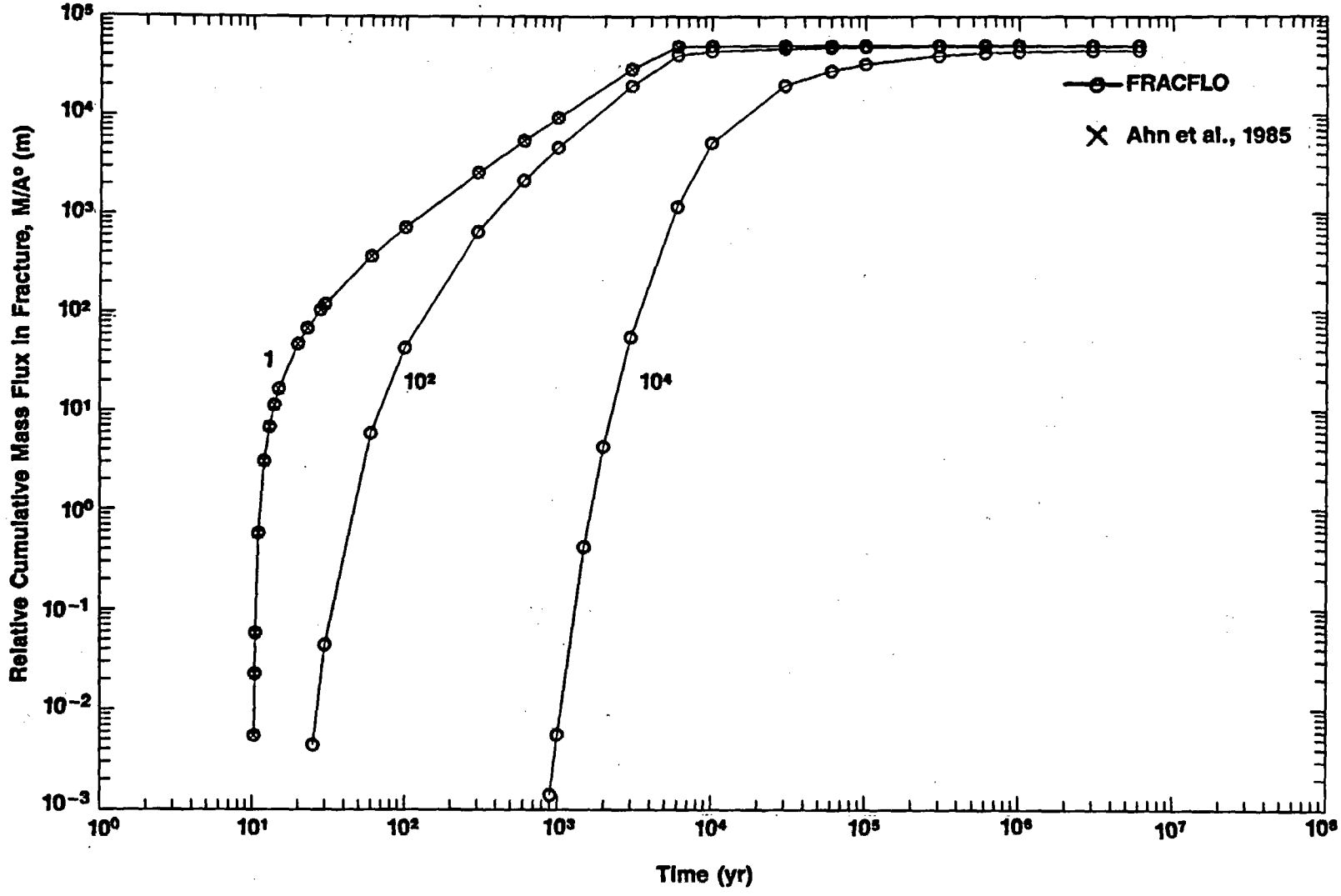

Figure 3-4c. Relative Cumulative Mass Flux of Np-237 in the Fracture Versus Time at $x = 100$ m, $y = 0$ m, and $D_{xx} = 0$ for Different Rock Matrix Retardation Factors ($R' = 1, 10^2, 10^4$) (Case 2: Band Release Mode)

Table 3-7a. Case 2 Results: Relative Concentration, Mass Flux, and Cumulative Mass Flux in the Fracture for Np-237 Over Time with Rock Matrix Retardation Factor R′ = 1 (Band Release Mode)

Time (yr)	Concentration A/A^{o}	Mass Flux F/A^{o} (m/yr)	Cumulative Mass Flux M/A^{o} (m)
1.000E+01	0.000E+00	0.000E+00	0.000E+00
1.010E+01	7.744E-08	7.744E-05	3.303E-07
1.020E+01	1.565E-03	1.565E-02	4.374E-04
1.030E+01	9.823E-03	9.823E-02	5.456E-03
1.040E+01	2.535E-02	2.535E-01	2.254E-02
1.050E+01	4.550E-02	4.550E-01	5.769E-02
1.100E+01	1.573E-01	1.573E+00	5.879E-01
1.200E+01	3.173E-01	3.173E+00	3.014E+00
1.300E+01	4.142E-01	4.142E+00	6.707E+00
1.400E+01	4.795E-01	4.795E+00	1.119E+01
1.500E+01	5.271E-01	5.271E+00	1.624E+01
2.000E+01	6.547E-01	6.547E+00	4.628E+01
2.300E+01	8.949E-01	8.949E+00	6.656E+01
2.800E+01	7.389E-01	7.389E+00	1.025E+02
3.000E+01	7.518E-01	7.518E+00	1.174E+02
6.000E+01	8.415E-01	8.415E+00	3.594E+02
1.000E+02	8.815E-01	8.815E+00	7.051E+02
3.000E+02	9.337E-01	9.337E+00	2.535E+03
6.000E+02	9.534E-01	9.534E+00	5.371E+03
1.000E+03	9.638E-01	9.638E+00	9.208E+03
3.000E+03	9.784E-01	9.784E+00	2.867E+04
6.000E+03	2.123E-02	2.123E-01	4.892E+04
1.000E+04	4.668E-03	4.668E-02	4.930E+04
3.000E+04	6.161E-04	6.161E-03	4.962E+04
6.000E+04	2.009E-04	2.009E-03	4.972E+04
1.000E+05	8.976E-05	8.976E-04	4.977E+04
3.000E+05	1.578E-05	1.578E-04	4.985E+04
6.000E+05	5.029E-06	5.029E-05	4.987E+04
1.000E+06	2.048E-06	2.048E-05	4.989E+04
3.000E+06	2.057E-07	2.057E-06	4.990E+04
6.000E+06	2.751E-08	2.751E-07	4.990E+04

Table 3-7b. Case 2 Results: Relative Concentration, Mass Flux, and Cumulative Mass Flux in the Fracture for Np-237 Over Time With Rock Matrix Retardation Factor R′ = 100 (Band Release Mode)

Time (yr)	Concentration A/A^{o}	Mass Flux F/A^{o} (m/yr)	Cumulative Mass Flux M/A^{o} (m)
1.000E+01	0.000E+00	0.000E+00	0.000E+00
1.500E+01	2.540E-10	2.540E-09	5.675E-10
2.000E+01	7.744E-06	7.744E-05	6.303E-05
2.100E+01	2.008E-05	2.008E-04	1.944E-04
2.230E+01	5.521E-05	5.521E-04	6.541E-04
2.500E+01	2.607E-04	2.607E-03	4.403E-03
3.000E+01	1.565E-03	1.565E-02	4.374E-02
6.000E+01	4.550E-02	4.550E-01	5.769E+00
1.000E+02	1.360E-01	1.360E+00	4.211E+01
3.000E+02	4.062E-01	4.062E+00	6.296E+02
6.000E+02	5.603E-01	5.603E+00	2.114E+03
1.000E+03	6.529E-01	6.529E+00	4.562E+03
3.000E+03	7.951E-01	7.951E+00	1.941E+04
6.000E+03	2.015E-01	2.015E+00	3.974E+04
1.000E+04	4.601E-02	4.601E-01	4.337E+04
3.000E+04	6.139E-03	6.139E-02	4.653E+04
6.000E+04	2.006E-03	2.006E-02	4.757E+04
1.000E+05	8.966E-04	8.966E-03	4.810E+04
3.000E+05	1.577E-04	1.577E-03	4.883E+04
6.000E+05	5.028E-05	5.028E-04	4.910E+04
1.000E+06	2.048E-05	2.048E-04	4.923E+04
3.000E+06	2.057E-06	2.057E-05	4.936E+04
6.000E+06	2.751E-07	2.751E-06	4.939E+04

Table 3-7c. Case 2 Results: Relative Concentration, Mass Flux, and Cumulative Mass Flux in the Fracture for Np-237 Over Time with Rock Matrix Retardation Factor R' = 10,000 (Band Release Mode)

Time (yr)	Concentration A/A^{o}	Mass Flux F/A^{o} (m/yr)	Cumulative Mass Flux M/A^{o} (m)
1.000E+02	2.982E-50	2.982E-49	2.347E-49
8.000E+02	4.864E-07	4.864E-06	2.565E-04
9.000E+02	2.132E-06	2.132E-05	1.401E-03
1.000E+03	6.966E-06	6.966E-05	5.567E-03
1.500E+03	2.485E-04	2.485E-03	4.147E-01
2.000E+03	1.522E-03	1.522E-02	4.217E+00
3.000E+03	9.692E-03	9.692E-02	5.354E+01
6.000E+03	6.752E-02	6.752E-01	1.134E+03
1.000E+04	1.114E-01	1.114E+00	5.079E+03
3.000E+04	4.272E-02	4.272E-01	1.957E+04
6.000E+04	1.688E-02	1.688E-01	2.755E+04
1.000E+05	8.100E-03	8.100E-02	3.220E+04
3.000E+05	1.525E-03	1.525E-02	3.905E+04
6.000E+05	4.946E-04	4.946E-03	4.184E+04
1.000E+06	2.028E-04	2.028E-03	4.291E+04
3.000E+06	2.050E-05	2.050E-04	4.428E+04
6.000E+06	2.746E-06	2.746E-05	4.453E+04

3.5.3 Case 3: Multiple Patch Source Subject to Step Release and Band Release

The two-dimensional solution restricted to the fracture plane was verified by means of a test example dealing with the transport of Cm-245 subject to a step and band release mode. The geometry of the source corresponds to an array of patch sources (11 in total) with an individual width of 5 meters and spaced at intervals of 5 meters. The list of parameters related to this case is given in Table 3-8. Test runs for four different times reported in Table 3-9 are in exact agreement with results predicted by MASCOT (see Gureghian, 1987) for the same input parameters. Note that the two-dimensional model in MASCOT simulates transport of a radionuclide decay chain in a fracture of unit thickness, whereby diffusion into the rock matrix is ignored.

Table 3-8. Input Parameters for Case 3

Species	Cm-245
Initial Concentration A^o (arbitrary unit of activity/L^3)	1
Type of Release Mode	Step and Band
Boundary Condition	Array of finite patch sources (total of 11)
Location	100.0 m downstream
y_1	100 m
d	5.0 m
Spacing Between Sources	5.0 m
u	10.0 m/yr
v	0 m/yr
D_{xx}	1,000 m^2/yr
D_{yy}	200 m^2/yr
D_{yx}	0.0 m^2/yr
D_p	0.0 m^2/yr
$T_{1/2}$	8,500 yr
T_L	10^5 yr
b	5×10^{-3} m yr
R	5,000
R'	1.0

Table 3-9. Case 3 Results: Relative Concentration in Fracture (A/A^o) for Cm-245

Lateral Distance (m)	Time			
	1.0×10^4 yr	5.0×10^4 yr	1.5×10^5 yr	2.0×10^5 yr
0.0	0.3004×10^{-5}	0.8548×10^{-4}	0.5897×10^{-7}	0.5568×10^{-9}
50.0	0.1083×10^{-2}	0.6852×10^{-3}	0.1358×10^{-6}	0.9476×10^{-9}
75.0	0.7469×10^{-2}	0.1687×10^{-2}	0.1835×10^{-6}	0.1443×10^{-8}
100.0	0.0237	0.3327×10^{-2}	0.2280×10^{-6}	0.1308×10^{-8}
125.0	0.0364	0.4678×10^{-2}	0.2600×10^{-6}	0.1419×10^{-8}
150.0	0.0393	0.5119×10^{-2}	0.2717×10^{-6}	0.1458×10^{-8}

Note: Values determined for this restricted case correspond exactly to values predicted by MASCOT (Gureghian, 1987) for the same input parameters.

3.5.4 Case 4: Two-Dimensional Transport of Tc-99 in Fracture and Rock Matrix

The results reported here illustrate the full application of the solutions dealing with the three types of concentration distribution at inlet, namely finite patch, multiple patch, and Gaussian distributed source, subject to a step and band release mode. The input parameters pertinent to these problems are reported in Table 3-10. Graphical interpretation of the numerical results yielded by the finite line and a Gaussian distributed source are reported in the form of concentration isopleths; these isopleths were generated using a bilinear interpolation scheme. The simulation times for all three test cases reported in the subsequent sections range between 2.5×10^4 and 5×10^4 years.

Case 4A - Finite Patch Source

Figures 3-5a (Step Release) and 3-5b (Band Release) show the relative concentration isopleths for Tc-99 in the fracture. Figures 3-5c and 3-5d give corresponding data at 1 m in the rock matrix, and Figures 3-5e and 3-5f at 5 m. The finite patch source is 50 m wide and centered at a distance of 350 m on the y-axis. Results indicate that the axis of symmetry of the plume follows to a reasonable approximation the same prescribed direction (northwest) of ground-water flow in the fracture plane. The area of the plume defined here by the relative concentration isopleth of 0.001 seems to decrease with increasing height. Tabulated results are given in Tables 3-11a, 3-11b, 3-11c, 3-11d, 3-11e, and 3-11f.

Table 3-10. Input Parameters Used in Simulation of Tc-99 in Fracture and Rock Matrix for Case 4

Boundary Type	Case 4A (FPS)	Case 4B (AFPS)	Case 4C (GDS)
u (m/yr)	2.	2.	2.
v (m/yr)	1.	0.	1.
a_L (m)	5	5	5
a_T (m)	2	2	2
D_p (m^2/yr)	10^{-2}	10^{-2}	10^{-2}
D_d (m^2/yr)	1.2×10^{-2}	1.2×10^{-2}	1.2×10^{-2}
τ	0.5	0.5	0.5
ϕ	10^{-2}	10^{-2}	10^{-2}
b (m)	5×10^{-3}	5×10^{-3}	5×10^{-3}
R	10	10	10
R′	100	100	100
T (yr)	10^4	--	10^4
$T_{1/2}$ (yr)	2.13×10^5	2.13×10^5	2.13×10^5
y_0 (m)	--	--	350
σ (m)	--	--	20
d (m)	50	10	--
y_1 (m)	350	100	--
y_2 (m)	--	200	--
y_3 (m)	--	300	--

Note: Initial concentration at the source A° (arbitrary unit of activity/L^3) = 1.

Key: FPS = Finite Patch Source
AFPS = Array of Finite Patch Sources
GDS = Gaussian Distributed Source

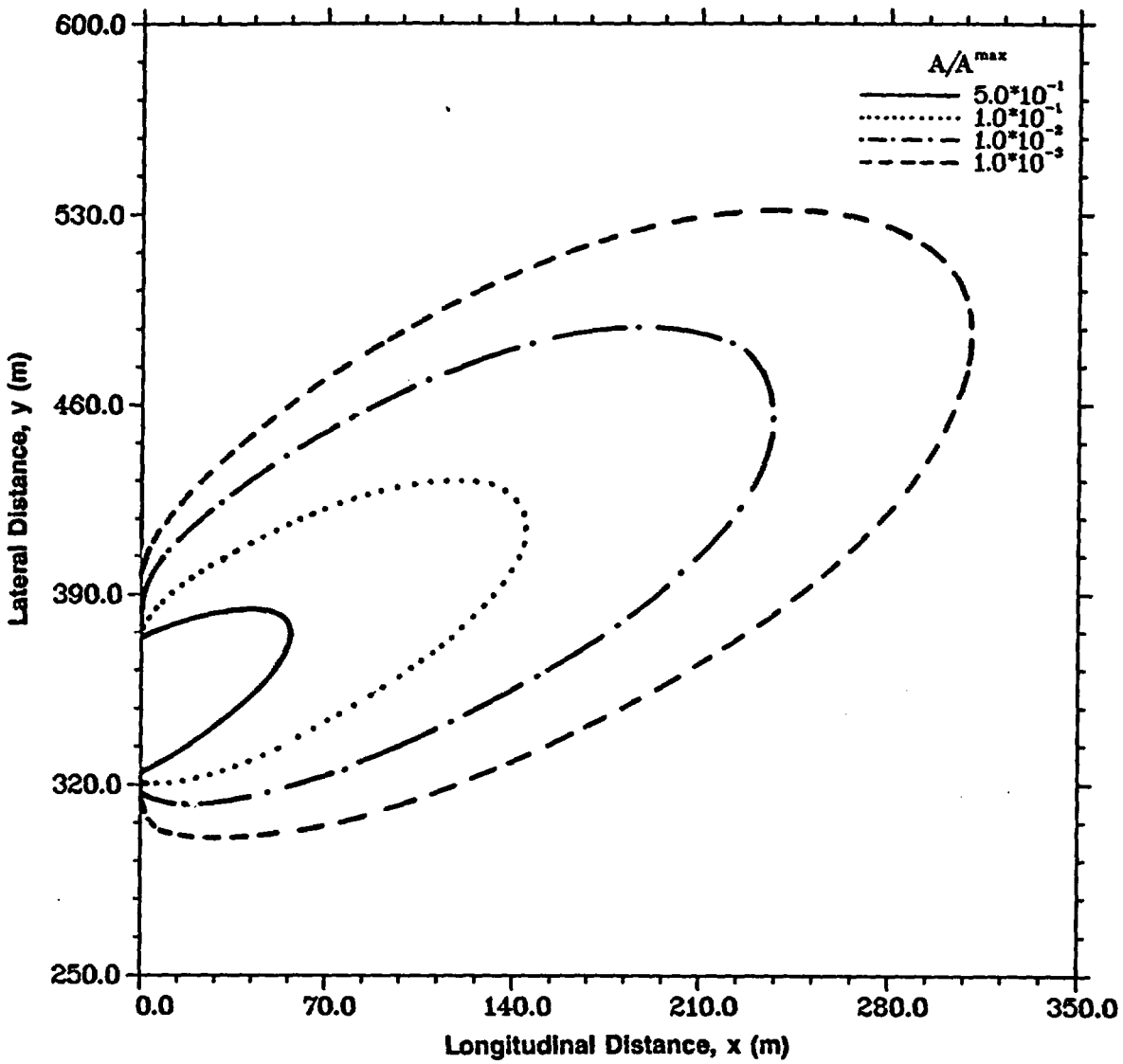

Figure 3-5a. Relative Concentration Isopleths for Tc-99 in the Fracture at z = 0 m and t = 5 x 10^3 yr, Step Release Mode (Case 4A: Finite Patch Source)

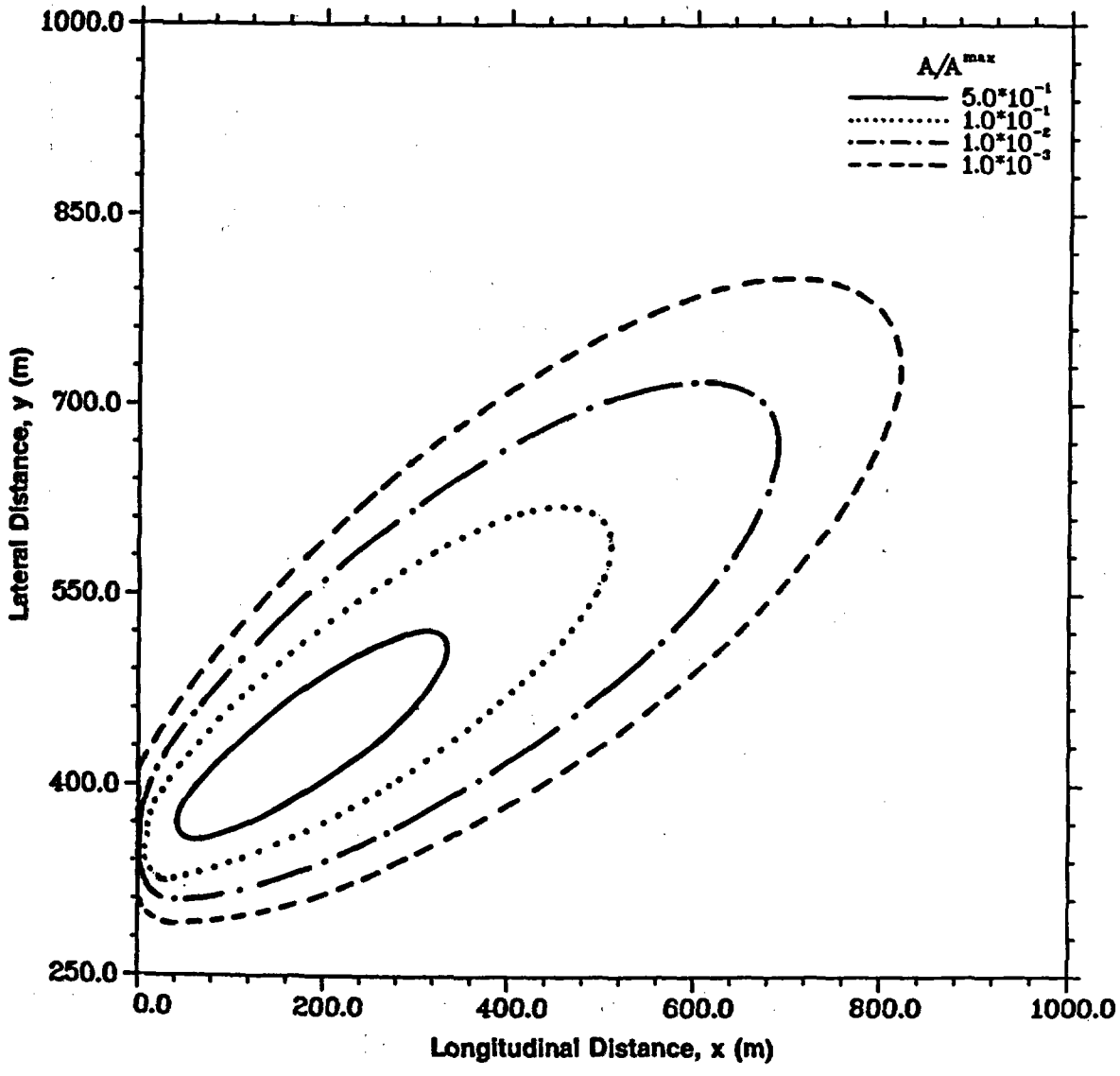

Figure 3-5b. Relative Concentration Isopleths for Tc-99 in the Fracture at z = 0 m and t = 2.5 × 10^4 yr, Band Release Mode (Case 4A: Finite Patch Source)

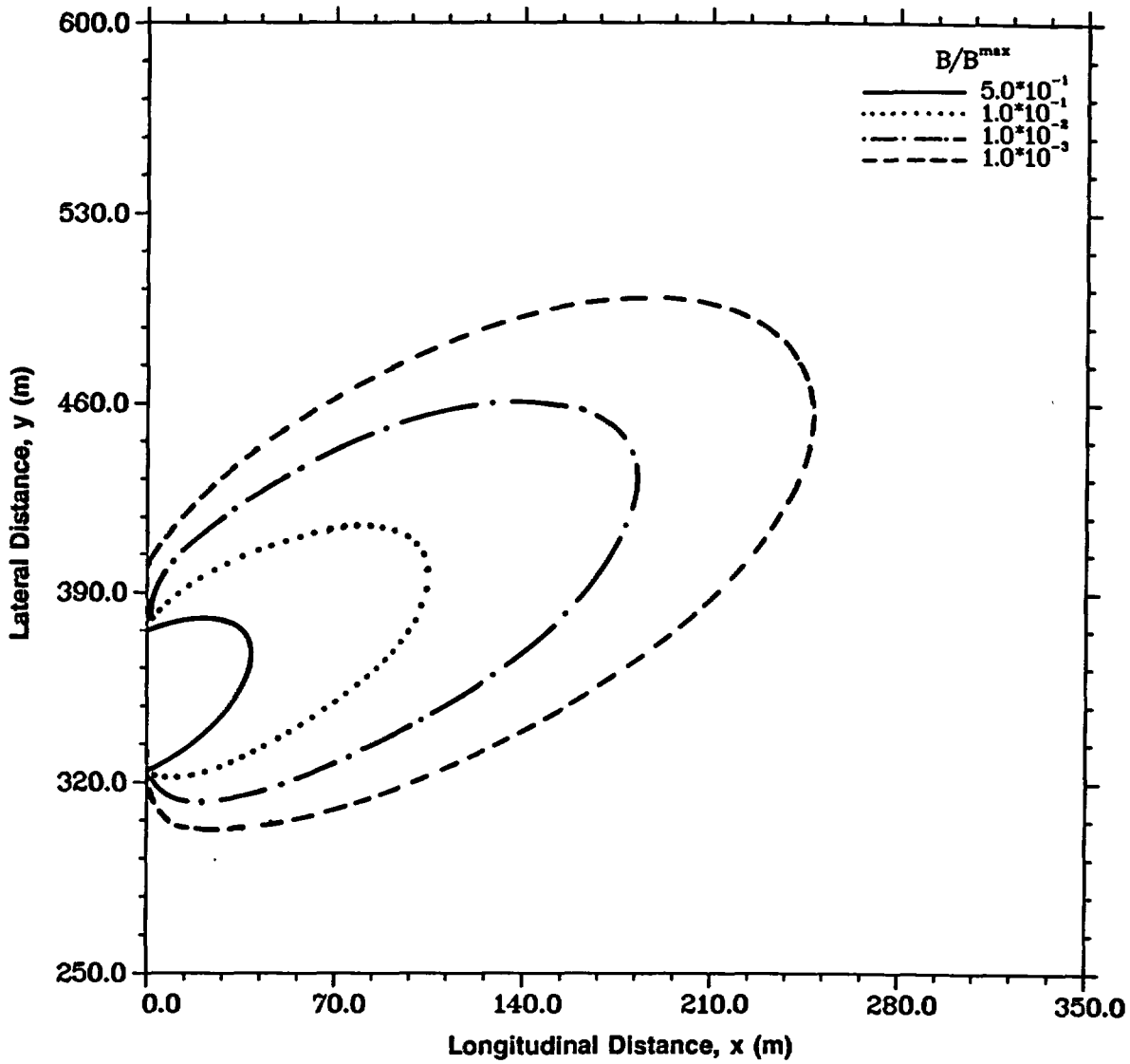

Figure 3-5c. Relative Concentration Isopleths for Tc-99 in the Rock Matrix at z = 1 m and t = 5 × 10^3 yr, Step Release Mode (Case 4A: Finite Patch Source)

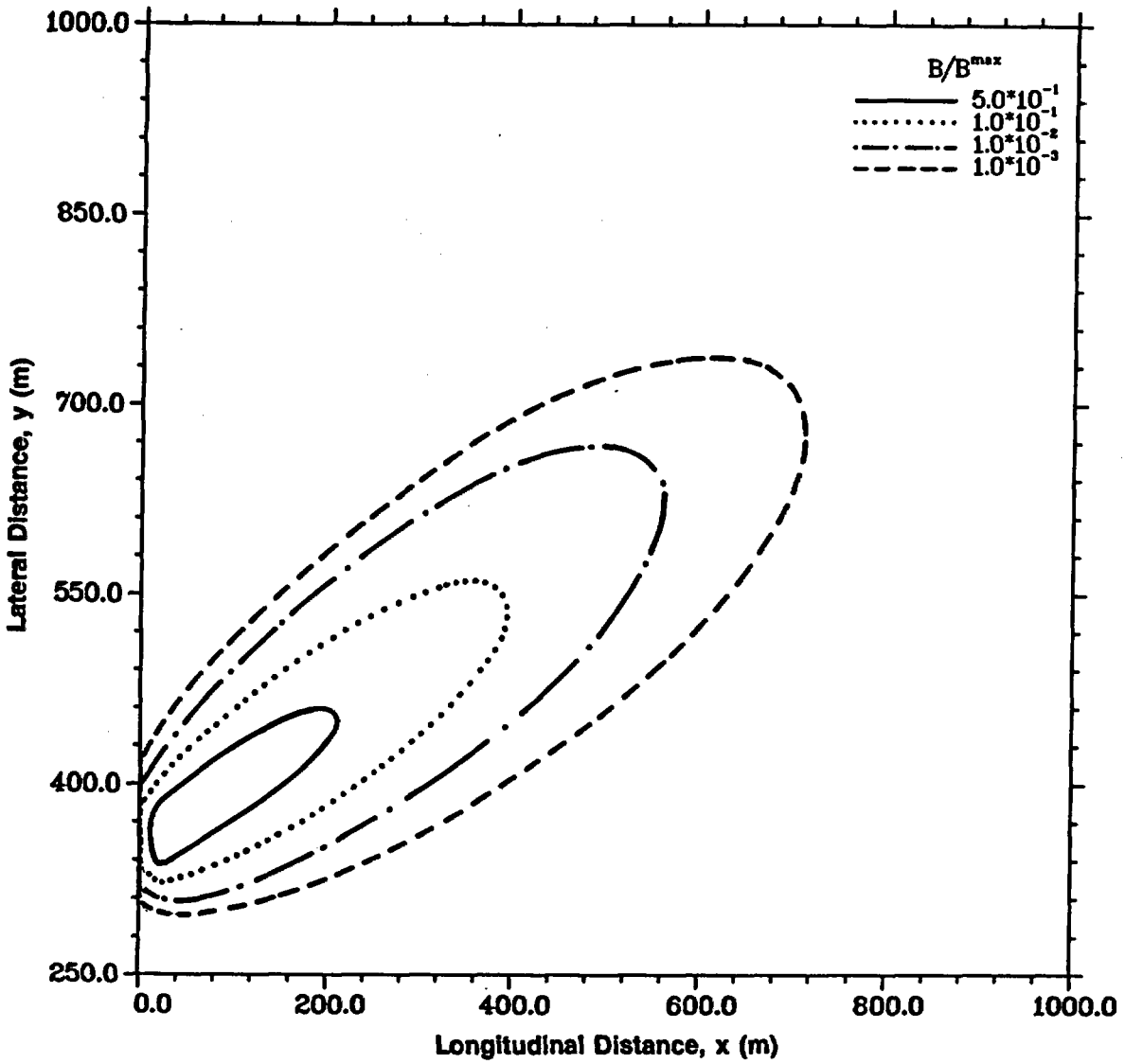

Figure 3-5d. Relative Concentration Isopleths for Tc-99 in the Rock Matrix at z = 1 m and t = 2.5 = 10^4 yr, Band Release Mode (Case 4A: Finite Patch Source)

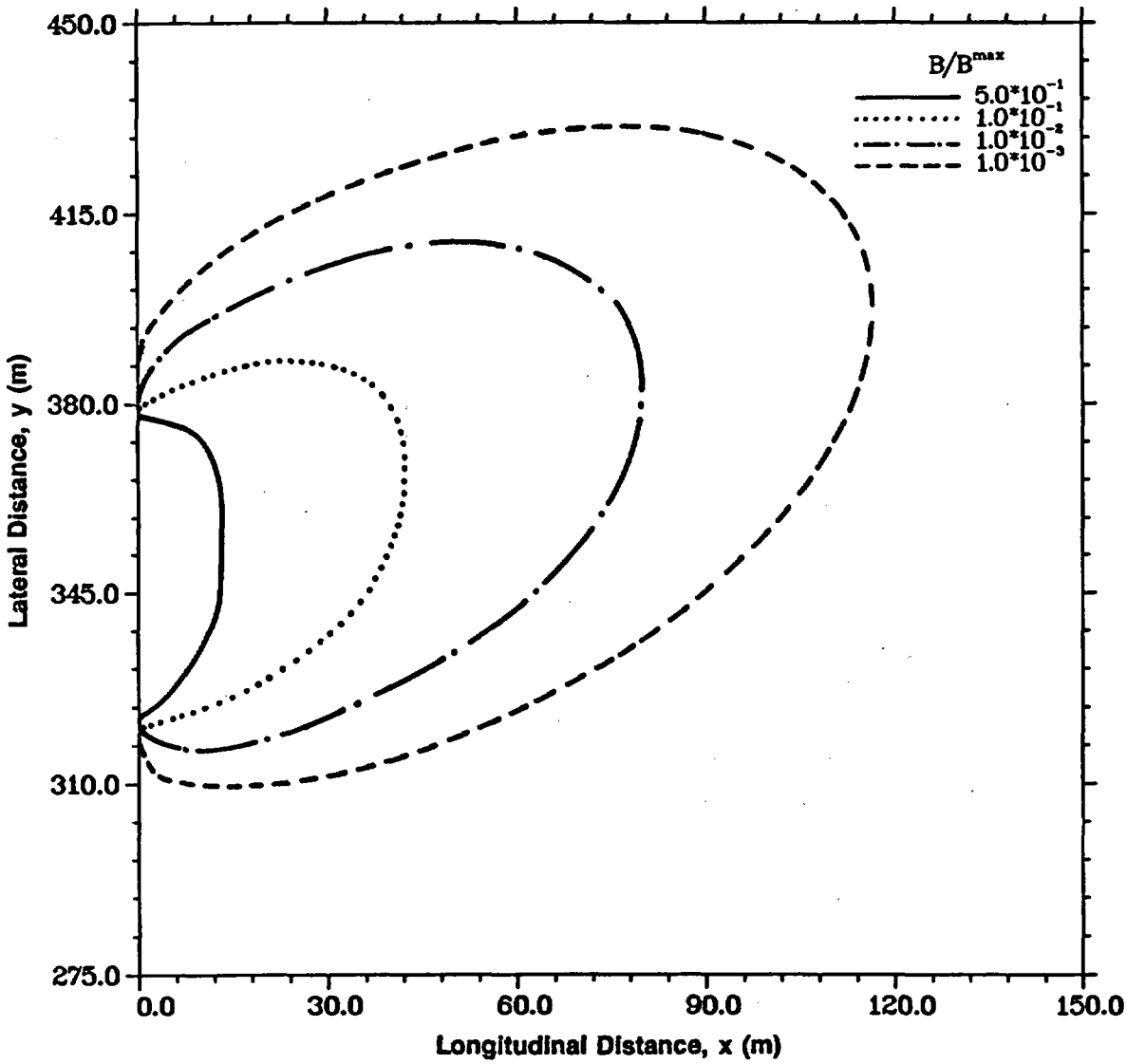

Figure 3-5e. Relative Concentration Isopleths for Tc-99 in the Rock Matrix at z = 5 m and t = 5 × 10³ yr, Step Release Mode (Case 4A: Finite Patch Source)

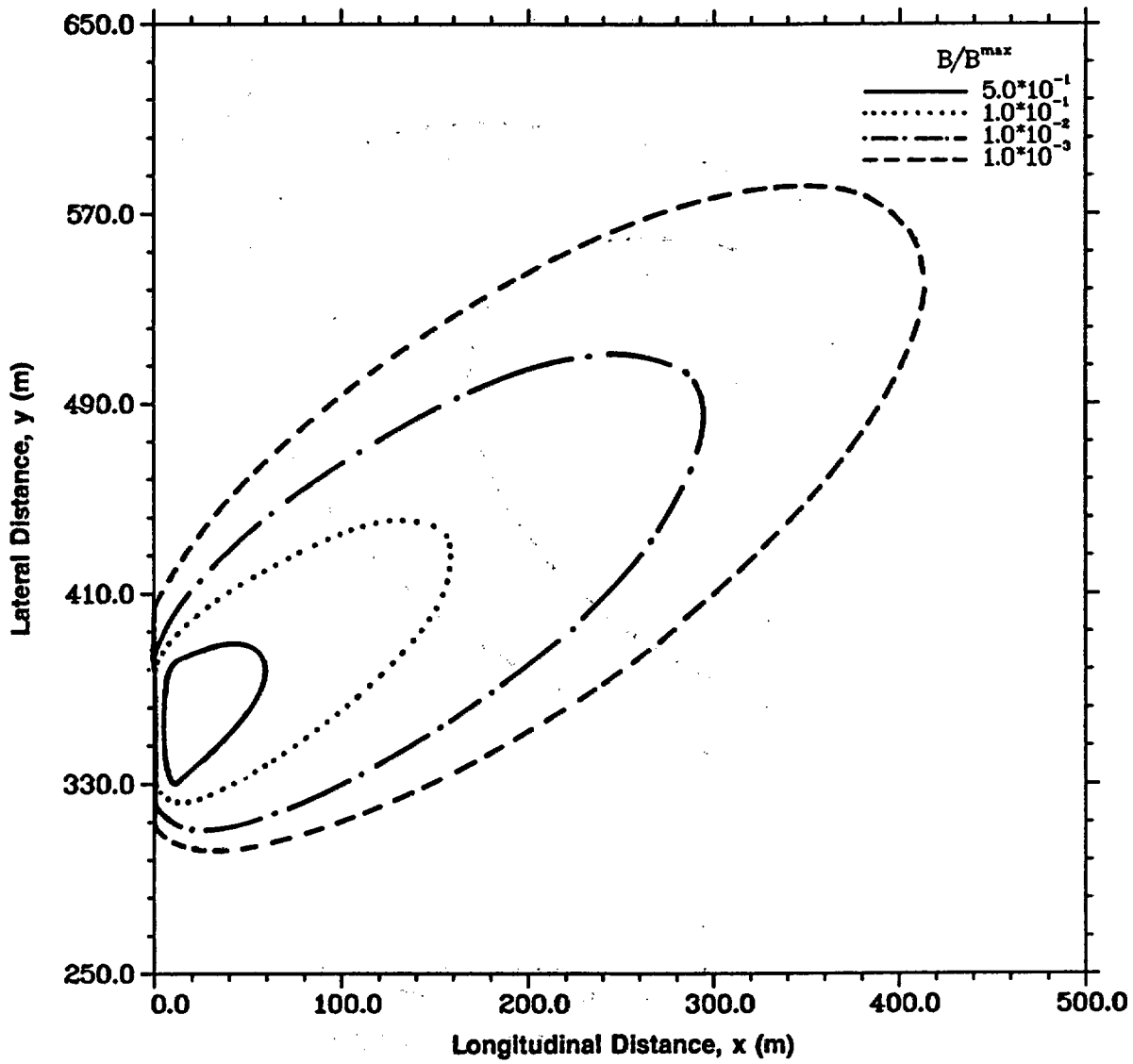

Figure 3-5f. Relative Concentration Isopleths for Tc-99 in the Rock Matrix at z = 5 m and t = 2.5 × 10^4 yr, Band Release Mode (Case 4A: Finite Patch Source)

Table 3-11a. Case 4A Results: Relative Concentration in the Fracture (A/A°) of Species Tc-99 at Time t = 5 x 10^3 yr and z = 0 m (Finite Patch Source, Step Release Mode)

Distance Along x-Axis (m)	Lateral Distance y (m)							
	250	300	350	400	450	500	550	600
0.0	0.00000E+00	0.00000E+00	0.98386E+00	0.00000E+00	0.00000E+00	0.00000E+00	0.00000E+00	0.00000E+00
50.0	0.12579E-07	0.44683E-03	0.33514E+00	0.26954E+00	0.18355E-02	0.28088E-05	0.26358E-08	0.16562E-11
100.0	0.97525E-08	0.98135E-04	0.46890E-01	0.23414E+00	0.30428E-01	0.26721E-03	0.62231E-06	0.68247E-09
150.0	0.25042E-08	0.12385E-04	0.51147E-02	0.73075E-01	0.50186E-01	0.26411E-02	0.21781E-04	0.55478E-07
200.0	0.34416E-09	0.11306E-05	0.45222E-03	0.12619E-01	0.25862E-01	0.53857E-02	0.16003E-03	0.11036E-05
250.0	0.30234E-10	0.78125E-07	0.31980E-04	0.14215E-02	0.65049E-02	0.37748E-02	0.34198E-03	0.64495E-05
300.0	0.18351E-11	0.41312E-08	0.17851E-05	0.11295E-03	0.96128E-03	0.12377E-02	0.28126E-03	0.13393E-04
350.0	0.79931E-13	0.16743E-09	0.77862E-07	0.65645E-05	0.91815E-04	0.22560E-03	0.10940E-03	0.11761E-04

Extracted data; complete data run is provided in microfiche form at the back of this report.

Table 3-11b. Case 4A Results: Relative Concentration in the Fracture (A/A°) of Species Tc-99 at Time t = 2.5 x 10^4 yr and z = 0 m (Finite Patch Source, Band Release Mode)

Distance Along x-Axis (m)	Lateral Distance y (m)								
	250	340	430	520	610	700	790	880	1000
0.0	0.00000E+00	0.00000E+00	0.00000E+00	0.00000E+00	0.00000E+00	0.00000E+00	0.00000E+00	0.00000E+00	0.00000E+00
100.0	0.12162E-07	0.48809E-02	0.33851E-01	0.54740E-04	0.57930E-08	0.25145E-12	0.65371E-17	0.11547E-21	0.32105E-28
200.0	0.40470E-08	0.42008E-03	0.55829E-01	0.95459E-02	0.19633E-04	0.43707E-08	0.30776E-12	0.10644E-16	0.55323E-23
300.0	0.39347E-09	0.23180E-04	0.11981E-01	0.35316E-01	0.14212E-02	0.28961E-05	0.93122E-09	0.93508E-13	0.13183E-18
400.0	0.20760E-10	0.92297E-06	0.10303E-02	0.18541E-01	0.73904E-02	0.13296E-03	0.24746E-06	0.95169E-10	0.50042E-15
500.0	0.72618E-12	0.27743E-07	0.51288E-04	0.31531E-02	0.69228E-02	0.80056E-03	0.83601E-05	0.13800E-07	0.33457E-12
600.0	0.18441E-13	0.64818E-09	0.17252E-05	0.25623E-03	0.20487E-02	0.10826E-02	0.53341E-04	0.36880E-06	0.45125E-10
700.0	0.35711E-15	0.12026E-10	0.42432E-07	0.12242E-04	0.26693E-03	0.48489E-03	0.91316E-04	0.23779E-05	0.14498E-08
800.0	0.54225E-17	0.17977E-12	0.79814E-09	0.38752E-06	0.18758E-04	0.93712E-04	0.55362E-04	0.47283E-05	0.13242E-07
900.0	0.65528E-19	0.21817E-14	0.11781E-10	0.87266E-08	0.80802E-06	0.93408E-05	0.14617E-04	0.35589E-05	0.40728E-07
1000.0	0.63461E-21	0.21551E-16	0.13833E-12	0.14591E-09	0.23164E-07	0.54197E-06	0.19533E-05	0.11926E-05	0.49040E-07

Extracted data; complete data run is provided in microfiche form at the back of this report.

Table 3-11c. Case 4A Results: Relative Concentration in the Rock Matrix (B/A°) of Species Tc-99 at Time t = 5 x 10^3 yr and z = 1 m (Finite Patch Source, Step Release Mode)

Distance Along x-Axis (m)	Lateral Distance y (m)							
	250	300	350	400	450	500	550	600
0.0	0.00000E+00	0.00000E+00	0.31458E+00	0.00000E+00	0.00000E+00	0.00000E+00	0.00000E+00	0.00000E+00
50.0	0.13977E-08	0.81458E-04	0.75550E-01	0.56706E-01	0.26329E-03	0.23440E-06	0.12132E-09	0.40865E-13
100.0	0.76290E-09	0.11877E-04	0.70738E-02	0.34394E-01	0.36552E-02	0.21137E-04	0.28992E-07	0.17722E-10
150.0	0.13004E-09	0.95871E-06	0.49666E-03	0.72388E-02	0.43991E-02	0.17267E-03	0.91879E-06	0.13856E-08
200.0	0.11464E-10	0.54775E-07	0.27616E-04	0.81839E-03	0.15529E-02	0.26336E-03	0.55379E-05	0.24306E-07
250.0	0.63203E-12	0.23345E-08	0.12089E-05	0.58835E-04	0.25883E-03	0.12955E-03	0.89786E-05	0.11596E-06
300.0	0.23716E-13	0.75332E-10	0.41290E-07	0.29271E-05	0.24757E-04	0.28653E-04	0.52900E-05	0.18439E-06
350.0	0.63173E-15	0.18483E-11	0.10925E-08	0.10504E-06	0.15022E-05	0.34308E-05	0.14150E-05	0.11786E-06

Extracted data; complete data run is provided in microfiche form at the back of this report.

Table 3-11d. Case 4A Results: Relative Concentration in the Rock Matrix (B/A°) of Species Tc-99 at Time t = 2.5 x 10^4 yr and z = 1 m (Finite Patch Source, Band Release Mode)

Distance Along x-Axis (m)	Lateral Distance y (m)								
	250	340	430	520	610	700	790	880	1000
0.0	0.00000E+00	0.00000E+00	0.00000E+00	0.00000E+00	0.00000E+00	0.00000E+00	0.00000E+00	0.00000E+00	0.00000E+00
100.0	0.11002E-07	0.67904E-02	0.43012E-01	0.44768E-04	0.31723E-08	0.98269E-13	0.19041E-17	0.25834E-22	0.51887E-29
200.0	0.25376E-08	0.33253E-03	0.45447E-01	0.65775E-02	0.10257E-04	0.17074E-08	0.91408E-13	0.24520E-17	0.92749E-24
300.0	0.18096E-09	0.12651E-04	0.69140E-02	0.19019E-01	0.64793E-03	0.10584E-05	0.26894E-09	0.21406E-13	0.22330E-19
400.0	0.72791E-11	0.37221E-06	0.44309E-03	0.77889E-02	0.28114E-02	0.43229E-04	0.66567E-07	0.20908E-10	0.83353E-16
500.0	0.19967E-12	0.86031E-08	0.16993E-04	0.10466E-02	0.21675E-02	0.22474E-03	0.20265E-05	0.28216E-08	0.53393E-13
600.0	0.40575E-14	0.15881E-09	0.45145E-06	0.68175E-04	0.52785E-03	0.25862E-03	0.11391E-04	0.68452E-07	0.67378E-11
700.0	0.63689E-16	0.23699E-11	0.89276E-08	0.26435E-05	0.56806E-04	0.97944E-04	0.16927E-04	0.39301E-06	0.19838E-09
800.0	0.78896E-18	0.28783E-13	0.13650E-09	0.68467E-07	0.33072E-05	0.15949E-04	0.88198E-05	0.68564E-06	0.16313E-08
900.0	0.77940E-20	0.28503E-15	0.16461E-11	0.12664E-08	0.11813E-06	0.13352E-05	0.19858E-05	0.44750E-06	0.44499E-08
1000.0	0.61695E-22	0.22995E-17	0.15811E-13	0.17401E-10	0.28045E-08	0.64817E-07	0.22476E-06	0.12878E-06	0.46928E-08

Extracted data; complete data run is provided in microfiche form at the back of this report.

Table 3-11e. Case 4A Results: Relative Concentration in the Rock Matrix (B/A°) of Species Tc-99 at Time t = 5 x 10^3 yr and z = 5 m (Finite Patch Source, Step Release Mode)

Distance Along x-Axis (m)	Lateral Distance y (m)							
	275	300	325	350	375	400	425	450
0.0	0.00000E+00	0.00000E+00	0.57886E-06	0.57886E-06	0.57886E-06	0.00000E+00	0.00000E+00	0.00000E+00
20.0	0.22878E-13	0.33048E-10	0.27753E-07	0.19452E-06	0.17304E-06	0.62845E-08	0.42301E-10	0.26916E-12
40.0	0.22503E-13	0.17438E-10	0.44602E-08	0.51896E-07	0.62159E-07	0.15087E-07	0.38552E-09	0.42240E-11
60.0	0.10969E-13	0.50788E-11	0.72979E-09	0.10976E-07	0.19826E-07	0.10491E-07	0.93927E-09	0.22851E-10
80.0	0.36502E-14	0.11440E-11	0.11788E-09	0.20439E-08	0.55327E-08	0.45305E-08	0.97816E-09	0.54480E-10
100.0	0.95304E-15	0.22272E-12	0.18574E-10	0.35290E-09	0.13431E-08	0.15439E-08	0.60145E-09	0.68955E-10
120.0	0.21001E-15	0.39253E-13	0.28376E-11	0.57622E-10	0.28812E-09	0.44823E-09	0.26538E-09	0.54418E-10
140.0	0.40724E-16	0.64054E-14	0.41881E-12	0.89673E-11	0.55755E-10	0.11406E-09	0.93575E-10	0.30330E-10

Extracted data; complete data run is provided in microfiche form at the back of this report.

Table 3-11f. Case 4A Results: Relative Concentration in the Rock Matrix (B/A°) of Species Tc-99 at Time t = 2.5 x 10^4 yr and z = 5 m (Finite Patch Source, Band Release Mode)

Distance Along x-Axis (m)	Lateral Distance y (m)								
	250	298	346	394	442	490	538	586	650
0.0	0.00000E+00	0.00000E+00	0.00000E+00	0.00000E+00	0.00000E+00	0.00000E+00	0.00000E+00	0.00000E+00	0.00000E+00
50.0	0.27986E-09	0.58028E-05	0.51103E-02	0.69345E-02	0.94709E-04	0.26464E-06	0.57627E-09	0.11487E-11	0.26113E-15
100.0	0.27039E-09	0.15229E-05	0.67305E-03	0.47028E-02	0.11116E-02	0.20386E-04	0.11431E-06	0.38879E-09	0.13561E-12
150.0	0.10098E-09	0.25872E-06	0.85627E-04	0.14870E-02	0.16073E-02	0.17217E-03	0.35230E-05	0.27905E-07	0.19888E-10
200.0	0.24046E-10	0.37367E-07	0.10633E-04	0.31564E-03	0.92323E-03	0.35670E-03	0.25512E-04	0.54184E-06	0.97498E-09
250.0	0.44211E-11	0.49024E-08	0.12772E-05	0.53435E-04	0.31789E-03	0.31334E-03	0.63699E-04	0.35558E-05	0.17846E-07
300.0	0.68515E-12	0.59811E-09	0.14760E-06	0.78328E-05	0.78609E-04	0.15856E-03	0.74645E-04	0.98699E-05	0.13796E-06
350.0	0.93621E-13	0.68556E-10	0.16353E-07	0.10347E-05	0.15432E-04	0.54743E-04	0.50849E-04	0.14083E-04	0.51333E-06
400.0	0.11569E-13	0.74193E-11	0.17335E-08	0.12578E-06	0.25543E-05	0.14265E-04	0.23175E-04	0.12023E-04	0.10406E-05
450.0	0.13124E-14	0.76007E-12	0.17555E-09	0.14230E-07	0.37003E-06	0.29939E-05	0.77553E-05	0.68685E-05	0.12797E-05
500.0	0.13800E-15	0.73811E-13	0.16962E-10	0.15087E-08	0.48050E-07	0.52875E-06	0.20309E-05	0.28468E-05	0.10426E-05

Extracted data; complete data run is provided in microfiche form at the back of this report.

Case 4B - Multiple Patch Source

Figures 3-6a, 3-6b, 3-6c, and 3-6d show the relative concentration, relative mass flux, magnitude and direction of mass flux, and cumulative mass flux profiles of Tc-99 at various distances x in the fracture. The figures depict stepwise release from three identical finite line sources 10 m wide and centered at 100 m, 200 m, and 300 m along the y-axis. The wave-like pattern, particularly at close distances from the source (denoting a relatively high concentration gradient in the transverse direction of the fracture), seems to be damped out at greater distances x. The impact of the lateral hydrodynamic dispersion mechanism on the migration process seems to manifest itself only at large distances from the source. Tabulated results are given in Tables 3-12a, 3-12b, 3-12c, and 3-12d.

Figures 3-6e, 3-6f, and 3-6g show the relative concentration profiles at different distances in the rock matrix. The shape of these curves is intimately related to the concentration profile in the fracture. This denotes that concentrations of Tc-99 (decreasing with the elevation z) are an immediate consequence of the diffusion mechanism, the sole process gearing the migration of the solute in the rock matrix. Results are given in Tables 3-12e, 3-12f, and 3-12g. Note that the superposition of the solution for a single line source has been adopted in this instance (see Equation 3-35).

Case 4C - Gaussian Distributed Source

Figures 3-7a (Step Release) and 3-7b (Band Release) show the relative concentration isopleths for Tc-99 in the fracture. Figures 3-7c and 3-7d give corresponding data at 1 m in the rock matrix, and Figures 3-7e and 3-7f at 5 m. The Gaussian source with a standard deviation of 20 is centered at a distance of 350 m on the y-axis. Conclusions very similar to the finite line source case may be drawn here, except the area of the plume is much larger; this is a consequence of the assumed concentration distribution at the source. Results are given in Tables 3-13a, 3-13b, 3-13c, 3-13d, 3-13e, and 3-13f.

Note: The maximum concentration in the fracture (A^{max}) and in the rock (B^{max}) is:

	z (m)	Case 4A		Case 4C	
		Step Release	Band Release	Step Release	Band Release
A^{max}	0.0	9.83681E-01	6.60038E-02	9.83861E-01	6.13422E-02
B^{max}	1.0	3.14576E-01	9.36598E-02	3.14576E-01	8.34140E-02
B^{max}	5.0	5.78862E-07	1.77803E-02	5.78862E-07	1.69540E-02

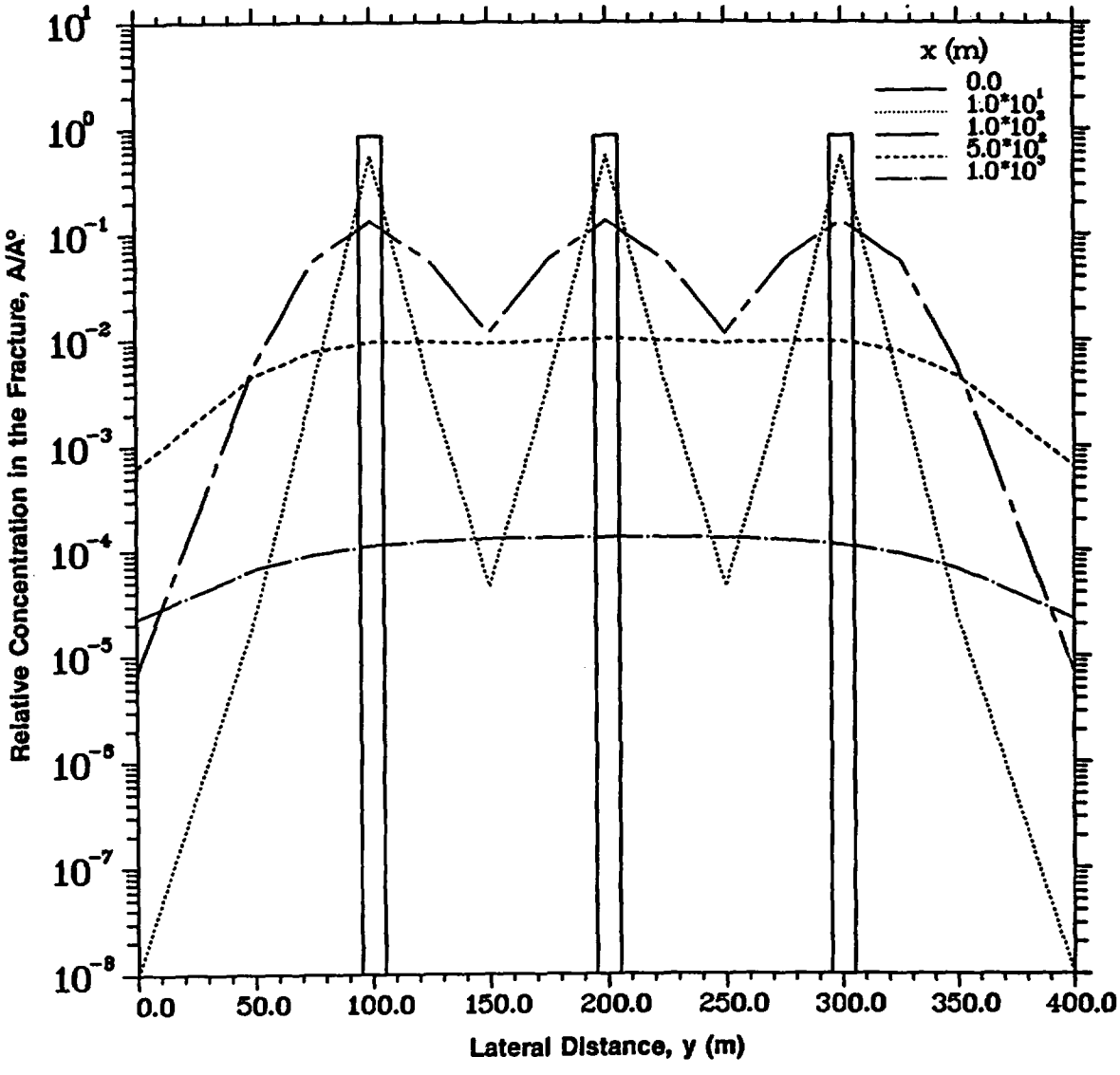

Figure 3-6a. Relative Concentration Profiles for Tc-99 in the Fracture at z = 0 m and t = 5 × 10⁴ yr (Case 4B: Multiple Patch Source)

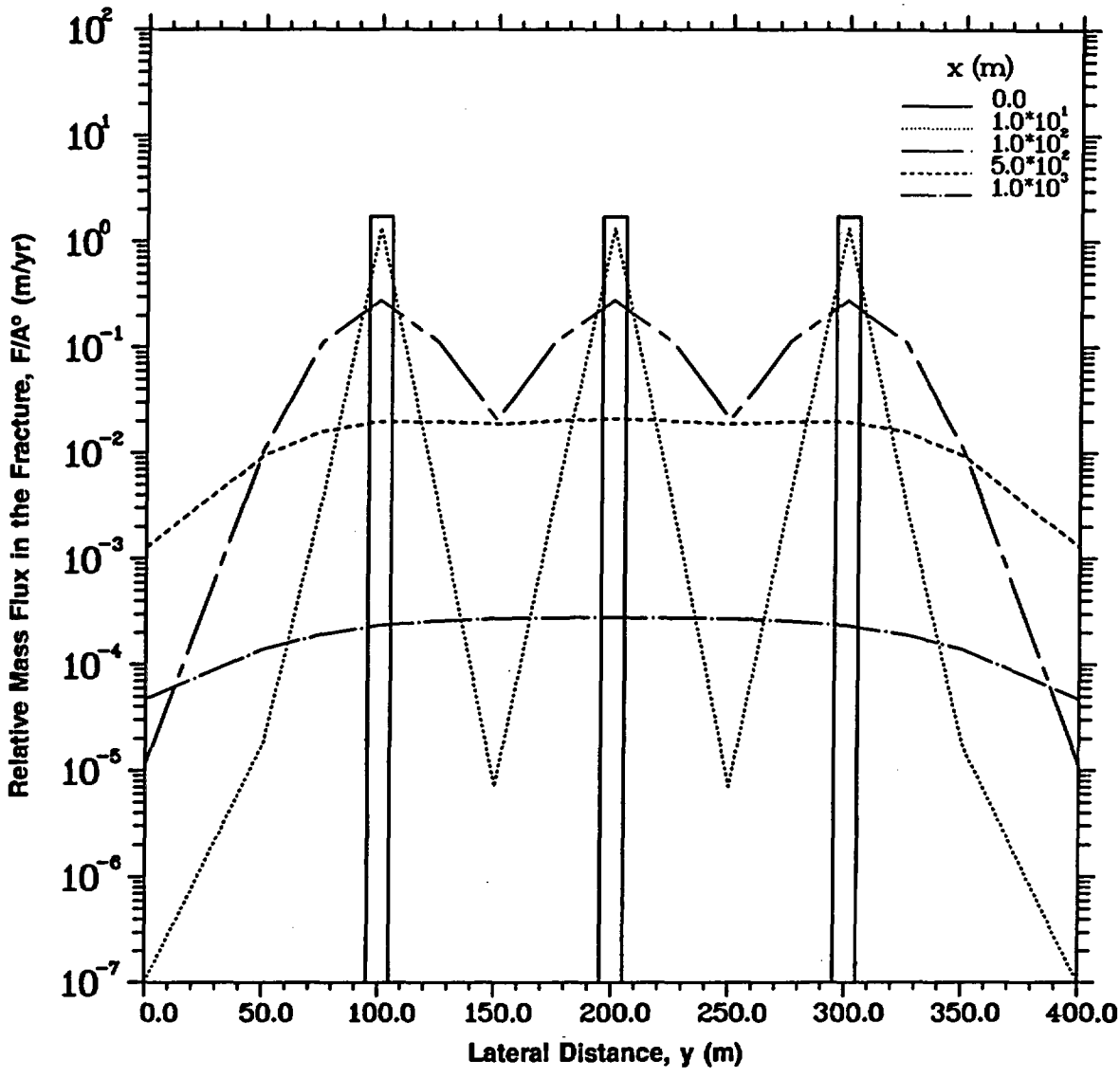

Figure 3-6b. Relative Mass Flux Profiles of Tc-99 in the Fracture at z = 0 m and t = 5 x 10^4 yr (Case 4B: Multiple Patch Source)

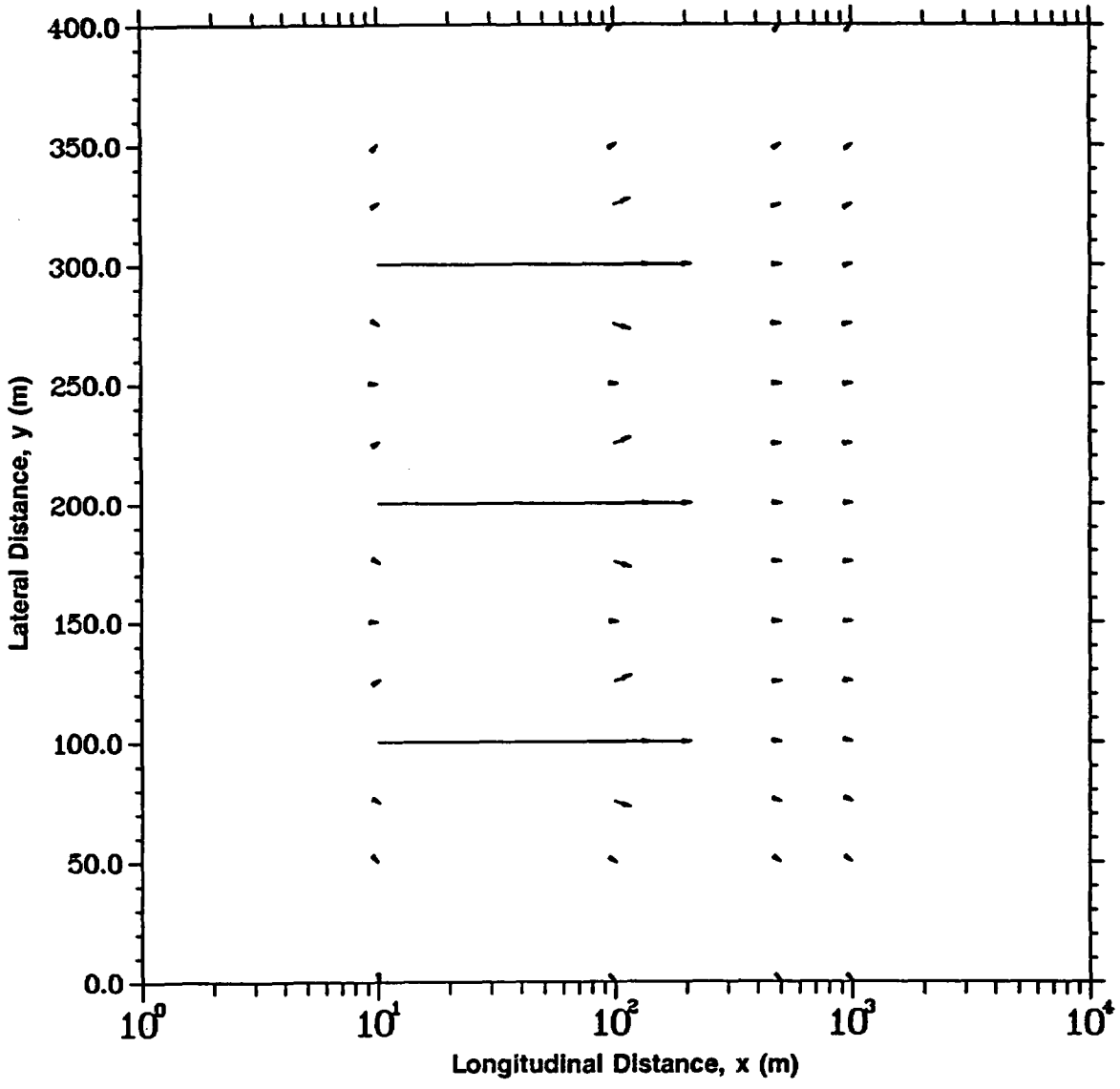

Figure 3-6c. Mass Flux Vector of Tc-99 at Discrete Points in the Fracture at z = 0 m and t = 5 × 10^4 yr (Case 4B: Multiple Patch Source)

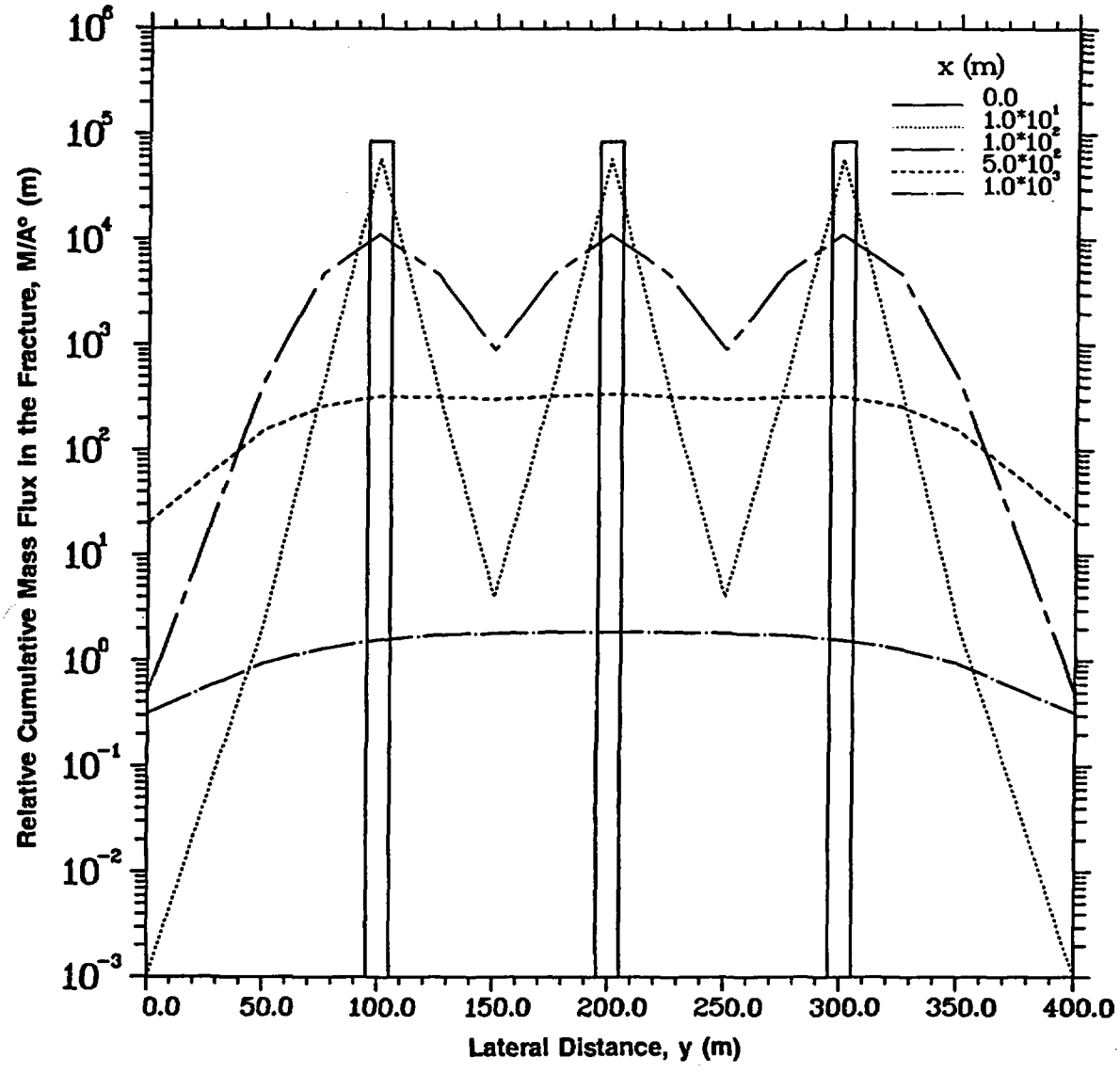

Figure 3-6d. Relative Cumulative Mass Flux of Tc-99 in the Fracture at z = 0 m and t = 5 × 10^4 yr (Case 4B: Multiple Patch Source)

Table 3-12a. Case 4B Results: Relative Concentration in the Fracture (A/A°) of Species Tc-99 at Time t = 5 x 10^4 yr (Multiple Patch Source, Step Release Mode)

Distance Along x-Axis (m)	Lateral Distance y (m)								
	0	50	75	100	125	150	175	200	225
0.0	0.00000E+00	0.00000E+00	0.00000E+00	0.84984E+00	0.00000E+00	0.00000E+00	0.00000E+00	0.84984E+00	0.00000E+00
10.0	0.22589E-08	0.22322E-04	0.36164E-02	0.54745E+00	0.36166E-02	0.44644E-04	0.36166E-02	0.54745E+00	0.36166E-02
100.0	0.69658E-05	0.56983E-02	0.55705E-01	0.13233E+00	0.55954E-01	0.11397E-01	0.55954E-01	0.13234E+00	0.55954E-01
500.0	0.62969E-03	0.45772E-02	0.76927E-02	0.95670E-02	0.95265E-02	0.91276E-02	0.96717E-02	0.10196E-01	0.96717E-02
1000.0	0.22405E-04	0.66408E-04	0.91350E-04	0.11092E-03	0.12283E-03	0.12882E-03	0.13167E-03	0.13258E-03	0.13167E-03

Distance Along x-Axis (m)	Lateral Distance y (m)					
	250	275	300	325	350	400
0.0	0.00000E+00	0.00000E+00	0.84984E+00	0.00000E+00	0.00000E+00	0.00000E+00
10.0	0.44644E-04	0.36166E-02	0.54745E+00	0.36164E-02	0.22322E-04	0.22589E-08
100.0	0.11397E-01	0.55954E-01	0.13233E+00	0.55705E-01	0.56983E-02	0.69658E-05
500.0	0.91276E-02	0.95265E-02	0.95670E-02	0.76927E-02	0.45772E-02	0.62969E-03
1000.0	0.12882E-03	0.12283E-03	0.11092E-03	0.91350E-04	0.66408E-04	0.22405E-04

Table 3-12b. Case 4B Results: X-Component of Relative Mass Flux in the Fracture ($F_x/A°$) (m/yr) of Species Tc-99 at Time t = 5 x 10^4 yr (Multiple Patch Source, Step Release Mode)

Distance Along x-Axis (m)	Lateral Distance y (m)								
	0	50	75	100	125	150	175	200	225
0.0	0.00000E+00	0.00000E+00	0.00000E+00	0.16997E+01	0.00000E+00	0.00000E+00	0.00000E+00	0.16997E+01	0.00000E+00
10.0	0.16273E-09	0.35515E-05	0.13841E-02	0.13279E+01	0.13841E-02	0.71030E-05	0.13841E-02	0.13279E+01	0.13841E-02
100.0	0.10477E-04	0.10326E-01	0.11116E+00	0.27572E+00	0.11156E+00	0.20651E-01	0.11156E+00	0.27573E+00	0.11156E+00
500.0	0.12741E-02	0.94271E-02	0.15913E-01	0.19803E-01	0.19668E-01	0.18801E-01	0.19958E-01	0.21076E-01	0.19958E-01
1000.0	0.47049E-04	0.14002E-03	0.19277E-03	0.23411E-03	0.25917E-03	0.27172E-03	0.27769E-03	0.27962E-03	0.27769E-03

Distance Along x-Axis (m)	Lateral Distance y (m)					
	250	275	300	325	350	400
0.0	0.00000E+00	0.00000E+00	0.16997E+01	0.00000E+00	0.00000E+00	0.00000E+00
10.0	0.71030E-05	0.13841E-02	0.13279E+01	0.13841E-02	0.35515E-05	0.16273E-09
100.0	0.20651E-01	0.11156E+00	0.27572E+00	0.11116E+00	0.10326E-01	0.10477E-04
500.0	0.18801E-01	0.19668E-01	0.19803E-01	0.15913E-01	0.94271E-02	0.12741E-02
1000.0	0.27172E-03	0.25917E-03	0.23411E-03	0.19277E-03	0.14002E-03	0.47049E-04

Table 3-12c. Case 4B Results: Y-Component of Relative Mass Flux in the Fracture (F_y/A^*) (m/yr) of Species Tc-99 at Time t = 5 x 10^4 yr (Multiple Patch Source, Step Release Mode)

Distance Along x-Axis (m)	Lateral Distance y (m)								
	0	50	75	100	125	150	175	200	225
0.0	0.00000E+00	0.00000E+00	0.00000E+00	0.00000E+00	0.00000E+00	0.00000E+00	0.00000E+00	0.00000E+00	0.00000E+00
10.0	-0.16164E-08	-0.17229E-04	-0.31871E-02	-0.16164E-08	0.31870E-02	-0.23525E-12	-0.31870E-02	0.00000E+00	0.31870E-02
100.0	-0.41551E-05	-0.25476E-02	-0.14886E-01	-0.41551E-05	0.14750E-01	-0.18757E-08	-0.14750E-01	0.00000E+00	0.14750E-01
500.0	-0.13090E-03	-0.49718E-03	-0.44698E-03	-0.13090E-03	0.93412E-04	-0.79211E-05	-0.13242E-03	0.00000E+00	0.13242E-03
1000.0	-0.25210E-05	-0.41419E-05	-0.36888E-05	-0.25209E-05	-0.13525E-05	-0.64885E-06	-0.29289E-06	0.00000E+00	0.29289E-06

Distance Along x-Axis (m)	Lateral Distance y (m)					
	250	275	300	325	350	400
0.0	0.00000E+00	0.00000E+00	0.00000E+00	0.00000E+00	0.00000E+00	0.00000E+00
10.0	0.23525E-12	-0.31870E-02	0.16164E-08	0.31871E-02	0.17229E-04	0.16164E-08
100.0	0.18757E-08	-0.14750E-01	0.41551E-05	0.14886E-01	0.25476E-02	0.41551E-05
500.0	0.79211E-05	-0.93412E-04	0.13090E-03	0.44698E-03	0.49718E-03	0.13090E-03
1000.0	0.64885E-06	0.13525E-05	0.25209E-05	0.36888E-05	0.41419E-05	0.25210E-05

Table 3-12d. Case 4B Results: Relative Cumulative Mass Flux in the Fracture (M/A°) of Species Tc-99 at Time t = 5 x 10^4 yr (Multiple Patch Source, Step Release Mode)

Distance Along x-Axis (m)	Lateral Distance y (m)								
	0	50	75	100	125	150	175	200	225
0.0	0.00000E+00	0.00000E+00	0.00000E+00	0.84984E+05	0.00000E+00	0.00000E+00	0.00000E+00	0.84984E+05	0.00000E+00
10.0	0.17748E-03	0.21667E+01	0.39886E+03	0.58232E+05	0.39887E+03	0.40058E+01	0.39887E+03	0.58232E+05	0.39887E+03
100.0	0.49956E+00	0.46355E+03	0.46768E+04	0.11201E+05	0.46947E+04	0.90234E+03	0.46947E+04	0.11202E+05	0.46947E+04
500.0	0.20545E+02	0.15410E+03	0.26090E+03	0.32476E+03	0.32175E+03	0.30691E+03	0.32635E+03	0.34516E+03	0.32635E+03
1000.0	0.31547E+00	0.94562E+00	0.13037E+01	0.15834E+01	0.17518E+01	0.18353E+01	0.18752E+01	0.18883E+01	0.18752E+01

Distance Along x-Axis (m)	Lateral Distance y (m)					
	250	275	300	325	350	400
0.0	0.00000E+00	0.00000E+00	0.84984E+05	0.00000E+00	0.00000E+00	0.00000E+00
10.0	0.40058E+01	0.39887E+03	0.58232E+05	0.39886E+03	0.21667E+01	0.17748E-03
100.0	0.90234E+03	0.46947E+04	0.11201E+05	0.46768E+04	0.46355E+03	0.49956E+00
500.0	0.30691E+03	0.32175E+03	0.32476E+03	0.26090E+03	0.15410E+03	0.20545E+02
1000.0	0.18353E+01	0.17518E+01	0.15834E+01	0.13037E+01	0.94562E+00	0.31547E+00

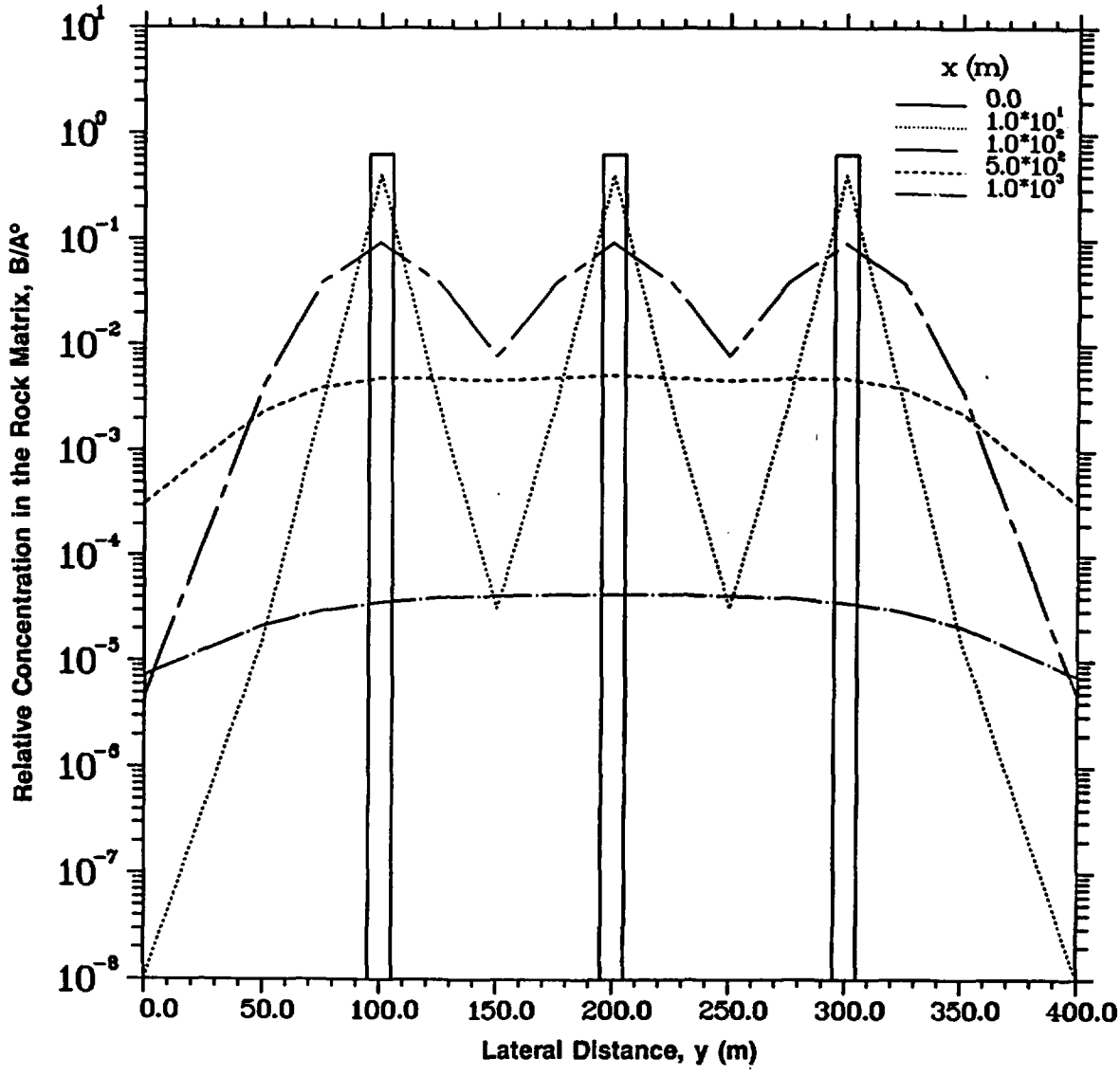

Figure 3-6e. Relative Concentration Profiles for Tc-99 in the Rock Matrix at z = 1 m and t = 5 × 10⁴ yr (Case 4B: Multiple Patch Source)

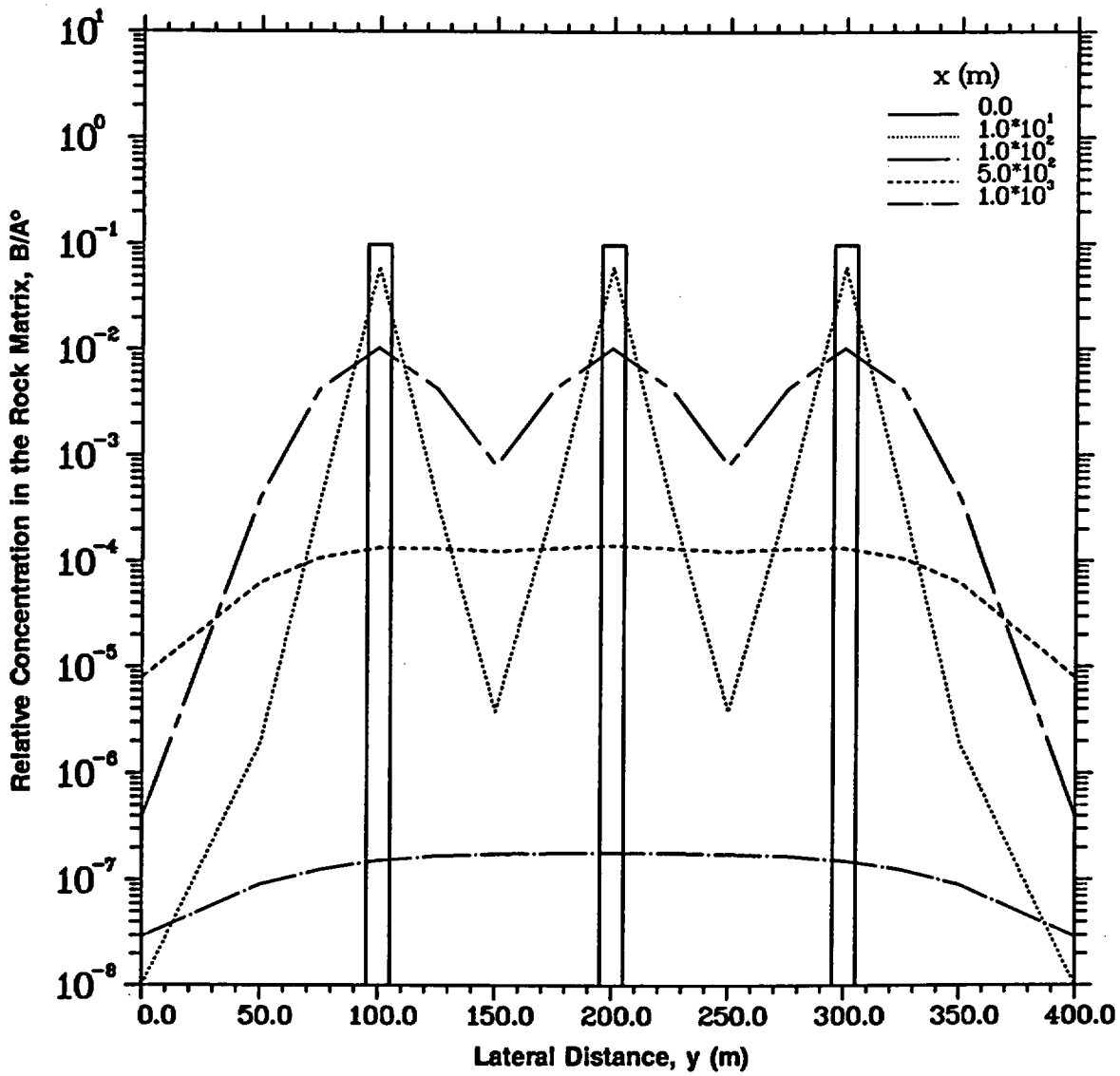

Figure 3-6f. Relative Concentration Profiles for Tc-99 in the Rock Matrix at z = 5 m and t = 5 × 10⁴ yr (Case 4B: Multiple Patch Source)

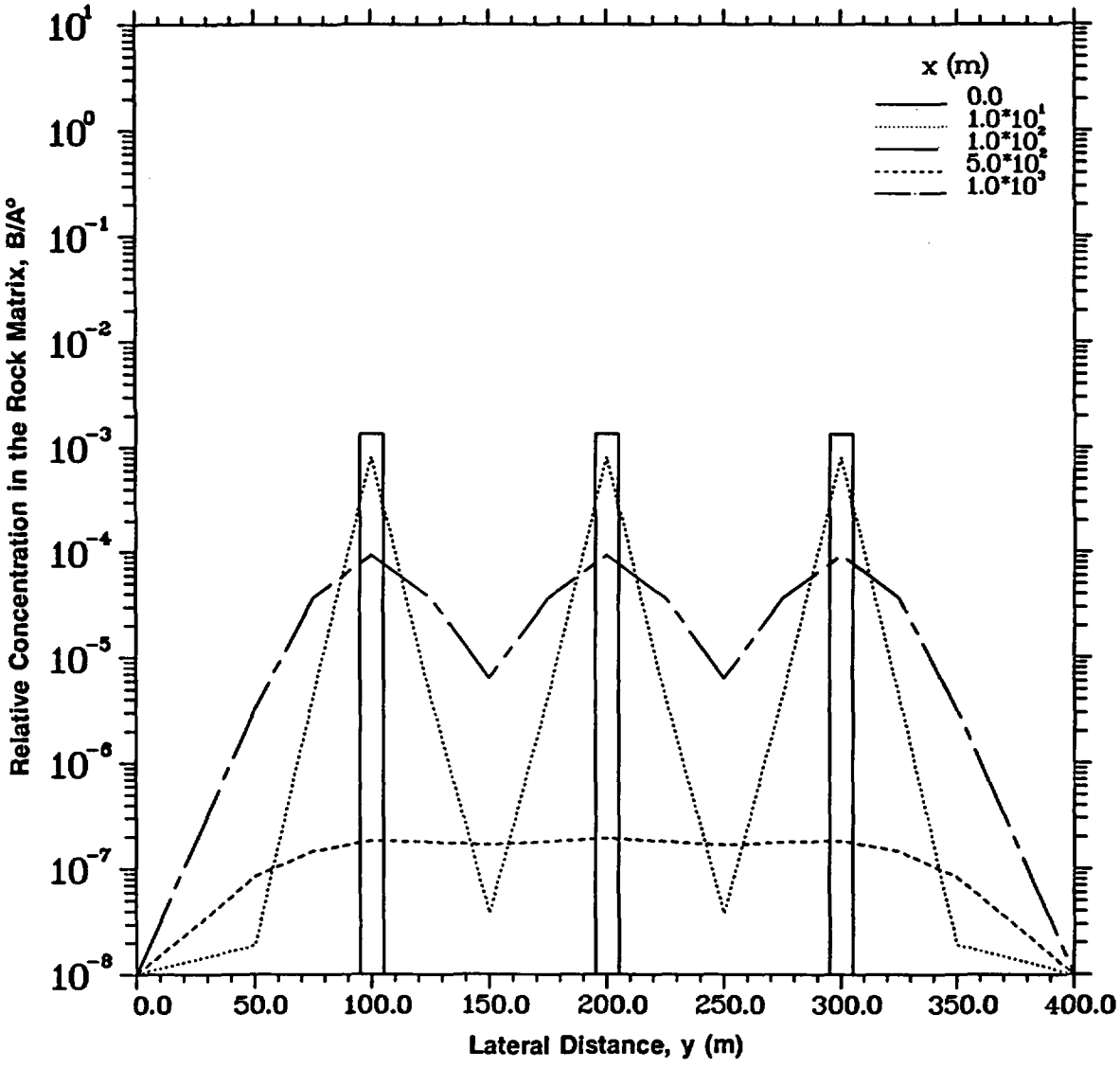

Figure 3-6g. Relative Concentration Profiles for Tc-99 in the Rock Matrix at z = 10 m and t = 5 × 10⁴ yr (Case 4B: Multiple Patch Source)

Table 3-12e. Case 4B Results: Relative Concentration in the Rock Matrix (B/A°) of Species Tc-99 at Time t = 5 x 10^4 yr and z = 1 m (Multiple Patch Source, Step Release Mode)

Distance Along x-Axis (m)	Lateral Distance y (m)								
	0	50	75	100	125	150	175	200	225
0.0	0.00000E+00	0.00000E+00	0.00000E+00	0.63995E+00	0.00000E+00	0.00000E+00	0.00000E+00	0.63995E+00	0.00000E+00
10.0	0.15277E-08	0.15988E-04	0.26612E-02	0.41011E+00	0.26613E-02	0.31976E-04	0.26613E-02	0.41011E+00	0.26613E-02
100.0	0.46080E-05	0.39390E-02	0.39052E-01	0.93251E-01	0.39221E-01	0.78780E-02	0.39221E-01	0.93256E-01	0.39221E-01
500.0	0.31534E-03	0.23278E-02	0.39265E-02	0.48858E-02	0.48546E-02	0.46425E-02	0.49265E-02	0.52008E-02	0.49265E-02
1000.0	0.72023E-05	0.21516E-04	0.29643E-04	0.36004E-04	0.39848E-04	0.41765E-04	0.42678E-04	0.42975E-04	0.42678E-04

Distance Along x-Axis (m)	Lateral Distance y (m)					
	250	275	300	325	350	400
0.0	0.00000E+00	0.00000E+00	0.63995E+00	0.00000E+00	0.00000E+00	0.00000E+00
10.0	0.31976E-04	0.26613E-02	0.41011E+00	0.26612E-02	0.15988E-04	0.15277E-08
100.0	0.78780E-02	0.39221E-01	0.93251E-01	0.39052E-01	0.39390E-02	0.46080E-05
500.0	0.46425E-02	0.48546E-02	0.48858E-02	0.39265E-02	0.23278E-02	0.31534E-03
1000.0	0.41765E-04	0.39848E-04	0.36004E-04	0.29643E-04	0.21516E-04	0.72023E-05

Table 3-12f. Case 4B Results: Relative Concentration in the Rock Matrix (B/A°) of Species Tc-99 at Time t = 5 x 10^4 yr and z = 5 m (Multiple Patch Source, Step Release Mode)

Distance Along x-Axis (m)	Lateral Distance y (m)								
	0	50	75	100	125	150	175	200	225
0.0	0.00000E+00	0.00000E+00	0.00000E+00	0.97058E-01	0.00000E+00	0.00000E+00	0.00000E+00	0.97058E-01	0.00000E+00
10.0	0.14128E-09	0.19188E-05	0.36208E-03	0.60685E-01	0.36210E-03	0.38376E-05	0.36210E-03	0.60685E-01	0.36210E-03
100.0	0.38599E-06	0.40198E-03	0.42483E-02	0.10386E-01	0.42640E-02	0.80396E-03	0.42640E-02	0.10387E-01	0.42640E-02
500.0	0.79661E-05	0.62754E-04	0.10749E-03	0.13408E-03	0.13200E-03	0.12521E-03	0.13374E-03	0.14204E-03	0.13374E-03
1000.0	0.29117E-07	0.89822E-07	0.12456E-06	0.15144E-06	0.16721E-06	0.17481E-06	0.17848E-06	0.17974E-06	0.17848E-06

Distance Along x-Axis (m)	Lateral Distance y (m)					
	250	275	300	325	350	400
0.0	0.00000E+00	0.00000E+00	0.97058E-01	0.00000E+00	0.00000E+00	0.00000E+00
10.0	0.38376E-05	0.36210E-03	0.60685E-01	0.36208E-03	0.19188E-05	0.14128E-09
100.0	0.80396E-03	0.42640E-02	0.10386E-01	0.42483E-02	0.40198E-03	0.38599E-06
500.0	0.12521E-03	0.13200E-03	0.13408E-03	0.10749E-03	0.62754E-04	0.79661E-05
1000.0	0.17481E-06	0.16721E-06	0.15144E-06	0.12456E-06	0.89822E-07	0.29117E-07

Table 3-12g. Case 4B Results: Relative Concentration in the Rock Matrix (B/A°) of Species Tc-99 at Time t = 5 x 10^4 yr and z = 10 m (Multiple Patch Source, Step Release Mode)

Distance Along x-Axis (m)	Lateral Distance y (m)								
	0	50	75	100	125	150	175	200	225
0.0	0.00000E+00	0.00000E+00	0.00000E+00	0.13376E-02	0.00000E+00	0.00000E+00	0.00000E+00	0.13376E-02	0.00000E+00
10.0	0.97461E-12	0.18991E-07	0.42751E-05	0.80714E-03	0.42752E-05	0.37982E-07	0.42752E-05	0.80714E-03	0.42752E-05
100.0	0.23254E-08	0.31752E-05	0.36657E-04	0.92602E-04	0.36767E-04	0.63503E-05	0.36767E-04	0.92604E-04	0.36767E-04
500.0	0.97542E-08	0.83654E-07	0.14622E-06	0.18303E-06	0.17800E-06	0.16699E-06	0.18000E-06	0.19277E-06	0.18000E-06
1000.0	0.33840E-11	0.10878E-10	0.15211E-10	0.18514E-10	0.20377E-10	0.21234E-10	0.21662E-10	0.21819E-10	0.21662E-10

Distance Along x-Axis (m)	Lateral Distance y (m)					
	250	275	300	325	350	400
0.0	0.00000E+00	0.00000E+00	0.13376E-02	0.00000E+00	0.00000E+00	0.00000E+00
10.0	0.37982E-07	0.42752E-05	0.80714E-03	0.42751E-05	0.18991E-07	0.97461E-12
100.0	0.63503E-05	0.36767E-04	0.92602E-04	0.36657E-04	0.31752E-05	0.23254E-08
500.0	0.16699E-06	0.17800E-06	0.18303E-06	0.14622E-06	0.83654E-07	0.97542E-08
1000.0	0.21234E-10	0.20377E-10	0.18514E-10	0.15211E-10	0.10878E-10	0.33840E-11

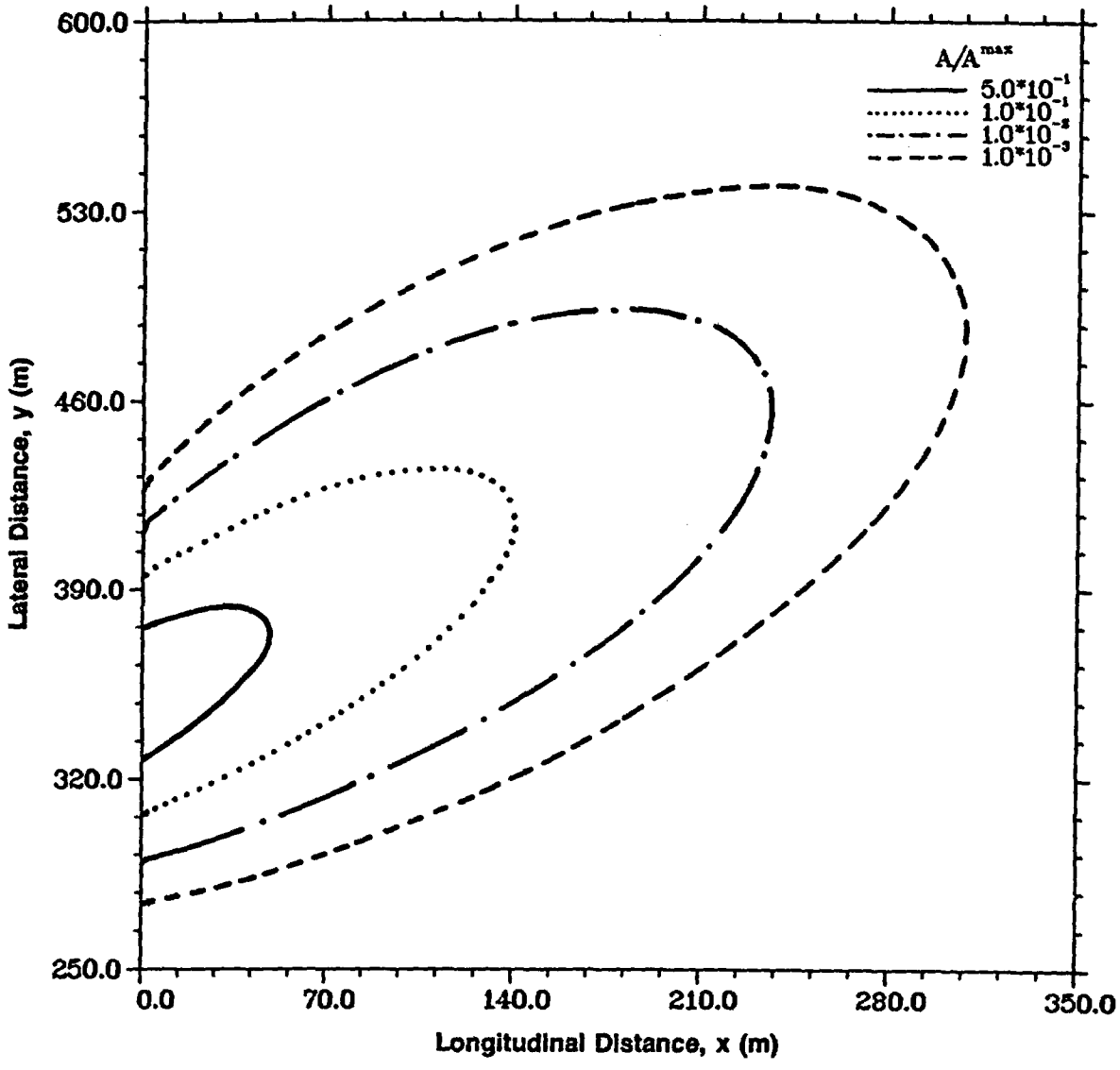

Figure 3-7a. Relative Concentration Isopleths for Tc-99 in the Fracture at z = 0 m and t = 5 × 10³ yr, Step Release Mode (Case 4C: Gaussian Distributed Source)

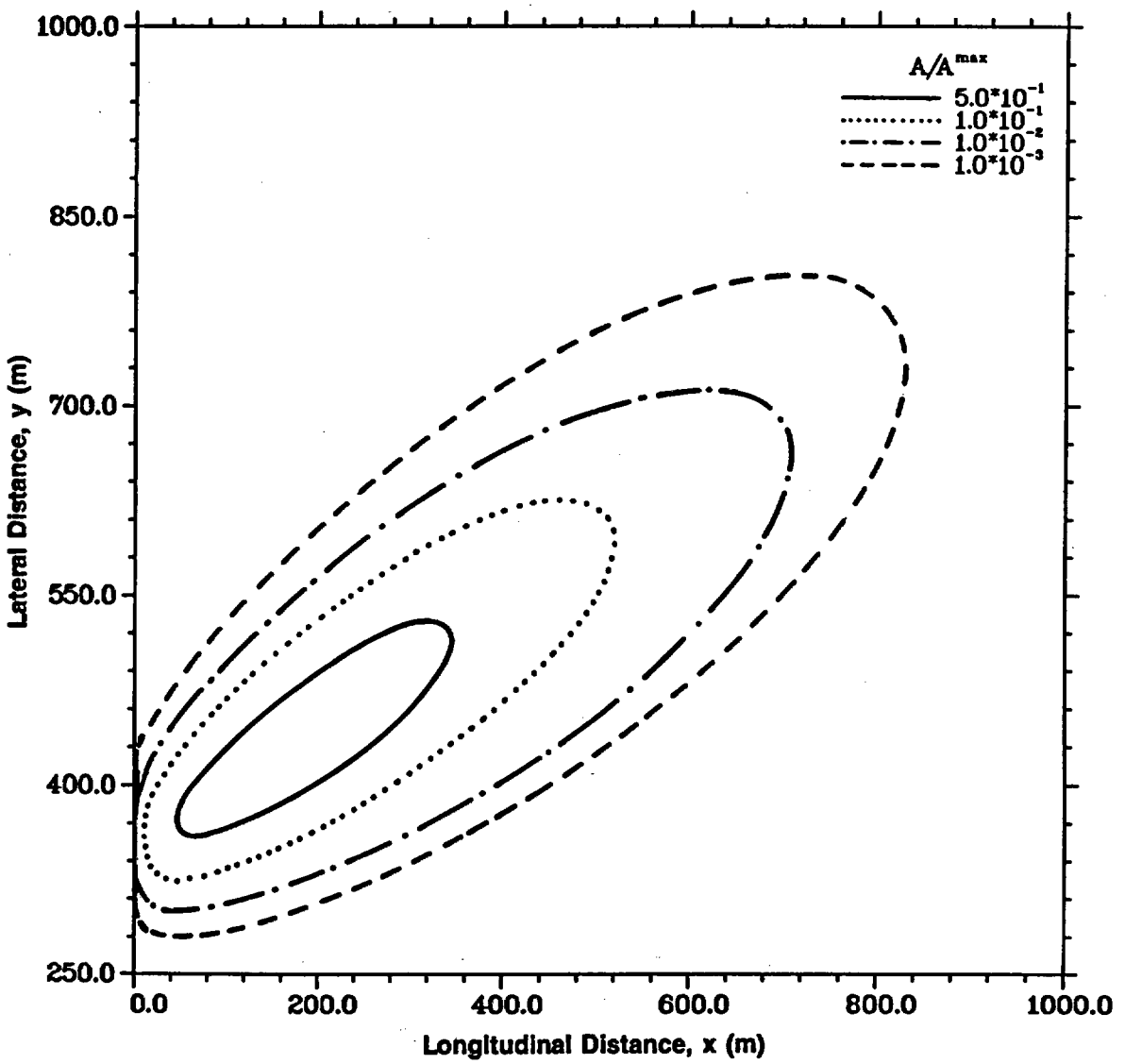

Figure 3-7b. Relative Concentration Isopleths for Tc-99 in the Fracture at z = 0 m and t = 2.5 × 10^4 yr, Band Release Mode (Case 4C: Gaussian Distributed Source)

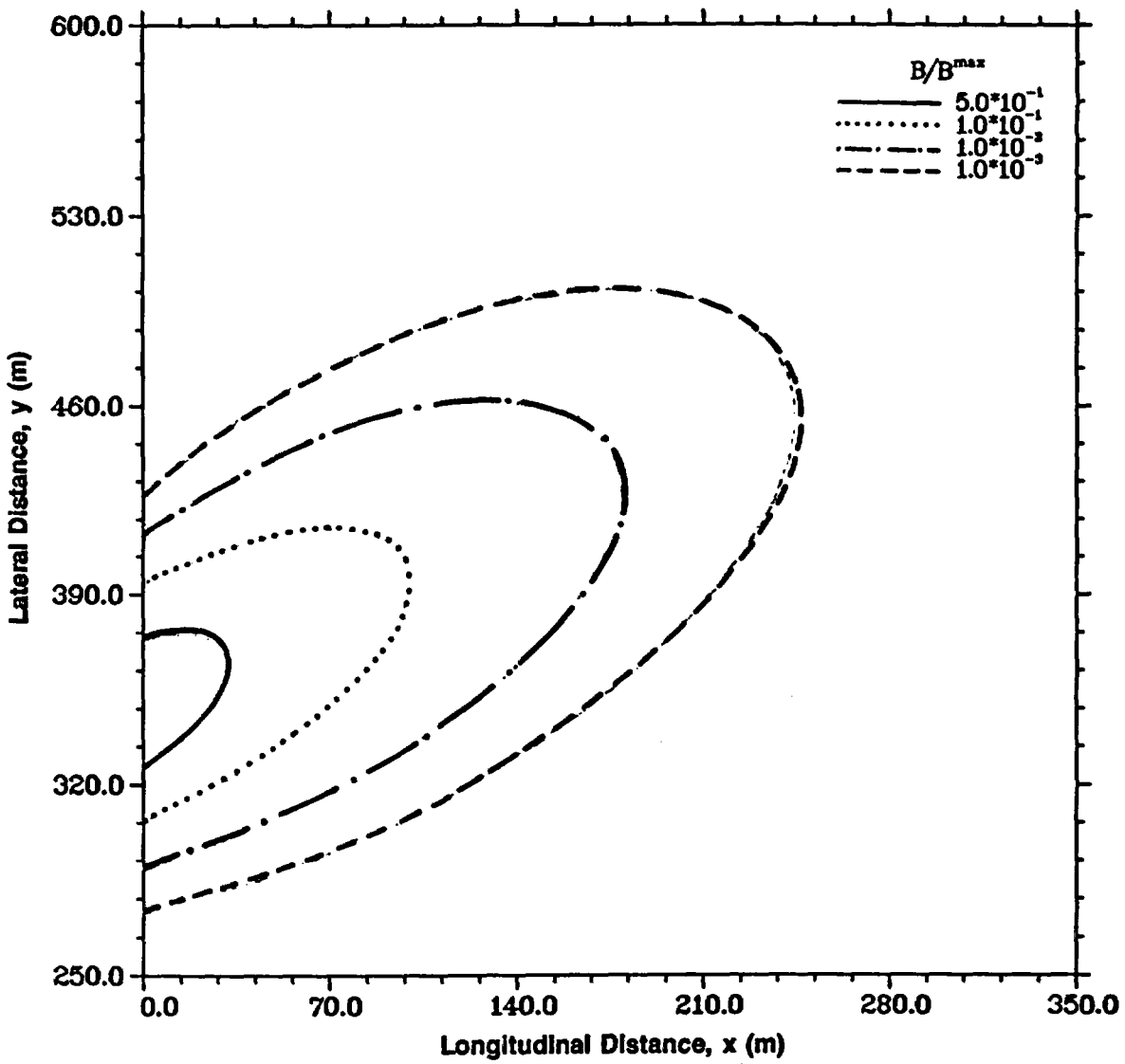

Figure 3-7c. Relative Concentration Isopleths for Tc-99 in the Rock Matrix at z = 1 m and t = 5 × 10³ yr, Step Release Mode (Case 4C: Gaussian Distributed Source)

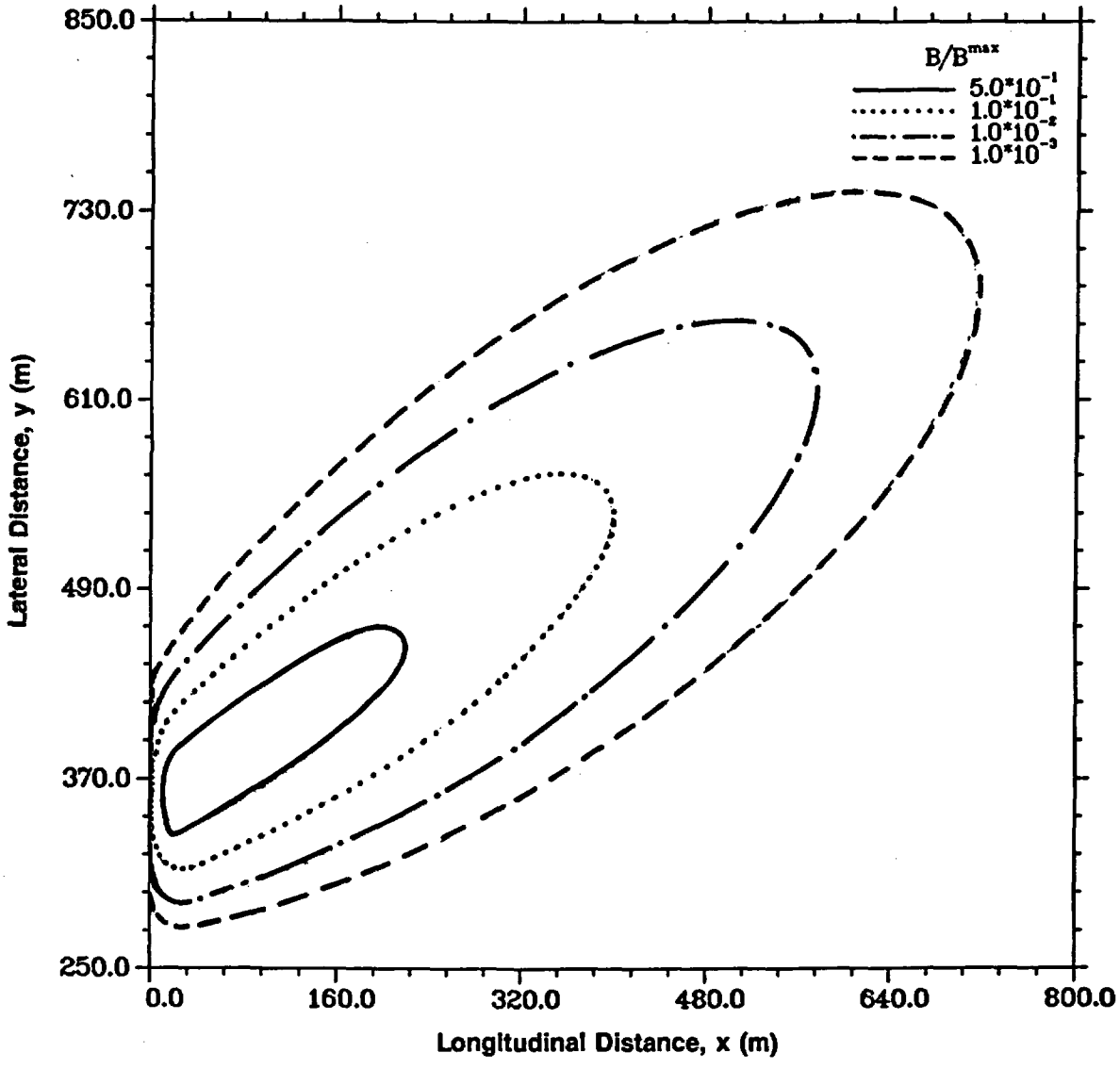

Figure 3-7d. Relative Concentration Isopleths for Tc-99 in the Rock Matrix at z = 1 m and t = 2.5 × 10^4 yr, Band Release Mode (Case 4C: Gaussian Distributed Source)

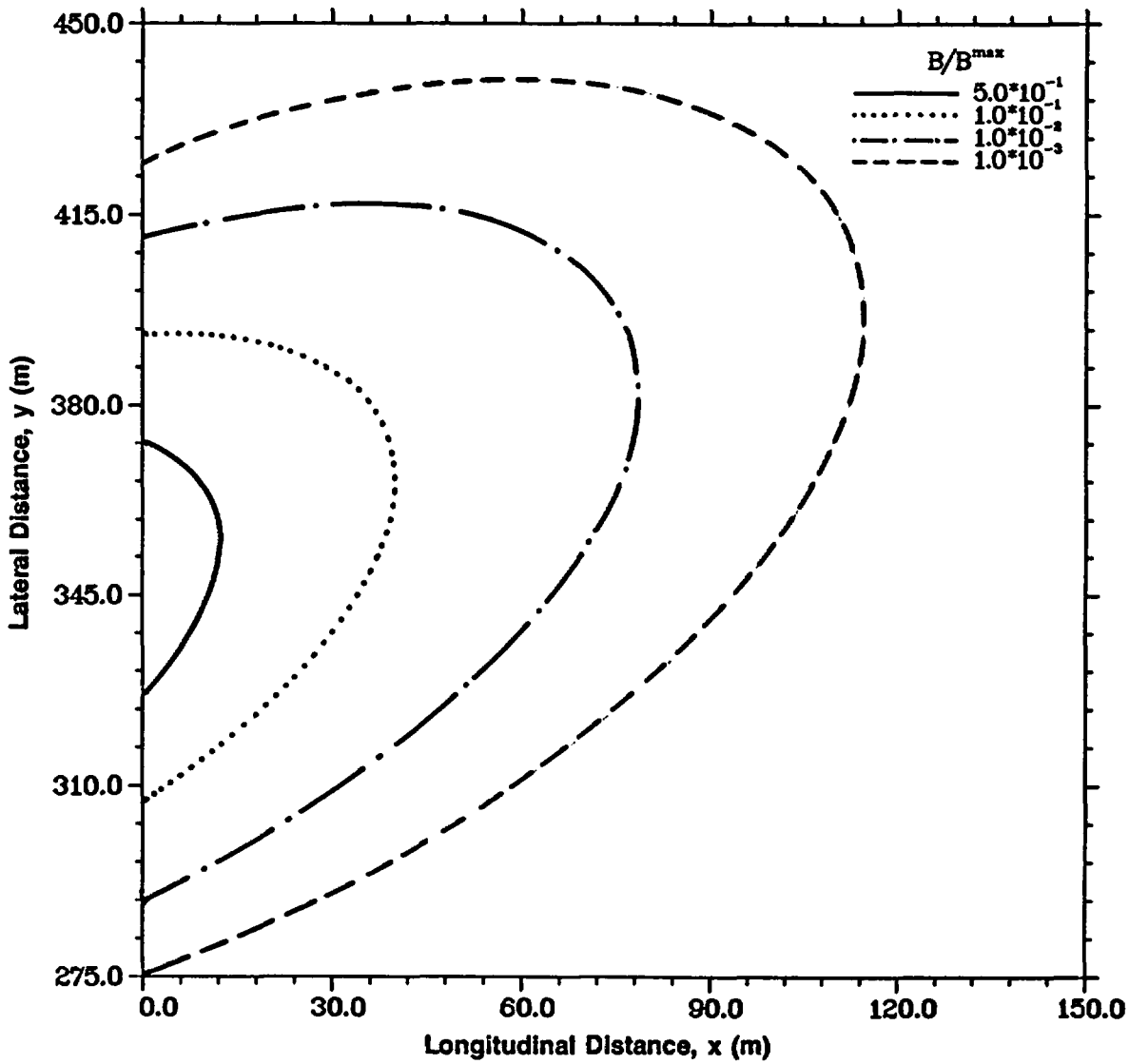

Figure 3-7e. Relative Concentration Isopleths for Tc-99 in the Rock Matrix at z = 5 m and t = 5 × 10^3 yr, Step Release Mode (Case 4C: Gaussian Distributed Source)

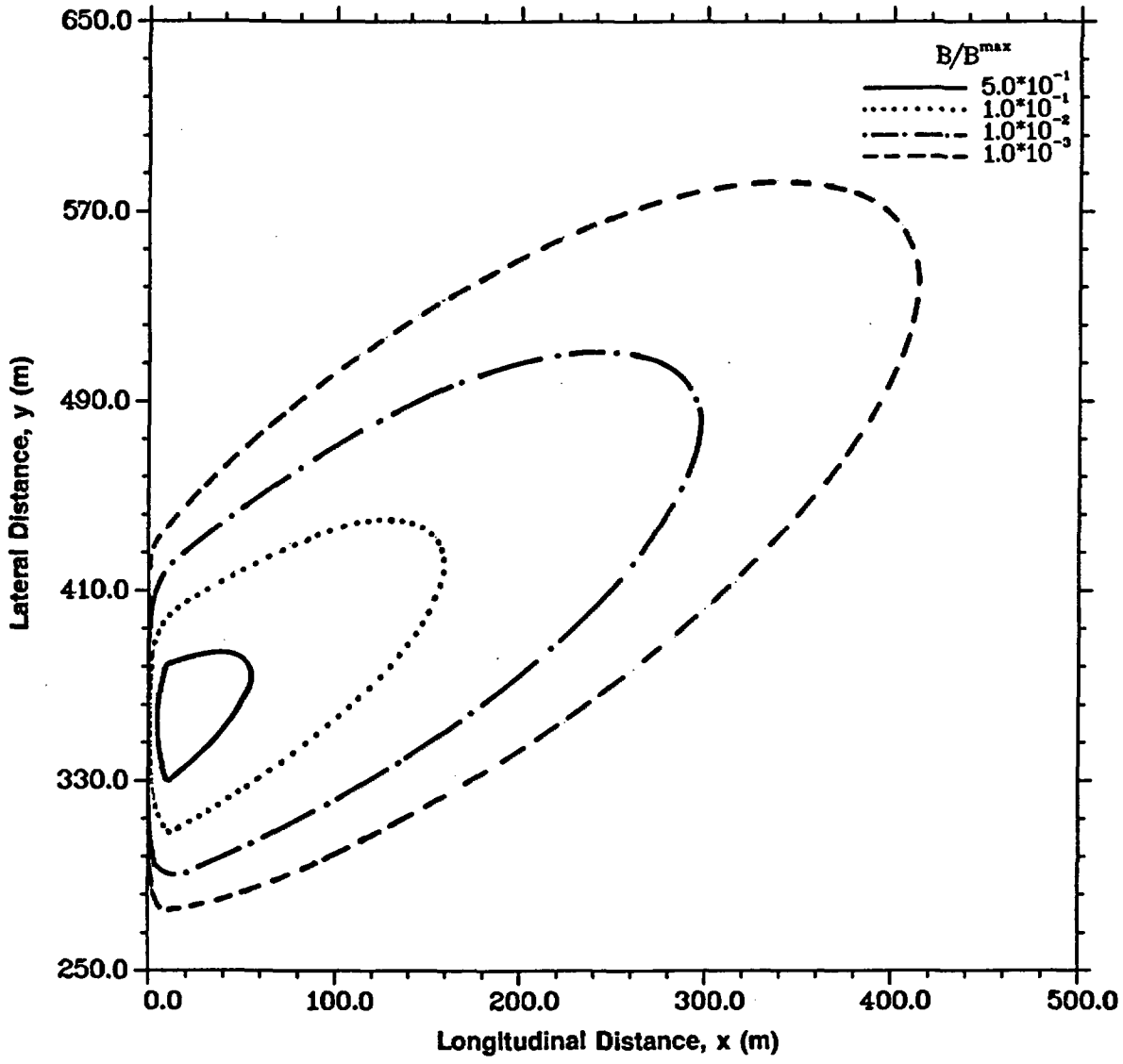

Figure 3-7f. Relative Concentration Isopleths for Tc-99 in the Rock Matrix at z = 5 m and t = 2.5 × 10^4 yr, Band Release Mode (Case 4C: Gaussian Distributed Source)

Table 3-13a. Case 4C Results: Relative Concentration in the Fracture (A/A°) of Species Tc-99 at Time t = 5 x 10^3 yr and z = 0 m (Gaussian Distributed Source, Step Release Mode)

Distance Along x-Axis (m)	Lateral Distance y (m)							
	250	300	350	400	450	500	550	600
0.0	0.36665E-05	0.43228E-01	0.98386E+00	0.43228E-01	0.36665E-05	0.60035E-12	0.18976E-21	0.11579E-33
50.0	0.30034E-05	0.61531E-02	0.31396E+00	0.27250E+00	0.69006E-02	0.21059E-04	0.27837E-07	0.23837E-10
100.0	0.67072E-06	0.77511E-03	0.59213E-01	0.21125E+00	0.41263E-01	0.81717E-03	0.36297E-05	0.64758E-08
150.0	0.92504E-07	0.81675E-04	0.81032E-02	0.68650E-01	0.50224E-01	0.42540E-02	0.66610E-04	0.30709E-06
200.0	0.90337E-08	0.69885E-05	0.84691E-03	0.12998E-01	0.24181E-01	0.62616E-02	0.29784E-03	0.36205E-05
250.0	0.65229E-09	0.47664E-06	0.68457E-04	0.16367E-02	0.61244E-02	0.38068E-02	0.46337E-03	0.13849E-04
300.0	0.35403E-10	0.25589E-07	0.42848E-05	0.14567E-03	0.94295E-03	0.11836E-02	0.31732E-03	0.21171E-04
350.0	0.14540E-11	0.10716E-08	0.20721E-06	0.94489E-05	0.95602E-04	0.21390E-03	0.11182E-03	0.15132E-04

Extracted data; complete data run is provided in microfiche form at the back of this report.

Table 3-13b. Case 4C Results: Relative Concentration in the Fracture (A/A°) of Species Tc-99 at Time t = 2.5 x 10^4 yr and z = 0 m (Gaussian Distributed Source, Band Release Mode)

Distance Along x-Axis (m)	Lateral Distance y (m)								
	250	340	430	520	610	700	790	880	100
0.0	0.00000E+00	0.00000E+00	0.00000E+00	0.00000E+00	0.00000E+00	0.00000E+00	0.00000E+00	0.00000E+00	0.00000E+00
100.0	0.32184E-06	0.75245E-02	0.33872E-01	0.12538E-03	0.20491E-07	0.11051E-11	0.33466E-16	0.67105E-21	0.21704E-27
200.0	0.47591E-07	0.84900E-03	0.53014E-01	0.11146E-01	0.38466E-04	0.12828E-07	0.11885E-11	0.50223E-16	0.32153E-22
300.0	0.32853E-08	0.53590E-04	0.12921E-01	0.34310E-01	0.18045E-02	0.54335E-05	0.24741E-08	0.32716E-12	0.61195E-18
400.0	0.14532E-09	0.23279E-05	0.12839E-02	0.17971E-01	0.76897E-02	0.17927E-03	0.46035E-06	0.23987E-09	0.17715E-14
500.0	0.45909E-11	0.74653E-07	0.72645E-04	0.32386E-02	0.67568E-02	0.89132E-03	0.11841E-04	0.25827E-07	0.89438E-12
600.0	0.10947E-12	0.18374E-08	0.27237E-05	0.28465E-03	0.20020E-02	0.10983E-02	0.63106E-04	0.54540E-06	0.93116E-10
700.0	0.20369E-14	0.35631E-10	0.73447E-07	0.14773E-04	0.26966E-03	0.47555E-03	0.97135E-04	0.29708E-05	0.24062E-08
800.0	0.30175E-16	0.55384E-12	0.14953E-08	0.50675E-06	0.19900E-04	0.91973E-04	0.55712E-04	0.52822E-05	0.18527E-07
900.0	0.35965E-18	0.69673E-14	0.23653E-10	0.12307E-07	0.90679E-06	0.93627E-05	0.14389E-04	0.37111E-05	0.50195E-07
1000.0	0.34635E-20	0.71201E-16	0.29544E-12	0.22077E-09	0.27569E-07	0.56154E-06	0.19221E-05	0.11970E-05	0.55242E-07

Extracted data; complete data run is provided in microfiche form at the back of this report.

Table 3-13c. Case 4C Results: Relative Concentration in the Rock Matrix (B/A°) of Species Tc-99 at Time t = 5 x 10^3 yr and z = 1 m (Gaussian Distributed Source, Step Release Mode)

Distance Along x-Axis (m)	Lateral Distance y (m)							
	250	300	350	400	450	500	550	600
0.0	0.11723E-05	0.13822E-01	0.31458E+00	0.13822E-01	0.11723E-05	0.19195E-12	0.60674E-22	0.37023E-34
50.0	0.55807E-06	0.13301E-02	0.70251E-01	0.58019E-01	0.12285E-02	0.25750E-05	0.20397E-08	0.99184E-12
100.0	0.78802E-07	0.10941E-03	0.89437E-02	0.30969E-01	0.52780E-02	0.79988E-04	0.23873E-06	0.26108E-09
150.0	0.68197E-08	0.73459E-05	0.80018E-03	0.67550E-02	0.44673E-02	0.30763E-03	0.35112E-05	0.10729E-07
200.0	0.41321E-09	0.39338E-06	0.53376E-04	0.83688E-03	0.14524E-02	0.31964E-03	0.11754E-04	0.10108E-06
250.0	0.18330E-10	0.16573E-07	0.27052E-05	0.67520E-04	0.24239E-03	0.13277E-03	0.13081E-04	0.29167E-06
300.0	0.60636E-12	0.54416E-09	0.10478E-06	0.37877E-05	0.24103E-04	0.27497E-04	0.61980E-05	0.32245E-06
350.0	0.15082E-13	0.13834E-10	0.31045E-08	0.15288E-06	0.15531E-05	0.32437E-05	0.14727E-05	0.16135E-06

Extracted data; complete data run is provided in microfiche form at the back of this report.

Table 3-13d. Case 4C Results: Relative Concentration in the Rock Matrix (B/A°) of Species Tc-99 at Time t = 2.5 x 10^4 yr and z = 1 m (Gaussian Distributed Source, Band Release Mode)

Distance Along x-Axis (m)	Lateral Distance y (m)							
	250	340	430	520	610	700	790	850
0.0	0.00000E+00	0.00000E+00	0.00000E+00	0.00000E+00	0.00000E+00	0.00000E+00	0.00000E+00	0.00000E+00
100.0	0.36372E-06	0.10627E-01	0.43651E-01	0.11383E-03	0.12561E-07	0.48001E-12	0.10753E-16	0.68856E-20
200.0	0.33242E-07	0.68658E-03	0.43003E-01	0.78487E-02	0.21326E-04	0.54145E-08	0.38337E-12	0.42031E-15
300.0	0.16256E-08	0.29898E-04	0.74371E-02	0.18516E-01	0.84152E-03	0.20778E-05	0.75861E-09	0.18907E-11
400.0	0.53920E-10	0.95937E-06	0.55238E-03	0.75352E-02	0.29453E-02	0.59615E-04	0.12867E-06	0.85046E-09
500.0	0.13229E-11	0.23643E-07	0.24146E-04	0.10725E-02	0.21174E-02	0.25270E-03	0.29346E-05	0.52918E-07
600.0	0.25092E-13	0.45950E-09	0.71658E-06	0.75628E-04	0.51519E-03	0.26330E-03	0.13638E-04	0.63714E-06
700.0	0.37713E-15	0.71649E-11	0.15562E-07	0.31892E-05	0.57284E-04	0.96109E-04	0.18113E-04	0.20073E-05
800.0	0.45490E-17	0.90497E-13	0.25789E-09	0.89629E-07	0.35030E-05	0.15640E-04	0.88975E-05	0.21215E-05

Extracted data; complete data run is provided in microfiche form at the back of this report.

Table 3-13e. Case 4C Results: Relative Concentration in the Rock Matrix (B/A°) of Species Tc-99 at Time t = 5 x 10^3 yr and z = 5 m (Gaussian Distributed Source, Step Release Mode)

Distance Along x-Axis (m)	Lateral Distance y (m)							
	275	300	325	350	375	400	425	450
0.0	0.51161E-09	0.25433E-07	0.26502E-06	0.57886E-06	0.26502E-06	0.25433E-07	0.51161E-09	0.21572E-11
15.0	0.15976E-09	0.72513E-08	0.83421E-07	0.23730E-06	0.16710E-06	0.29953E-07	0.14707E-08	0.23521E-10
30.0	0.47971E-10	0.20351E-08	0.25367E-07	0.89434E-07	0.88866E-07	0.25629E-07	0.23090E-08	0.74963E-10
45.0	0.13924E-10	0.56127E-09	0.74792E-08	0.31513E-07	0.41602E-07	0.17628E-07	0.25527E-08	0.14147E-09
60.0	0.39188E-11	0.15193E-09	0.21433E-08	0.10498E-07	0.17610E-07	0.10294E-07	0.22067E-08	0.18984E-09
75.0	0.10716E-11	0.40321E-10	0.59783E-09	0.33322E-08	0.68626E-08	0.52811E-08	0.15814E-08	0.19804E-09
90.0	0.28503E-12	0.10484E-10	0.16247E-09	0.10133E-08	0.24938E-08	0.24363E-08	0.97508E-09	0.16943E-09
105.0	0.73820E-13	0.26692E-11	0.43048E-10	0.29638E-09	0.85296E-09	0.10276E-08	0.53088E-09	0.12325E-09
120.0	0.18625E-13	0.66504E-12	0.11125E-10	0.83639E-10	0.27650E-09	0.40116E-09	0.26006E-09	0.78227E-10
135.0	0.45799E-14	0.16209E-12	0.28048E-11	0.22822E-10	0.85406E-10	0.14632E-09	0.11626E-09	0.44163E-10
150.0	0.10979E-14	0.38631E-13	0.69004E-12	0.60318E-11	0.25240E-10	0.50226E-10	0.47956E-10	0.22511E-10

Extracted data; complete data run is provided in microfiche form at the back of this report.

Table 3-13f. Case 4C Results: Relative Concentration in the Rock Matrix (B/A°) of Species Tc-99 at Time t = 2.5 x 10^4 yr and z = 5 m (Gaussian Distributed Source, Band Release Mode)

Distance Along x-Axis (m)	Lateral Distance y (m)								
	250	298	346	394	442	490	538	586	650
0.0	0.00000E+00	0.00000E+00	0.00000E+00	0.00000E+00	0.00000E+00	0.00000E+00	0.00000E+00	0.00000E+00	0.00000E+00
50.0	0.57630E-07	0.91711E-04	0.50477E-02	0.64542E-02	0.28725E-03	0.15481E-05	0.39670E-08	0.84172E-11	0.49017E-15
100.0	0.14673E-07	0.12429E-04	0.92623E-03	0.42433E-02	0.13240E-02	0.48264E-04	0.44709E-06	0.20067E-08	0.85777E-12
150.0	0.27246E-08	0.16385E-05	0.14547E-03	0.14340E-02	0.15410E-02	0.23255E-03	0.76997E-05	0.90671E-07	0.91827E-10
200.0	0.42832E-09	0.20797E-06	0.20745E-04	0.34007E-03	0.86048E-03	0.37698E-03	0.37124E-04	0.11467E-05	0.31500E-08
250.0	0.60182E-10	0.25304E-07	0.27493E-05	0.64689E-04	0.30565E-03	0.30306E-03	0.73468E-04	0.54526E-05	0.41198E-07
300.0	0.77501E-11	0.29446E-08	0.34219E-06	0.10552E-04	0.80068E-04	0.15052E-03	0.76537E-04	0.12236E-04	0.24118E-06
350.0	0.92694E-12	0.32726E-09	0.40215E-07	0.15313E-05	0.16836E-04	0.52785E-04	0.49510E-04	0.15350E-04	0.72750E-06
400.0	0.10375E-12	0.34707E-10	0.44754E-08	0.20200E-06	0.29928E-05	0.14234E-04	0.22245E-04	0.12193E-04	0.12713E-05
450.0	0.10917E-13	0.35094E-11	0.47236E-09	0.24548E-07	0.46486E-06	0.31232E-05	0.75043E-05	0.67223E-05	0.14149E-05
500.0	0.10830E-14	0.33810E-12	0.47324E-10	0.27715E-08	0.64492E-07	0.57959E-06	0.20085E-05	0.27531E-05	0.10815E-05

Extracted data; complete data run is provided in microfiche form at the back of this report.

PART 2

4.0 MULTIPLE PARALLEL FRACTURE CASE WITH FINITE DIFFUSION FIELD: SERIES SOLUTION

4.1 NON-ZERO LONGITUDINAL DISPERSION

The Laplace transformation of Equation 2-11 with its associated boundary condition Equations 3-1 and 3-2 subject to its initial and boundary conditions Equations 2-15, 2-18c, and 3-45 has a solution of the form given by

$$\bar{B}\,(x,y,z,s) = \cosh[r_b\,(z-L)]\mathrm{sech}[r_b(b-L)]\;\bar{A}\;(x,y,s) \tag{4-1}$$

where r_b is given by Equation 3-5a. The transformed diffusive flux at the interface of the fracture and rock matrix is given by

$$\bar{J} = -\phi D_e \frac{\partial \bar{B}}{\partial z}\,(x,y,b,s) = -\phi D_e r_b \tanh[r_b(b-L)]\;\bar{A}\,(x,y,s)\ . \tag{4-2}$$

4.1.1 Fracture

After proper substitution of the transform of the diffusive flux given by Equation 4-2 into the Laplace transformation of Equation 2-10 and applying subsequently the Fourier integral transform (see Equations 3-7 to 3-21), we then obtain an expression identical to Equation 3-21 in which the term corresponding to r_a given by Equation 3-22c will now take the following form

$$r_a = -R(s+\lambda) - c_f(s+\lambda)^{1/2}\tanh\left[c_r(L-b)(s+\lambda)^{1/2}\right] \tag{4-3}$$

whereas the remaining components of Equation 3-21 given by Equations 3-22a, 3-22b, and 3-22d will remain unaltered. Following the same procedure as outlined before (see Equations 3-24 to 3-42), the inverse Fourier integral transform will then have the same form as Equation 3-42. Rewriting the latter we have

$$\bar{A}\,(x,y,s) = A^o \int_0^\infty \psi(x,\sigma)E_\Omega\,\theta(s)e^{r_a X}\,d\sigma\ . \tag{4-4}$$

To find the inverse Laplace transform of the above equation, we write

$$L^{-1}\theta(s)e^{r_a X} = e^{-\lambda t}L^{-1}\exp(-R\chi s)G_F(s) \tag{4-5}$$

where

$$G_F(s) = \frac{\exp[-\varepsilon\sqrt{s}\tanh\beta\sqrt{s}]}{s} \tag{4-6}$$

with

$$\varepsilon = c_f X = \frac{\Phi}{b}(R'D_p)^{1/2}X \tag{4-7a}$$

$$\beta = c_r(L-b) = \left(\frac{R'}{D_p}\right)^{1/2}(L-b) \ . \tag{4-7b}$$

Expanding the numerator of Equation 4-6 in power series we find that

$$G_F(s) = \frac{1}{s} - \frac{\varepsilon}{\sqrt{s}}\tanh\beta\sqrt{s} + \frac{\varepsilon^2}{2!}\tanh^2\beta\sqrt{s} - \frac{\varepsilon^3}{3!}\sqrt{s}\tanh^3\beta\sqrt{s} + \ldots \tag{4-8}$$

which may also be written as

$$G_F(s) = \frac{1}{s} + \sum_{n=1}^{\infty}(-1)^n\frac{\varepsilon^n}{n!}g_n(s) \tag{4-9}$$

where

$$g_n(s) = \begin{cases} s^{(n-1)/2}\dfrac{\tanh^n\beta\sqrt{s}}{\sqrt{s}} & , n = 1, 3, 5, \ldots \\ s^{(n-2)/2}\tanh^n\beta\sqrt{s} & , n = 2, 4, 6, \ldots \end{cases} \tag{4-10}$$

The exponential series expansion for $\tanh\beta\sqrt{s}$ may be written as

$$\tanh\beta\sqrt{s} = \sum_{k=0}^{\infty} a_k e^{-2k\beta\sqrt{s}} \tag{4-11}$$

where

$$a_k = \begin{cases} 1 & , k = 0 \\ 2(-1)^k & , k \geq 1 \end{cases} \tag{4-12}$$

and the corresponding series for $\tanh \beta\sqrt{s}$ raised to the nth power (Gradshteyn and Ryzhik, 1980, p. 14) is given by

$$\tanh^n \beta\sqrt{s} = \sum_{k=0}^{\infty} {}_n\bar{b}_k e^{-2k\beta\sqrt{s}} \tag{4-13}$$

where

$$ {}_n\bar{b}_k = \begin{cases} 1 & , k = 0 \quad (4\text{-}14a) \\ \frac{1}{k} \sum_{i=1}^{k} \left(i(n+1)-k\right) a_i \, {}_n\bar{b}_{k-i} & , k \geq 1 \; . \quad (4\text{-}14b) \end{cases}$$

Substitution of Equation 4-13 in Equation 4-10 yields

$$g_n(s) = \begin{cases} s^{(n-1)/2} \sum_{k=0}^{\infty} {}_n\bar{b}_k \frac{e^{-2k\beta\sqrt{s}}}{\sqrt{s}} & , n = 1, 3, 5, \ldots \\ s^{(n-2)/2} \sum_{k=0}^{\infty} {}_n\bar{b}_k e^{-2k\beta\sqrt{s}} & , n = 2, 4, 6, \ldots \end{cases} \tag{4-15}$$

Using the inverse transforms of $e^{-a\sqrt{s}}/\sqrt{s}$, $e^{-a\sqrt{s}}$, $1/\sqrt{s}$, and $s^{n+1/2}$ (see Appendix A, Eqs. A.2-2 through A.2-4 and A.3-10) and applying the differentiation theorem (Eq. A.1-3), the inverse Laplace transform of $G_F(s)$ (see Eq. 4-6) may then be written as

$$G_F(t) = L^{-1}\{G_F(s)\} = g(t) + \sum_{n=1}^{\infty} (-1)^n \frac{\varepsilon^n}{n!} \bar{g}_n(t) \tag{4-16}$$

where

$$g(t) = 1 + \sum_{n=1}^{\infty} (-1)^n \frac{\varepsilon^n}{n!} \left[\frac{1}{\sqrt{\pi t^n}} \prod_{i=0}^{(n-3)/2} \left(\frac{1+2i}{2} \right) \right] \quad n = 1,3,5,\ldots \tag{4-17}$$

and

$$\bar{g}_n(t) = \begin{cases} \frac{1}{\sqrt{\pi}} \sum_{k=1}^{\Omega_0} {}_n\bar{b}_k \frac{d^{(n-1)/2}}{dt^{(n-1)/2}} \left[\frac{e^{-(k\beta)^2/t}}{\sqrt{t}} \right] & n = 1, 3, 5, \ldots \quad (4\text{-}18a) \\ \frac{1}{2\sqrt{\pi}} \sum_{k=1}^{\Omega_0} {}_n\bar{b}_k (2k\beta) \frac{d^{(n-2)/2}}{dt^{(n-2)/2}} \left[\frac{e^{-(k\beta)^2/t}}{\sqrt{t^3}} \right] & n = 2, 4, 6, \ldots \quad (4\text{-}18b) \end{cases}$$

Expansion of the first member of Equation 4-17 in series form yields

$$g(t) = 1 - \frac{2}{\sqrt{\pi}} \left[\frac{\varepsilon}{2\sqrt{t}} - \frac{1}{3}\left(\frac{\varepsilon}{2\sqrt{t}}\right)^3 + \frac{1}{10}\left(\frac{\varepsilon}{2\sqrt{t}}\right)^5 - \ldots + \ldots \right] . \tag{4-19}$$

Noting that the second member of the above equation corresponds to the exponential series form of the error function (see Eq. 3-60b) with argument $\varepsilon = c_f X$, Equation 4-18a becomes

$$g(t) = 1 - \mathrm{erf}\left(\frac{\varepsilon}{2\sqrt{t}}\right) = \mathrm{erfc}\left(\frac{c_f X}{2\sqrt{t}}\right) \tag{4-20}$$

and Equation 4-16 may now be written as

$$G_F(t) = \mathrm{erfc}\left(\frac{c_f X}{2\sqrt{t}}\right) + \sum_{n=1}^{\infty} (-1)^n \frac{\varepsilon^n}{n!} \bar{g}_n(t) . \tag{4-21}$$

The derivative terms in Equations 4-18a and 4-18b are obtained after using Leibnitz's theorem for differentiation of a product (Abramowitz and Stegun, 1972) (see also Appendix C):

$$\frac{d^n}{dt^n}(t^p e^{a/t}) = t^{(p-n)} e^{a/t} \sum_{r=0}^{n} \binom{n}{r} \prod_{i=1}^{n-r} (p-i+1) \cdot (-1)^r \sum_{m=1}^{r} \prod_{j=1}^{m-1} (r-j) \binom{r}{m-1} \left(\frac{a}{t}\right)^{r-m+1} \tag{4-22}$$

where

$$a = -(k\beta)^2 \tag{4-23a}$$

and

$$p = \begin{cases} -\frac{1}{2} & , n = 1, 3, 5, \ldots \\ -\frac{3}{2} & , n = 2, 4, 6, \ldots \end{cases} \tag{4-23b}$$

Because of the slow convergence exhibited by such an approach, particularly when the value of $c_f X$ becomes large, an alternative form of the second member of Equation 4-21 was sought. Writing

$$\alpha_k = \frac{k\beta}{\sqrt{t}} \tag{4-24a}$$

$$h = \frac{\varepsilon}{2\sqrt{t}} \tag{4-24b}$$

expansion of the second member of Equation 4-21 using Equations 4-18, 4-22, and 4-24a yields

$$\sum_{n=1}^{\infty} (-1)^n \frac{\varepsilon^n}{n!} \bar{g}_n(t) = \sum_{k=1}^{\Omega_0} \frac{1}{\sqrt{\pi}} e^{-a_k^2} \left[{}_1\bar{b}_k \frac{\varepsilon}{\sqrt{t}} - {}_2\bar{b}_k \frac{\varepsilon^2}{2!} \frac{a_k}{t} + {}_3\bar{b}_k \frac{\varepsilon^3}{3!} \frac{1}{\sqrt{t^3}} \left(a_k^2 - \frac{1}{2} \right) \right.$$

$$\left. - {}_4\bar{b}_k \frac{\varepsilon^4}{4!} \frac{a_k}{t^2} \left(a_k^2 - \frac{3}{2} \right) + {}_5\bar{b}_k \frac{\varepsilon^5}{5!} \frac{1}{\sqrt{t^5}} (a_k^4 - 3a_k^2 + \frac{3}{4}) - \ldots \right] . \tag{4-25}$$

With the nth derivative of the error function (Abramowitz and Stegun, 1972, p. 298) defined as

$$\frac{d^{n+1}}{dz^{n+1}} \operatorname{erf}(z) = (-1)^n \frac{2}{\sqrt{\pi}} H_n(z) e^{-z^2}, n = 0, 1, 2, 3, \ldots \tag{4-26}$$

where H_n are the Hermite polynomials (see Appendix A.4) and using Taylor's theorem, we may write

$$\operatorname{erf}(a_k + h) = \operatorname{erf}(a_k) + h \frac{d}{da_k} \left(\operatorname{erf}(a_k) \right) + \frac{h^2}{2!} \frac{d^2}{da_k^2} \left(\operatorname{erf}(a_k) \right) + \frac{h^3}{3!} \frac{d^3}{da_k^3} \left(\operatorname{erf}(a_k) \right) + \ldots \tag{4-27}$$

Expanding the right-hand side using Equation 4-26, the above equation becomes

$$\operatorname{erf}(a_k + \frac{\varepsilon}{2\sqrt{t}}) = \operatorname{erf}(a_k) + \frac{1}{\sqrt{\pi}} e^{-a_k^2} \left[\frac{\varepsilon}{\sqrt{t}} - \frac{\varepsilon^2}{2!} \frac{a_k}{t} + \frac{\varepsilon^3}{3!} \frac{1}{\sqrt{t^3}} \left(a_k^2 - \frac{1}{2} \right) \right.$$

$$\left. - \frac{\varepsilon^4}{4!} \frac{a_k}{t^2} \left(a_k^2 - \frac{3}{2} \right) + \frac{\varepsilon^5}{5!} \frac{1}{\sqrt{t^5}} \left(a_k^4 - 3a_k^2 + \frac{3}{4} \right) - \ldots \right] . \tag{4-28}$$

Comparing Equations 4-25 and 4-28, we find

$$H_1(t) = \sum_{n=1}^{\infty} (-1)^n \frac{\varepsilon^n}{n!} g_n(t) = \sum_{k=1}^{\Omega_0} \sum_{m=1}^{k} a_{km} \varepsilon^m \frac{d^m}{d\varepsilon^m} \left[\operatorname{erf}\left(a_k + \frac{\varepsilon}{2\sqrt{t}} \right) \right] \tag{4-29}$$

with

$$a_{ij} = 0 \quad , j > i \tag{4-30a}$$

$$a_{i1} = - \frac{{}_1\bar{b}_i}{c_{11}} = (-1)^{i+1}(2) \tag{4-30b}$$

$$a_{ij} = \left((-1)^j \, {}_j\bar{b}_i\right) - \sum_{k=1}^{j-1} c_{kj} \cdot a_{ik}/c_{jj}, \; j > 1 \tag{4-30c}$$

where

$$c_{ij} = (-1)^{j+1} \prod_{k=0}^{i-1} (j-k) \;, \; j \geq i \tag{4-30d}$$

$$c_{ij} = 0 \;, \; j < i \;. \tag{4-30e}$$

A set of values for ${}_i\bar{b}_j$, a_{ij}, and c_{ij} is reported in Tables 4-1a, 4-1b, and 4-1c.

Equation 4-21 now may be written as

$$G_F(t) = \mathrm{erfc}\left(\frac{c_f X}{2\sqrt{t}}\right) + \sum_{k=1}^{\Omega_o} \sum_{m=1}^{k} a_{km} (c_f X)^m \frac{d^m}{d\varepsilon^m} \left[\mathrm{erf}\left(\frac{2k\beta + \varepsilon}{2\sqrt{t}}\right)\right] \;. \tag{4-31a}$$

where

$$\frac{d^{n+1}}{d\varepsilon^{n+1}} \left[\mathrm{erf}(z)\right] = (-1)^n \frac{2}{\sqrt{\pi}} H_n(z) e^{-z^2} \left(\frac{1}{2\sqrt{t}}\right)^{n+1} , \; n = 0,1,2,3,\ldots \tag{4-31b}$$

and

$$z = \frac{2k\beta + \varepsilon}{2\sqrt{t}} \tag{4-31c}$$

Substituting Equation 4-31 into Equation 4-5 and applying subsequently the translation theorem (Eq. A.1-1), the inverse Laplace transform of Equation 4-4 yielding the solution of the concentration in the fracture may be written as

$$A(x,y,t) = A^o e^{-\lambda t} \int_0^\infty \psi(x,\sigma) E_\Omega \, G_F(t - R\chi) \, U(t - R\chi) d\sigma \;. \tag{4-32}$$

Note that when the contribution of the second member of Equation 4-31a becomes negligible, the above equation will be identical to Equation 3-43. Discussions pertaining to the magnitude of Ω_0 will be deferred to Section 4.5.

Table 4-1. Sets of Values for Equations 4-30a Through 4-30e

a. Listing of Coefficients $\bar{b}_{ij}$

i\j	0	1	2	3	4	5	6	7	8	9	10
1	1	-2	2	-2	2	-2	2	-2	2	-2	2
2	1	-4	8	-12	16	-20	24	-28	32	-36	40
3	1	-6	18	-38	66	-102	146	-198	258	-326	402
4	1	-8	32	-88	192	-360	608	-952	1408	-1992	2720
5	1	-10	50	-170	450	-1002	1970	-3530	5890	-9290	14002
6	1	-12	72	-292	912	-2364	5336	-10836	20256	-35436	58728
7	1	-14	98	-462	1666	-4942	12642	-28814	59906	-115598	209762
8	1	-16	128	-688	2816	-9424	27008	-68464	157184	-332688	658048
9	1	-18	162	-978	4482	-16722	53154	-148626	374274	-864146	1854882
10	1	-20	200	-1340	6800	-28004	97880	-299660	822560	-2060980	4780008
11	1	-22	242	-1782	9922	-44726	170610	-568150	1690370	-4573910	11414898
12	1	-24	288	-2312	14016	-68664	284000	-1022760	3281280	-9545560	25534368

Table 4-1. (Continued)

b. Listing of Coefficients a_{ij} (Derivatives of Error Function)

i\j	1	2	3	4	5	6	7	8	9	10	11	12
1	2.0											
2	-2.0	-2.0										
3	2.0	4.0	1.333E+00									
4	-2.0	-6.0	-4.000E+00	-6.667E-01								
5	2.0	8.0	8.000E+00	2.667E+00	2.667E-01							
6	-2.0	-10.0	-1.333E+01	-6.667E+00	-1.333E+00	-8.889E-02						
7	2.0	12.0	2.000E+01	1.333E+01	4.000E+00	5.333E-01	2.540E-02					
8	-2.0	-14.0	-2.800E+01	-2.333E+01	-9.333E+00	-1.867E+00	-1.778E-01	-6.349E-03				
9	2.0	16.0	3.733E+01	3.733E+01	1.867E+01	4.978E+00	7.111E-01	5.079E-02	1.411E-03			
10	-2.0	-18.0	-4.800E+01	-5.600E+01	-3.360E+01	-1.120E+01	-2.133E+00	-2.286E-01	-1.270E-02	-2.822E-04		
11	2.0	20.0	6.000E+01	8.000E+01	5.600E+01	2.240E+01	5.333E+00	7.619E-01	6.349E-02	2.822E-03	5.131E-05	
12	-2.0	-22.0	-7.333E+01	-1.100E+02	-8.800E+01	-4.107E+01	-1.173E+01	-2.095E+00	-2.328E-01	-1.552E-02	-5.644E-04	-8.551E-06

c. Listing of Coefficients c_{ij}

i\j	1	2	3	4	5	6	7	8	9	10	11	12
1	1	-2	3	-4	5	-6	7	-8	9	-10	11	-12
2	0	-2	6	-12	20	-30	42	-56	72	-90	110	-132
3	0	0	6	-24	60	-120	210	-336	504	-720	990	-1320
4	0	0	0	-24	120	-360	840	-1680	3024	-5040	7920	-11880
5	0	0	0	0	120	-720	2520	-6720	15120	-30240	55440	-95040
6	0	0	0	0	0	-720	5040	-20160	60480	-151200	332640	-665280
7	0	0	0	0	0	0	5040	-40320	181440	-604800	1663200	-3991680
8	0	0	0	0	0	0	0	-40320	362880	-1814400	6652800	-19958400
9	0	0	0	0	0	0	0	0	362880	-3628800	19958400	-79833600
10	0	0	0	0	0	0	0	0	0	-3628800	39916800	-239500800
11	0	0	0	0	0	0	0	0	0	0	39916800	-479001600
12	0	0	0	0	0	0	0	0	0	0	0	-479001600

4.1.2 Rock Matrix

Substitution of Equation 4-4 into Equation 4-1 gives the transformation of the concentration in the rock as

$$\bar{B}\,(x,y,z,s) = A^{o}\int_{0}^{\infty}\psi(x,\sigma)E_{\Omega}\theta(s)e^{r_a X}\cosh[r_b(z-L)]\mathrm{sech}[r_b(b-L)]d\sigma \quad . \tag{4-33}$$

To find the inverse Laplace transform of the above equation, we write

$$L^{-1}\theta(s)e^{r_a X}\cosh[r_b(z-L)]\mathrm{sech}[r_b(b-L)] = e^{-\lambda t}L^{-1}\exp(-R\chi s)\ \cdot\ G_R(s) \tag{4-34}$$

where

$$G_R(s) = G_F(s)\,\frac{\cosh\mu\sqrt{s}}{\cosh\beta\sqrt{s}}\ ,\ (\beta>\mu) \tag{4-35}$$

with

$$\mu = c_r(L-z) = \left(\frac{R'}{D_e}\right)^{1/2}(L-z)\ . \tag{4-36}$$

Writing

$$H(s) = \frac{\cosh\mu\sqrt{s}}{\cosh\beta\sqrt{s}} = \frac{e^{\mu\sqrt{s}}+e^{-\mu\sqrt{s}}}{e^{\beta\sqrt{s}}+e^{-\beta\sqrt{s}}} = \left[e^{(\mu-\beta)\sqrt{s}}+e^{-(\mu+\beta)\sqrt{s}}\right]\left(1+e^{-2\beta\sqrt{s}}\right)^{-1} \tag{4-37}$$

expanding the second term on the right-hand side into a binomial series, we find that

$$H(s) = \sum_{i=1}^{\infty}(-1)^{i+1}\left[e^{-[(2i-1)\beta-\mu]\sqrt{s}}+e^{-[(2i-1)\beta+\mu]\sqrt{s}}\right]\ . \tag{4-38}$$

Substituting Equation 4-9 and Equation 4-38 into Equation 4-35, we obtain after some algebraic manipulation the equation

$$G_R(s) = \tilde{g}(s) + \sum_{n=1}^{\infty}(-1)^n\frac{\varepsilon^n}{n!}\tilde{\tilde{g}}_n(s) \tag{4-39}$$

where

$$\tilde{g}(s) = \frac{H(s)}{s} \tag{4-40}$$

and

$$\tilde{\tilde{g}}_n(s) = \begin{cases} s^{(n-1)/2} \sum_{i=0}^{\infty} {}_n\bar{b}_i \sum_{j=1}^{\infty} (-1)^{j+1} \sum_{k=1}^{2} \dfrac{e^{-{}^kY_{ij}\sqrt{s}}}{\sqrt{s}} & n = 1, 3, 5, \ldots \quad (4\text{-}41a) \\ s^{(n-2)/2} \sum_{i=0}^{\infty} {}_n\bar{b}_i \sum_{j=1}^{\infty} (-1)^{j+1} \sum_{k=1}^{2} e^{-{}^kY_{ij}\sqrt{s}} & n = 2, 4, 6, \ldots \quad (4\text{-}41b) \end{cases}$$

with

$${}^1Y_{ij} = [2(i+j) - 1]\beta - \mu \tag{4-42a}$$

$${}^2Y_{ij} = [2(i+j) - 1]\beta + \mu \quad . \tag{4-42b}$$

Using the inverse transforms of $e^{-a\sqrt{s}}/s$, $e^{-a\sqrt{s}}/\sqrt{s}$, and $e^{-a\sqrt{s}}$ (see Appendix A, Eqs. A.2-1 through A.2-3) and applying as before the multiplication theorem strictly to the second member on the right-hand side of Equation 4-39, the inverse Laplace transform of $G_R(s)$ may then be written as

$$G_R(t) = L^{-1}\{G_R(s)\} = \tilde{g}(t) + \sum_{n=1}^{\infty} (-1)^n \frac{\varepsilon^n}{n!} \tilde{\tilde{g}}_n(t) \tag{4-43}$$

where

$$\tilde{g}(t) = \sum_{i=1}^{\Omega'} (-1)^{i+1} \sum_{k=1}^{2} \left(\operatorname{erfc}\left[\frac{{}^kY_{0i}}{2\sqrt{t}} \right] \right) \tag{4-44}$$

and

$$g_n(t) = \begin{cases} \dfrac{1}{\sqrt{\pi}} \displaystyle\sum_{i=0}^{\Omega_1''} {}_n\bar{b}_i \sum_{j=1}^{\Omega_2''} (-1)^{j+1} \sum_{k=1}^{2} \frac{d^{(n-1)/2}}{dt^{(n-1)/2}} \left[\frac{e^{-\left({}^kY_{ij}\right)^2/4t}}{\sqrt{t}} \right] & n = 1, 3, 5, \ldots \quad (4\text{-}45a) \\ \dfrac{1}{2\sqrt{\pi}} \displaystyle\sum_{i=0}^{\Omega_1''} {}_n\bar{b}_i \sum_{j=1}^{\Omega_2''} (-1)^{j+1} \sum_{k=1}^{2} \left({}^kY_{ij}\right) \frac{d^{(n-2)/2}}{dt^{(n-2)/2}} \left[\frac{e^{-\left({}^kY_{ij}\right)^2/4t}}{\sqrt{t^3}} \right] & n = 2, 4, 6, \ldots \quad (4\text{-}45b) \end{cases}$$

By taking an approach similar to the one outlined in the previous section (see Eqs. 4-24 through 4-29) with ${}^kY_{ij}/2\sqrt{t}$ substituting for α_k, it may be shown that the second member of Equation 4-43 is written as

$$\sum_{n=1}^{\infty} (-1)^n \frac{\varepsilon^n}{n!} \tilde{\tilde{g}}_n(t) = \tilde{\tilde{g}}_1(t) + \tilde{\tilde{g}}_2(t) \tag{4-46}$$

$$g_1(t) = \sum_{i=1}^{\Omega_1''} (-1)^i \sum_{k=1}^{2} \operatorname{erf}\left[\frac{{}^kY_{0i} + \varepsilon}{2\sqrt{t}} \right] - \sum_{i=1}^{\Omega'} (-1)^i \sum_{k=1}^{2} \operatorname{erf}\left[\frac{{}^kY_{0i}}{2\sqrt{t}} \right]$$

$$= \sum_{i=1}^{\Omega_0''} (-1)^{i+1} \sum_{k=1}^{2} \operatorname{erfc}\left[\frac{{}^kY_{0i} + \varepsilon}{2\sqrt{t}} \right] - \sum_{i=1}^{\Omega'} (-1)^{i+1} \sum_{k=1}^{2} \operatorname{erfc}\left[\frac{{}^kY_{0i}}{2\sqrt{t}} \right] \tag{4-47}$$

and

$$\tilde{\tilde{g}}_2(t) = \sum_{i=1}^{\Omega_1''} \sum_{j=1}^{\Omega_2''} (-1)^{j+1} \sum_{k=1}^{2} \sum_{m=1}^{i} a_{im} \varepsilon^m \frac{d^m}{d\varepsilon^m} \left[\operatorname{erf}\left(\frac{{}^kY_{ij} + \varepsilon}{2\sqrt{t}} \right) \right] . \tag{4-48}$$

Note that Equation 4-47 corresponds to the terms in the summation series given by Equations 4-45a and 4-45b with i set to zero, in which case ${}_nb_0$ is equal to unity for all values of n (see Eq. 4-41a). The result for this set of conditions is a correspondence between the left-hand side of Equation 4-46 and $g_1(t)$ given by Equation 4-47 which becomes exact after premultiplying the latter by minus one.

Combining Equations 4-44 and 4-47, we have

$$\tilde{g}(t) + \tilde{\tilde{g}}_1(t) = \sum_{i=1}^{\Omega_0''} (-1)^{i+1} \sum_{k=1}^{2} \operatorname{erfc}\left[\frac{{}^{k}Y_{0i} + \varepsilon}{2\sqrt{t}}\right] \tag{4-49}$$

Hence Equation 4-43 becomes

$$G_R(t) = \sum_{i=1}^{\Omega_0''} (-1)^{i+1} \sum_{k=1}^{2} \operatorname{erfc}\left[\frac{{}^{k}Y_{i0}+c_f X}{2\sqrt{t}}\right] + \sum_{i=1}^{\Omega_1''} \sum_{j=1}^{\Omega_2''} (-1)^{j+1} \sum_{k=1}^{2} \sum_{m=1}^{i} a_{im}(c_f X)^m \frac{d^m}{d\varepsilon^m}\left[\operatorname{erf}\left(\frac{{}^{k}Y_{ij}+\varepsilon}{2\sqrt{t}}\right)\right] \tag{4-50}$$

Substituting Equation 4-31 into Equation 4-34 and applying subsequently the translation theorem (Eq. A.1-1), the inverse Laplace transform of Equation 4-25 yielding the solution of the concentration in the rock then may be written as

$$B(x,y,z,t) = A^o e^{-\lambda t} \int_0^\infty \psi(x,\sigma) E_\Omega G_R(t - R\chi)\, U(t - R\chi) d\sigma \quad . \tag{4-51}$$

It may be worthwhile noting that under some circumstances Equation 4-51 will become identical to Equation 3-45 (see Section 4.5 for discussion). Details regarding the integration of Equations 4-32 and 4-51 may be found in Appendix B.

4.1.3 Mass Flux

The general equation for the mass flux in the fracture is given by Equation 3-53 in which the Laplace transforms of the derivative terms $\partial\bar{A}/\partial x$ and $\partial\bar{A}/\partial y$ have the same form as Equations 3-55 and 3-56, with the noted difference that the coefficient of χ in the exponential argument is given in this instance by Equation 4-3.

The evaluation of $\partial\bar{A}/\partial x$ requires a new estimate of the x-derivative of $e^{r_a \chi}$ based on Equation 4-3 and in this case Equation 3-55 becomes

$$\frac{\partial \bar{A}}{\partial x} = A^o \int_0^\infty \theta(s) e^{r_a \chi} \psi(x,\sigma)\,[2a_1(\sigma - a_1 x)E_\Omega + E_\Omega^x - E_\Omega \bar{\beta} f_1(s+\lambda)] d\sigma \tag{4-52}$$

where

$$f_1(s) = Rs + c_f \sqrt{s} \tanh \beta \sqrt{s} \tag{4-53}$$

and α_1, $\bar{\beta}$ are given by Equations 3-57b and 3-59, and E_Ω^x by either Equation 3-62 or Equation 3-64, all depending upon the type of boundary condition imposed at the source. Writing

$$L^{-1}\theta(s)e^{r_a X} f_1(s+\lambda) = e^{-\lambda t} L^{-1} \exp(-R\chi s)\, G_F^*(s) \tag{4-54}$$

where

$$G_F^*(s) = G_F(s) \cdot f_1(s) \tag{4-55a}$$

$$= RsG_F(s) - c_f \frac{d}{d\varepsilon}\left[G_F(s)\right] \tag{4-55b}$$

with $G_F(s)$ given by Equation 4-9. Using Equation 4-31 and applying Theorem A.1.3a to $sG_F(s)$ in Equation 4-55b, and subsequently Theorem A.1-1, the inverse Laplace transform of Equation 4-52 becomes

$$\frac{\partial A}{\partial x} = A^o e^{-\lambda t} \int_0^\infty \psi(x,\sigma)\Bigg[(2\alpha_1(\sigma-\alpha_1 x)E_\Omega + E_\Omega^x)\, G_F(t-R\chi) - E_\Omega \bar{\beta}\Bigg[R\Bigg(\frac{\bar{\varepsilon}}{\sqrt{\pi}} \frac{e^{-\bar{\varepsilon}^2/(t-R\chi)}}{\sqrt{(t-R\chi)^3}} + \tag{4-56}$$

$$\sum_{n=1}^{\infty} (-1)^n \frac{\varepsilon^n}{n!} \bar{g}'_n(t-R\chi)\Bigg) + c_f\Bigg(\frac{1}{\sqrt{\pi}} \frac{e^{-\bar{\varepsilon}^2/(t-R\chi)}}{\sqrt{(t-R\chi)}} - \sum_{n=1}^{\infty} (-1)^n \frac{\varepsilon^{n-1}}{(n-1)!} \bar{g}_n(t-R\chi)\Bigg)\Bigg]\Bigg] U(t-R\chi)d\sigma$$

where $\bar{g}'_n(t)$ corresponds to the time derivative of $g_n(t)$ given by Equations 4-18.

The inverse Laplace transform of the y-derivative of A which has a form identical to Equation 3-68b may be written as

$$\frac{\partial A}{\partial y} = A^o e^{-\lambda t} \int_0^\infty \psi(x,\sigma) E_\Omega^y\, G_F(t-R\chi) U(t-R\chi) d\sigma \tag{4-57}$$

where E_Ω^x, E_Ω^y, $\bar{\varepsilon}$, and $G_F(t)$ are given by Equations 3-63, 3-65, 3-67d, and 4-31a, respectively.

Referring to Equation 4-25 we have

$$H_2(t) = \sum_{n=1}^{\infty} (-1)^n \frac{\varepsilon^n}{n!} \bar{g}'_n(t) = \sum_{k=1}^{\Omega_o} \frac{1}{\sqrt{\pi}} e^{-a_k^2} \left[{}_1\bar{b}_k \frac{\varepsilon}{\sqrt{t^3}} (a_k^2 - \frac{1}{2}) - {}_2\bar{b}_k \frac{\varepsilon^2}{2!} \frac{a_k}{t^2} (a_k^2 - \frac{3}{2}) \right.$$

$$\left. + {}_3\bar{b}_k \frac{\varepsilon^3}{3!} \frac{1}{\sqrt{t^5}} \left(a_k^4 - 3a_k^2 + \frac{3}{4} \right) - \ldots \right] \tag{4-58}$$

Comparing Equations 4-58 and 4-28 we find

$$H_2(t) = \sum_{k=1}^{\Omega_o} \sum_{m=1}^{k} a_{km} \varepsilon^m \frac{d^{m+2}}{d\varepsilon^{m+2}} \left[\mathrm{erf}\left(\frac{2k\beta + \varepsilon}{2\sqrt{t}} \right) \right] . \tag{4-59}$$

Referring to Equation 4-29 and differentiating both sides with respect to ε yields

$$H_3(t) = \sum_{n=1}^{\infty} (-1)^n \frac{\varepsilon^{n-1}}{(n-1)!} g_n(t) = \sum_{k=1}^{\Omega_o} \sum_{m=1}^{k} a_{km} \left[m \varepsilon^{m-1} \frac{d^m}{d\varepsilon^m} \left[\mathrm{erf}\left(\frac{2k\beta + \varepsilon}{2\sqrt{t}} \right) \right] \right.$$

$$\left. + \varepsilon^m \frac{d^{m+1}}{d\varepsilon^{m+1}} \left[\mathrm{erf}\left(\frac{2k\beta + \varepsilon}{2\sqrt{t}} \right) \right] \right] \tag{4-60}$$

The components of the mass flux given by Equations 3-54 may now be written as

$$F_i = A^o e^{-\lambda t} \int_0^{\infty} \psi(x,\sigma) \left[{}_iF_1 \cdot G_F(t - R\chi) + {}_iF_2^* \left[R\left(\frac{\bar{\varepsilon}}{\sqrt{\pi}} \frac{e^{-\bar{\varepsilon}^2/(t-R\chi)}}{\sqrt{(t-R\chi)^3}} \right.\right.\right.$$

$$\left.\left.\left. + H_2(t - R\chi) \right) + c_f \left(\frac{1}{\sqrt{\pi}} \frac{e^{-\bar{\varepsilon}^2/(t-R\chi)}}{\sqrt{(t-R\chi)}} - H_3(t - R\chi) \right) \right] \right] U(t - R\chi)\, d\sigma \ , \ (i = x,y) \tag{4-61}$$

with

$${}_iF_2^* = D_{ix} E_\Omega \bar{\beta} \ , \ (i = x,y) \tag{4-62}$$

where ${}_xF_1$, ${}_yF_1$, $G_F(t)$, $H_2(t)$, and $H_3(t)$ are given by Equations 3-67a, 3-67c, 4-31, 4-59, and 4-60, respectively.

4.1.4 Cumulative Mass Flux

The cumulative mass flux may be written as

$$M(t) = \int_{R_X}^{t} F(\tau)\, d\tau \tag{4-63}$$

where $F(\tau)$ is given by Equation 3-70b.

Unidimensional Flow ($F_y = 0$)

Substituting for $F(\tau)$ given by Equation 4-61a and interchanging the order of integration (see Eqs. 3-71 through 3-73), the above equation may now be written as

$$M(t) = A^0 \int_{f(t)}^{\infty} \psi(x,\sigma) \left[{}_x\bar{F}_1 J_0 + {}_xF_2^* [R(I_2 + J_2) + c_f(I_3 - J_3)] \right] U(t - R_X) d\sigma \tag{4-64}$$

where ${}_x\bar{F}_1$ and ${}_xF_2^*$ are given by Equations 3-74a and 4-62, and

$$J_0 = \int_{R_X}^{t} e^{-\lambda\tau} G_F(\tau) d\tau = I_1 + J_1 \tag{4-65}$$

$$I_1 = \int_{R_X}^{t} e^{-\lambda\tau} \operatorname{erfc}\left[\frac{\bar{\varepsilon}}{\sqrt{t - R_X}} \right] d\tau = K_0(\bar{\varepsilon}) + \frac{\bar{\varepsilon}\, e^{-\lambda R_X}}{\lambda\sqrt{\pi}} K_2(\bar{\varepsilon}) \tag{4-66}$$

$$J_1 = \int_{R_X}^{t} H_1(\tau) e^{-\lambda\tau}\, d\tau \tag{4-67}$$

$$I_2 = \frac{\bar{\varepsilon}\, e^{-\lambda R_X}}{\sqrt{\pi}} \int_0^{t - R_X} \frac{e^{-\lambda t - \frac{\bar{\varepsilon}^2}{\tau}}}{\sqrt{\tau^3}}\, d\tau = \frac{\bar{\varepsilon}\, e^{-\lambda R_X}}{\sqrt{\pi}} K_2(\bar{\varepsilon}) \tag{4-68}$$

$$J_2 = \int_{R_X}^{t} H_2(\tau) e^{-\lambda\tau} d\tau \tag{4-69}$$

$$I_3 = \frac{e^{-\lambda R_X}}{\sqrt{\pi}} \int_{R_X}^{t} \frac{e^{-\lambda\tau - \frac{\bar{\varepsilon}^2}{\tau}}}{\sqrt{\tau}} d\tau = \frac{e^{-\lambda R_X}}{\sqrt{\pi}} K_1(\bar{\varepsilon}) \tag{4-70}$$

$$J_3 = \int_{R_X}^{t} H_3(\tau) e^{-\lambda\tau} d\tau \tag{4-71}$$

where K_0, K_1, and K_2 are given by Equations 3-79a, 3-81, and 3-82, and H_1, H_2, and H_3 are given by Equations 4-29, 4-59, and 4-60, respectively. Writing

$$\bar{\xi}_k = k\beta + \bar{\varepsilon} \tag{4-72}$$

and while noting that

$$\int_{R_X}^{t} e^{-\lambda\tau} \frac{d^n}{d\varepsilon^n} \left[\mathrm{erf}\left(\frac{\bar{\xi}_k}{\sqrt{\tau - R_X}} \right) \right] d\tau = \frac{d^n}{d\varepsilon^n} \left[L\left(\bar{\xi}_k \right) \right] \tag{4-73}$$

where

$$L\left(\bar{\xi}_k \right) = e^{-\lambda R_X} \int_0^{t-R_X} e^{-\lambda\tau} \mathrm{erf}\left(\frac{\bar{\xi}_k}{\sqrt{\tau}} \right) d\tau \ . \tag{4-74}$$

integration by parts yields

$$L(\bar{\xi}_k) = -\frac{e^{-\lambda t}}{\lambda} \mathrm{erf}\left(\frac{\bar{\xi}_k}{\sqrt{t - R_X}} \right) + \frac{e^{-\lambda R_X}}{\lambda} - \frac{\bar{\xi}_k e^{-\lambda R_X}}{\lambda\sqrt{\pi}} \int_0^{t-R_X} \frac{e^{-\lambda\tau - \frac{\bar{\xi}_k^2}{\tau}}}{\sqrt{\tau^3}} d\tau$$

$$= -\frac{e^{-\lambda t}}{\lambda} \mathrm{erf}\left(\frac{\bar{\xi}_k}{\sqrt{t - R_X}} \right) + \frac{e^{-\lambda R_X}}{\lambda} - \frac{\bar{\xi}_k e^{-\lambda R_X}}{\lambda\sqrt{\pi}} K_2(\bar{\xi}_k) \ . \tag{4-75}$$

Substituting for $K_2(\bar{\xi}_k)$ (Eq. 3-82) in the last term of the above equation, it may then be shown that

$$\frac{d^n}{d\varepsilon^n} \left[L(\bar{\xi}_k) \right] = -\frac{e^{-\lambda t}}{\lambda} \frac{d^n}{d\varepsilon^n} \left[\mathrm{erf}\left(\frac{\bar{\xi}_k}{\sqrt{t - R_X}} \right) \right] - \frac{e^{-\lambda R_X}}{2\lambda} \left[\lambda^{n/2} e^{2\bar{\xi}_k\sqrt{\lambda}} + (-1)^n \lambda^{n/2} e^{-2\bar{\xi}_k\sqrt{\lambda}} \right.$$

$$\left. - \frac{d^n}{d\varepsilon^n} \left[e^{2\bar{\xi}_k\sqrt{\lambda}} \mathrm{erf}\left(\frac{\bar{\xi}_k}{\sqrt{t - R_X}} + \sqrt{\lambda(t - R_X)} \right) + e^{-2\bar{\xi}_k\sqrt{\lambda}} \mathrm{erf}\left(\frac{\bar{\xi}_k}{\sqrt{t - R_X}} - \sqrt{\lambda(t - R_X)} \right) \right] \right] \tag{4-76}$$

The last member of the above equation may be evaluated using Leibnitz's theorem for differentiation (Eq. C-6 along with Eq. C-3) and Equation 4-31b. Using the above notations, Equations 4-67, 4-69, and 4-71 may now be written as

$$J_1 = \sum_{k=1}^{\Omega_o} \sum_{m=1}^{k} a_{km} \varepsilon^m \frac{d^m}{d\varepsilon^m} [L(\bar{\xi}_k)] \tag{4-77}$$

$$J_2 = \sum_{k=1}^{\Omega_o} \sum_{m=1}^{k} a_{km} \varepsilon^m \frac{d^{m+2}}{d\varepsilon^{m+2}} [L(\bar{\xi}_k)] \ . \tag{4-78}$$

$$J_3 = \sum_{k=1}^{\Omega_o} \sum_{m=1}^{k} a_{km} \left[m\varepsilon^{m-1} \frac{d^m}{d\varepsilon^m} [L(\bar{\xi}_k)] + \varepsilon^m \frac{d^{m+1}}{d\varepsilon^{m+1}} [L(\bar{\xi}_k)] \right] \tag{4-79}$$

Reverting to Equation 4-64 and using the above notations, this becomes

$$M(t) = A^o \int_0^\infty \psi(\chi,\sigma) \left[{}_x\bar{F}_1 [K_o(\bar{\varepsilon}) + \frac{\bar{\varepsilon}\, e^{-\lambda R\chi}}{\lambda\sqrt{\pi}} K_2(\bar{\varepsilon}) + J_1] \right.$$

$$\left. + {}_xF_2^* \left[R\left(\frac{\bar{\varepsilon}\, e^{-\lambda R\chi}}{\sqrt{\pi}} K_2(\bar{\varepsilon}) + J_2 \right) + c_f \left(\frac{e^{-\lambda R\chi}}{\sqrt{\pi}} K_1(\bar{\varepsilon}) - J_3 \right) \right] \right] U(t - R\chi) \ . \tag{4-80}$$

4.2 NO LONGITUDINAL DISPERSION

With the streamlines assumed normal to the source (i.e., $v = 0$) and neglecting the longitudinal dispersion effects (i.e., $D_{xx} = D_{xy} = 0$), Equations 4-1 to 4-3 are still satisfied. In this case, the solution in the fracture and rock matrix may be obtained from Equations 4-32 and 4-51 after implementing on the one hand the relation given by Equation 3-50 and proper substitution for the correspondence of the variables ε (i.e., ε') and χ (i.e., χ') on the other hand, to yield

$$A(x,y,t) = A^o e^{-\lambda t} E_\Omega G_F'(t - R\chi')\, U(t - R\chi') \tag{4-81}$$

$$B(x,y,z,t) = A^o e^{-\lambda t} E_\Omega G_R'(t - R\chi')\, U(t - R\chi') \tag{4-82}$$

where

$$G_F'(t) = \mathrm{erfc}\left(\frac{c_f \chi'}{2\sqrt{t}} \right) + \sum_{k=1}^{\Omega_o} \sum_{m=1}^{k} a_{km} (c_f \chi')^m \frac{d^m}{d\varepsilon'^m} \left[\mathrm{erf}\left(\frac{2k\beta + \varepsilon'}{2\sqrt{t}} \right) \right] \tag{4-83}$$

$$G_R'(t) = \sum_{i=1}^{\Omega_0''} (-1)^{i+1} \sum_{k=1}^{2} \operatorname{erfc}\left[\frac{{}^{k}Y_{i0} + c_f X'}{2\sqrt{t}}\right]$$

$$+ \sum_{i=1}^{\Omega_1''} \sum_{j=1}^{\Omega_2''} (-1)^{j+1} \sum_{k=1}^{2} \sum_{m=1}^{i} a_{im}(c_f X') \frac{d^m}{d\varepsilon'^m} \left[\operatorname{erf}\left(\frac{{}^{k}Y_{ij} + \varepsilon'}{2\sqrt{t}}\right)\right] \tag{4-84}$$

Note that χ' corresponds to x/u.

Based on Equations 3-50 and 3-70b, the mass flux and cumulative mass flux in the fracture may be obtained from Equations 4-61 and 4-80.

$$F(t) = A^o e^{-\lambda t} F_3 G_F'(t - R\chi') U(t - R\chi') \tag{4-85}$$

$$M(t) = A^o F_3 \left(K_o(\bar{\bar{\varepsilon}}) + \frac{\bar{\bar{\varepsilon}} e^{-\lambda R\chi'}}{\lambda\sqrt{\pi}} K_2(\bar{\bar{\varepsilon}}) + J_1' \right) U(t - R\chi') \tag{4-86}$$

where

$$J_1' = \sum_{k=1}^{\Omega_0} \sum_{m=1}^{k} a_{km} (\varepsilon')^m \frac{d^m}{d(\varepsilon')^m} [L(\bar{\bar{\xi}}_k)] \tag{4-87}$$

$$\bar{\bar{\xi}}_k = k\beta + \bar{\bar{\varepsilon}} \tag{4-88a}$$

$$\bar{\bar{\varepsilon}} = \frac{\varepsilon'}{2} = \frac{c_f X'}{2} \tag{4-88b}$$

and functions K_0, K_2, and F_3 are given by Equations 3-79a, 3-82, and 3-88, respectively.

4.3 SOLUTION FOR BAND RELEASE

The general form of the solution for the finite-duration band release mode based on the boundary condition given by Equation 2-20 and which uses the superposition technique (see Foglia et al., 1979) may be written as

$${}^{b}A(x,y,t) = A(x,y,t; A^o) - A(x,y,t-T; A^o e^{-\lambda T}) U(t-T) \tag{4-89}$$

$${}^{b}B(x,y,z,t) = B(x,y,z,t; B^o) - B(x,y,z,t-T; B^o e^{-\lambda T}) U(t-T) \tag{4-90}$$

where T corresponds to the leach duration and superscript b indicates the band release solution.

4.4 CONVERGENCE OF SERIES

The solutions presented in this section include for the most part components in the form of series. Although tentative limits of their upper bound for the longitudinal dispersion-free solutions have been proposed in Section 4.5, these might converge prematurely, particularly when the ratio of $\varepsilon/2\sqrt{t}$ becomes excessively smaller than unity.

Convergence of these series is assumed to be reached when the following criteria are simultaneously met, i.e., for a given series the absolute percentage relative error in two consecutive steps of the summation process is less than or equal to 0.1 and the absolute difference at these steps is less than or equal to 10^{-6}.

With a series at the nth step of its evaluation defined as

$$S_n = \sum_{i=1}^{n} a_i \tag{4-91}$$

the first convergence criterion corresponds to

$$\left| \frac{S_m - S_{m-1}}{S_m} \right| \leq 10^{-3}; m = n-1, n \text{ (relative error)} \tag{4-92a}$$

whereas the second corresponds to

$$\left| S_n - S_{n-1} \right| \leq 10^{-6} \text{ . (absolute error)} \tag{4-92b}$$

4.5 REMARKS

The series solution presented in this section includes a combination of complementary error function and multiple derivatives of the error function. The number of significant terms in the series summation is dependent to a large extent upon the argument of the error functions. Past a certain threshold the argument will render subsequent terms in the series negligibly small and, therefore, these terms may be neglected. For example, an argument for the error function corresponding to 5.5 will render both complementary error function and its derivatives negligibly small. Since the argument of the exponential term in the derivative expression of the error function emerges as the square of its argument, the argument of the exponential and error function are accordingly related. In the related computer code, the error function is evaluated internally (Cody, 1969) and assigned its

maximum value of one when its argument (i.e., ARG′) becomes greater or equal to the square root of the maximum permissible value of the exponential argument (i.e., ARG) as allowed by the computer.

An estimate of some tentative limits for the values of Ω_0'', Ω_1'', and Ω_2'' (see Eqs. 4-31a and 4-50) may be obtained after equating the argument of the complementary error function and exponential argument appearing in the derivative terms of the error functions to ARG′ and ARG, respectively. Moreover, it may also be shown that the reported solutions are dependent on some dimensionless numbers, such as the Fourier number defined as

$$Fo = \frac{D_p(t - R\chi)}{R'(L-b)^2} \quad , \tag{4-93}$$

a dimensionless number determining the penetration of the solute front into the rock matrix over a given period of time, which is analogous to the theory of heat conduction in solids. Thus, the larger the Fourier number, the greater the elapsed time for the diffusion process.

4.5.1 Fracture

In order to determine a limiting value for Ω_0 in Equation 4-31a, we write

$$\frac{(2\Omega_0\beta + c_f\chi)^2}{4(t - R\chi)} \leq ARG \quad . \tag{4-94}$$

Substituting for β (see Eq. 4-7b) and using Equation 4-94, we find that

$$\Omega_0 \leq \left[(ARG\ Fo)^{1/2} - P_0\right] \tag{4-95}$$

where P_0 is a dimensionless number defined as

$$P_0 = \frac{\phi D_p \chi}{2b(L-b)} \quad . \tag{4-96}$$

Note that in this case the second member on the right-hand side of Equation 4-31a would contribute to the solution in the fracture only when

$$Fo \geq \frac{1}{ARG}\left[1 + P_0\right]^2 \tag{4-97}$$

.as otherwise Equation 4-31a now reduces to

$$G_F(t) = \mathrm{erfc}\left(\frac{c_f X}{2\sqrt{t}}\right), \mathrm{Fo} < \frac{1}{\mathrm{ARG}}\left[1 + P_0\right]^2 \tag{4-98}$$

which indicates that for this specific range of values of Fo based on a value for ARG greater than 30, the solutions of the concentration in the fracture for infinite and finite diffusion into the rock matrix become practically identical.

4.5.2 Rock

Referring to the argument of the complementary error function term in Equation 4-50, which is obtained after setting k = 1 (see Eq. 4-42a), the limiting value of Ω_0 may be found after writing

$$\frac{(2\Omega_0'' - 1)\beta - \mu + c_f X}{2\sqrt{t - R_X}} \leq \mathrm{ARG}' \quad . \tag{4-99}$$

Substituting for β and μ, we find that

$$\Omega_0'' \leq \mathrm{ARG}'\,\mathrm{Fo}^{1/2} + \frac{1}{2}\left(\frac{L-z}{L-b}\right) + \frac{1}{2} - P_0 \tag{4-100}$$

where μ is given by Equation 4-36. It may be shown that Ω_0 will take its lowest value corresponding to unity when Fo satisfies the following condition

$$\mathrm{Fo} \geq \frac{1}{\mathrm{ARG}}\left[\frac{1}{2}\left(\frac{z-b}{L-b}\right) + P_0\right]^2 \tag{4-101}$$

as otherwise Equation 4-50 now reduces to

$$G_r(t) = \mathrm{erfc}\left(\frac{c_r(z-b) + c_f X}{2\sqrt{t}}\right), \mathrm{Fo} < \frac{1}{\mathrm{ARG}}\left[\frac{1}{2}\left(\frac{z-b}{L-b}\right) + P_0\right]^2 \quad . \tag{4-102}$$

Since in this case the second member of Equation 4-50 cannot be evaluated, the solution of the concentration in the rock matrix becomes identical to the single fracture case.

Referring to the second term in Equation 4-50 and selecting the smallest argument (i.e., ${}^1\gamma_{ij}/4t$ where ${}^1\gamma_{ij}$ is given by Equation 4-42a), the value for Ω_1'' may be found after writing

$$\frac{[(2m-1)\beta - \mu c_f \chi]^2}{4(t-R\chi)} \leq \mathrm{ARG} \tag{4-103}$$

where $m = \Omega_1^{\alpha''} = \Omega_2''$. Substituting for β and μ, we have

$$m \leq (\mathrm{ARG}\, F_0)^{1/2} + \left(\frac{L-z}{L-b}\right) + \frac{1}{2} - P_0 \tag{4-104}$$

and in this case the number of summations corresponds to

$$\sum_{i=1}^{m} i \ .$$

Note that in the evaluation of χ, the value of the variable σ is taken to correspond to σ_{UL} given by Equation B.1-11b (see Appendix B). When the longitudinal dispersion effects are ignored, then χ is substituted by χ'. The reader may easily observe that for a given value of the dimensionless number $c_f \chi/2\sqrt{t}$, this particular solution method loses its viability with increasing values of the Fourier number. However, of interest are values of $c_f\chi/2\sqrt{t} \leq 0.1$ which render the terms associated to the innermost series summation in Equations 4-31a, 4-50, 4-60, 4-61a, 4-77, 4-78, 4-79, 4-84, and 4-87 negligibly small (i.e., $<10^{-6}$) past the sixth term of the summation. Consequently, in such instances the series solution may conveniently substitute the contour integration solution (see Chapter 5), in which convergence characteristics are adversely affected by decreasing values of the dimensionless number.

5.0 MULTIPLE PARALLEL FRACTURE CASE WITH FINITE DIFFUSION FIELD: CONTOUR INTEGRATION

5.1 FRACTURE

Rewriting Equation 4-4:

$$\bar{A}(x,y,s) = \int_0^\infty \psi(x,\sigma)E_\Omega A^o\theta(s)e^{{}^r a^X} d\sigma \tag{5-1}$$

The inverse Laplace transform of the above equation may be sought after using the Bromwich complex inversion formula (Carslaw and Jaeger, 1958) and applying the Translation, Linear Transformation, and Convolution Theorems to the last two terms of Equation 5-1.

$$L^{-1}\left[\theta(s)e^{{}^r a^X}\right] = L^{-1}\left[\frac{\exp[-R_X(s+\lambda)]}{(s+\lambda)} \exp\left[-c_f X(s+\lambda)^{1/2}\tanh(c_r(L-b)(s+\lambda)^{1/2})\right]\right]$$

$$= e^{-\lambda t}\int_0^{t-R_X} G_F(\tau,\varepsilon,\beta)d\tau \tag{5-2}$$

where

$$G_F(\tau,\varepsilon,\beta) = L^{-1}\left[\exp[-\varepsilon(s)^{1/2}\tanh(\beta(s)^{1/2})]\right] = \frac{1}{\pi}\int_0^\infty \eta\exp(\beta_r)\cos(\beta_\ell)d\eta \tag{5-3}$$

with

$$\varepsilon = c_f X \tag{5-4a}$$

$$\beta = c_r(L-b) \tag{5-4b}$$

$$\beta_r = -\frac{\varepsilon\eta}{2}\left[\frac{\sinh(\beta\eta) - \sin(\beta\eta)}{\cosh(\beta\eta) + \cos(\beta\eta)}\right] \tag{5-4c}$$

$$\beta_\ell = \frac{\eta^2\tau}{2} - \gamma_\ell \tag{5-4d}$$

$$\gamma_\ell = \frac{\varepsilon\eta}{2}\left[\frac{\sinh(\beta\eta) + \sin(\beta\eta)}{\cosh(\beta\eta) + \cos(\beta\eta)}\right] . \tag{5-4e}$$

Note that Equation 5-3 was derived by Skopp and Warrick (1974).

Writing the last term under the integral sign in Equation 5-3 (i.e., $\cos\beta_\ell$) in a more explicit form using Equation 5-4d, we have

$$\cos(\beta_\ell) = \cos\left(\frac{\eta^2}{2}\tau\right)\cos(\gamma_\ell) + \sin\left(\frac{\eta^2}{2}\tau\right)\sin(\gamma_\ell) \ . \tag{5-5}$$

Integration of Equation 5-3 with respect to τ using Equation 5-5, we obtain

$$G_F(t-R\chi,\varepsilon,\beta) = \int_0^{t-R\chi} G_F(\tau,\varepsilon,\beta)d\tau = \frac{2}{\pi}\int_0^\infty \frac{\exp(\beta_r)}{\eta}[\sin(v)\cos(\gamma_\ell) + [1-\cos(v)]\sin(\gamma_\ell)]d\eta \tag{5-6}$$

where

$$v = \frac{\eta^2(t-R\chi)}{2} = \frac{\eta^2}{2}\left(t - \frac{Rx^2}{4D_{xx}\sigma^2}\right) \ . \tag{5-7}$$

Using the formula

$$\sin(a+b) = \sin(a)\cos(b) + \cos(a)\sin(b) \tag{5-8}$$

the inverse Laplace transform of Equation 5-3 yielding the final solution of the concentration in a system of parallel fractures may be written as

$$A(x,y,t) = \frac{2}{\pi}A^o e^{-\lambda t}\int_0^\infty \psi(x,\sigma)E_\Omega \int_0^\infty \frac{\exp(\beta_r)}{\eta}\cdot[\sin(\gamma_\ell) + \sin(v-\gamma_\ell)]U(t-R\chi)d\eta d\sigma \tag{5-9}$$

where χ, γ_ℓ, and v are given by Equations 3-22d, 5-4e, and 5-7, respectively.

5.2 ROCK MATRIX

Substitution of Equation 5-1 in Equation 4-1 gives

$$\overline{B}(x,y,z,s) = A^o\int_0^\infty \psi(x,\sigma)E_\Omega\theta(s)e^{r_a\chi}\cosh[r_b(z-L)]\mathrm{sech}[r_b(b-L)]d\sigma \tag{5-10}$$

The inverse Laplace transform of Equation 5-10 after substituting for r_b (see Equation 3-5a) may be obtained (see Appendix A, Equation A.2-5) from

$$L^{-1}\frac{\cosh\left[\mu(s)^{1/2}\right]\mathrm{sech}\left[\beta(s)^{1/2}\right]}{s} = 1 - \sum_{n=0}^{\infty}\Gamma_\delta\exp(-\delta^2 t) \tag{5-11}$$

where

$$\mu = c_r (L - z) \tag{5-12a}$$

$$\delta = \frac{(2n+1)\pi}{2\beta} \tag{5-12b}$$

$$\Gamma_\delta = (-1)^n \frac{4}{(2n+1)\pi} \cos(\delta\mu) \ . \tag{5-12c}$$

Using Equations 5-3 and 5-11, the inverse Laplace transform of Equation 5-10 is obtained after applying the Translation, Linear Transformation, and Convolution Theorems, respectively. This may be written as

$$B(x,y,z,t) = \frac{A^0}{\pi} e^{-\lambda t} \int_0^\infty \psi(x,\sigma) E_\Omega \int_0^\infty \eta \exp(\beta_r) \, . \int_0^{t-R\chi} \cos(\beta_\ell) \, . \, [1 - \sum_{n=0}^{\infty} \Gamma_\delta \exp[-\delta^2(t-\tau)]]$$

$$U(t - R\chi) d\tau \, d\eta \, d\sigma \ . \tag{5-13}$$

Note that $\cos(\beta_\ell)$ is given by Equation 5-5. Integration of Equation 5-13 with respect to τ while making use of the following formulae

$$\int e^{az} \sin bz \, dz = \frac{e^{az}}{a^2 + b^2} (a \sin bz - b \cos bz) \tag{5-14a}$$

$$\int e^{az} \cos bz \, dz = \frac{e^{az}}{a^2 + b^2} (a \cos bz + b \sin bz) \tag{5-14a}$$

$$\cos(a+b) = \cos(a)\cos(b) - \sin(a)\sin(b) \tag{5-14c}$$

will then yield a tentative solution of the concentration in the rock matrix. This may be written as

$$B(x,y,z,t) = \frac{A^0}{\pi} e^{-\lambda t} \int_0^\infty \psi(x,\sigma) E_\Omega \int_0^\infty \eta \exp(\beta_r) \Big\{ \frac{2}{\eta^2} [\sin(\gamma_\ell) + \sin(v - \gamma_\ell)] - \sum_{m=0}^{\infty} \frac{\Gamma_\delta}{\delta^4 + \eta^4/4} [\exp(-\delta^2 R\chi)$$

$$[\delta^2 \cos(v - \gamma_\ell) + \frac{\eta^2}{2} \sin(v - \gamma_\ell)] - \exp(-\delta^2 t)[\delta^2 \cos(\gamma_\ell) - \frac{\eta^2}{2} \sin(\gamma_\ell)]] \, U(t - R\chi) \Big\} d\eta \, d\sigma \tag{5-15}$$

where χ, γ_ℓ, v, δ, and Γ_δ are given by Equations 3-22d, 5-4e, 5-7, 5-12b, and 5-12c, respectively.

Because of the slow convergence registered by the solution given by Equation 5-15 for small Fourier numbers and its deficiency to cope adequately with large Fourier numbers (i.e., >20) since Equation 5-11 reduces to one in such a case, an alternative solution based on a contour integration along the imaginary axis was sought.

Referring to Equation 5-10 and applying to this the Convolution Theorem yields

$$B(x,y,z,t) = A^{o}e^{-\lambda t}\int_0^{\infty}\psi(x,\sigma)E_{\Omega}\int_0^{t}G_R(\tau,\varepsilon,\beta,\mu)\,d\tau d\sigma\;U(t-R\chi) \tag{5-16}$$

where

$$G_R(\tau,\varepsilon,\beta,\mu) = L^{-1}\exp\left[-\varepsilon(s)^{1/2}\tanh\beta(s)^{1/2}\right]\frac{\cosh\mu(s)^{1/2}}{\cosh\beta(s)^{1/2}} \tag{5-17}$$

Substituting $s = i\eta^2/2$ and and $s = -i\eta^2/2$ on the positive and negative parts of the imaginary axis in the above equation and using the following relations

$$\cosh(z) = \cosh x\cos y + i\sinh x\sin y \tag{5-18}$$

$$\tanh(z) = \frac{\sinh 2x + i\sin 2y}{\cosh 2x + \cos 2y} \tag{5-19}$$

and multiplying both numerator and denominator of Equation 5-17 by the conjugate of Equation 5-18 yields

$$G_R(\tau,\varepsilon,\beta,\mu) = \frac{1}{8\pi}\int_0^{\infty}\sum_{m=1}^{2}\sum_{n=1}^{2}\sum_{p=1}^{2}\frac{\eta}{\delta_1}\exp\left[\beta_r + (-1)^{m+1}\frac{\beta\eta}{2} + (-1)^{n+1}\frac{\mu\eta}{2}\right]\cdot$$

$$\exp\left[i(-1)^{p+1}\left(\frac{\eta^2\tau}{2} - \gamma_\ell + (-1)^m\frac{\beta\eta}{2} - (-1)^n\frac{\mu\eta}{2}\right)\right]d\eta \tag{5-20}$$

where

$$\delta_1 = \cosh^2\left(\frac{\beta\eta}{2}\right)\cos^2\left(\frac{\beta\eta}{2}\right) + \sinh^2\left(\frac{\beta\eta}{2}\right)\sin^2\left(\frac{\beta\eta}{2}\right) \tag{5-21}$$

and β_r is given by Equation 5-4c.

Recognizing the following relation

$$e^{i\theta} = \cos\theta + i\sin\theta \tag{5-22}$$

Equation 5-20 may now be written as

$$G_R(\tau,\varepsilon,\beta,\mu) = \frac{1}{4\pi}\int_0^\infty \sum_{m=1}^{2}\sum_{n=1}^{2} \frac{\eta}{\delta_1} \exp[\bar{\beta}_r]\cos[\bar{\beta}_\ell]\,d\eta \tag{5-23}$$

where

$$\bar{\beta}_r = \beta_r + (-1)^{m+1}\frac{\beta\eta}{2} + (-1)^{n+1}\frac{\mu\eta}{2} \tag{5-24a}$$

$$\bar{\beta}_\ell = \frac{\eta^2\tau}{2} - \bar{\gamma}_\ell \tag{5-24b}$$

$$\bar{\gamma}_\ell = \gamma_\ell + (-1)^{m+1}\frac{\beta\eta}{2} - (-1)^{n+1}\frac{\mu\eta}{2} \tag{5-24c}$$

Noting that Equations 5-23 and 5-24b have forms similar to Equations 5-3 and 5-4d, integration of $\cos[\beta_\ell]$ with respect to τ, following identical steps given by Equations 5-5 through 5-8, will then yield the final solution of the concentration in the rock matrix which may be written as

$$B(x,y,z,t) = \frac{1}{2\pi}A^o e^{-\lambda t}\int_0^\infty \psi(x,\sigma)E_\Omega \int_0^\infty \sum_{m=1}^{2}\sum_{n=1}^{2} \frac{\exp(\bar{\beta}_r)}{\delta_1\eta}[\sin(\bar{\gamma}_\ell)+\sin(v-\bar{\gamma}_\ell)]U(t-R\chi)d\eta d\delta \tag{5-25}$$

where v is given by Equation 5-7.

5.3 MASS FLUX

The general form of the equation for the mass flux in the fracture is given by Equation 3-53. This requires the evaluation of the derivatives terms $\partial A/\partial x$ and $\partial A/\partial y$. Referring to Equation 5-9, one obtains

$$\frac{\partial A}{\partial x} = A^o e^{-\lambda t}\int_0^\infty \psi(x,\sigma)\,[(2a_1(\sigma-a_1x)E_\Omega + E_\Omega^x)G_F(t-R\chi,\varepsilon,\beta)$$

$$+ E_\Omega G_F^x(t-R\chi,\varepsilon,\beta)]\,U(t-R\chi)\,d\sigma \tag{5-26}$$

$$\frac{\partial A}{\partial y} = A^o e^{-\lambda t}\int_0^\infty \psi(x,\sigma)\,E_\Omega^y G_F(t-R\chi,\varepsilon,\beta)\,U(t-R\chi)\,d\sigma \tag{5-27}$$

with

$$G_F^x(t-R\chi,\varepsilon,\beta) = \frac{2}{\pi}\int_0^\infty \frac{\exp(\beta_r)}{\eta}\,\bar{\beta}\left(c_f\zeta_r(\sin(\gamma_\ell)) + \sin(v-\gamma_\ell) + c_f\zeta_\ell\cos(\gamma_\ell)\right.$$

$$\left. - \left(\frac{R\eta^2}{2} + c_f\zeta_\ell\right)\cos(v-\gamma_\ell)\right)d\eta \tag{5-28a}$$

$$\zeta_\ell = \gamma_\ell/\varepsilon = \frac{\eta}{2}\left[\frac{\sinh(\beta\eta)+\sin(\beta\eta)}{\cosh(\beta\eta)+\cos(\beta\eta)}\right] \tag{5-28b}$$

$$\zeta_r = \beta_r/\varepsilon = -\frac{\eta}{2}\left[\frac{\sinh(\beta\eta)-\sin(\beta\eta)}{\cosh(\beta\eta)+\cos(\beta\eta)}\right] \tag{5-28c}$$

and terms given earlier as follows: α_1 by Equation 3-57b, β by Equations 3-59, E_Ω^x by Equation 3-62 or 3-64, and E_Ω^x by Equation 3-63 or 3-65.

With the proper substitution of Equations 5-9 and 5-26 into Equations 3-54 we find the solution for the components of the mass flux in the fracture written as

$$F_i = \frac{2}{\pi}A^o e^{-\lambda t}\int_0^\infty \psi(x,\sigma)\int_0^\infty \frac{\exp(\beta_r)}{\eta}\left[\left(\sin(\gamma_\ell)+\sin(v-\gamma_\ell)\right){}_iF_1\right.$$

$$\left. - {}_iF_2^*\left(c_f\zeta_r(\sin(\gamma_\ell)+\sin(v-\gamma_\ell)) + \cos(\gamma_\ell)c_f\zeta_\ell - \cos(v-\gamma_\ell)\left(\frac{R\eta^2}{2}+c_f\zeta_\ell\right)\right)\right]U(t-R\chi)d\eta d\sigma\ ,(i = x,y) \tag{5-29}$$

where ${}_iF_1$ and ${}_iF_2^*$ are given by Equations 3-67a and 4-62.

5.4 CUMULATIVE MASS FLUX

The general form of the equation describing the cumulative mass flux in the fracture is given by Equation 4-63.

Unidimensional Flow ($F_y = 0$)

Defining

$$I_1(t,\eta,v,\gamma_\ell,\chi) = \int_0^t e^{-\lambda\tau}\sin(\gamma_\ell)\,U(t-R\chi)d\tau \tag{5-30a}$$

$$= \int_{R\chi}^{t} e^{-\lambda\tau} \sin(\gamma_\ell) d\tau \tag{5-30b}$$

$$= \frac{\sin(\gamma_\ell)}{\lambda} (e^{-\lambda R\chi} - e^{-\lambda t}) \tag{5-30c}$$

and

$$I_2(t, \eta, v, \gamma_\ell, \chi) = \int_0^t e^{-\lambda\tau} \sin\left(\frac{\eta^2(\tau - R\chi)}{2} - \gamma_\ell\right) U(t - R\chi) d\tau \tag{5-31a}$$

$$= e^{-\lambda R\chi} \int_0^t e^{-\lambda\tau} \sin\left(\frac{\eta^2\tau}{2} - \gamma_\ell\right) d\tau \ . \tag{5-31b}$$

Recognizing the following integral (Abramowitz and Stegun, 1972),

$$\int e^{ax} \sin(bx + c) dx = \frac{e^{ax}}{a^2 + b^2} [a \sin(bx + c) - b \cos(bx + c)] \tag{5-32}$$

we may evaluate I_2 as

$$I_2(t, \eta, v, \gamma_\ell, \chi) = \frac{1}{\lambda^2 + \eta^4/4} \left[e^{-\lambda R\chi} \left(\frac{\eta^2}{2} \cos(\gamma_\ell) - \lambda \sin(\gamma_\ell) - e^{-\lambda t} \left(\frac{\eta^2}{2} \cos(v - \gamma_\ell) + \lambda \sin(v - \gamma_\ell) \right) \right) \right]. \tag{5-33}$$

$$J_1(t, \eta, v, \gamma_\ell, \chi) = \int_0^t e^{-\lambda\tau} \cos(\gamma_\ell) U(t - R\chi) d\tau \tag{5-34a}$$

$$= e^{-\lambda R\chi} \int_0^{t - R\chi} e^{-\lambda\tau} \cos(\gamma_\ell) d\tau = \frac{\cos(\gamma_\ell)}{\lambda} (e^{-\lambda R\chi} - e^{-\lambda t}) \tag{5-34b}$$

$$J_2(t, \eta, v, \gamma_\ell, \chi) = \int_0^t e^{-\lambda\tau} \cos(v - \gamma_\ell) U(t - R\chi) d\tau = e^{-\lambda R\chi} \int_0^{t - R\chi} e^{-\lambda\tau} \cos\left(\frac{\eta^2}{2} \tau - \gamma_\ell\right) d\tau \tag{5-35}$$

Recognizing the following integral (Abramowitz and Stegun, 1972)

$$\int e^{ax} \cos(bx + c) dx = \frac{e^{ax}}{a^2 + b^2} [a \cos(bx + c) + b \sin(bx + c)] \tag{5-36}$$

we may evaluate J_2 as

$$J_2(t, \eta, v, \gamma_\ell, \chi) = \frac{1}{\lambda^2+\eta^4/4}\left[e^{-\lambda R\chi}\left(\frac{\eta^2}{2}\sin(\gamma_\ell)+\lambda\cos(\gamma_\ell)\right)+e^{-\lambda t}\left(\frac{\eta^2}{2}\sin(v-\gamma_\ell)-\lambda\cos(v-\gamma_\ell)\right)\right] \tag{5-37}$$

The cumulative mass flux is then given by

$$M(t) = \frac{2}{\pi}A^o\int_0^\infty\int_0^\infty \psi(x,\sigma)\frac{\exp(\beta_r)}{\eta}\left[{}_x\overline{F}_1\sum_{k=1}^{2} I_k(t, \eta, v, \gamma_\ell, \chi)\right.$$

$$\left. - {}_xF_2^*\left(c_f\zeta_r\sum_{k=1}^{2} I_k(t,\eta,v,\gamma_\ell,\chi)+c_f\zeta_\ell J_1(t,\eta,v,\gamma_\ell,\chi)\right)-\left(\frac{R\eta^2}{2}+c_f\zeta_\ell\right)J_2(t,\eta,v,\gamma_\ell,\chi)\right]U(t-R\chi)d\eta d\sigma \tag{5-38}$$

where ${}_x\overline{F}_1$ and ${}_xF_2^*$ are given by Equations 3-74a and 4-62. Details regarding the integration of Equations 5-9, 5-25, 5-29, and 5-38 may be found in Appendix B.

5.5 NO LONGITUDINAL DISPERSION

With the streamlines assumed normal to the source (i.e., $v = 0$) and neglecting the longitudinal dispersion effects (i.e., $D_{xx} = D_{xy} = 0$), Equation 5-1 is still satisfied. In this case, the solutions in the fracture and the rock matrix are given by Equations 5-9 and 5-25 after implementing the relation given by Equation 3-50 to yield

$$A(x,y,t) = \frac{2}{\pi}A^o e^{-\lambda t}E_\Omega\int_0^\infty \frac{\exp(\beta_r')}{\eta}[\sin(\gamma_\ell') + \sin(v'-\gamma_\ell')]\,U(t-R\chi')d\eta \tag{5-39}$$

$$B(x,y,z,t) = \frac{1}{2\pi}A^o e^{-\lambda t}E_\Omega\int_0^\infty \sum_{m=1}^{2}\sum_{n=1}^{2}\frac{\exp(\overline{\beta}_r')}{\delta_1\eta}[\sin(\overline{\gamma}_\ell') + \sin(v'-\overline{\gamma}_\ell')]\,U(t-R\chi')\,d\eta \tag{5-40}$$

where

$$\varepsilon' = c_f\chi' = c_f\frac{x}{u} \tag{5-41a}$$

$$\overline{\gamma}_\ell' = \gamma_\ell(\varepsilon') \tag{5-41b}$$

$$v' = v(\chi') = \frac{\eta^2}{2}(t - R\chi') = \frac{\eta^2}{2}(t - R\frac{x}{u}) \tag{5-41c}$$

$$\beta_r' = \beta_r(\varepsilon') \tag{5-41d}$$

$$\bar{\beta}_r' = \bar{\beta}_r(\varepsilon') \tag{5-41e}$$

and δ_1 is given by Equation 5-21.

The mass flux at any point in the fracture may be obtained after substitution of Equation 5-29a (with $F_2^* = 0$) and Equation 5-29b into Equation 3-70b to yield

$$F(t) = \frac{2}{\pi} A^o e^{-\lambda t} F_3 \int_0^\infty \frac{\exp(\beta_r')}{\eta} \left[\sin(\gamma_\ell') - \sin(v' - \gamma_\ell') \right] U(t - R\chi')\, d\eta \tag{5-42}$$

where F_3 is given by Equation 3-88.

Similarly the cumulative mass flux is obtained after substitution of Equation 5-42 into Equation 4-63 and written as

$$M(t) = \frac{2}{\pi} A^o F_3 \int_0^\infty \frac{\exp(\beta_r')}{\eta} \sum_{k=1}^{2} I_k(t, \eta, v', \gamma_\ell', \chi')\, U(t - R\chi')\, d\eta \ . \tag{5-43}$$

6.0 DISCUSSION AND RESULTS FOR MULTIPLE PARALLEL FRACTURE CASE WITH FINITE DIFFUSION

The solutions for the multiple parallel fracture case using series and the contour integration presented in Chapters 4 and 5 were verified by comparing their individual performance against each other. The reported test cases included one- and two-dimensional simulations of the general form of the mass transport equation, as well as to the longitudinal dispersion-free form. Two types of radionuclide release modes were considered, step and band.

6.1 DISCUSSION OF CASE 5: SPATIAL VARIATION OF CONCENTRATION OF Np-237

This test case deals with the migration of Np-237 in a one-dimensional flow domain, where the concentration at the source is subjected to a step and a band release mode. To this effect, the flow field is assumed unidimensional (i.e., $v = 0$, $D_{yy} = D_{yx} = 0$). The concentration at the source was simulated by means of a plane source of infinite width, whereas the parallel set of fractures with an aperture of 0.005 m were assumed to be 20 m apart. The input data for this test case are presented in Table 6-1. Results reported for Cases 5A and 5B are obtained through the longitudinal dispersion-free form of the general solution. Note that in the case of the rock matrix, results were obtained for a point in space located 100 m downstream from the source. It may be added that the Fourier numbers encountered in these simulations ranged between approximately 0.01 and 1.0.

6.1.1 Results for Case 5A: Step Release Mode

Figures 6-1a, 6-1b, 6-1c, and 6-1d show a comparison of the relative concentration, mass flux, and cumulative mass flux in the fracture and the rock matrix for several points in time (i.e., $t = 10^4$, 6×10^4, 2×10^5, and 10^6 years). Results reported in Tables 6-2a through 6-2e indicate that the two solution methods reported in Chapters 4 and 5 yield identical results, with the exception of points located close to the source, where the contour integration solution in the case of the fracture seems to display a poor converging characteristic, particularly with increasing times. Upon examination of the values of the dimensionless number $\varepsilon/2\sqrt{t\text{-}R_X}$ at those points which exhibit these undesirable features, it was noted these were in all cases less than or equal to 0.1. This supports the independent investigations reported also in Appendix B. As indicated in Appendix B, the solution denotes slow convergence properties in this critical region of the flow domain. Note that in the case of the rock matrix, the concentration profile corresponding to $t = 10^4$ years is identical to one which might have been obtained using the single fracture solution, since in this instance the Fourier number is about 0.01 with $P_0 = 0.01$, which satisfies the criterion proposed in Equation 4-98.

Table 6-1. Input Parameters for Case 5

Species	Np-237
Initial Concentration A^o (arbitrary unit of activity/L^3)	1
Type of Release Mode	Case 5A: Step Case 5B: Band
Boundary Condition	Infinite Plane Source
x	100.0 m (Case 5B)
y	0.0 m
d	∞
u	10.0 m/yr
v	0.0 m/yr
D_{xx}	0.0 m^2/yr
D_{yy}	0.0 m^2/yr
D_{yx}	0.0 m^2/yr
D_p	0.01 m^2/yr
L	10.0 m
$T_{1/2}$	2.14×10^6 yr
T_L	3×10^4 yr
b	0.005 m
Φ	10^{-2}
R	1
R′	100

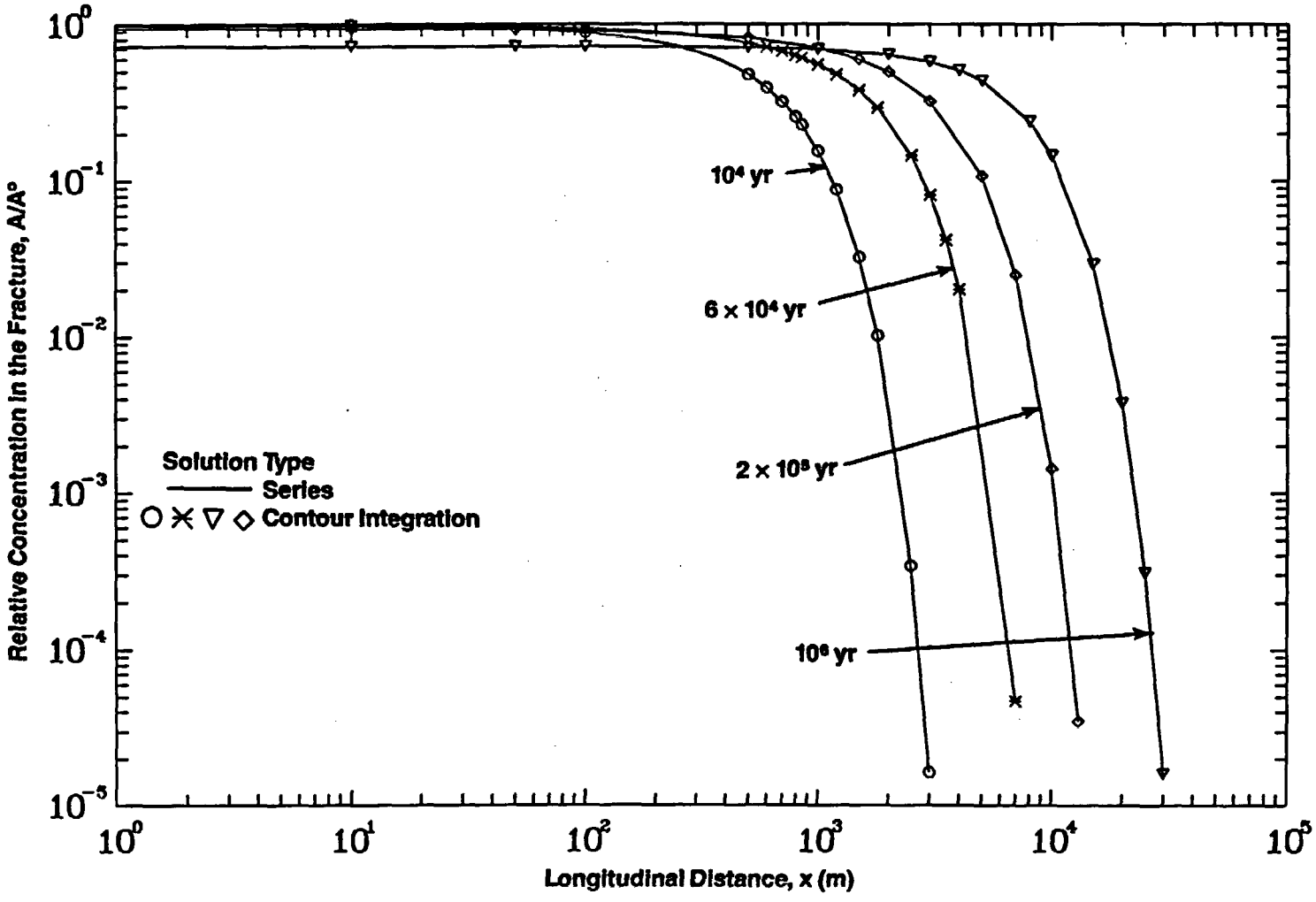

Figure 6-1a. Comparison of Spatial Variation of Relative Concentration of Np-237 in the Fracture for Different Times (Case 5A: Multiple Parallel Fractures, Step Release Mode, No Longitudinal Dispersion)

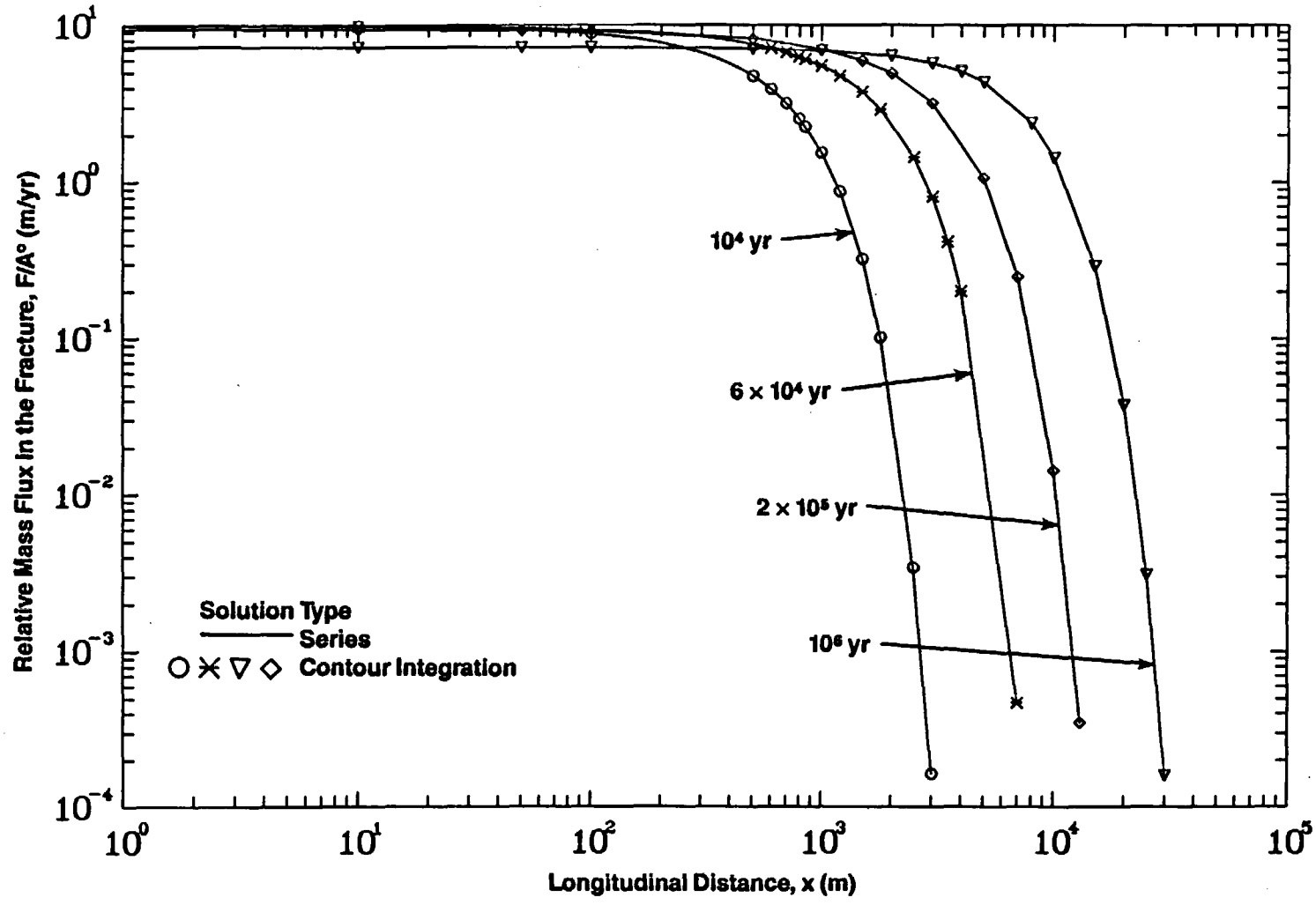

Figure 6-1b. Comparison of Spatial Variation of Relative Mass Flux of Np-237 in the Fracture for Different Times (Case 5A: Multiple Parallel Fractures, Step Release Mode, No Longitudinal Dispersion)

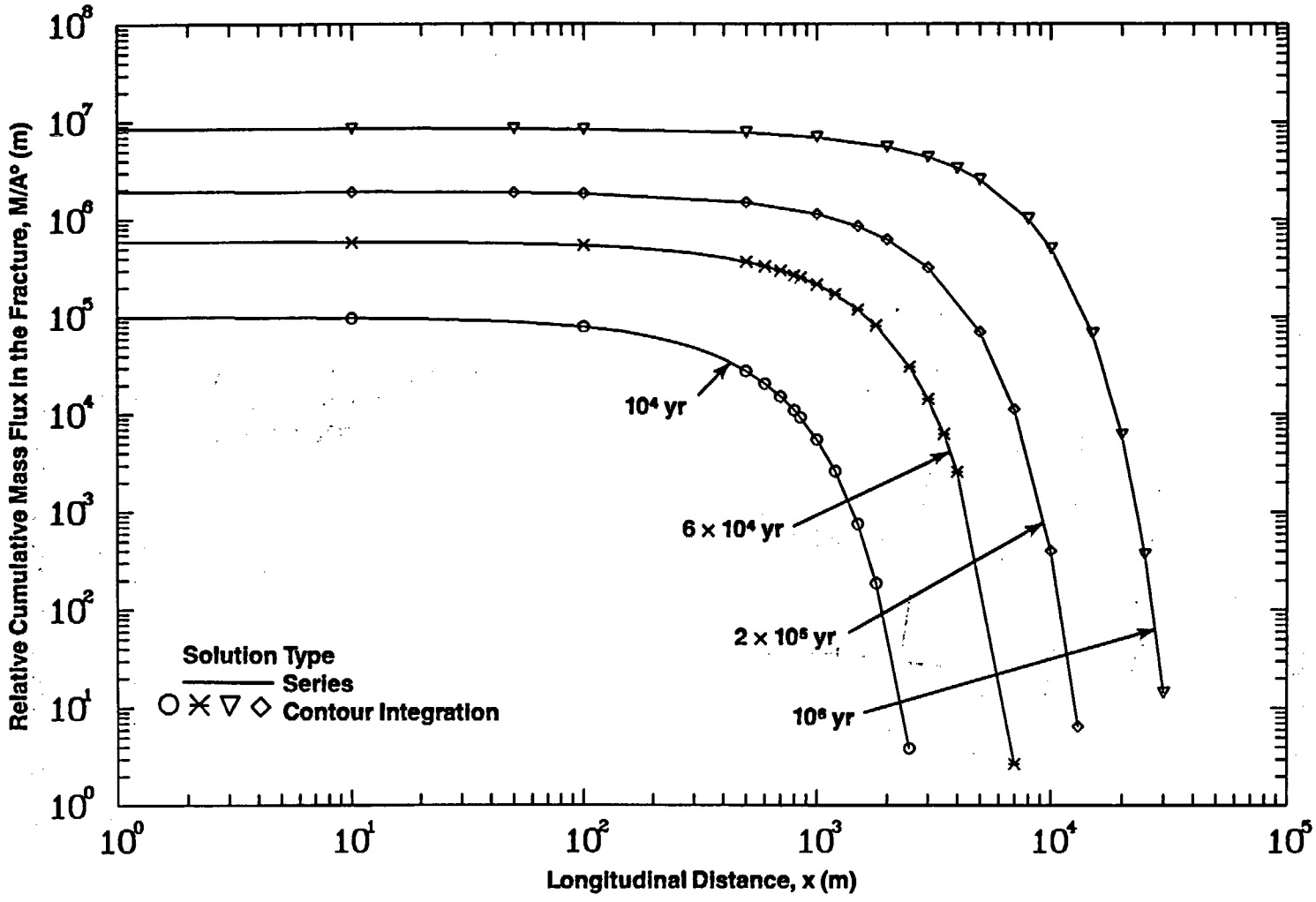

Figure 6-1c. Comparison of Spatial Variation of Relative Cumulative Mass Flux of Np-237 in the Fracture for Different Times (Case 5A: Multiple Parallel Fractures, Step Release Mode, No Longitudinal Dispersion)

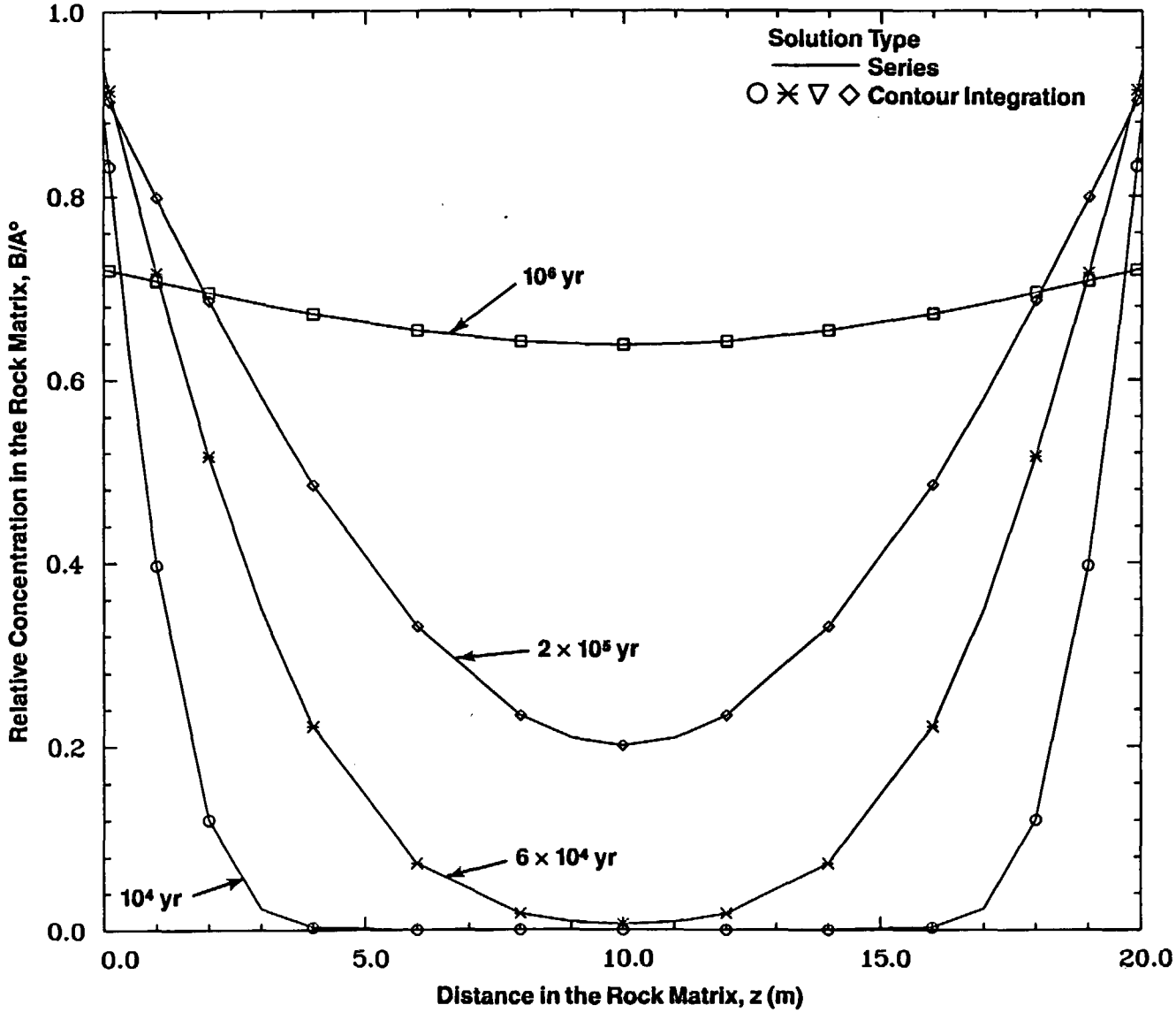

Figure 6-1d. Comparison of Spatial Variation of Relative Concentration of Np-237 in the Rock Matrix for Different Times (Case 5A: Multiple Parallel Fractures, Step Release Mode, No Longitudinal Dispersion)

Table 6-2a. Case 5A Results: Comparison of Relative Concentration, Mass Flux, and Cumulative Mass Flux in the Fracture for Np-237 at Time t = 10^4 yr (Step Release Mode)

Longitudinal Distance x (m)	Concentration A/A^o SS	Concentration A/A^o CIS	Mass Flux F/A^o (m/yr) SS	Mass Flux F/A^o (m/yr) CIS	Cumulative Mass Flux M/A^o (m) SS	Cumulative Mass Flux M/A^o (m) CIS
1.000E+00	9.956E-01		9.956E+00		9.961E+04	
2.000E+00	9.945E-01		9.945E+00		9.939E+04	
5.000E+00	9.911E-01		9.911E+00		9.871E+04	
1.000E+01	9.855E-01	9.886E-01	9.855E+00	9.886E+00	9.759E+04	9.693E+04
2.000E+01	9.743E-01		9.743E+00		9.539E+04	
5.000E+01	9.406E-01		9.406E+00		8.901E+04	
1.000E+02	8.846E-01	8.846E-01	8.846E+00	8.846E+00	7.913E+04	7.913E+04
1.500E+02	8.292E-01		8.292E+00		7.014E+04	
2.000E+02	7.746E-01		7.746E+00		6.200E+04	
2.500E+02	7.210E-01		7.210E+00		5.463E+04	
3.000E+02	6.687E-01		6.687E+00		4.799E+04	
3.500E+02	6.180E-01		6.180E+00		4.203E+04	
4.000E+02	5.690E-01		5.690E+00		3.669E+04	
4.500E+02	5.219E-01		5.219E+00		3.192E+04	
5.000E+02	4.769E-01	4.769E-01	4.769E+00	4.769E+00	2.769E+04	2.769E+04
6.000E+02	3.934E-01	3.934E-01	3.934E+00	3.934E+00	2.062E+04	2.062E+04
7.000E+02	3.195E-01	3.195E-01	3.195E+00	3.195E+00	1.515E+04	1.515E+04
8.000E+02	2.552E-01	2.552E-01	2.552E+00	2.552E+00	1.097E+04	1.097E+04
8.500E+02	2.266E-01	2.266E-01	2.266E+00	2.266E+00	9.287E+03	9.287E+03
1.000E+03	1.547E-01	1.547E-01	1.547E+00	1.547E+00	5.509E+03	5.509E+03
1.200E+03	8.748E-02	8.748E-02	8.748E-01	8.748E-01	2.604E+03	2.604E+03
1.500E+03	3.246E-02	3.246E-02	3.246E-01	3.246E-01	7.508E+02	7.508E+02
1.800E+03	1.017E-02	1.017E-02	1.017E-01	1.017E-01	1.863E+02	1.863E+02
2.500E+03	3.417E-04	3.417E-04	3.417E-03	3.417E-03	3.867E+00	3.867E+00
3.000E+03	1.644E-05	1.645E-05	1.644E-04	1.645E-04	1.381E-01	1.381E-01

SS : Series Solution
CIS : Contour Integration Solution

Table 6-2b. Case 5A Results: Comparison of Relative Concentration, Mass Flux, and Cumulative Mass Flux in the Fracture for Np-237 at Time t = 6 x 10^4 yr (Step Release Mode)

Longitudinal Distance x (m)	Concentration A/A_o SS	Concentration A/A_o CIS	Mass Flux F/A_o (m/yr) SS	Mass Flux F/A_o (m/yr) CIS	Cumulative Mass Flux M/A_o (m) SS	Cumulative Mass Flux M/A_o (m) CIS
1.000E+00	9.803E-01		9.803E+00		5.937E+05	
2.000E+00	9.799E-01		9.799E+00		5.931E+05	
5.000E+00	9.785E-01		9.785E+00		5.915E+05	
1.000E+01	9.762E-01	9.792E-01	9.762E+00	9.792E+00	5.887E+05	5.805E+05
2.000E+01	9.717E-01		9.717E+00		5.833E+05	
5.000E+01	9.582E-01		9.582E+00		5.672E+05	
1.000E+02	9.356E-01	9.357E-01	9.356E+00	9.357E+00	5.412E+05	5.411E+05
1.500E+02	9.131E-01		9.131E+00		5.161E+05	
2.000E+02	8.906E-01		8.906E+00		4.919E+05	
2.500E+02	8.682E-01		8.682E+00		4.687E+05	
3.000E+02	8.459E-01		8.459E+00		4.463E+05	
3.500E+02	8.237E-01		8.237E+00		4.248E+05	
4.000E+02	8.016E-01		8.016E+00		4.042E+05	
4.500E+02	7.796E-01		7.796E+00		3.844E+05	
5.000E+02	7.579E-01	7.579E-01	7.579E+00	7.579E+00	3.653E+05	3.653E+05
6.000E+02	7.149E-01	7.149E-01	7.149E+00	7.149E+00	3.295E+05	3.295E+05
7.000E+02	6.727E-01	6.727E-01	6.727E+00	6.727E+00	2.967E+05	2.967E+05
8.000E+02	6.316E-01	6.316E-01	6.316E+00	6.316E+00	2.665E+05	2.665E+05
8.500E+02	6.114E-01	6.114E-01	6.114E+00	6.114E+00	2.524E+05	2.524E+05
1.000E+03	5.525E-01	5.525E-01	5.525E+00	5.525E+00	2.138E+05	2.138E+05
1.200E+03	4.786E-01	4.786E-01	4.786E+00	4.786E+00	1.701E+05	1.701E+05
1.500E+03	3.785E-01	3.785E-01	3.785E+00	3.785E+00	1.187E+05	1.187E+05
1.800E+03	2.922E-01	2.922E-01	2.922E+00	2.922E+00	8.119E+04	8.119E+04
2.500E+03	1.452E-01	1.452E-01	1.452E+00	1.452E+00	3.084E+04	3.084E+04
3.000E+03	8.091E-02	8.091E-02	8.091E-01	8.091E-01	1.435E+04	1.435E+04
3.500E+03	4.188E-02	4.188E-02	4.188E-01	4.188E-01	6.261E+03	6.261E+03
4.000E+03	2.010E-02	2.010E-02	2.010E-01	2.010E-01	2.557E+03	2.557E+03
7.000E+03	4.706E-05	4.706E-05	4.706E-04	4.706E-04	2.658E+00	2.657E+00

SS : Series Solution
CIS : Contour Integration Solution

Table 6-2c. Case 5A Results: Comparison of Relative Concentration, Mass Flux, and Cumulative Mass Flux in Fracture for Np-237 at Time t = 2 x 10^5 yr (Step Release Mode)

Longitudinal Distance x (m)	Concentration A/A_o SS	Concentration A/A_o CIS	Mass Flux F/A_o (m/yr) SS	Mass Flux F/A_o (m/yr) CIS	Cumulative Mass Flux M/A_o (m) SS	Cumulative Mass Flux M/A_o (m) CIS
1.000E+00	9.370E-01		9.370E+00		1.936E+06	
1.000E+01	9.349E-01	9.373E-01	9.349E+00	9.373E+00	1.927E+06	1.900E+06
5.000E+01	9.256E-01	9.262E-01	9.256E+00	9.262E+00	1.888E+06	1.888E+06
1.000E+02	9.139E-01	9.140E-01	9.139E+00	9.140E+00	1.840E+06	1.840E+06
5.000E+02	8.205E-01	8.205E-01	8.205E+00	8.205E+00	1.490E+06	1.490E+06
1.000E+03	7.057E-01	7.057E-01	7.057E+00	7.057E+00	1.131E+06	1.131E+06
1.500E+03	5.962E-01	5.962E-01	5.962E+00	5.962E+00	8.453E+05	8.453E+05
2.000E+03	4.945E-01	4.945E-01	4.945E+00	4.945E+00	6.223E+05	6.223E+05
3.000E+03	3.212E-01	3.212E-01	3.212E+00	3.212E+00	3.215E+05	3.215E+05
5.000E+03	1.063E-01	1.063E-01	1.063E+00	1.063E+00	6.987E+04	6.987E+04
7.000E+03	2.492E-02	2.492E-02	2.492E-01	2.492E-01	1.128E+04	1.128E+04
1.000E+04	1.428E-03	1.428E-03	1.428E-02	1.428E-02	3.984E+02	3.984E+02
1.300E+04	3.484E-05	3.484E-05	3.484E-04	3.484E-04	6.464E+00	6.464E+00

SS : Series Solution
CIS : Contour Integration Solution

Table 6-2d. Case 5A Results: Comparison of Relative Concentration, Mass Flux, and Cumulative Mass Flux in the Fracture for Np-237 at Time t = 10^6 yr (Step Release Mode)

Longitudinal Distance x (m)	Concentration A/A_o SS	Concentration A/A_o CIS	Mass Flux F/A_o (m/yr) SS	Mass Flux F/A_o (m/yr) CIS	Cumulative Mass Flux M/A_o (m) SS	Cumulative Mass Flux M/A_o (m) CIS
1.000E+00	7.233E-01		7.233E+00		8.540E+06	
1.000E+01	7.231E-01	7.240E-01	7.231E+00	7.240E+00	8.525E+06	8.407E+06
5.000E+01	7.221E-01	7.233E-01	7.221E+00	7.233E+00	8.456E+06	8.458E+06
1.000E+02	7.208E-01	7.209E-01	7.208E+00	7.209E+00	8.371E+06	8.371E+06
5.000E+02	7.087E-01	7.087E-01	7.087E+00	7.087E+00	7.707E+06	7.707E+06
1.000E+03	6.895E-01	6.895E-01	6.895E+00	6.895E+00	6.926E+06	6.926E+06
2.000E+03	6.393E-01	6.393E-01	6.393E+00	6.393E+00	5.523E+06	5.523E+06
3.000E+03	5.770E-01	5.770E-01	5.770E+00	5.770E+00	4.333E+06	4.333E+06
4.000E+03	5.073E-01	5.073E-01	5.073E+00	5.073E+00	3.344E+06	3.344E+06
5.000E+03	4.352E-01	4.352E-01	4.352E+00	4.352E+00	2.539E+06	2.539E+06
8.000E+03	2.393E-01	2.393E-01	2.393E+00	2.393E+00	1.009E+06	1.009E+06
1.000E+04	1.445E-01	1.445E-01	1.445E+00	1.445E+00	5.042E+05	5.042E+05
1.500E+04	2.923E-02	2.923E-02	2.923E-01	2.923E-01	6.761E+04	6.761E+04
2.000E+04	3.756E-03	3.756E-03	3.756E-02	3.756E-02	6.104E+03	6.104E+03
2.500E+04	3.086E-04	3.086E-04	3.086E-03	3.086E-03	3.663E+02	3.663E+02
3.000E+04	1.606E-05	1.606E-05	1.606E-04	1.606E-04	1.436E+01	1.436E+01

SS : Series Solution
CIS : Contour Integration Solution

Table 6-2e. Case 5A Results: Comparison of Relative Concentration in the Rock Matrix for Np-237 for Different Times at Longitudinal Distance x = 100 m (Step Release Mode)

Time :	10^4 yr		6×10^4 yr		2×10^5 yr		10^6 yr	
Vertical Distance z (m)	SS	B/A^o CIS	SS	B/A^o CIS	SS	B/A^o CIS	SS	B/A^o CIS
5.000E-03	8.846E-01		9.356E-01		9.139E-01		7.208E-01	
1.000E-02	8.818E-01		9.345E-01		9.133E-01		7.207E-01	
2.000E-02	8.763E-01		9.322E-01		9.122E-01		7.206E-01	
4.000E-02	8.652E-01		9.277E-01		9.098E-01		7.203E-01	
8.000E-02	8.430E-01		9.187E-01		9.052E-01		7.198E-01	
1.000E-01	8.320E-01	8.320E-01	9.142E-01	9.142E-01	9.028E-01	9.028E-01	7.195E-01	7.195E-01
2.000E-01	7.774E-01		8.917E-01		8.911E-01		7.182E-01	
5.000E-01	6.209E-01		8.248E-01		8.562E-01		7.143E-01	
1.000E+00	3.966E-01	3.966E-01	7.160E-01	7.160E-01	7.985E-01	7.985E-01	7.077E-01	7.077E-01
2.000E+00	1.201E-01	1.201E-01	5.162E-01	5.162E-01	6.863E-01	6.863E-01	6.950E-01	6.950E-01
3.000E+00	2.372E-02		3.495E-01		5.809E-01		6.829E-01	
4.000E+00	2.990E-03	2.990E-03	2.215E-01	2.215E-01	4.850E-01	4.850E-01	6.718E-01	6.718E-01
6.000E+00	1.168E-05	1.168E-05	7.232E-02	7.232E-02	3.300E-01	3.300E-01	6.534E-01	6.534E-01
8.000E+00	6.704E-09	6.704E-09	1.806E-02	1.806E-02	2.333E-01	2.333E-01	6.417E-01	6.417E-01
9.000E+00	7.739E-11		8.993E-03		2.087E-01		6.387E-01	
1.000E+01	1.095E-12	1.095E-12	6.370E-03	6.370E-03	2.005E-01	2.005E-01	6.377E-01	6.377E-01
1.100E+01	7.739E-11		8.993E-03		2.087E-01		6.387E-01	
1.200E+01	6.704E-09	6.704E-09	1.806E-02	1.806E-02	2.333E-01	2.333E-01	6.417E-01	6.417E-01
1.400E+01	1.168E-05	1.168E-05	7.232E-02	7.232E-02	3.300E-01	3.300E-01	6.534E-01	6.534E-01
1.600E+01	2.990E-03	2.990E-03	2.215E-01	2.215E-01	4.850E-01	4.850E-01	6.718E-01	6.718E-01
1.700E+01	2.372E-02		3.495E-01		5.809E-01		6.829E-01	
1.800E+01	1.201E-01	1.201E-01	5.162E-01	5.162E-01	6.863E-01	6.863E-01	6.950E-01	6.950E-01
1.900E+01	3.966E-01	3.966E-01	7.160E-01	7.160E-01	7.985E-01	7.985E-01	7.077E-01	7.077E-01
1.950E+01	6.209E-01		8.248E-01		8.562E-01		7.143E-01	
1.980E+01	7.774E-01		8.917E-01		8.911E-01		7.182E-01	
1.990E+01	8.320E-01	8.320E-01	9.142E-01	9.142E-01	9.028E-01	9.028E-01	7.195E-01	7.195E-01
1.992E+01	8.430E-01		9.187E-01		9.052E-01		7.198E-01	
1.996E+01	8.652E-01		9.277E-01		9.098E-01		7.203E-01	
1.998E+01	8.763E-01		9.322E-01		9.122E-01		7.206E-01	
1.999E+01	8.818E-01		9.345E-01		9.133E-01		7.207E-01	
1.9995E+01	8.846E-01		9.356E-01		9.139E-01		7.208E-01	

SS : Series Solution
CIS : Contour Integration Solution

6.1.2 Results for Case 5B: Band Release Mode

Figures 6-2a, 6-2b, 6-2c, and 6-2d show the relative concentration, mass flux, and cumulative mass flux in the fracture and the rock matrix for several points in time (i.e., $t = 10^4, 6 \times 10^4, 2 \times 10^5$, and 10^6 years). Results reported in Tables 6-3a through 6-3d suggest similar conclusions as in the former case.

6.2 DISCUSSION OF CASE 6: TEMPORAL VARIATION OF CONCENTRATION OF Np-237, INFLUENCE OF LONGITUDINAL DISPERSION

This test case deals with the time-dependent migration of Np-237 in a one-dimensional flow domain, where longitudinal dispersion effects are considered and the concentration at the source is subjected to a step and band release mode. The observation point where the breakthrough curves are monitored is located at a distance of 500 m down gradient. The input data reported in Table 6-4 are essentially similar to those of Case 5, except for the fracture spacing, which in this instance is assigned a value of 0.6 m; in addition, three values for D_x corresponding to 10, 100, and 1000 m^2/yr were used with the main intent of verifying the two solution methods pertaining to the general form of the transport equation.

The Fourier numbers encountered in these simulations ranged approximately between 0.1 and 23, whereas the Peclet number Pe in the fracture (i.e., $Pe = uL/D_x$, where $L = 500$ m) ranged between 5 and ∞. Figures 6-3a through 6-3d present a comparison of the relative concentration, mass flux, cumulative mass flux in the fracture, and the concentration at a distance $z = 0.3$ m in the rock matrix for the step release mode; Figures 6-4a through 6-4d show corresponding plots for the band release mode. Results reported in Tables 6-5 and 6-6 show excellent agreement between the two solutions, except for very small times where the slight discrepancy displayed by the contour integration solution seems to be virtually eliminated with increasing values of the longitudinal dispersion. The impact of this parameter on the solution is reflected in the value of χ, the magnitude of which is inversely proportional to D_x; hence, for a given time t and position x the smaller χ, the higher the value of the Fourier number Fo. Results also indicate that the influence of the longitudinal dispersion effects become important for values of this parameter greater than 10 m^2/yr throughout the leaching period, beyond which the dispersive effects become less accentuated except for the case of the largest selected hypothetical value of 1000 m^2/yr. Note that in all cases reported for the rock matrix, the new contour integration based solution derived in Chapter 5 displayed a high degree of accuracy and acceptable convergence properties.

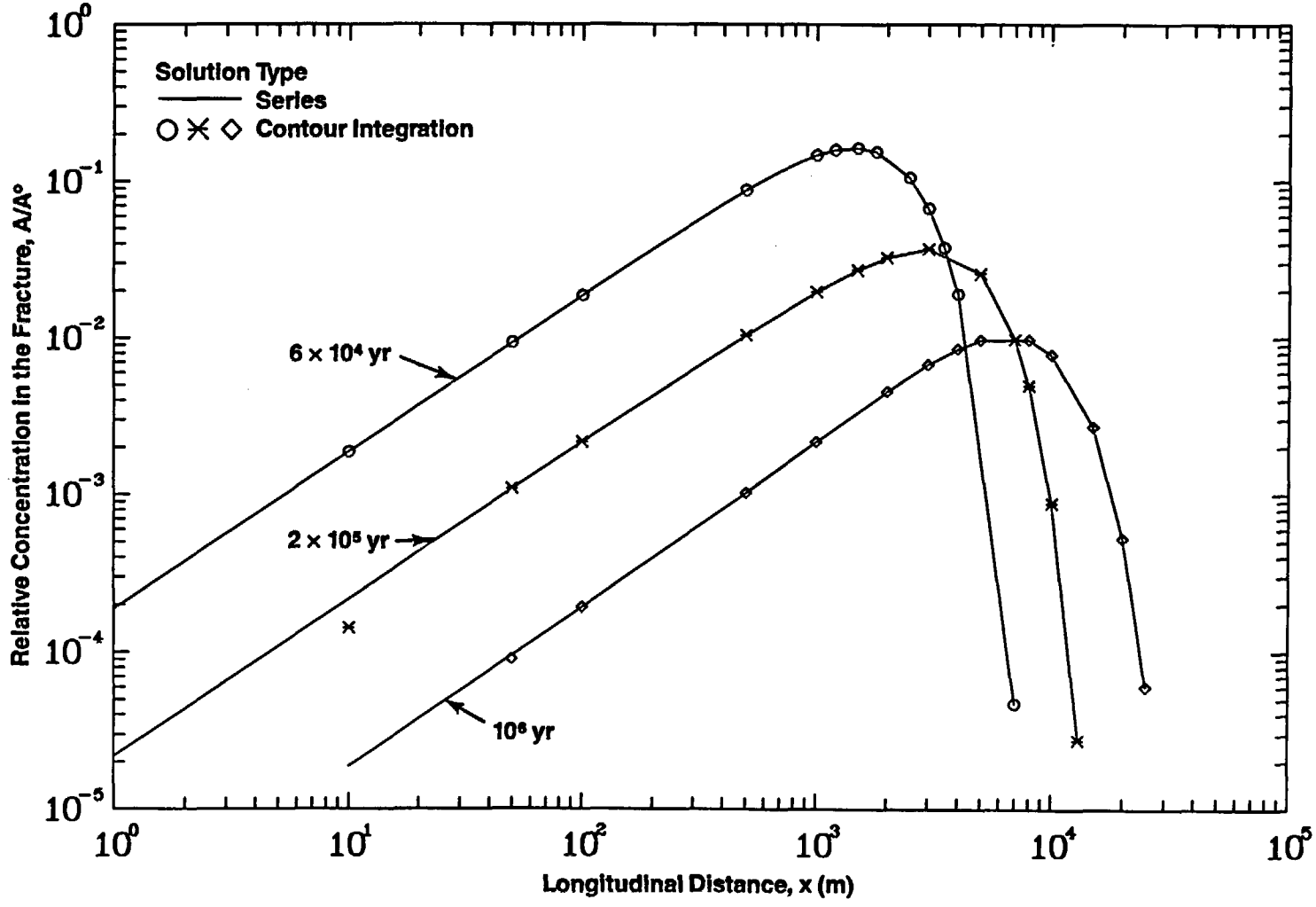

Figure 6-2a. Comparison of Spatial Variation of Relative Concentration of Np-237 in the Fracture for Different Times (Case 5B: Multiple Parallel Fractures, Band Release Mode, No Longitudinal Dispersion)

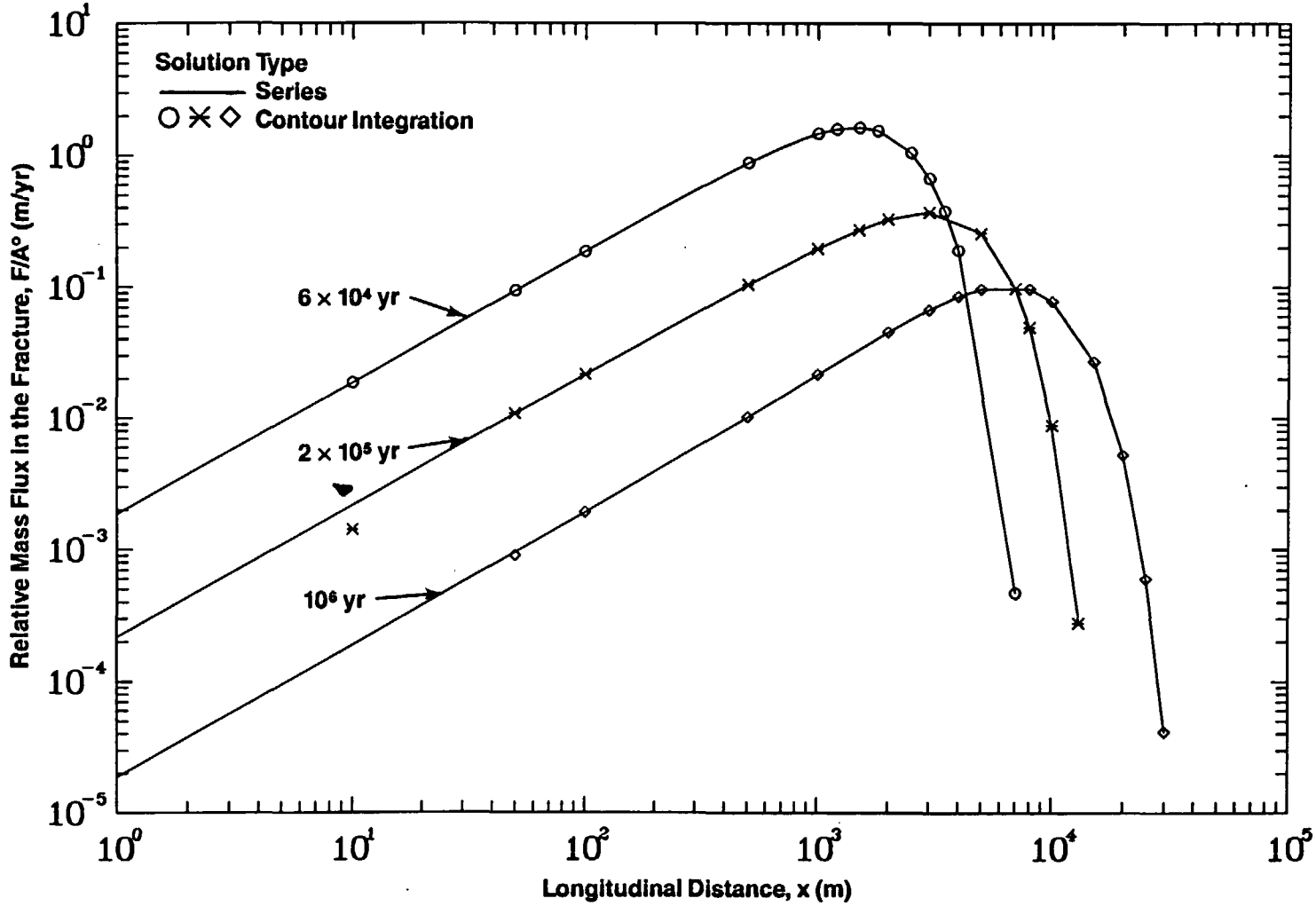

Figure 6-2b. Comparison of Spatial Variation of Relative Mass Flux of Np-237 in the Fracture for Different Times (Case 5B: Multiple Parallel Fractures, Band Release Mode, No Longitudinal Dispersion)

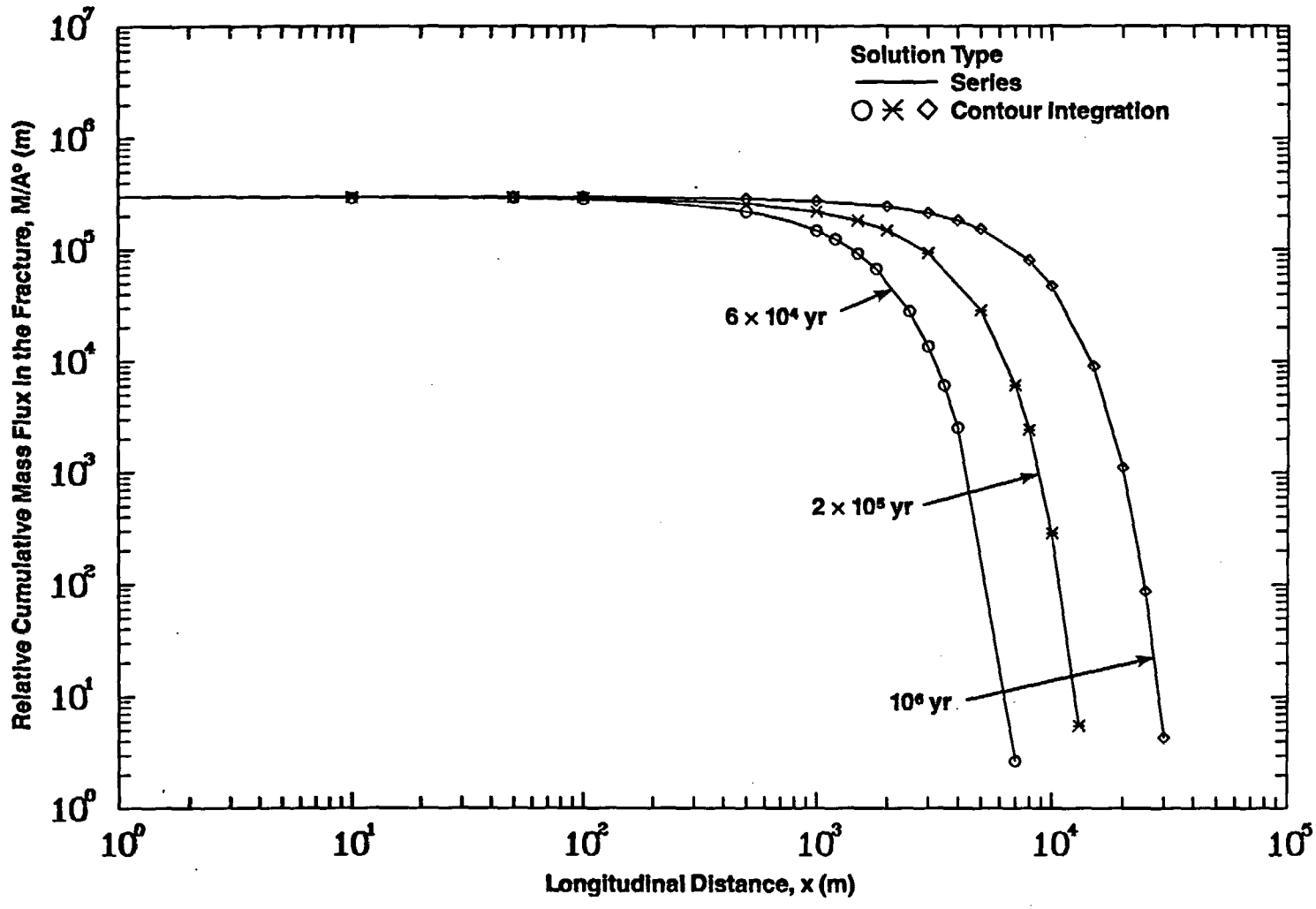

Figure 6-2c. Comparison of Spatial Variation of Relative Cumulative Mass Flux of Np-237 in the Fracture for Different Times (Case 5B: Multiple Parallel Fractures, Band Release Mode, No Longitudinal Dispersion)

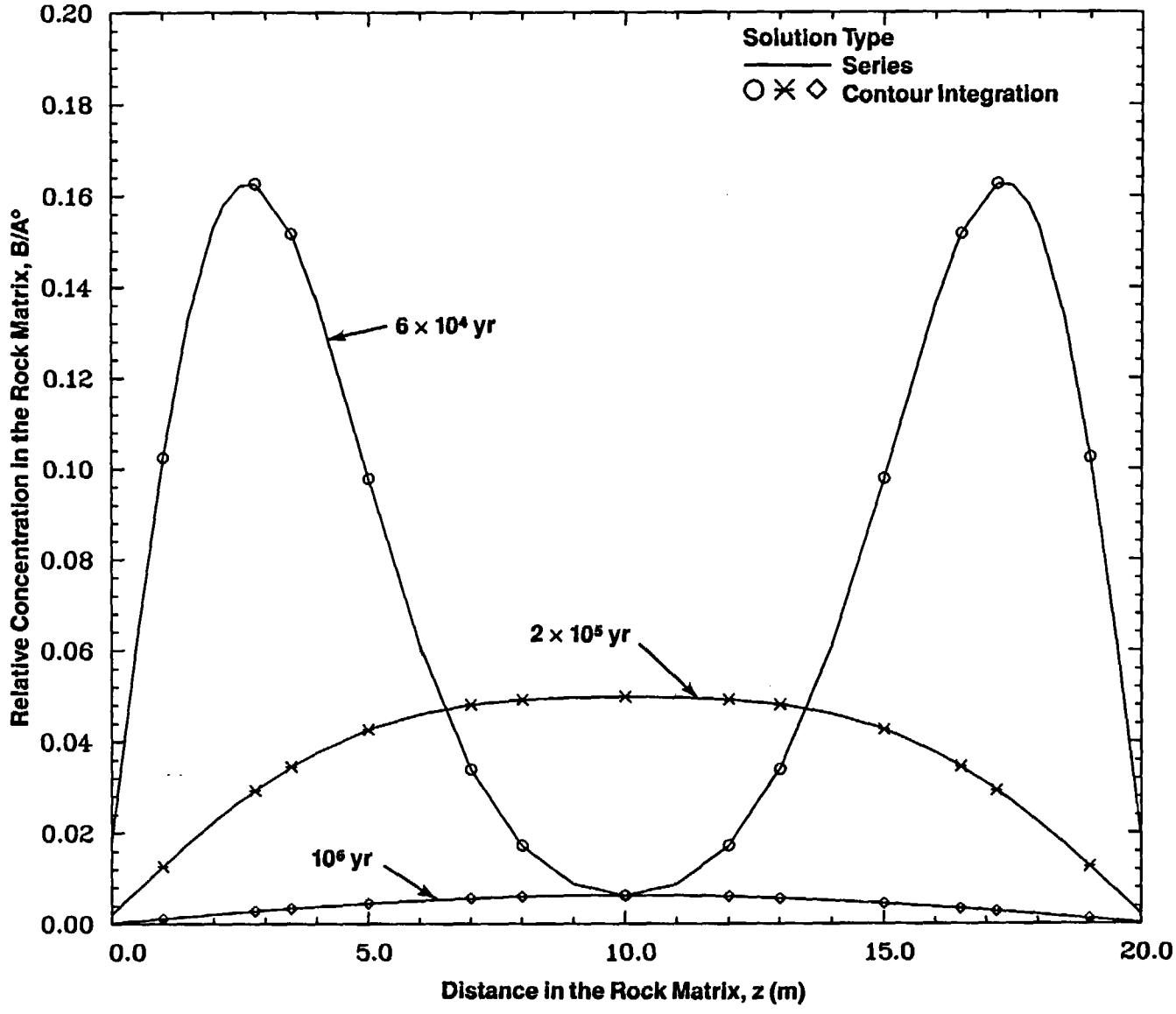

Figure 6-2d. Comparison of Spatial Variation of Relative Concentration of Np-237 in the Rock Matrix for Different Times (Case 5B: Multiple Parallel Fractures, Band Release Mode, No Longitudinal Dispersion)

Table 6-3a. Case 5B Results: Comparison of Relative Concentration, Mass Flux, and Cumulative Mass Flux in the Fracture for Np-237 at Time t = 6 x 10^4 yr (Band Release Mode)

Longitudinal Distance x (m)	Concentration A/A^o SS	Concentration A/A^o CIS	Mass Flux F/A^o (m/yr) SS	Mass Flux F/A^o (m/yr) CIS	Cumulative Mass Flux M/A^o (m) SS	Cumulative Mass Flux M/A^o (m) CIS
1.000E+00	1.871E-04		1.871E-03		2.984E+05	
1.000E+01	1.871E-03	1.867E-03	1.871E-02	1.867E-02	2.969E+05	2.928E+05
5.000E+01	9.353E-03	9.352E-03	9.353E-02	9.352E-02	2.904E+05	2.904E+05
1.000E+02	1.867E-02	1.868E-02	1.867E-01	1.868E-01	2.822E+05	2.822E+05
2.000E+02	3.709E-02		3.709E-01		2.660E+05	
4.000E+02	7.208E-02		7.208E-01		2.342E+05	
5.000E+02	8.817E-02	8.817E-02	8.817E-01	8.817E-01	2.188E+05	2.188E+05
6.000E+02	1.030E-01		1.030E+00		2.037E+05	
7.000E+02	1.165E-01		1.165E+00		1.891E+05	
8.000E+02	1.284E-01		1.284E+00		1.749E+05	
8.500E+02	1.337E-01		1.337E+00		1.680E+05	
1.000E+03	1.471E-01	1.471E-01	1.471E+00	1.471E+00	1.482E+05	1.482E+05
1.200E+03	1.587E-01	1.587E-01	1.587E+00	1.587E+00	1.240E+05	1.240E+05
1.500E+03	1.632E-01	1.632E-01	1.632E+00	1.632E+00	9.244E+04	9.244E+04
1.800E+03	1.545E-01	1.545E-01	1.545E+00	1.545E+00	6.688E+04	6.688E+04
2.500E+03	1.056E-01	1.056E-01	1.056E+00	1.056E+00	2.793E+04	2.793E+04
3.000E+03	6.735E-02	6.735E-02	6.735E-01	6.735E-01	1.355E+04	1.355E+04
3.500E+03	3.791E-02	3.791E-02	3.791E-01	3.791E-01	6.072E+03	6.072E+03
4.000E+03	1.911E-02	1.911E-02	1.911E-01	1.911E-01	2.518E+03	2.518E+03
7.000E+03	4.705E-05	4.705E-05	4.705E-04	4.705E-04	2.657E+00	2.657E+00

SS : Series Solution
CIS : Contour Integration Solution

Table 6-3b. Case 5B Results: Comparison of Relative Concentration, Mass Flux, and Cumulative Mass Flux in the Fracture for Np-237 at Time t = 2 x 10^5 yr (Band Release Mode)

Longitudinal Distance x (m)	Concentration A/A_o SS	Concentration A/A_o CIS	Mass Flux F/A_o (m/yr) SS	Mass Flux F/A_o (m/yr) CIS	Cumulative Mass Flux M/A_o (m) SS	Cumulative Mass Flux M/A_o (m) CIS
1.000E+00	2.178E-05		2.178E-04		2.985E+05	
1.000E+01	2.177E-04	1.415E-04	2.177E-03	1.415E-03	2.977E+05	2.936E+05
5.000E+01	1.085E-03	1.085E-03	1.085E-02	1.085E-02	2.944E+05	2.944E+05
1.000E+02	2.163E-03	2.163E-03	2.163E-02	2.163E-02	2.903E+05	2.903E+05
5.000E+02	1.044E-02	1.044E-02	1.044E-01	1.044E-01	2.578E+05	2.578E+05
1.000E+03	1.968E-02	1.968E-02	1.968E-01	1.968E-01	2.188E+05	2.188E+05
1.500E+03	2.723E-02	2.723E-02	2.723E-01	2.723E-01	1.822E+05	1.822E+05
2.000E+03	3.275E-02	3.275E-02	3.275E-01	3.275E-01	1.489E+05	1.489E+05
3.000E+03	3.712E-02	3.712E-02	3.712E-01	3.712E-01	9.361E+04	9.361E+04
5.000E+03	2.581E-02	2.581E-02	2.581E-01	2.581E-01	2.857E+04	2.857E+04
7.000E+03	9.805E-03	9.805E-03	9.805E-02	9.805E-02	6.038E+03	6.038E+03
8.000E+03	4.965E-03	4.965E-03	4.965E-02	4.965E-02	2.404E+03	2.404E+03
1.000E+04	8.827E-04	8.827E-04	8.827E-03	8.827E-03	2.842E+02	2.842E+02
1.300E+04	2.772E-05	2.771E-05	2.772E-04	2.771E-04	5.484E+00	5.484E+00

SS : Series Solution
CIS : Contour Integration Solution

Table 6-3c. Case 5B Results: Comparison of Relative Concentration, Mass Flux, and Cumulative Mass Flux in the Fracture for Np-237 at Time t = 10^6 yr (Band Release Mode)

Longitudinal Distance x (m)	Concentration A/A_o SS	Concentration A/A_o CIS	Mass Flux F/A_o (m/yr) SS	Mass Flux F/A_o (m/yr) CIS	Cumulative Mass Flux M/A_o (m) SS	Cumulative Mass Flux M/A_o (m) CIS
1.000E+00	1.884E-06		1.884E-05		2.985E+05	
1.000E+01	1.887E-05		1.887E-04		2.983E+05	
5.000E+01	9.504E-05	9.013E-05	9.504E-04	9.013E-04	2.973E+05	2.974E+05
1.000E+02	1.918E-04	1.918E-04	1.918E-03	1.918E-03	2.961E+05	2.961E+05
5.000E+02	1.019E-03	1.019E-03	1.019E-02	1.019E-02	2.860E+05	2.860E+05
1.000E+03	2.154E-03	2.154E-03	2.154E-02	2.154E-02	2.725E+05	2.725E+05
2.000E+03	4.538E-03	4.538E-03	4.538E-02	4.538E-02	2.436E+05	2.436E+05
3.000E+03	6.756E-03	6.756E-03	6.756E-02	6.756E-02	2.131E+05	2.131E+05
4.000E+03	8.527E-03	8.527E-03	8.527E-02	8.527E-02	1.825E+05	1.825E+05
5.000E+03	9.703E-03	9.703E-03	9.703E-02	9.703E-02	1.530E+05	1.530E+05
8.000E+03	9.715E-03	9.715E-03	9.715E-02	9.715E-02	7.976E+04	7.976E+04
1.000E+04	7.819E-03	7.819E-03	7.819E-02	7.819E-02	4.684E+04	4.684E+04
1.500E+04	2.710E-03	2.710E-03	2.710E-02	2.710E-02	8.971E+03	8.971E+03
2.000E+04	5.236E-04	5.236E-04	5.236E-03	5.236E-03	1.101E+03	1.101E+03
2.500E+04	6.019E-05	6.019E-05	6.019E-04	6.019E-04	8.644E+01	8.644E+01
3.000E+04	4.159E-06	4.159E-06	4.159E-05	4.159E-05	4.287E+00	4.287E+00

SS : Series Solution
CIS : Contour Integration Solution

Table 6-3d. Case 5B Results: Comparison of Relative Concentration in the Rock Matrix for Np-237 for Different Times at Longitudinal Distance x = 100 m (Band Release Mode)

Time :	6×10^4 yr		2×10^5 yr		10^6 yr	
Vertical Distance z (m)	B/A^o SS	CIS	B/A^o SS	CIS	B/A^o SS	CIS
5.000E-03	1.867E-02		2.163E-03		1.918E-04	
5.000E-01	6.316E-02		7.445E-03		6.737E-04	
1.000E+00	1.025E-01	1.025E-01	1.266E-02	1.266E-02	1.156E-03	1.156E-03
1.500E+00	1.331E-01		1.768E-02		1.632E-03	
2.000E+00	1.532E-01		2.243E-02		2.098E-03	
2.200E+00	1.581E-01		2.423E-02		2.282E-03	
2.500E+00	1.622E-01		2.684E-02		2.552E-03	
2.800E+00	1.627E-01	1.627E-01	2.930E-02	2.930E-02	2.817E-03	2.817E-03
3.500E+00	1.517E-01	1.517E-01	3.448E-02	3.448E-02	3.411E-03	3.411E-03
4.000E+00	1.365E-01		3.765E-02		3.812E-03	
5.000E+00	9.785E-02	9.785E-02	4.268E-02	4.268E-02	4.543E-03	4.543E-03
6.000E+00	6.112E-02		4.607E-02		5.166E-03	
7.000E+00	3.395E-02	3.395E-02	4.813E-02	4.813E-02	5.667E-03	5.667E-03
8.000E+00	1.726E-02	1.726E-02	4.921E-02	4.921E-02	6.033E-03	6.033E-03
9.000E+00	8.818E-03		4.969E-02		6.256E-03	
1.000E+01	6.308E-03	6.308E-03	4.982E-02	4.982E-02	6.332E-03	6.332E-03
1.100E+01	8.818E-03		4.969E-02		6.256E-03	
1.200E+01	1.726E-02	1.726E-02	4.921E-02	4.921E-02	6.033E-03	6.033E-03
1.300E+01	3.395E-02	3.395E-02	4.813E-02	4.813E-02	5.667E-03	5.667E-03
1.400E+01	6.112E-02		4.607E-02		5.166E-03	
1.500E+01	9.785E-02	9.785E-02	4.268E-02	4.268E-02	4.543E-03	4.543E-03
1.600E+01	1.365E-01		3.765E-02		3.812E-03	
1.650E+01	1.517E-01	1.517E-01	3.448E-02	3.448E-02	3.411E-03	3.412E-03
1.720E+01	1.627E-01	1.627E-01	2.930E-02	2.930E-02	2.817E-03	2.817E-03
1.750E+01	1.622E-01		2.684E-02		2.552E-03	
1.780E+01	1.581E-01		2.423E-02		2.282E-03	
1.800E+01	1.532E-01		2.243E-02		2.098E-03	
1.850E+01	1.331E-01		1.768E-02		1.632E-03	
1.900E+01	1.025E-01	1.025E-01	1.266E-02	1.266E-02	1.156E-03	1.156E-03
1.950E+01	6.316E-02		7.445E-03		6.737E-04	
2.000E+01	1.867E-02		2.163E-03		1.918E-04	

SS : Series Solution
CIS : Contour Integration Solution

Table 6-4. Input Parameters for Case 6

Species	Np-237
Initial Concentration A° (arbitrary unit of activity/L^3)	1
Type of Release Mode	Case 6A: Step Case 6B: Band
Boundary Condition	Infinite Plane Source
x	500.0 m
y	0.0 m
z	0.3 m
d	∞
u	10.0 m/yr
v	0.0 m/yr
D_{xx}	0, 10, 100, 1000 m^2/yr
D_{yy}	0.0 m^2/yr
D_{yx}	0.0 m^2/yr
D_p	0.01 m^2/yr
L	0.3 m
$T_{1/2}$	2.14×10^6 yr
T_L	1×10^4 yr
b	0.005 m
Φ	10^{-2}
R	1
R′	100

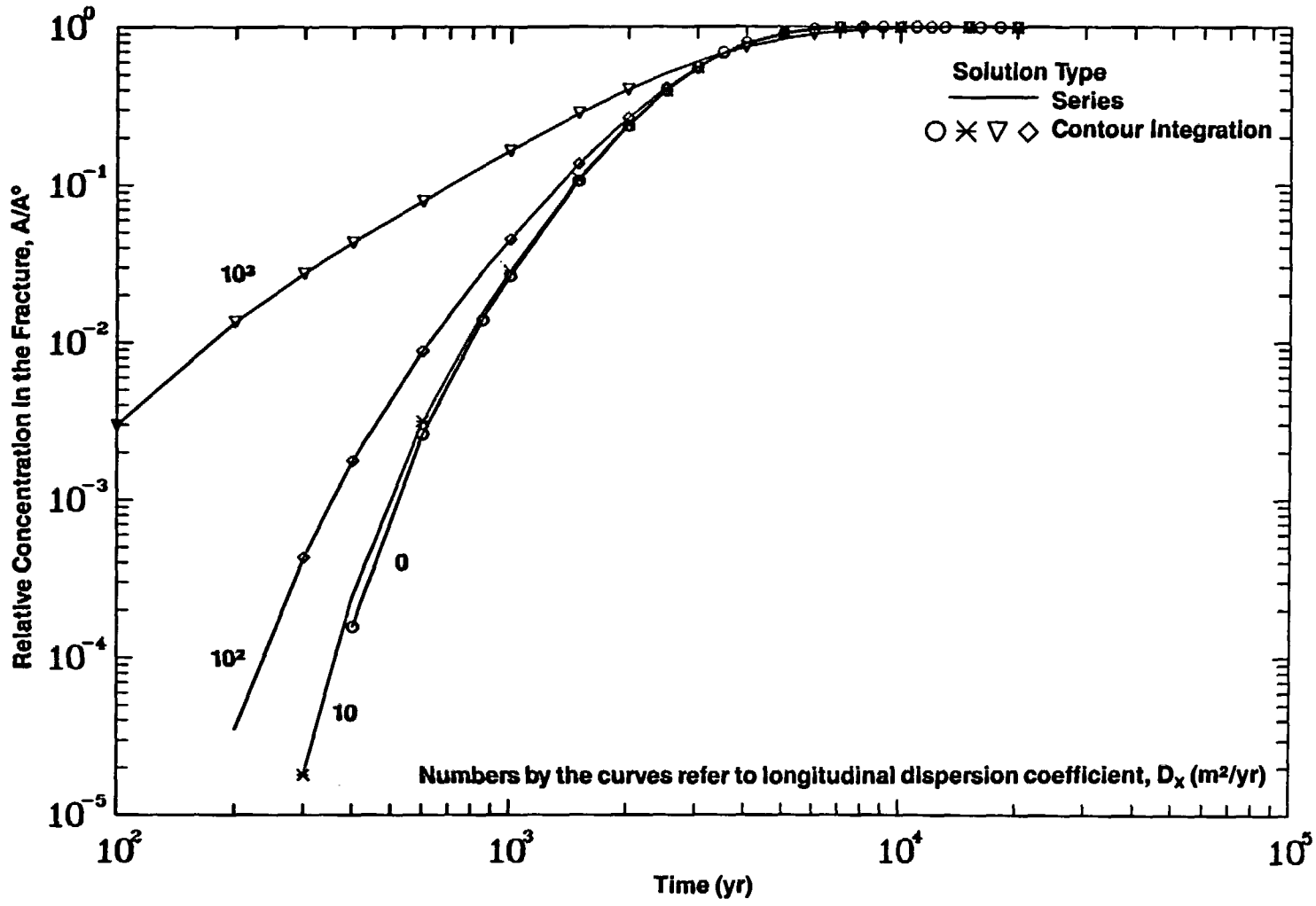

Figure 6-3a. Comparison of Temporal Variation of Relative Concentration of Np-237 in the Fracture for D_{xx} = 0, 10, 100, 1000 m²/yr (Case 6A: Multiple Parallel Fractures, Step Release Mode)

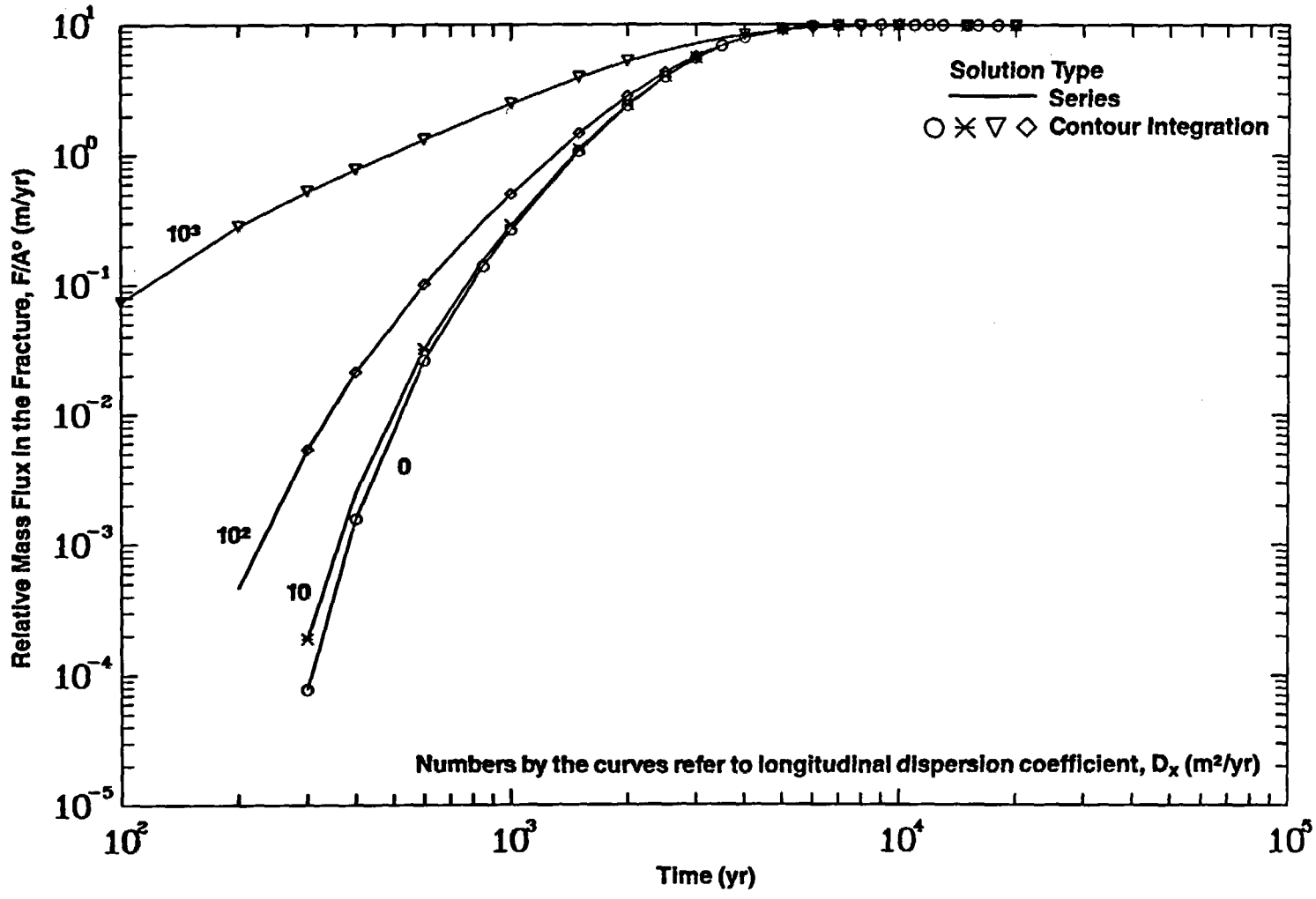

Figure 6-3b. Comparison of Temporal Variation of Relative Mass Flux of Np-237 in the Fracture for D_{xx} = 0, 10, 100, 1000 m²/yr (Case 6A: Multiple Parallel Fractures, Step Release Mode)

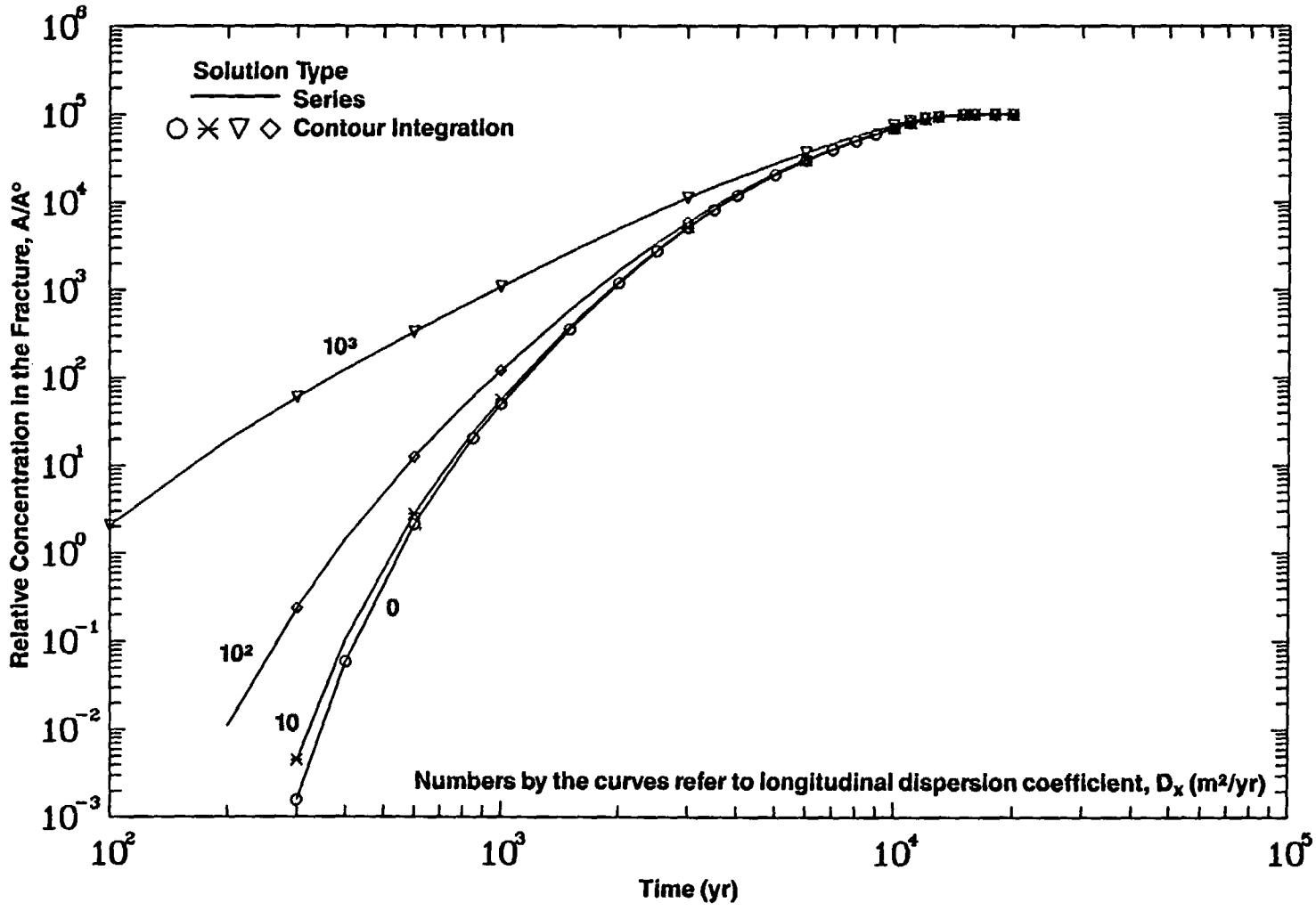

Figure 6-3c. Comparison of Temporal Variation of Relative Cumulative Mass Flux of Np-237 in the Fracture for D_{xx} = 0, 10, 100, 1000 m^2/yr (Case 6A: Multiple Parallel Fractures, Step Release Mode)

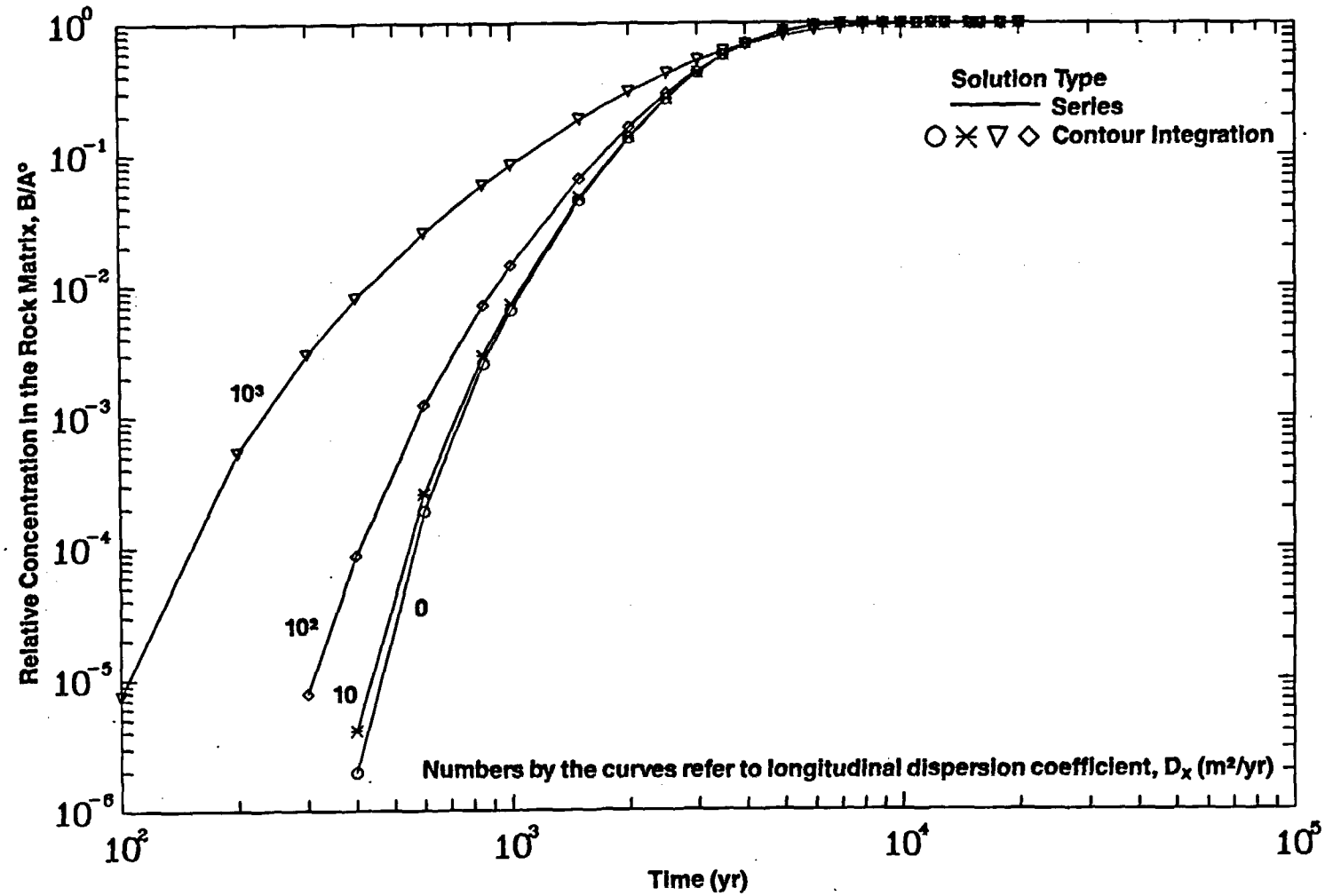

Figure 6-3d. Comparison of Temporal Variation of Relative Concentration of Np-237 in the Rock Matrix at Elevation z = 0.3 m for D_{xx} = 0, 10, 100, 1000 m²/yr (Case 6A: Multiple Parallel Fractures, Step Release Mode)

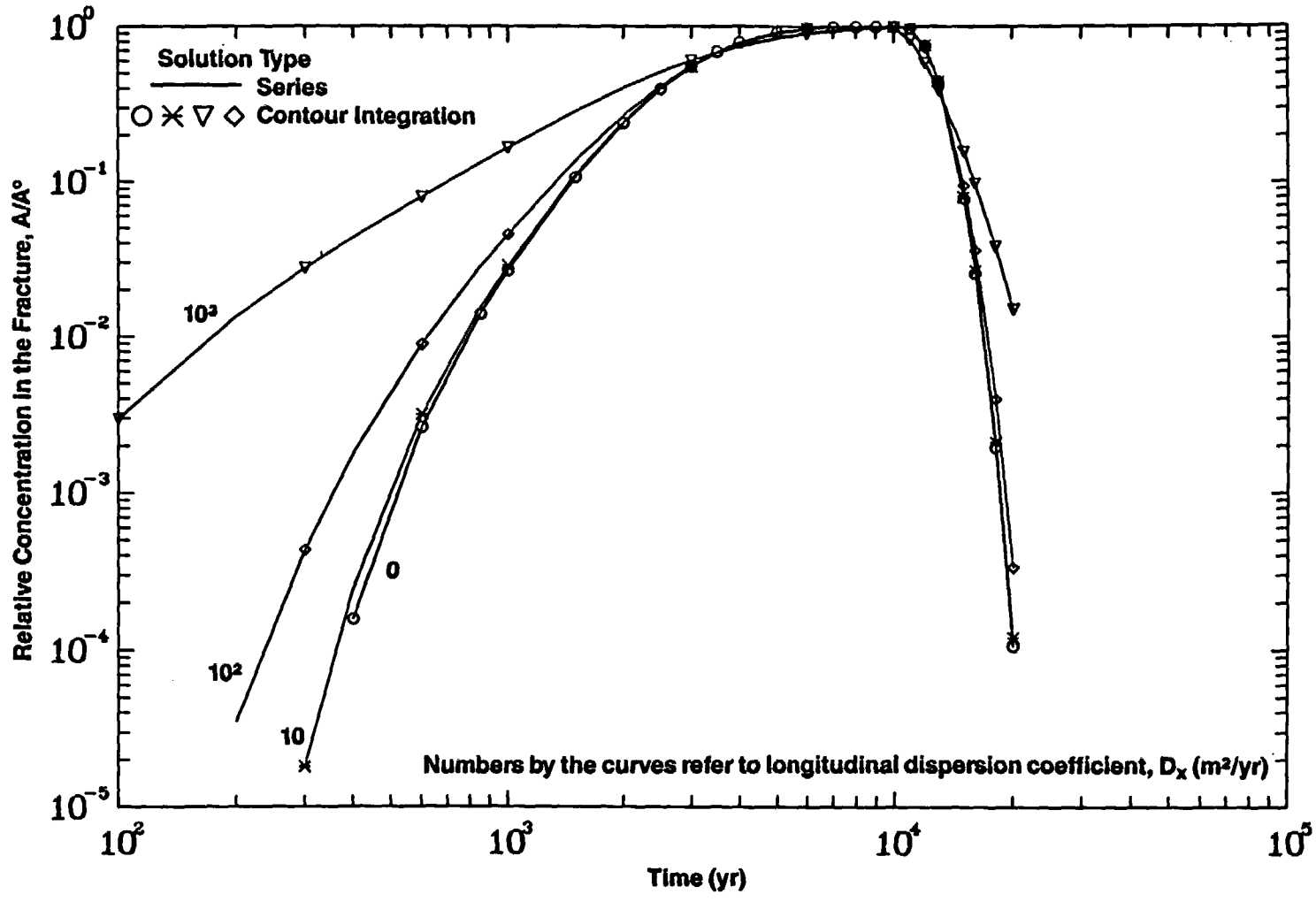

Figure 6-4a. Comparison of Temporal Variation of Relative Concentration of Np-237 in the Fracture for D_{xx} = 0, 10, 100, 1000 m²/yr (Case 6B: Multiple Parallel Fractures, Band Release Mode)

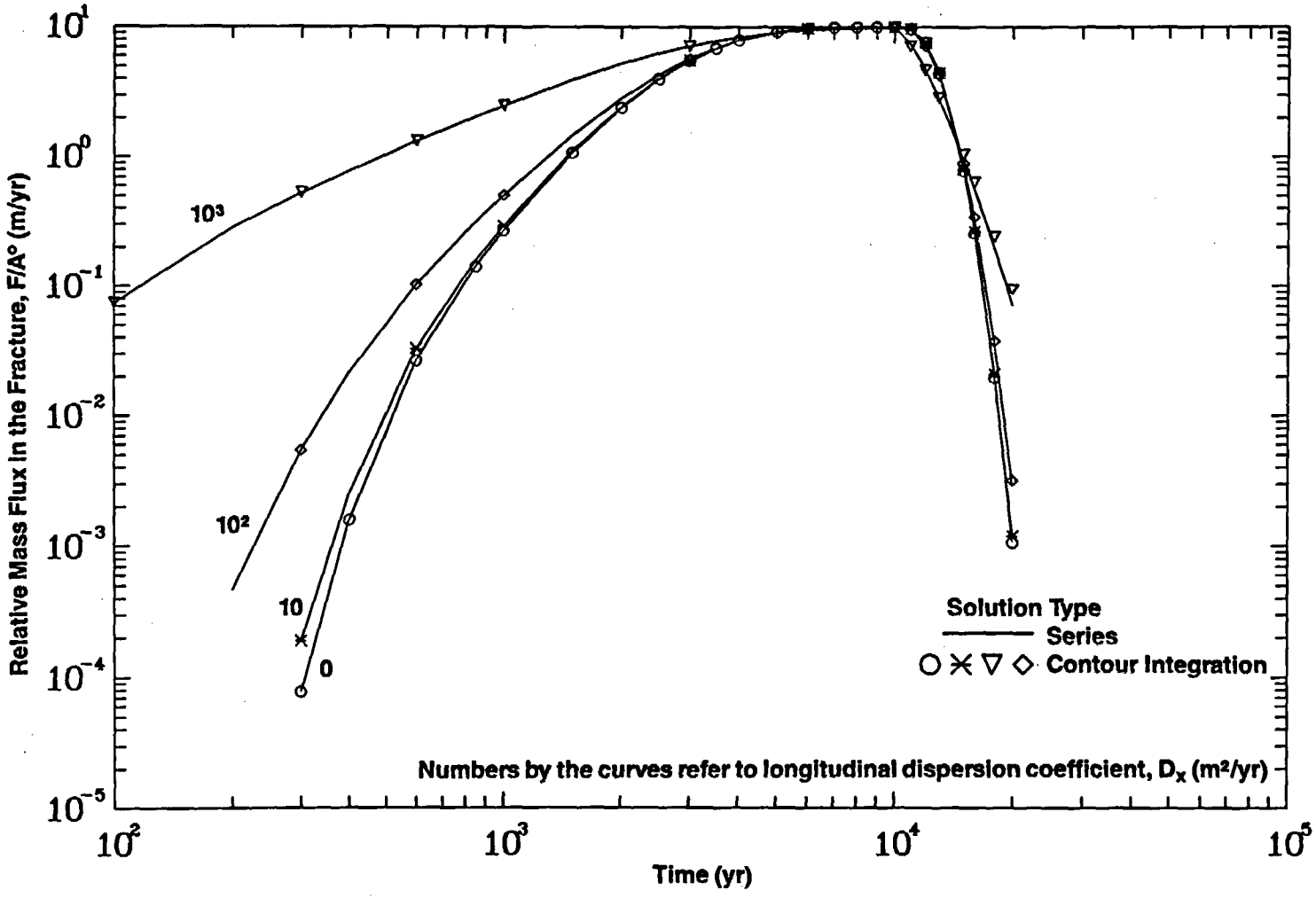

Figure 6-4b. Comparison of Temporal Variation of Relative Mass Flux of Np-237 in the Fracture for D_{xx} = 0, 10, 100, 1000 m²/yr (Case 6B: Multiple Parallel Fractures, Band Release Mode)

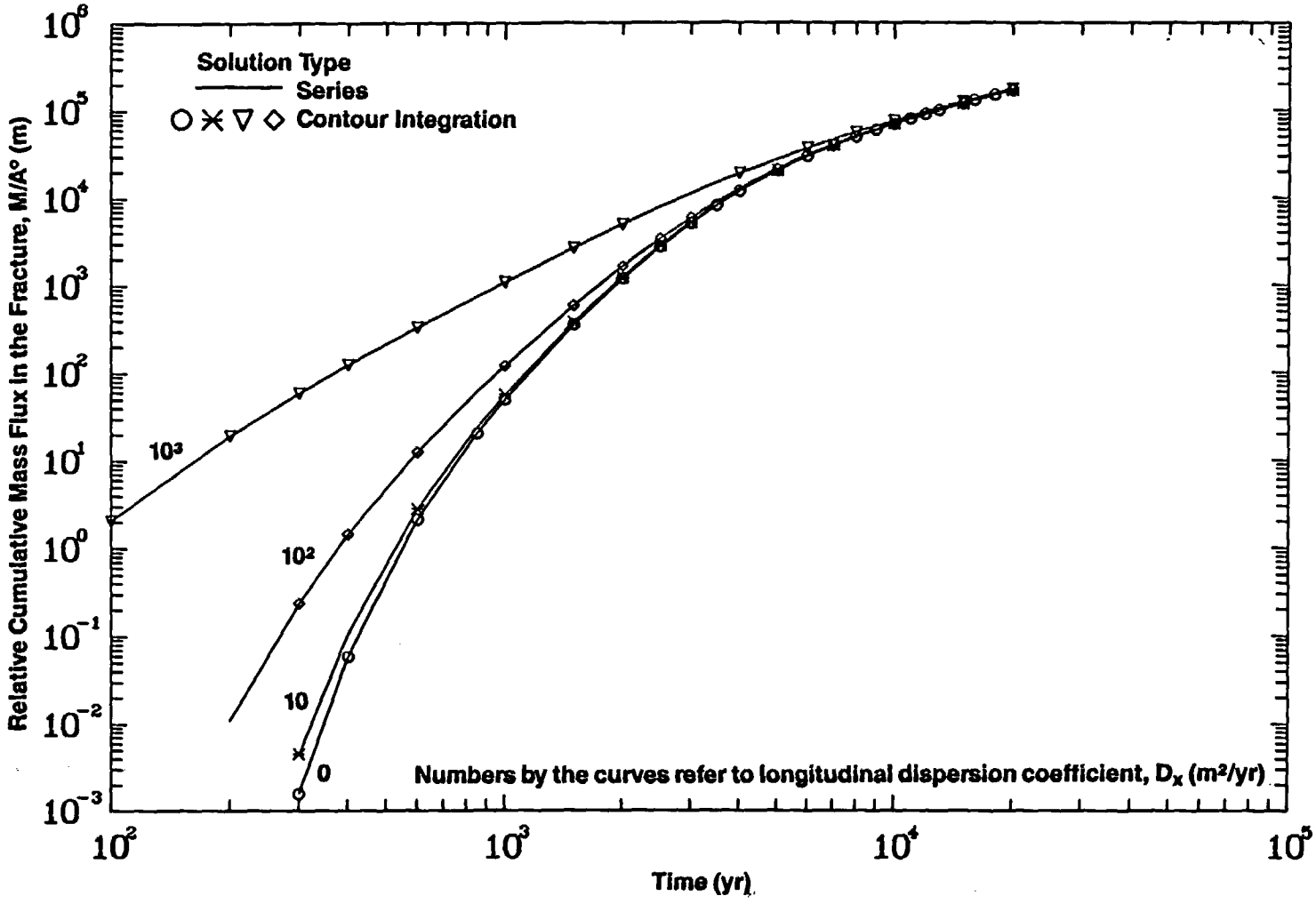

Figure 6-4c. Comparison of Temporal Variation of Relative Cumulative Mass Flux of Np-237 in the Fracture for D_{xx} = 0, 10, 100, 1000 m^2/yr (Case 6B: Multiple Parallel Fractures, Band Release Mode)

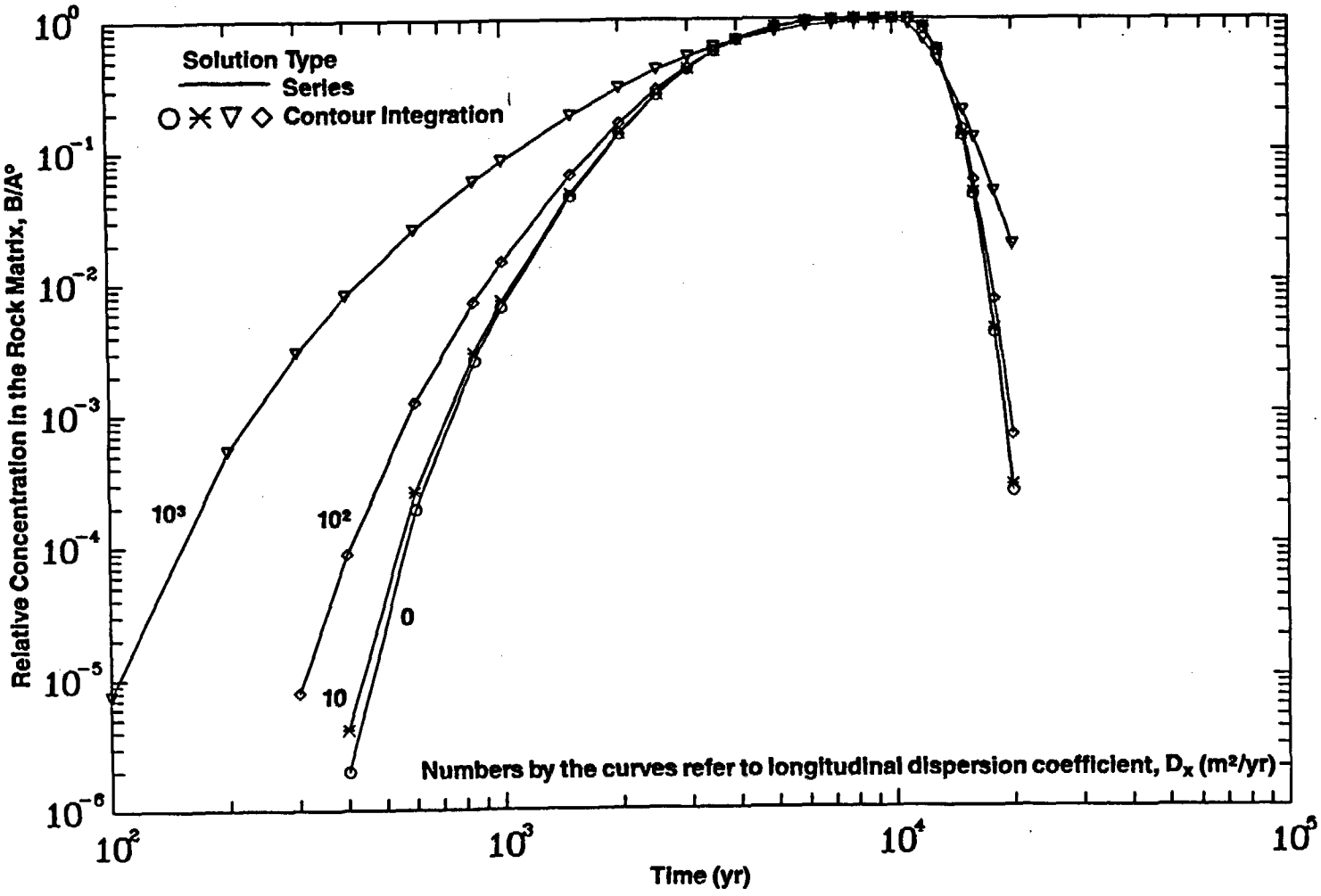

Figure 6-4d. Comparison of Temporal Variation of Relative Concentration of Np-237 in the Rock Matrix at Elevation z = 0.3 m for D_{xx} = 0, 10, 100, 1000 m²/yr (Case 6B: Multiple Parallel Fractures, Band Release Mode)

Table 6-5a. Case 6A Results: Comparison of Relative Concentration, Mass Flux, and Cumulative Mass Flux in the Fracture for Np-237 at x = 500 m, D_{xx} = 0 (Step Release Mode)

Time	Concentration A/A_o		Mass Flux F/A_o (m/yr)		Cumulative Mass Flux M/A_o (m)	
t (yr)	SS	CIS	SS	CIS	SS	CIS
1.000E+02	1.524E-23	7.679E-09	1.524E-22	7.679E-08	1.453E-22	-5.481E-08
2.000E+02	7.764E-09	1.916E-08	7.764E-08	1.916E-07	6.122E-07	4.868E-07
3.000E+02	7.744E-06	7.735E-06	7.744E-05	7.735E-05	1.576E-03	1.576E-03
4.000E+02	1.571E-04	1.571E-04	1.571E-03	1.571E-03	5.866E-02	5.866E-02
6.000E+02	2.618E-03	2.617E-03	2.618E-02	2.617E-02	2.135E+00	2.135E+00
8.500E+02	1.391E-02	1.391E-02	1.391E-01	1.391E-01	2.047E+01	2.047E+01
1.000E+03	2.664E-02	2.664E-02	2.664E-01	2.664E-01	5.027E+01	5.027E+01
1.500E+03	1.067E-01	1.067E-01	1.067E+00	1.067E+00	3.593E+02	3.593E+02
2.000E+03	2.383E-01	2.383E-01	2.383E+00	2.383E+00	1.205E+03	1.205E+03
2.500E+03	3.965E-01	3.965E-01	3.965E+00	3.965E+00	2.787E+03	2.787E+03
3.000E+03	5.531E-01	5.531E-01	5.531E+00	5.531E+00	5.166E+03	5.166E+03
3.500E+03	6.884E-01	6.884E-01	6.884E+00	6.884E+00	8.281E+03	8.281E+03
4.000E+03	7.938E-01	7.938E-01	7.938E+00	7.938E+00	1.200E+04	1.200E+04
5.000E+03	9.205E-01	9.205E-01	9.205E+00	9.205E+00	2.065E+04	2.065E+04
6.000E+03	9.726E-01	9.726E-01	9.726E+00	9.726E+00	3.016E+04	3.016E+04
7.000E+03	9.903E-01	9.903E-01	9.903E+00	9.903E+00	3.999E+04	3.999E+04
8.000E+03	9.955E-01	9.955E-01	9.955E+00	9.955E+00	4.993E+04	4.993E+04
9.000E+03	9.966E-01	9.966E-01	9.966E+00	9.966E+00	5.989E+04	5.989E+04
1.000E+04	9.967E-01	9.967E-01	9.967E+00	9.967E+00	6.986E+04	6.986E+04
1.100E+04	9.964E-01	9.964E-01	9.964E+00	9.964E+00	7.982E+04	7.982E+04
1.200E+04	9.961E-01	9.961E-01	9.961E+00	9.961E+00	8.978E+04	8.978E+04
1.300E+04	9.958E-01	9.958E-01	9.958E+00	9.958E+00	9.974E+04	9.974E+04
1.500E+04	9.952E-01	9.952E-01	9.952E+00	9.952E+00	1.197E+05	1.197E+05
1.600E+04	9.948E-01	9.948E-01	9.948E+00	9.948E+00	1.296E+05	1.296E+05
1.800E+04	9.942E-01	9.942E-01	9.942E+00	9.942E+00	1.495E+05	1.495E+05
2.000E+04	9.935E-01	9.935E-01	9.935E+00	9.935E+00	1.694E+05	1.694E+05

SS : Series Solution
CIS : Contour Integration Solution

Table 6-5b. Case 6A Results: Comparison of Relative Concentration, Mass Flux, and Cumulative Mass Flux in the Fracture for Np-237 at x = 500 m, D_{xx} = 10 m^2/yr (Step Release Mode)

Time	Concentration A/A_o		Mass Flux F/A_o (m/yr)		Cumulative Mass Flux M/A_o (m)	
t (yr)	SS	CIS	SS	CIS	SS	CIS
1.000E+02	6.075E-16	6.210E-09	6.971E-15	5.718E-08	1.632E-14	-5.634E-08
2.000E+02	7.686E-08		8.175E-07		8.626E-06	
3.000E+02	1.807E-05	1.807E-05	1.880E-04	1.880E-04	4.515E-03	4.515E-03
4.000E+02	2.438E-04		2.511E-03		1.050E-01	
6.000E+02	3.152E-03	3.152E-03	3.215E-02	3.215E-02	2.805E+00	2.805E+00
8.500E+02	1.531E-02		1.553E-01		2.385E+01	
1.000E+03	2.859E-02	2.859E-02	2.895E-01	2.895E-01	5.659E+01	5.659E+01
1.500E+03	1.100E-01	1.100E-01	1.110E+00	1.110E+00	3.824E+02	3.824E+02
2.000E+03	2.414E-01	2.414E-01	2.429E+00	2.429E+00	1.251E+03	1.251E+03
2.500E+03	3.983E-01	3.983E-01	4.001E+00	4.001E+00	2.854E+03	2.854E+03
3.000E+03	5.533E-01	5.533E-01	5.551E+00	5.551E+00	5.248E+03	5.248E+03
3.500E+03	6.872E-01		6.888E+00		8.369E+03	
4.000E+03	7.920E-01		7.932E+00		1.209E+04	
5.000E+03	9.188E-01	9.188E-01	9.194E+00	9.194E+00	2.073E+04	2.073E+04
6.000E+03	9.716E-01		9.718E+00		3.023E+04	
7.000E+03	9.899E-01	9.899E-01	9.900E+00	9.900E+00	4.006E+04	4.006E+04
8.000E+03	9.953E-01		9.953E+00		4.999E+04	
9.000E+03	9.966E-01		9.966E+00		5.995E+04	
1.000E+04	9.966E-01	9.966E-01	9.966E+00	9.966E+00	6.992E+04	6.992E+04
1.100E+04	9.964E-01		9.964E+00		7.988E+04	
1.200E+04	9.961E-01		9.961E+00		8.984E+04	
1.300E+04	9.958E-01		9.958E+00		9.980E+04	
1.500E+04	9.952E-01	9.952E-01	9.952E+00	9.952E+00	1.197E+05	1.197E+05
1.600E+04	9.948E-01		9.948E+00		1.297E+05	
1.800E+04	9.942E-01		9.942E+00		1.496E+05	
2.000E+04	9.935E-01	9.935E-01	9.935E+00	9.935E+00	1.694E+05	1.694E+05

SS : Series Solution
CIS : Contour Integration Solution

Table 6-5c. Case 6A Results: Comparison of Relative Concentration, Mass Flux, and Cumulative Mass Flux in the Fracture for Np-237 at x = 500 m, D_{xx} = 100 m^2/yr (Step Release Mode)

Time	Concentration A/A^o		Mass Flux F/A^o (m/yr)		Cumulative Mass Flux M/A^o (m)	
t (yr)	SS	CIS	SS	CIS	SS	CIS
1.000E+02	7.101E-08	7.284E-08	1.082E-06	1.048E-06	8.641E-06	8.586E-06
2.000E+02	3.515E-05		4.648E-04		1.103E-02	
3.000E+02	4.314E-04	4.314E-04	5.354E-03	5.354E-03	2.371E-01	2.371E-01
4.000E+02	1.771E-03	1.771E-03	2.118E-02	2.118E-02	1.449E+00	1.449E+00
6.000E+02	8.850E-03	8.850E-03	1.015E-01	1.015E-01	1.253E+01	1.253E+01
8.500E+02	2.789E-02		3.110E-01		6.140E+01	
1.000E+03	4.541E-02	4.541E-02	5.004E-01	5.004E-01	1.216E+02	1.216E+02
1.500E+03	1.366E-01	1.366E-01	1.466E+00	1.466E+00	5.931E+02	5.931E+02
2.000E+03	2.670E-01	2.670E-01	2.815E+00	2.815E+00	1.652E+03	1.652E+03
2.500E+03	4.141E-01	4.141E-01	4.309E+00	4.309E+00	3.432E+03	3.432E+03
3.000E+03	5.564E-01	5.564E-01	5.732E+00	5.732E+00	5.949E+03	5.949E+03
3.500E+03	6.799E-01		6.949E+00		9.129E+03	
4.000E+03	7.785E-01		7.907E+00		1.285E+04	
5.000E+03	9.042E-01	9.042E-01	9.110E+00	9.110E+00	2.143E+04	2.143E+04
6.000E+03	9.623E-01		9.654E+00		3.085E+04	
7.000E+03	9.854E-01	9.854E-01	9.866E+00	9.866E+00	4.063E+04	4.063E+04
8.000E+03	9.935E-01		9.939E+00		5.054E+04	
9.000E+03	9.959E-01		9.961E+00		6.049E+04	
1.000E+04	9.964E-01	9.964E-01	9.965E+00	9.965E+00	7.046E+04	7.046E+04
1.100E+04	9.964E-01		9.964E+00		8.042E+04	
1.200E+04	9.961E-01		9.961E+00		9.038E+04	
1.300E+04	9.958E-01		9.958E+00		1.003E+05	
1.500E+04	9.952E-01	9.952E-01	9.952E+00	9.952E+00	1.203E+05	1.203E+05
1.600E+04	9.948E-01		9.948E+00		1.302E+05	
1.800E+04	9.942E-01		9.942E+00		1.501E+05	
2.000E+04	9.935E-01	9.935E-01	9.935E+00	9.935E+00	1.700E+05	1.700E+05

SS : Series Solution
CIS : Contour Integration Solution

Table 6-5d. Case 6A Results: Comparison of Relative Concentration, Mass Flux, and Cumulative Mass Flux in the Fracture for Np-237 at x = 500 m, D_{xx} = 1000 m^2/yr (Step Release Mode)

Time	Concentration A/A_o		Mass Flux F/A_o (m/yr)		Cumulative Mass Flux M/A_o (m)	
t (yr)	SS	CIS	SS	CIS	SS	CIS
1.000E+02	2.974E-03	2.974E-03	7.435E-02	7.435E-02	2.089E+00	2.089E+00
2.000E+02	1.356E-02	1.356E-02	2.839E-01	2.839E-01	1.947E+01	1.947E+01
3.000E+02	2.761E-02	2.761E-02	5.271E-01	5.271E-01	5.989E+01	5.989E+01
4.000E+02	4.347E-02	4.347E-02	7.816E-01	7.816E-01	1.252E+02	1.252E+02
6.000E+02	7.951E-02	7.951E-02	1.321E+00	1.321E+00	3.349E+02	3.349E+02
8.500E+02	1.315E-01		2.043E+00		7.546E+02	
1.000E+03	1.654E-01	1.654E-01	2.488E+00	2.488E+00	1.094E+03	1.094E+03
1.500E+03	2.850E-01	2.850E-01	3.938E+00	3.938E+00	2.705E+03	2.705E+03
2.000E+03	4.032E-01	4.032E-01	5.230E+00	5.230E+00	5.006E+03	5.006E+03
2.500E+03	5.109E-01		6.304E+00		7.898E+03	
3.000E+03	6.041E-01		7.162E+00		1.127E+04	
3.500E+03	6.823E-01		7.830E+00		1.503E+04	
4.000E+03	7.465E-01	7.465E-01	8.344E+00	8.344E+00	1.908E+04	1.908E+04
5.000E+03	8.399E-01		9.031E+00		2.780E+04	
6.000E+03	8.991E-01	8.991E-01	9.424E+00	9.424E+00	3.704E+04	3.704E+04
7.000E+03	9.360E-01		9.649E+00		4.659E+04	
8.000E+03	9.588E-01	9.588E-01	9.778E+00	9.779E+00	5.631E+04	5.631E+04
9.000E+03	9.728E-01		9.853E+00		6.613E+04	
1.000E+04	9.815E-01	9.815E-01	9.896E+00	9.896E+00	7.600E+04	7.600E+04
1.100E+04	9.868E-01		9.920E+00		8.591E+04	
1.200E+04	9.900E-01		9.934E+00		9.584E+04	
1.300E+04	9.919E-01		9.941E+00		1.058E+05	
1.500E+04	9.936E-01	9.936E-01	9.945E+00	9.945E+00	1.257E+05	1.257E+05
1.600E+04	9.938E-01		9.944E+00		1.356E+05	
1.800E+04	9.938E-01		9.940E+00		1.555E+05	
2.000E+04	9.934E-01	9.933E-01	9.935E+00	9.934E+00	1.754E+05	1.754E+05

SS : Series Solution
CIS : Contour Integration Solution

Table 6-5e. Case 6A Results: Comparison of Temporal Variation of Relative Concentration in the Rock Matrix for Np-237 for Different D_{xx} at Longitudinal Distance x = 500 m (Step Release Mode)

D_{xx} (m^2/yr) :	0.0		10.0		100.0		1000.0	
Time t (yr)	B/A^o SS	CIS	B/A^o SS	CIS	B/A^o SS	CIS	B/A^o SS	CIS
1.000E+02	0.000E+00	3.766E-09	6.157E-25	3.905E-09	9.750E-13	4.272E-09	7.493E-06	7.497E-06
2.000E+02	1.524E-13	1.052E-09	7.697E-12	1.278E-09	9.503E-08	9.818E-08	5.347E-04	5.347E-04
3.000E+02	1.396E-08	2.134E-08	5.839E-08	6.426E-08	7.818E-06	7.822E-06	3.000E-03	3.000E-03
4.000E+02	1.970E-06	1.969E-06	4.104E-06	4.105E-06	8.733E-05	8.734E-05	8.054E-03	8.054E-03
6.000E+02	1.897E-04	1.897E-04	2.564E-04	2.564E-04	1.227E-03	1.227E-03	2.551E-02	2.551E-02
8.500E+02	2.527E-03	2.527E-03	2.930E-03	2.930E-03	7.096E-03	7.096E-03	5.887E-02	5.887E-02
1.000E+03	6.550E-03	6.550E-03	7.294E-03	7.294E-03	1.436E-02	1.436E-02	8.392E-02	8.392E-02
1.500E+03	4.540E-02	4.540E-02	4.759E-02	4.759E-02	6.595E-02	6.595E-02	1.861E-01	1.861E-01
2.000E+03	1.341E-01	1.341E-01	1.372E-01	1.372E-01	1.621E-01	1.621E-01	3.017E-01	3.017E-01
2.500E+03	2.662E-01	2.662E-01	2.689E-01	2.689E-01	2.914E-01	2.914E-01	4.161E-01	4.161E-01
3.000E+03	4.191E-01	4.191E-01	4.206E-01	4.206E-01	4.337E-01	4.337E-01	5.206E-01	5.206E-01
3.500E+03	5.684E-01	5.684E-01	5.684E-01	5.684E-01	5.702E-01	5.702E-01	6.114E-01	6.114E-01
4.000E+03	6.971E-01	6.971E-01	6.959E-01	6.959E-01	6.884E-01	6.884E-01	6.877E-01	6.877E-01
5.000E+03	8.708E-01	8.708E-01	8.689E-01	8.689E-01	8.542E-01	8.542E-01	8.014E-01	8.014E-01
6.000E+03	9.523E-01	9.523E-01	9.509E-01	9.509E-01	9.393E-01	9.393E-01	8.747E-01	8.747E-01
7.000E+03	9.833E-01	9.833E-01	9.827E-01	9.827E-01	9.762E-01	9.762E-01	9.207E-01	9.207E-01
8.000E+03	9.933E-01	9.933E-01	9.931E-01	9.931E-01	9.902E-01	9.902E-01	9.493E-01	9.493E-01
9.000E+03	9.960E-01	9.960E-01	9.960E-01	9.960E-01	9.948E-01	9.948E-01	9.669E-01	9.669E-01
1.000E+04	9.965E-01	9.965E-01	9.965E-01	9.965E-01	9.961E-01	9.961E-01	9.778E-01	9.778E-01
1.100E+04	9.964E-01	9.964E-01	9.964E-01	9.964E-01	9.963E-01	9.963E-01	9.845E-01	9.845E-01
1.200E+04	9.961E-01	9.961E-01	9.961E-01	9.961E-01	9.961E-01	9.961E-01	9.885E-01	9.885E-01
1.300E+04	9.958E-01	9.958E-01	9.958E-01	9.958E-01	9.958E-01	9.958E-01	9.910E-01	9.910E-01
1.500E+04	9.952E-01	9.952E-01	9.952E-01	9.952E-01	9.952E-01	9.952E-01	9.932E-01	9.932E-01
1.600E+04	9.948E-01	9.948E-01	9.948E-01	9.948E-01	9.948E-01	9.948E-01	9.936E-01	9.936E-01
1.800E+04	9.942E-01	9.942E-01	9.942E-01	9.942E-01	9.942E-01	9.942E-01	9.937E-01	9.937E-01
2.000E+04	9.935E-01	9.935E-01	9.935E-01	9.935E-01	9.935E-01	9.935E-01	9.933E-01	9.933E-01

SS : Series Solution
CIS : Contour Integration Solution

Table 6-6a. Case 6B Results: Comparison of Relative Concentration, Mass Flux, and Cumulative Mass Flux in the Fracture for Np-237 at x = 500 m, $D_{xx} = 0$ (Band Release Mode)

Time	Concentration A/A^o		Mass Flux F/A^o (m/yr)		Cumulative Mass Flux M/A^o (m)	
t (yr)	SS	CIS	SS	CIS	SS	CIS
1.000E+02	1.524E-23	7.679E-09	1.524E-22	7.679E-08	1.453E-22	-5.481E-08
2.000E+02	7.764E-09	1.916E-08	7.764E-08	1.916E-07	6.122E-07	4.868E-07
3.000E+02	7.744E-06	7.735E-06	7.744E-05	7.735E-05	1.576E-03	1.576E-03
4.000E+02	1.571E-04	1.571E-04	1.571E-03	1.571E-03	5.866E-02	5.866E-02
6.000E+02	2.618E-03	2.617E-03	2.618E-02	2.617E-02	2.135E+00	2.135E+00
8.500E+02	1.391E-02	1.391E-02	1.391E-01	1.391E-01	2.047E+01	2.047E+01
1.000E+03	2.664E-02	2.664E-02	2.664E-01	2.664E-01	5.027E+01	5.027E+01
1.500E+03	1.067E-01	1.067E-01	1.067E+00	1.067E+00	3.593E+02	3.593E+02
2.000E+03	2.383E-01	2.383E-01	2.383E+00	2.383E+00	1.205E+03	1.205E+03
2.500E+03	3.965E-01	3.965E-01	3.965E+00	3.965E+00	2.787E+03	2.787E+03
3.000E+03	5.531E-01	5.531E-01	5.531E+00	5.531E+00	5.166E+03	5.166E+03
3.500E+03	6.884E-01	6.884E-01	6.884E+00	6.884E+00	8.281E+03	8.281E+03
4.000E+03	7.938E-01	7.938E-01	7.938E+00	7.938E+00	1.200E+04	1.200E+04
5.000E+03	9.205E-01	9.205E-01	9.205E+00	9.205E+00	2.065E+04	2.065E+04
6.000E+03	9.726E-01	9.726E-01	9.726E+00	9.726E+00	3.016E+04	3.016E+04
7.000E+03	9.903E-01	9.903E-01	9.903E+00	9.903E+00	3.999E+04	3.999E+04
8.000E+03	9.955E-01	9.955E-01	9.955E+00	9.955E+00	4.993E+04	4.993E+04
9.000E+03	9.966E-01	9.966E-01	9.966E+00	9.966E+00	5.989E+04	5.989E+04
1.000E+04	9.967E-01	9.967E-01	9.967E+00	9.967E+00	6.986E+04	6.986E+04
1.100E+04	9.699E-01	9.699E-01	9.699E+00	9.699E+00	7.977E+04	7.977E+04
1.200E+04	7.586E-01	7.586E-01	7.586E+00	7.586E+00	8.858E+04	8.858E+04
1.300E+04	4.445E-01	4.445E-01	4.445E+00	4.445E+00	9.459E+04	9.459E+04
1.500E+04	7.763E-02	7.763E-02	7.763E-01	7.763E-01	9.907E+04	9.907E+04
1.600E+04	2.541E-02	2.541E-02	2.541E-01	2.541E-01	9.954E+04	9.954E+04
1.800E+04	1.940E-03	1.939E-03	1.940E-02	1.939E-02	9.973E+04	9.973E+04
2.000E+04	1.060E-04	1.059E-04	1.060E-03	1.059E-03	9.974E+04	9.974E+04

SS : Series Solution
CIS : Contour Integration Solution

Table 6-6b. Case 6B Results: Comparison of Relative Concentration, Mass Flux, and Cumulative Mass Flux in the Fracture for Np-237 at x = 500 m, D_{xx} = 10 m^2/yr (Band Release Mode)

Time	Concentration A/A^o		Mass Flux F/A^o (m/yr)		Cumulative Mass Flux M/A^o (m)	
t (yr)	SS	CIS	SS	CIS	SS	CIS
1.000E+02	6.075E-16	6.210E-09	6.971E-15	5.719E-08	1.632E-14	-5.634E-08
2.000E+02	7.686E-08		8.175E-07		8.626E-06	
3.000E+02	1.807E-05	1.807E-05	1.880E-04	1.880E-04	4.515E-03	4.515E-03
4.000E+02	2.438E-04		2.511E-03		1.050E-01	
6.000E+02	3.152E-03	3.152E-03	3.215E-02	3.215E-02	2.805E+00	2.805E+00
8.500E+02	1.531E-02		1.553E-01		2.385E+01	
1.000E+03	2.859E-02	2.859E-02	2.895E-01	2.895E-01	5.659E+01	5.659E+01
1.500E+03	1.100E-01		1.110E+00		3.824E+02	
2.000E+03	2.414E-01		2.429E+00		1.251E+03	
2.500E+03	3.983E-01		4.001E+00		2.854E+03	
3.000E+03	5.533E-01	5.533E-01	5.551E+00	5.551E+00	5.248E+03	5.248E+03
3.500E+03	6.872E-01		6.888E+00		8.369E+03	
4.000E+03	7.920E-01		7.932E+00		1.209E+04	
5.000E+03	9.188E-01		9.194E+00		2.073E+04	
6.000E+03	9.716E-01	9.716E-01	9.718E+00	9.718E+00	3.023E+04	3.023E+04
7.000E+03	9.899E-01		9.900E+00		4.006E+04	
8.000E+03	9.953E-01		9.953E+00		4.999E+04	
9.000E+03	9.966E-01		9.966E+00		5.995E+04	
1.000E+04	9.966E-01	9.966E-01	9.966E+00	9.966E+00	6.992E+04	6.992E+04
1.100E+04	9.679E-01	9.679E-01	9.676E+00	9.676E+00	7.983E+04	7.983E+04
1.200E+04	7.555E-01	7.555E-01	7.540E+00	7.540E+00	8.860E+04	8.860E+04
1.300E+04	4.443E-01	4.443E-01	4.425E+00	4.425E+00	9.457E+04	9.457E+04
1.500E+04	7.936E-02	7.936E-02	7.871E-01	7.871E-01	9.905E+04	9.905E+04
1.600E+04	2.640E-02	2.640E-02	2.613E-01	2.613E-01	9.953E+04	9.953E+04
1.800E+04	2.094E-03	2.094E-03	2.066E-02	2.066E-02	9.973E+04	9.973E+04
2.000E+04	1.195E-04	1.195E-04	1.174E-03	1.176E-03	9.974E+04	9.974E+04

SS : Series Solution
CIS : Contour Integration Solution

Table 6-6c. Case 6B Results: Comparison of Relative Concentration, Mass Flux, and Cumulative Mass Flux in the Fracture for Np-237 at x = 500 m, D_{xx} = 100 m^2/yr (Band Release Mode)

Time	Concentration A/A^o		Mass Flux F/A^o (m/yr)		Cumulative Mass Flux M/A^o (m)	
t (yr)	SS	CIS	SS	CIS	SS	CIS
1.000E+02	7.101E-08	7.284E-08	1.082E-06	1.048E-06	8.641E-06	8.586E-06
2.000E+02	3.515E-05		4.648E-04		1.103E-02	
3.000E+02	4.314E-04	4.314E-04	5.354E-03	5.354E-03	2.371E-01	2.371E-01
4.000E+02	1.771E-03		2.118E-02		1.449E+00	
6.000E+02	8.850E-03	8.850E-03	1.015E-01	1.015E-01	1.253E+01	1.253E+01
8.500E+02	2.789E-02		3.110E-01		6.140E+01	
1.000E+03	4.541E-02	4.541E-02	5.004E-01	5.004E-01	1.216E+02	1.216E+02
1.500E+03	1.366E-01		1.466E+00		5.931E+02	
2.000E+03	2.670E-01		2.815E+00		1.652E+03	
2.500E+03	4.141E-01		4.309E+00		3.432E+03	
3.000E+03	5.564E-01	5.564E-01	5.732E+00	5.732E+00	5.949E+03	5.949E+03
3.500E+03	6.799E-01		6.949E+00		9.129E+03	
4.000E+03	7.785E-01		7.907E+00		1.285E+04	
5.000E+03	9.042E-01		9.110E+00		2.143E+04	
6.000E+03	9.623E-01	9.623E-01	9.654E+00	9.654E+00	3.085E+04	3.085E+04
7.000E+03	9.854E-01		9.866E+00		4.063E+04	
8.000E+03	9.935E-01		9.939E+00		5.054E+04	
9.000E+03	9.959E-01		9.961E+00		6.049E+04	
1.000E+04	9.964E-01	9.964E-01	9.965E+00	9.965E+00	7.046E+04	7.046E+04
1.100E+04	9.511E-01	9.511E-01	9.465E+00	9.465E+00	8.030E+04	8.030E+04
1.200E+04	7.300E-01	7.300E-01	7.155E+00	7.155E+00	8.874E+04	8.874E+04
1.300E+04	4.411E-01	4.411E-01	4.245E+00	4.245E+00	9.441E+04	9.441E+04
1.500E+04	9.392E-02	9.392E-02	8.712E-01	8.712E-01	9.889E+04	9.889E+04
1.600E+04	3.569E-02	3.569E-02	3.255E-01	3.255E-01	9.945E+04	9.945E+04
1.800E+04	3.941E-03	3.940E-03	3.484E-02	3.483E-02	9.971E+04	9.971E+04
2.000E+04	3.351E-04	3.345E-04	2.877E-03	2.874E-03	9.974E+04	9.974E+04

SS : Series Solution
CIS : Contour Integration Solution

Table 6-6d. Case 6B Results: Comparison of Relative Concentration, Mass Flux, and Cumulative Mass Flux in the Fracture for Np-237 at x = 500 m, D_{xx} = 1,000 m^2/yr (Band Release Mode)

Time	Concentration A/A_o		Mass Flux F/A_o (m/yr)		Cumulative Mass Flux M/A_o (m)	
t (yr)	SS	CIS	SS	CIS	SS	CIS
1.000E+02	2.974E-03	2.974E-03	7.435E-02	7.435E-02	2.089E+00	2.089E+00
2.000E+02	1.356E-02		2.839E-01		1.947E+01	
3.000E+02	2.761E-02	2.761E-02	5.271E-01	5.271E-01	5.989E+01	5.989E+01
4.000E+02	4.347E-02		7.816E-01		1.252E+02	
6.000E+02	7.951E-02	7.951E-02	1.321E+00	1.321E+00	3.349E+02	3.349E+02
8.500E+02	1.315E-01		2.043E+00		7.546E+02	
1.000E+03	1.654E-01	1.654E-01	2.488E+00	2.488E+00	1.094E+03	1.094E+03
1.500E+03	2.850E-01		3.938E+00		2.705E+03	
2.000E+03	4.032E-01		5.230E+00		5.006E+03	
2.500E+03	5.109E-01		6.304E+00		7.898E+03	
3.000E+03	6.041E-01	6.041E-01	7.162E+00	7.162E+00	1.127E+04	1.127E+04
3.500E+03	6.823E-01		7.830E+00		1.503E+04	
4.000E+03	7.465E-01		8.344E+00		1.908E+04	
5.000E+03	8.399E-01		9.031E+00		2.780E+04	
6.000E+03	8.991E-01	8.991E-01	9.424E+00	9.424E+00	3.704E+04	3.704E+04
7.000E+03	9.360E-01		9.649E+00		4.659E+04	
8.000E+03	9.588E-01		9.778E+00		5.631E+04	
9.000E+03	9.728E-01		9.853E+00		6.613E+04	
1.000E+04	9.815E-01	9.815E-01	9.896E+00	9.896E+00	7.600E+04	7.600E+04
1.100E+04	8.219E-01	8.220E-01	7.441E+00	7.441E+00	8.482E+04	8.482E+04
1.200E+04	5.881E-01	5.881E-01	4.721E+00	4.721E+00	9.085E+04	9.085E+04
1.300E+04	3.897E-01	3.897E-01	2.803E+00	2.803E+00	9.454E+04	9.454E+04
1.500E+04	1.563E-01	1.563E-01	9.434E-01	9.433E-01	9.796E+04	9.796E+04
1.600E+04	9.762E-02	9.762E-02	5.505E-01	5.509E-01	9.869E+04	9.869E+04
1.800E+04	3.808E-02	3.808E-02	1.933E-01	1.932E-01	9.937E+04	9.937E+04
2.000E+04	1.504E-02	1.498E-02	7.076E-02	6.906E-02	9.961E+04	9.961E+04

SS : Series Solution
CIS : Contour Integration Solution

Table 6-6e. Case 6B Results: Comparison of Temporal Variation of Relative Concentration in the Rock Matrix for Np-237 for Different D_{xx} at Longitudinal Distance x = 500 m (Band Release Mode)

D_{xx} (m^2/yr) :	0.0		10.0		100.0		1000.0	
Time t (yr)	B/A^o SS	CIS	B/A^o SS	CIS	B/A^o SS	CIS	B/A^o SS	CIS
1.000E+02	0.000E+00	3.766E-09	6.157E-25	3.905E-09	9.750E-13	4.272E-09	7.493E-06	7.497E-06
2.000E+02	1.524E-13	1.052E-09	7.697E-12	1.278E-09	9.503E-08	9.818E-08	5.347E-04	5.347E-04
3.000E+02	1.396E-08	2.134E-08	5.839E-08	6.426E-08	7.818E-06	7.822E-06	3.000E-03	3.000E-03
4.000E+02	1.970E-06	1.969E-06	4.104E-06	4.105E-06	8.733E-05	8.734E-05	8.054E-03	8.054E-03
6.000E+02	1.897E-04	1.897E-04	2.564E-04	2.564E-04	1.227E-03	1.227E-03	2.551E-02	2.551E-02
8.500E+02	2.527E-03	2.527E-03	2.930E-03	2.930E-03	7.096E-03	7.096E-03	5.887E-02	5.887E-02
1.000E+03	6.550E-03	6.550E-03	7.294E-03	7.294E-03	1.436E-02	1.436E-02	8.392E-02	8.392E-02
1.500E+03	4.540E-02	4.540E-02	4.759E-02	4.759E-02	6.595E-02	6.595E-02	1.861E-01	1.861E-01
2.000E+03	1.341E-01	1.341E-01	1.372E-01	1.372E-01	1.621E-01	1.621E-01	3.017E-01	3.017E-01
2.500E+03	2.662E-01	2.662E-01	2.689E-01	2.689E-01	2.914E-01	2.914E-01	4.161E-01	4.161E-01
3.000E+03	4.191E-01	4.191E-01	4.206E-01	4.206E-01	4.337E-01	4.337E-01	5.206E-01	5.206E-01
3.500E+03	5.684E-01	5.684E-01	5.684E-01	5.684E-01	5.702E-01	5.702E-01	6.114E-01	6.114E-01
4.000E+03	6.971E-01	6.971E-01	6.959E-01	6.959E-01	6.884E-01	6.884E-01	6.877E-01	6.877E-01
5.000E+03	8.708E-01	8.708E-01	8.689E-01	8.689E-01	8.542E-01	8.542E-01	8.014E-01	8.014E-01
6.000E+03	9.523E-01	9.523E-01	9.509E-01	9.509E-01	9.393E-01	9.393E-01	8.747E-01	8.747E-01
7.000E+03	9.833E-01	9.833E-01	9.827E-01	9.827E-01	9.762E-01	9.762E-01	9.207E-01	9.207E-01
8.000E+03	9.933E-01	9.933E-01	9.931E-01	9.931E-01	9.902E-01	9.902E-01	9.493E-01	9.493E-01
9.000E+03	9.960E-01	9.960E-01	9.960E-01	9.960E-01	9.948E-01	9.948E-01	9.669E-01	9.669E-01
1.000E+04	9.965E-01	9.965E-01	9.965E-01	9.965E-01	9.961E-01	9.961E-01	9.778E-01	9.778E-01
1.100E+04	9.899E-01	9.899E-01	9.891E-01	9.891E-01	9.819E-01	9.819E-01	9.008E-01	9.008E-01
1.200E+04	8.624E-01	8.624E-01	8.594E-01	8.594E-01	8.345E-01	8.345E-01	6.878E-01	6.878E-01
1.300E+04	5.781E-01	5.781E-01	5.766E-01	5.766E-01	5.635E-01	5.635E-01	4.721E-01	4.721E-01
1.500E+04	1.272E-01	1.272E-01	1.290E-01	1.290E-01	1.437E-01	1.437E-01	1.943E-01	1.943E-01
1.600E+04	4.566E-02	4.566E-02	4.696E-02	4.696E-02	5.853E-02	5.853E-02	1.217E-01	1.217E-01
1.800E+04	4.052E-03	4.052E-03	4.313E-03	4.313E-03	7.214E-03	7.214E-03	4.744E-02	4.744E-02
2.000E+04	2.492E-04	2.492E-04	2.766E-04	2.763E-04	6.658E-04	6.657E-04	1.867E-02	1.868E-02

SS : Series Solution
CIS : Contour Integration Solution

6.3 DISCUSSION OF CASE 7: TWO-DIMENSIONAL TRANSPORT OF Tc-99 IN FRACTURE AND ROCK MATRIX

The results reported in this section illustrate the application of the series solution to a two-dimensional problem dealing with the migration of Tc-99 in a system of parallel fractures, where the concentration distribution at inlet is simulated by a set of three finite line sources and subject to a step release mode. In this instance, fluid flow is assumed to be in a direction normal to the upstream boundary; longitudinal dispersion effects are ignored. Concentration, mass flux, and cumulative mass flux in the fracture, as well as the concentration in the rock matrix, are computed at observation points located along lines downstream from the upstream boundary and parallel to it. A list of the input parameters referred to this problem is reported in Table 6-7.

The simulation time for all the investigated cases corresponds to 5×10^4 years. Figures 6-5a, 6-5b, 6-5c, and 6-5d show the relative concentration, mass flux, mass flux vector, and cumulative mass flux profiles at various distances. Corresponding tabulated results are given in Tables 6-8a, 6-8b, 6-8c, and 6-8d. Note that the concentration gradient in the transverse direction of the fracture, which is relatively important at short axial distances from the source, becomes smaller with increasing distance. As far as the lateral extent of the plume is concerned, the magnitude is greater at large distances from the source. This is a logical consequence of the large effective dispersion time which, in this instance, is proportional to the distance x and inversely proportional to the velocity u. Similar conclusions may be drawn for the mass flux and cumulative mass flux results.

Figures 6-5e, 6-5f, and 6-5g show the relative concentration profiles in the rock matrix at elevations of 0.1 m, 0.5 m, and 1.0 m. Tabulated results are given in Tables 6-8e, 6-8f, and 6-8g. The migration mechanism of Tc-99 in the rock matrix downstream from the source which is solely due to the diffusive effects is proportional to the concentration gradient prevailing at the fracture walls and the effective diffusive time given by $t_{eff} = t - x/u$. This suggests that either at short distances x from the source or for large velocities, the effective diffusive time is likely to enhance the migration process to the rock matrix.

Table 6-7. Input Parameters Used in Simulation of Tc-99 in Fracture and Rock Matrix for Case 7

Boundary Type	AFPS
Initial Concentration A° (arbitrary unit of activity/L^3)	1
Species	Tc-99
Type of Release Mode	Step
u (m/yr)	2
v (m/yr)	0
D_{xx} (m^2/yr)	0
D_{yy} (m^2/yr)	5
D_{yx} (m^2/yr)	0.0
D_e (m^2/yr)	10^{-2}
ϕ	10^{-2}
L(m)	1.0
b (m)	5×10^{-3}
R	10
R′	100
t (yr)	5×10^4
$T_{1/2}$ (yr)	2.13×10^5
d (m)	10
y_1 (m)	100
y_2 (m)	200
y_3 (m)	300

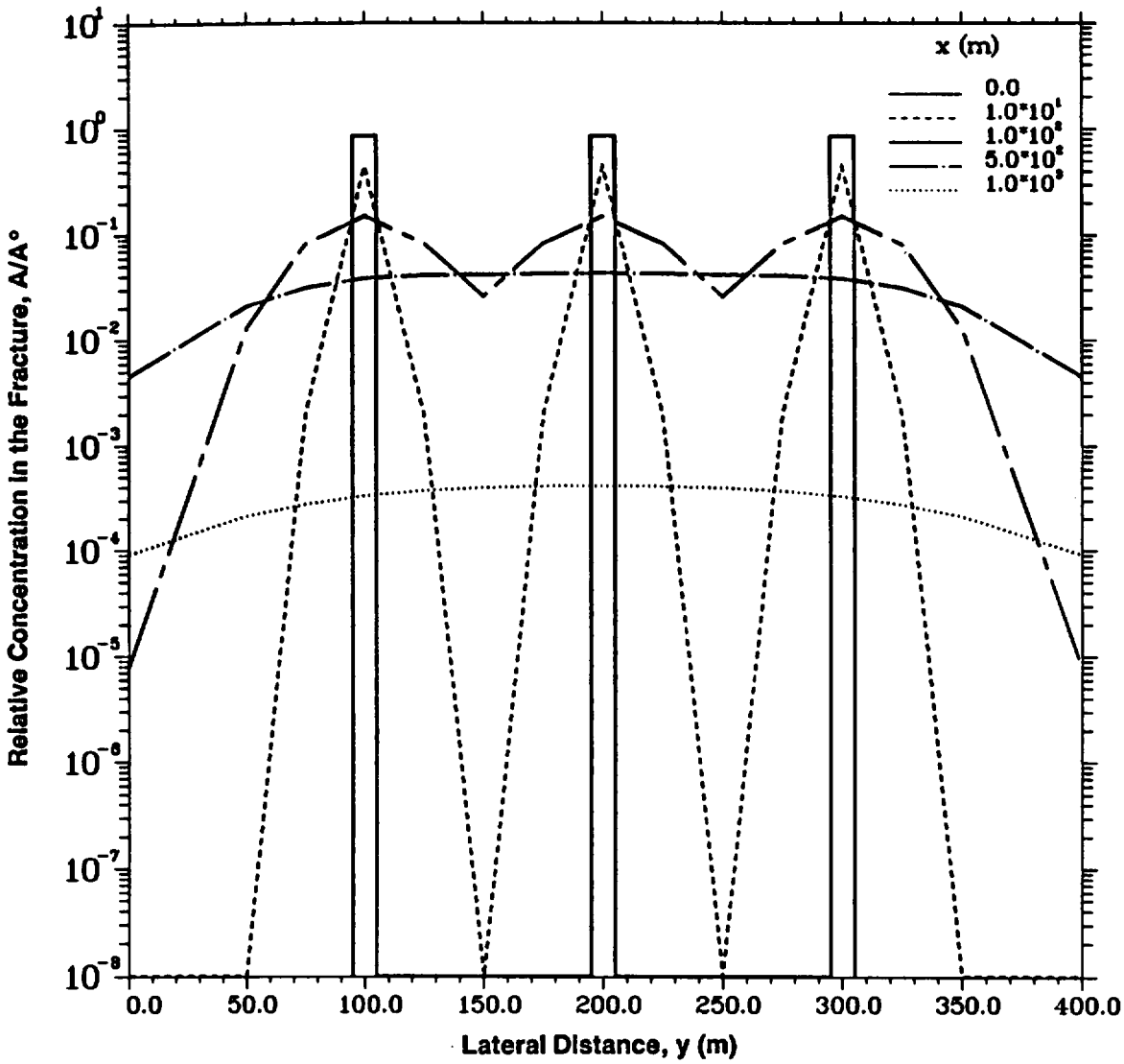

Figure 6-5a. Relative Concentration Profiles for Tc-99 in the Fracture at z = 0 m and t = 5 × 10⁴ yr (Case 7: Multiple Patch Source)

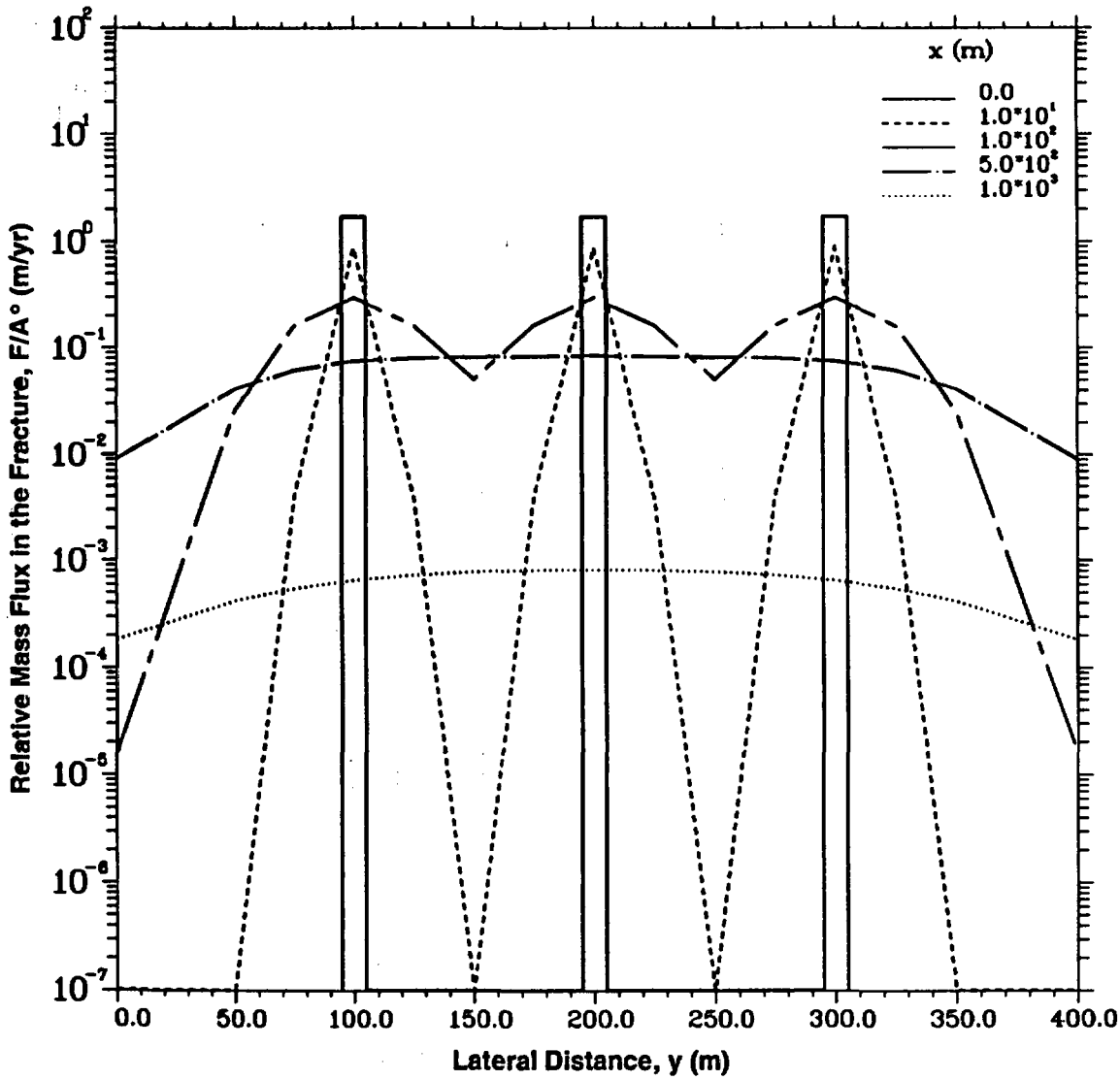

Figure 6-5b. Relative Mass Flux Profiles for Tc-99 in the Fracture at z = 0 m and t = 5 × 10⁴ yr (Case 7: Multiple Patch Source)

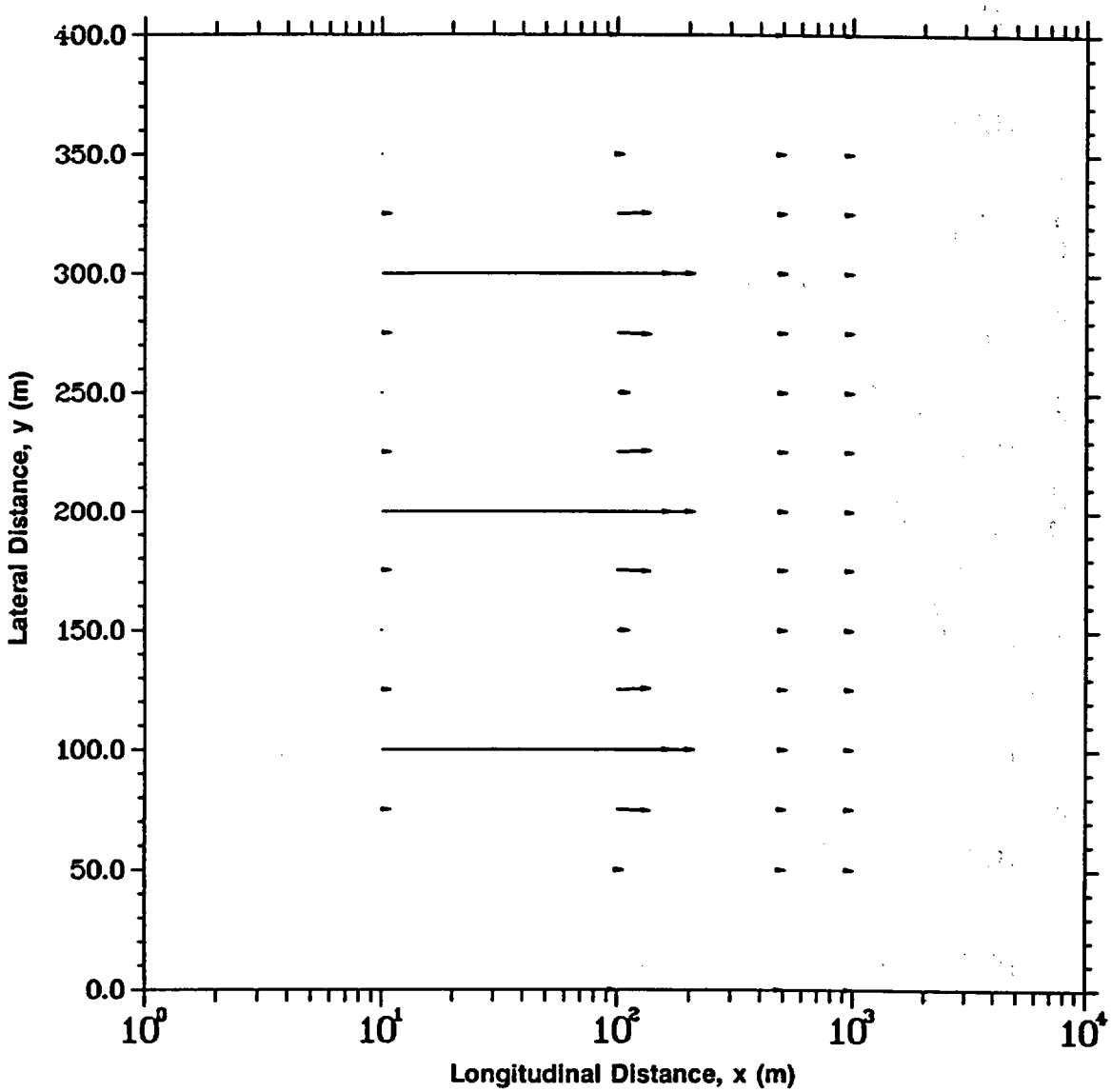

Figure 6-5c. Mass Flux Vector of Tc-99 at Discrete Points in the Fracture at z = 0 m and t = 5 × 10^4 (Case 7: Multiple Patch Source)

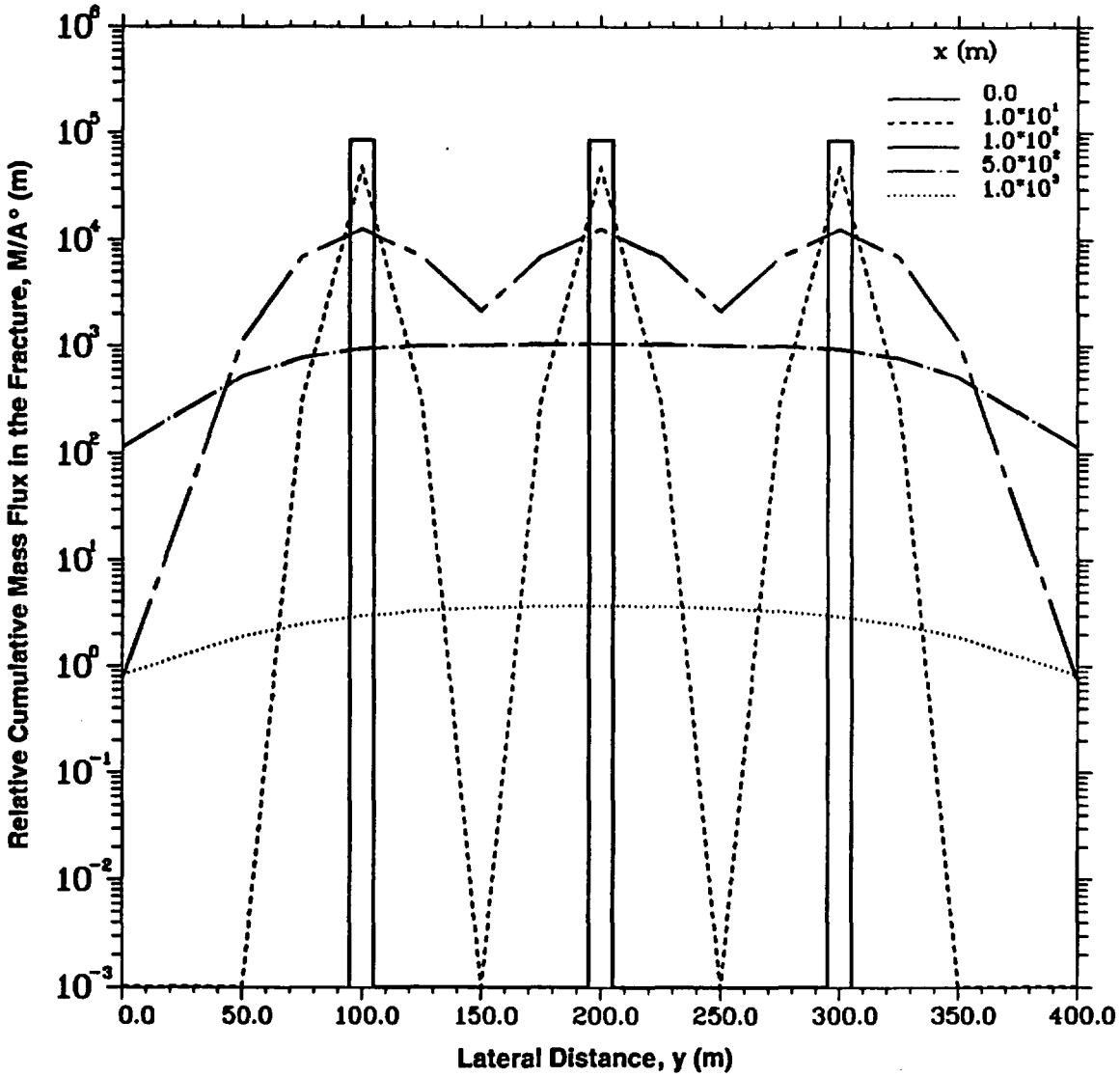

Figure 6-5d. Relative Cumulative Mass Flux Profiles for Tc-99 in the Fracture at z = 0 m and t = 5 × 10⁴ yr (Case 7: Multiple Patch Source)

Table 6-8a. Case 7 Results: Relative Concentration in the Fracture (A/A°) of Species Tc-99 at Time t = 5 x 10^4 yr (Multiple Patch Source)

Distance Along x-Axis (m)	Lateral Distance y (m)							
	0	50	75	100	125	150	175	200
0.0	0.00000E+00	0.00000E+00	0.00000E+00	0.84984E+00	0.00000E+00	0.00000E+00	0.00000E+00	0.84984E+00
10.0	0.00000E+00	0.83543E-10	0.19783E-02	0.44234E+00	0.19783E-02	0.16709E-09	0.19783E-02	0.44234E+00
100.0	0.80045E-05	0.12844E-01	0.81219E-01	0.15019E+00	0.81812E-01	0.25688E-01	0.81812E-01	0.15019E+00
500.0	0.45706E-02	0.20708E-01	0.31031E-01	0.38034E-01	0.40523E-01	0.41038E-01	0.41934E-01	0.42582E-01
1000.0	0.91901E-04	0.21058E-03	0.27449E-03	0.32931E-03	0.36965E-03	0.39511E-03	0.40839E-03	0.41242E-03

Distance Along x-Axis (m)	Lateral Distance y (m)						
	225	250	275	300	325	350	400
0.0	0.00000E+00	0.00000E+00	0.00000E+00	0.84984E+00	0.00000E+00	0.00000E+00	0.00000E+00
10.0	0.19783E-02	0.16709E-09	0.19783E-02	0.44234E+00	0.19783E-02	0.83543E-10	0.00000E+00
100.0	0.81812E-01	0.25688E-01	0.81812E-01	0.15019E+00	0.81219E-01	0.12844E-01	0.80045E-05
500.0	0.41934E-01	0.41038E-01	0.40523E-01	0.38034E-01	0.31031E-01	0.20708E-01	0.45706E-02
1000.0	0.40839E-03	0.39511E-03	0.36965E-03	0.32931E-03	0.27449E-03	0.21058E-03	0.91901E-04

Table 6-8b. Case 7 Results: X-Component of Relative Mass Flux in the Fracture ($F_x/A°$) (m/yr) of Species Tc-99 at Time t = 5 x 10^4 yr (Multiple Patch Source)

Distance Along x-Axis (m)	Lateral Distance y (m)							
	0	50	75	100	125	150	175	200
0.0	0.00000E+00	0.00000E+00	0.00000E+00	0.16997E+01	0.00000E+00	0.00000E+00	0.00000E+00	0.16997E+01
10.0	0.00000E+00	0.16709E-09	0.39565E-02	0.88468E+00	0.39565E-02	0.33417E-09	0.39565E-02	0.88468E+00
100.0	0.16009E-04	0.25688E-01	0.16244E+00	0.30037E+00	0.16362E+00	0.51376E-01	0.16362E+00	0.30039E+00
50.0	0.91411E-02	0.41416E-01	0.62062E-01	0.76068E-01	0.81047E-01	0.82077E-01	0.83869E-01	0.85163E-01
1000.0	0.18380E-03	0.42115E-03	0.54898E-03	0.65862E-03	0.73930E-03	0.79021E-03	0.81678E-03	0.82485E-03

Distance Along x-Axis (m)	Lateral Distance y (m)						
	225	250	275	300	325	350	400
0.0	0.00000E+00	0.00000E+00	0.00000E+00	0.16997E+01	0.00000E+00	0.00000E+00	0.00000E+00
10.0	0.39565E-02	0.33417E-09	0.39565E-02	0.88468E+00	0.39565E-02	0.16709E-09	0.00000E+00
100.0	0.16362E+00	0.51376E-01	0.16362E+00	0.30037E+00	0.16244E+00	0.25688E-01	0.16009E-04
500.0	0.83869E-01	0.82077E-01	0.81047E-01	0.76068E-01	0.62062E-01	0.41416E-01	0.91411E-02
1000.0	0.81678E-03	0.79021E-03	0.73930E-03	0.65862E-03	0.54898E-03	0.42115E-03	0.18380E-03

Table 6-8c. Case 7 Results: Y-Component of Relative Mass Flux in the Fracture ($F_y/A°$) (m/yr) of Species Tc-99 at Time t = 5 x 10^4 (Multiple Patch Source)

Distance Along x-Axis (m)	Lateral Distance y (m)							
	0	50	75	100	125	150	175	200
0.0	0.00000E+00	0.00000E+00	0.00000E+00	0.00000E+00	0.00000E+00	0.00000E+00	0.00000E+00	0.00000E+00
10.0	0.00000E+00	-0.37829E-19	-0.10152E-04	0.00000E+00	0.10152E-04	0.00000E+00	-0.10152E-04	0.00000E+00
100.0	-0.74314E-10	-0.95598E-04	-0.19109E-02	-0.13943E-05	0.18827E-02	-0.16103E-11	-0.18827E-02	0.00000E+00
500.0	-0.99371E-05	-0.10545E-03	-0.13614E-03	-0.82693E-04	-0.17755E-04	-0.11022E-04	-0.21179E-04	0.00000E+00
1000.0	-0.20985E-06	-0.65550E-06	-0.79083E-06	-0.75126E-06	-0.57235E-06	-0.35286E-06	-0.16051E-06	0.00000E+00

Distance Along x-Axis (m)	Lateral Distance y (m)						
	225	250	275	300	325	350	400
0.0	0.00000E+00	0.00000E+00	0.00000E+00	0.00000E+00	0.00000E+00	0.00000E+00	0.00000E+00
10.0	0.10152E-04	0.00000E+00	-0.10152E-04	0.00000E+00	0.10152E-04	0.37829E-19	0.00000E+00
100.0	0.18827E-02	0.16103E-11	-0.18827E-02	0.13943E-05	0.19109E-02	0.95598E-04	0.74314E-10
500.0	0.21179E-04	0.11022E-04	0.17755E-04	0.82693E-04	0.13614E-03	0.10545E-03	0.99371E-05
1000.0	0.16051E-06	0.35286E-06	0.57235E-06	0.75126E-06	0.79083E-06	0.65550E-06	0.20985E-06

Table 6-8d. Case 7 Results: Relative Cumulative Mass Flux in the Fracture (M/A°) of Species Tc-99 at Time t = 5 x 10^4 yr (Multiple Patch Source)

Distance Along x-Axis (m)	Lateral Distance y (m)							
	0	50	75	100	125	150	175	200
0.0	0.00000E+00	0.00000E+00	0.00000E+00	0.84984E+05	0.00000E+00	0.00000E+00	0.00000E+00	0.84984E+05
10.0	0.00000E+00	0.22269E-04	0.31258E+03	0.46961E+05	0.31258E+03	0.17739E-04	0.31258E+03	0.46961E+05
100.0	0.75635E+00	0.11213E+04	0.69374E+04	0.12732E+05	0.69851E+04	0.21778E+04	0.69851E+04	0.12733E+05
500.0	0.11507E+03	0.51944E+03	0.77769E+03	0.95286E+03	0.10151E+04	0.10280E+04	0.10505E+04	0.10667E+04
1000.0	0.83547E+00	0.19126E+01	0.24926E+01	0.29900E+01	0.33560E+01	0.35870E+01	0.37076E+01	0.37442E+01

Distance Along x-Axis (m)	Lateral Distance y (m)						
	225	250	275	300	325	350	400
0.0	0.00000E+00	0.00000E+00	0.00000E+00	0.84984E+05	0.00000E+00	0.00000E+00	0.00000E+00
10.0	0.31258E+03	0.17739E-04	0.31258E+03	0.46961E+05	0.31258E+03	0.22269E-04	0.00000E+00
100.0	0.69851E+04	0.21778E+04	0.69851E+04	0.12732E+05	0.69374E+04	0.11213E+04	0.75635E+00
500.0	0.10505E+04	0.10280E+04	0.10151E+04	0.95286E+03	0.77769E+03	0.51944E+03	0.11507E+03
1000.0	0.37076E+01	0.35870E+01	0.33560E+01	0.29900E+01	0.24926E+01	0.19126E+01	0.83547E+00

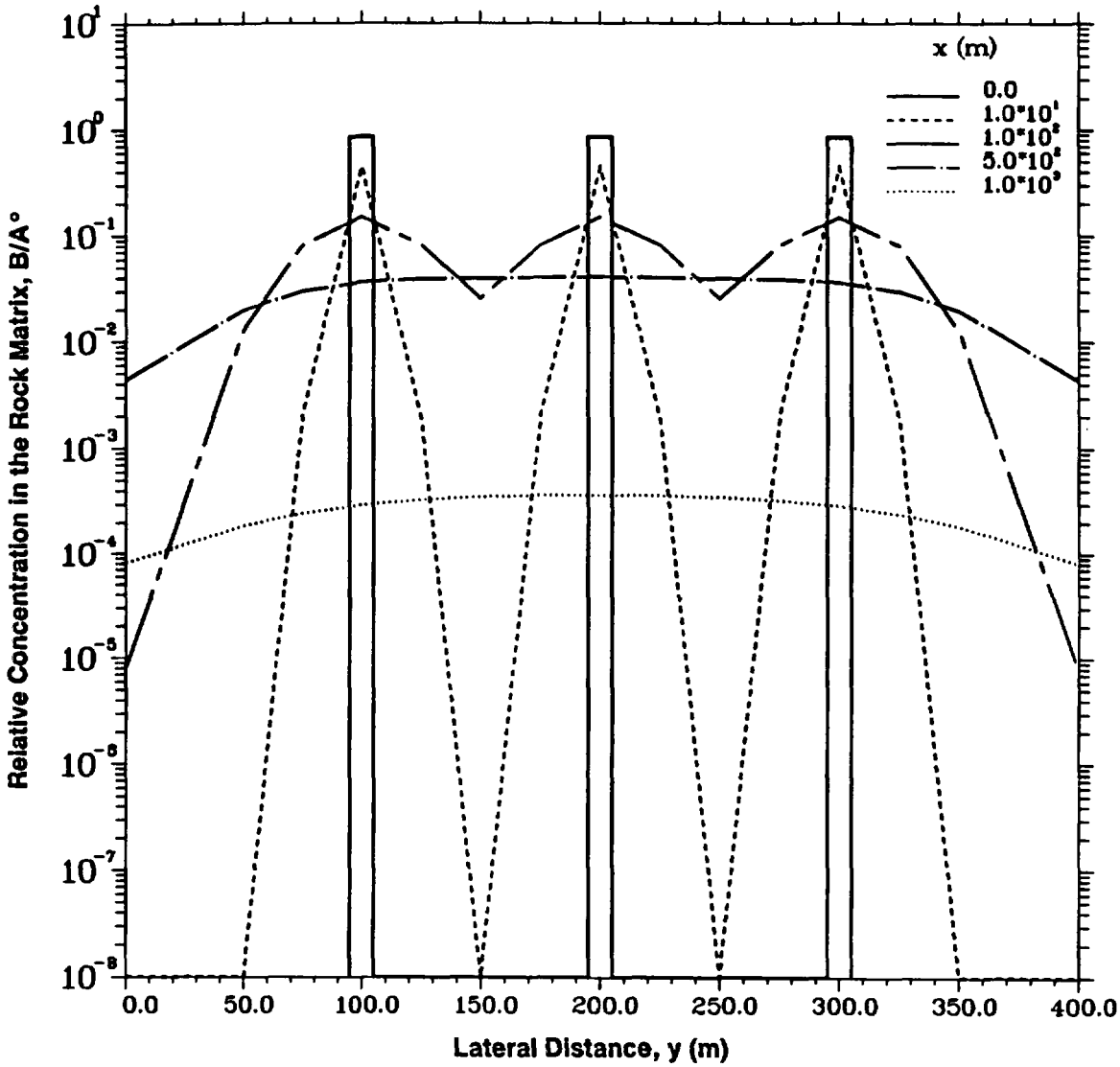

Figure 6-5e. Relative Concentration Profiles for Tc-99 in the Rock Matrix at $z = 0.1$ m and $t = 5 \times 10^4$ yr (Case 7: Multiple Patch Source)

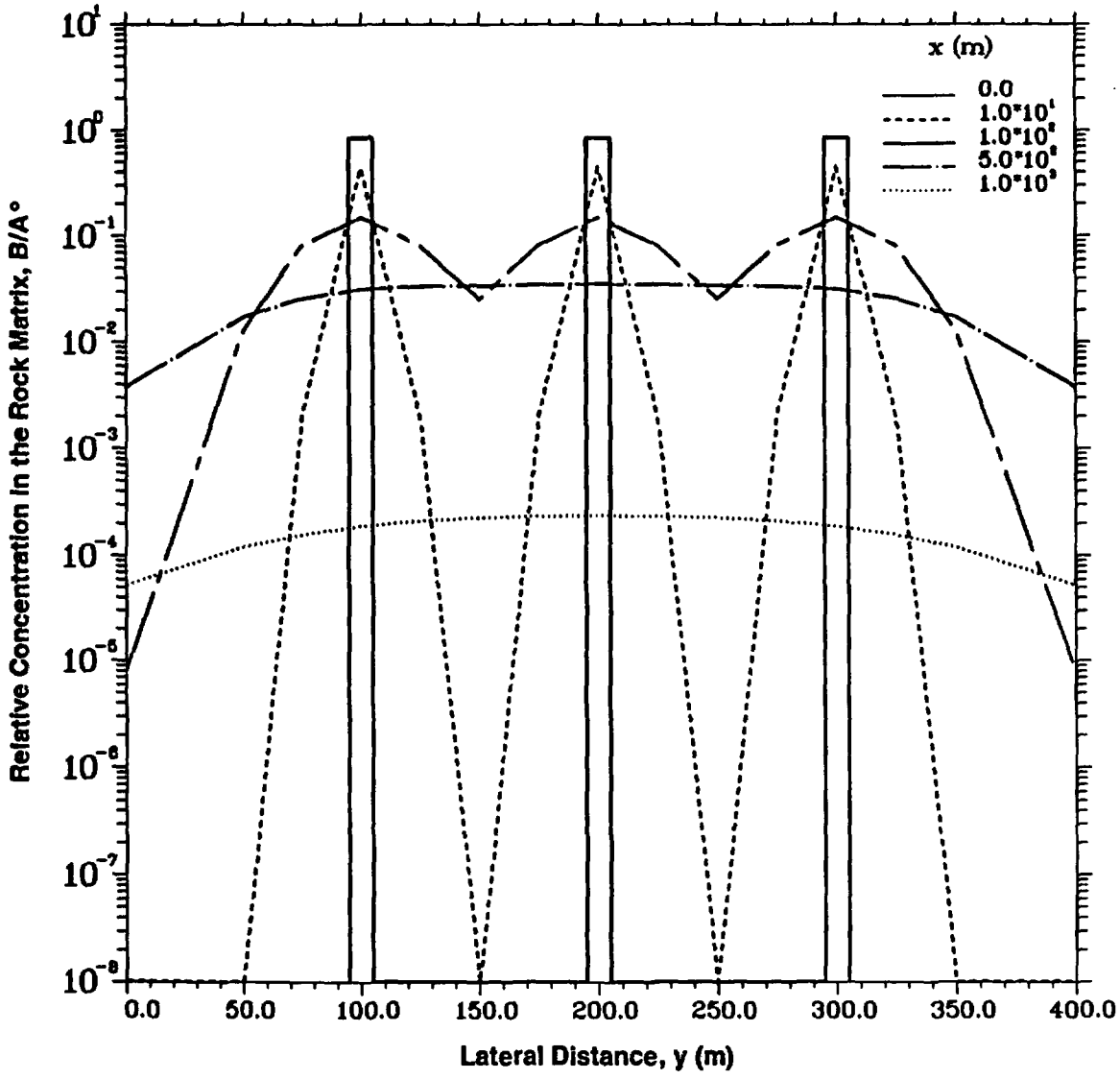

Figure 6-5f. Relative Concentration Profiles for Tc-99 in the Rock Matrix at $z = 0.5$ m and $t = 5 \times 10^4$ yr (Case 7: Multiple Patch Source)

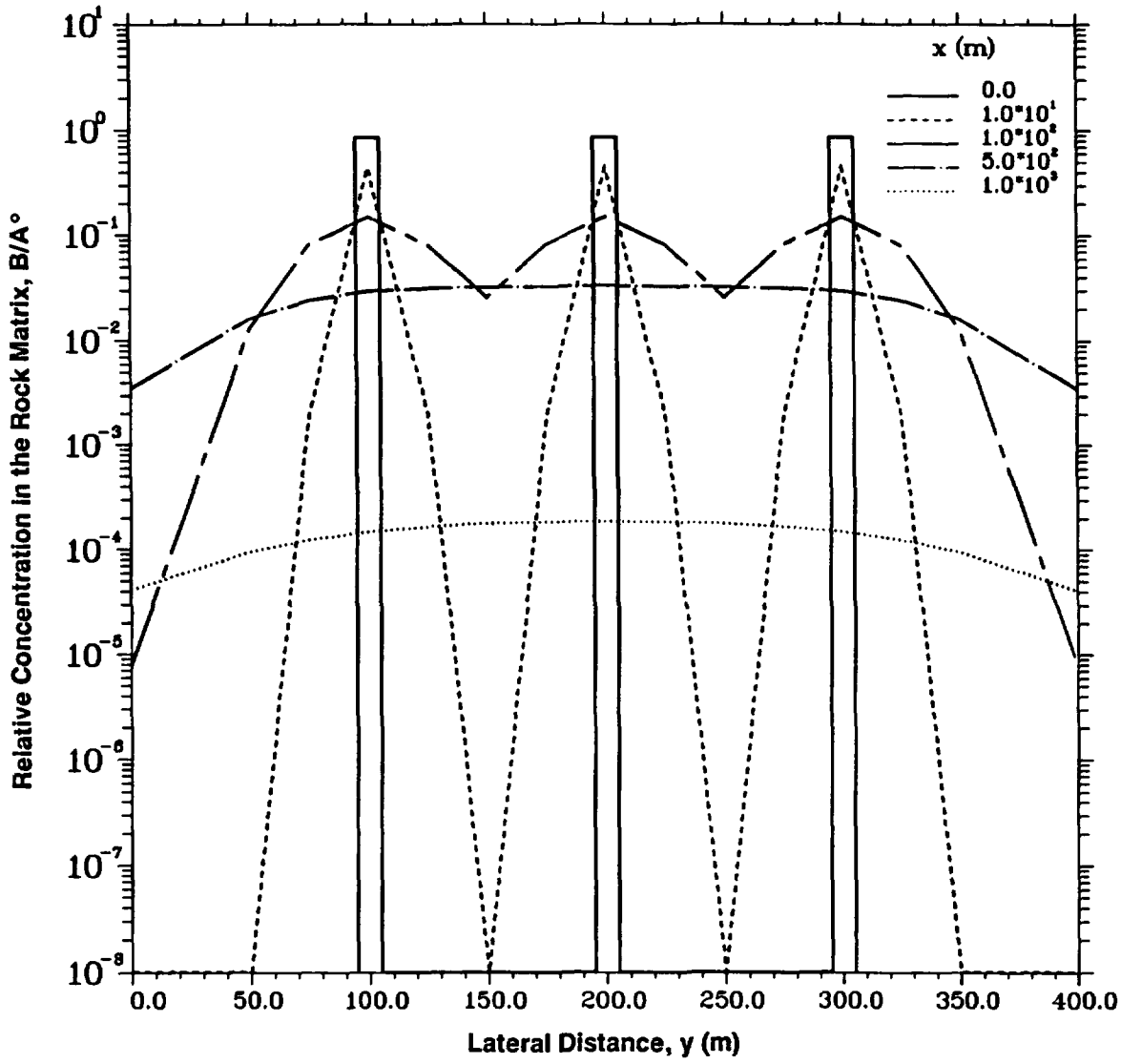

Figure 6-5g. Relative Concentration Profiles for Tc-99 in the Rock Matrix at $z = 1.0$ m and $t = 5 \times 10^4$ yr (Case 7: Multiple Patch Source)

Table 6-8e. Case 7 Results: Relative Concentration in the Rock Matrix (B/A°) of Species Tc-99 at Time t = 5 x 10^4 yr and z = 0.1 m (Multiple Patch Source)

Distance Along x-Axis (m)	Lateral Distance y (m)							
	0	50	75	100	125	150	175	200
0.0	0.00000E+00	0.00000E+00	0.00000E+00	0.84984E+00	0.00000E+00	0.00000E+00	0.00000E+00	0.84984E+00
10.0	0.00000E+00	0.83542E-10	0.19783E-02	0.44234E+00	0.19783E-02	0.16708E-09	0.19783E-02	0.44234E+00
100.0	0.80010E-05	0.12838E-01	0.81183E-01	0.15012E+00	0.81776E-01	0.25677E-01	0.81776E-01	0.15013E+00
500.0	0.43848E-02	0.19867E-01	0.29770E-01	0.36489E-01	0.38877E-01	0.39371E-01	0.40230E-01	0.40851E-01
1000.0	0.81726E-04	0.18726E-03	0.24410E-03	0.29285E-03	0.32872E-03	0.35136E-03	0.36317E-03	0.36676E-03

Distance Along x-Axis (m)	Lateral Distance y (m)						
	225	250	275	300	325	350	400
0.0	0.00000E+00	0.00000E+00	0.00000E+00	0.84984E+00	0.00000E+00	0.00000E+00	0.00000E+00
10.0	0.19783E-02	0.16708E-09	0.19783E-02	0.44234E+00	0.19783E-02	0.83542E-10	0.00000E+00
100.0	0.81776E-01	0.25677E-01	0.81776E-01	0.15012E+00	0.81183E-01	0.12838E-01	0.80010E-05
500.0	0.40230E-01	0.39371E-01	0.38877E-01	0.36489E-01	0.29770E-01	0.19867E-01	0.43848E-02
1000.0	0.36317E-03	0.35136E-03	0.32872E-03	0.29285E-03	0.24410E-03	0.18726E-03	0.81726E-04

Table 6-8f. Case 7 Results: Relative Concentration in the Rock Matrix (B/A°) of Species Tc-99 at Time t = 5 x 10^4 yr and z = 0.5 m (Multiple Patch Source)

Distance Along x-Axis (m)	Lateral Distance y (m)							
	0	50	75	100	125	150	175	200
0.0	0.00000E+00	0.00000E+00	0.00000E+00	0.84983E+00	0.00000E+00	0.00000E+00	0.00000E+00	0.84983E+00
10.0	0.00000E+00	0.83541E-10	0.19782E-02	0.44233E+00	0.19782E-02	0.16708E-09	0.19782E-02	0.44233E+00
100.0	0.79888E-05	0.12819E-01	0.81060E-01	0.14989E+00	0.81652E-01	0.25638E-01	0.81652E-01	0.14990E+00
500.0	0.38077E-02	0.17252E-01	0.25852E-01	0.31686E-01	0.33760E-01	0.34189E-01	0.34935E-01	0.35474E-01
1000.0	0.53000E-04	0.12144E-03	0.15830E-03	0.18991E-03	0.21318E-03	0.22786E-03	0.23552E-03	0.23785E-03

Distance Along x-Axis (m)	Lateral Distance y (m)						
	225	250	275	300	325	350	400
0.0	0.00000E+00	0.00000E+00	0.00000E+00	0.84983E+00	0.00000E+00	0.00000E+00	0.00000E+00
10.0	0.19782E-02	0.16708E-09	0.19782E-02	0.44233E+00	0.19782E-02	0.83541E-10	0.00000E+00
100.0	0.81652E-01	0.25638E-01	0.81652E-01	0.14989E+00	0.81060E-01	0.12819E-01	0.79888E-05
500.0	0.34935E-01	0.34189E-01	0.33760E-01	0.31686E-01	0.25852E-01	0.17252E-01	0.38077E-02
1000.0	0.23552E-03	0.22786E-03	0.21318E-03	0.18991E-03	0.15830E-03	0.12144E-03	0.53000E-04

Table 6-8g. Case 7 Results: Relative Concentration in the Rock Matrix (B/A°) of Species Tc-99 at Time t = 5 x 10^4 yr and z = 1.0 m (Multiple Patch Source)

Distance Along x-Axis (m)	Lateral Distance y (m)							
	0	50	75	100	125	150	175	200
0.0	0.00000E+00	0.00000E+00	0.00000E+00	0.84983E+00	0.00000E+00	0.00000E+00	0.00000E+00	0.84983E+00
10.0	0.00000E+00	0.83541E-10	0.19782E-02	0.44233E+00	0.19782E-02	0.16708E-09	0.19782E-02	0.44233E+00
100.0	0.79828E-05	0.12809E-01	0.80999E-01	0.14978E+00	0.81591E-01	0.25618E-01	0.81591E-01	0.14979E+00
500.0	0.35505E-02	0.16086E-01	0.24105E-01	0.29546E-01	0.31479E-01	0.31880E-01	0.32576E-01	0.33078E-01
1000.0	0.41546E-04	0.95195E-04	0.12409E-03	0.14887E-03	0.16711E-03	0.17862E-03	0.18462E-03	0.18645E-03

Distance Along x-Axis (m)	Lateral Distance y (m)						
	225	250	275	300	325	350	400
0.0	0.00000E+00	0.00000E+00	0.00000E+00	0.84983E+00	0.00000E+00	0.00000E+00	0.00000E+00
10.0	0.19782E-02	0.16708E-09	0.19782E-02	0.44233E+00	0.19782E-02	0.83541E-10	0.00000E+00
100.0	0.81591E-01	0.25618E-01	0.81591E-01	0.14978E+00	0.80999E-01	0.12809E-01	0.79828E-05
500.0	0.32576E-01	0.31880E-01	0.31479E-01	0.29546E-01	0.24105E-01	0.16086E-01	0.35505E-02
1000.0	0.18462E-03	0.17862E-03	0.16711E-03	0.14887E-03	0.12409E-03	0.95195E-04	0.41546E-04

7.0 SUMMARY AND CONCLUSIONS

Analytical solutions have been derived for predicting the two-dimensional transport of a radionuclide with no precursor in a single planar fracture as well as a system of parallel fractures coupled with the one-dimensional diffusive transport in the rock matrix. The solution for the mass and cumulative mass flux in the fracture and the longitudinal dispersion-free form of these solutions have also been investigated.

The solutions related to the fracture are designed for an unbounded medium (semi-infinite in the axial direction and infinite in the lateral direction); solutions related to the rock matrix consider a semi-infinite medium for the case of single fracture and a finite domain for the multiple fracture case. The initial concentration in both the fracture and the rock is assumed to be zero. The geometry and concentrations of the waste form at the source correspond to a finite patch (or multiple patch) or a Gaussian distributed source subject to decay in all cases. Furthermore, the radionuclide release modes considered in this study focus on the step and band release modes.

Two sets of solutions for the multiple parallel fracture case were derived; one based on a series approximation and the other based on contour integration are ideally suited to cope with small and large Fourier numbers, respectively. In particular, the new solution for the multiple parallel fracture case related to the rock matrix improved considerably the viability of its numerical evaluation by way of bypassing the restrictions inherent to a convolution-based solution.

An efficient transformation technique of the integration interval encountered in these solutions was derived, guaranteeing maximum stability and convergence. The Gauss-Legendre quadrature scheme was adopted to perform the integration. Note that in the multiple parallel fracture case, an efficient iterative quadrature scheme was devised to take care of the oscillatory nature of the integrand encountered in the solution based on contour integration.

In the case of the single fracture, the reported solutions were verified by means of available one- and two-dimensional analytical solutions; in the multiple parallel fracture case, the verification process was accomplished after comparing the results yielded by the two newly developed solutions, thus providing reasonable confidence to prospective users in utilizing them for verifying numerical codes.

Although overlooking longitudinal dispersion effects may lead to slightly conservative predictions both in terms of the maximum concentration in the system and the local concentration of a nuclide, yet the enhancement of the computational viability of the reported solutions in such a case cannot be underestimated. The need for a quadrature scheme is eliminated, except for the solution based on contour integration. These solutions also may be conveniently used for assessing the long-term geohydrochemical performance of a high-level nuclear waste repository located in fractured geologic media subjected to a water intrusion scenario.

8.0 REFERENCES

Abramowitz, M., and I. A. Stegun, 1972. Handbook of Mathematical Functions, Dover Publications, Inc., New York, NY.

Ahn, J., P. L. Chambré, and T. H. Pigford, 1985. Nuclide Migration Through a Planar Fissure with Matrix Diffusion, LBL-19249, Lawrence Berkeley Laboratory and Department of Nuclear Engineering, University of California, Berkeley, CA.

Ahn, J., P. L. Chambré, and T. H. Pigford, 1986. Radionuclide Migration Through Fractured Rock: Effects of Multiple Fractures and Two-Member Decay Chains, Earth Sciences Division, Lawrence Berkeley Laboratory and Department of Nuclear Engineering, University of California, Berkeley, CA.

Babcock, R. E., D. W. Green, and R. H. Perry, 1966. "Longitudinal Dispersion Mechanisms in Packed Beds," A.I.Ch.E. Journal, Vol. 12, No. 5, p. 922.

Barker, J. A., 1982. "Laplace Transform Solutions for Solute Transport in Fissured Aquifers," Advanced Water Resources, Vol. 5, No. 2, pp. 98-104.

Bear, J., 1972. Dynamics of Fluid in Porous Media, American Elsevier Publishing Co., New York, NY.

Carnahan, B., H. A. Luther, and J. O. Wilkes, 1969. Applied Numerical Methods, John Wiley and Sons, Inc., New York, NY.

Carslaw, H. S., and J. C. Jaeger, 1958. Conduction of Heat in Solids, 2nd ed., Clarendon Press, Oxford, UK.

Chambré, P. L., T. H. Pigford, A. Fujita, T. Kanki, A. Kobayashi, H. Lung, D. Ting, Y. Sato, and S. J. Zavoshy, 1982. Analytical Performance Models for Geologic Repositories Vol. II, LBL-14842, Lawrence Berkeley Laboratory, University of California, Berkeley, CA.

Chen, C. S., 1986. "Solutions for Radionuclide Transport From an Injection Well into a Single Fracture in a Porous Formation," Water Resources Research, Vol. 22, No. 4, pp. 508-518.

Cody, W. J., 1969. "Rational Chebyshev Approximation for the Error Functions," Mathematics of Computation, Vol. 23, No. 107, pp. 631-637.

Davis, G. B., and C. D. Johnston, 1984. "Comment on 'Contaminant Transport in Fractured Porous Media: Analytical Solutions for a System of Parallel Fractures,'" Water Resources Research, Vol. 20, No. 9, pp. 1321-1322.

Foglia, M., F. Iwamoto, M. Harada, P. L. Chambre, and T. H. Pigford, 1979. "The Superposition Equation for the Band Release of Decaying Radionuclides Through Sorbing Media," UCB-NE-3335, University of California at Berkeley, ANS Transactions, Volume 33, pp. 384-386.

Gradshteyn, I. S., and I. M. Ryzhik, 1980. Table of Integrals, Series, and Products, Academic Press, New York, NY, p. 1160.

Grisak, G. E., and J. F. Pickens, 1981. "An Analytical Solution for Solute Transport Through Fracture Media with Matrix Diffusion," Journal of Hydrology, Vol. 52, pp. 47-57.

Gureghian, A.B., 1987. Analytical Solutions for Multidimensional Transport of a Four-Member Radionuclide Decay Chain in Ground Water, BMI/OCRD-25, Office of Crystalline Repository Development, Battelle Memorial Institute, Columbus, OH, p. 162.

Hodgkinson, D. P., and P. R. Maul, 1985. One-Dimensional Modelling of Radionuclide Migration Through Permeable and Fractured Rock of Arbitrary Length Decay Chains Using Numerical Inversion of Laplace Transforms, AERE-11889, AERE-Harwell, Oxfordshire, UK, p. 36.

Kanki, T., A. Fujita, P. L. Chambre, and T. H. Pigford, 1981. Transport of Radionuclides Through Fractured Media, UCB-NE-4009, Lawrence Berkeley Laboratory, University of California, Earth Sciences Division, Berkeley, CA.

Moreno, L., and A. Rasmuson, 1986. "Contaminant Transport Through a Fractured Porous Rock: Impact of the Inlet Boundary Condition on the Concentration Profile in the Rock Matrix," Water Resources Research, Vol. 22, No. 12, pp. 1728-1730.

Neretnieks, I., 1980. "Diffusion in the Rock Matrix: An Important Factor in Radionuclide Retardation?" Journal of Geophysical Research, Vol. 85, pp. 4379-4397.

Neretnieks, I., T. Eriksen, and P. Tahtinen, 1982. "Tracer Movement in a Single Fissure in Granitic Rock: Some Experimental Results and Their Interpretation," Water Resources Research, Vol. 18, No. 4, pp. 849-858.

Rasmuson, A., and I. Neretnieks, 1980. "Exact Solution of a Model for Diffusion in Particles and Longitudinal Dispersion in Packed Beds," A.I.Ch.E. Journal, Vol. 26, pp. 686-690.

Rasmuson, A., and I. Neretnieks, 1981. "Migration of Radionuclides in Fissured Rock: The Influence of Micropore Diffusion and Longitudinal Dispersion," Journal of Geophysical Research, Vol. 86, pp. 3749-3758.

Rasmuson, A., and I. Neretnieks, 1986. "Radionuclide Transport in Fast Channels in Crystalline Rock," Water Resources Research, Vol. 22, pp. 1247-1256.

Rasmuson, A., 1984. "Migration of Radionuclides in Fissured Rock: Analytical Solutions for the Case of Constant Source Strength," Water Resources Research, Vol. 20, No. 10, pp. 1435-1442.

Rickert, P. G., R. G. Strickert, and M. G. Seitz, 1979. Nuclide Migration in Fractured Porous Rock, American Chemical Society, pp. 167-197.

Rosen, J. B., 1952. "Kinetics of a Fixed Bed System for Solid Diffusion into Spherical Particles," Journal of Chemical Physics, Vol. 20, p. 387.

Skopp, J., and A. W. Warrick, 1974. "A Two-Phase Model for the Miscible Displacement of Reactive Solutes in Soils," Soil Science Society of America Proceedings, Vol. 38, No. 4, pp. 545-550.

Sneddon, L. N., 1951. Fourier Transforms, McGraw-Hill Book Co., New York, NY.

Stroud, A. H., and D. Secrest, 1966. Gaussian Quadrature Formulas, Prentice-Hall, Inc., Englewood Cliffs, NJ.

Sudicky, E. A., and E. O. Frind, 1982. "Contaminant Transport in Fractured Porous Media: Analytical Solution for a System of Parallel Fractures," Water Resources Research, Vol. 18, No. 6, pp. 1634-1642.

Sudicky, E. A., and E. O. Frind, 1984. "Contaminant Transport in Fractured Porous Media: Analytical Solution for a Two-Member Decay Chain in a Single Fracture," Water Resources Research, Vol. 20, No. 7, pp. 1021-1029.

Tang, D. H., E. O. Frind, and E. A. Sudicky, 1981. "Contaminant Transport in Fractured Porous Media: Analytical Solution for a Single Fracture," Water Resources Research, Vol. 17, No. 3, pp. 555-565.

Van Genuchten, M. T., D. H. Tang, and R. Guennelon, 1984. "Some Exact Solutions for Solute Transport Through Soils Containing Large Cylindrical Macropores," Water Resources Research, Vol. 20, pp. 335-346.

APPENDIX A

THEOREMS, LAPLACE TRANSFORMS, AND DERIVATIVES

In this appendix, a selected number of theorems, inverse Laplace transforms, and derivatives is reported.

A.1 THEOREMS

The operations for the Laplace transformation reported in Chapters 1 to 4 require, in some cases, the use of the following theorems.

A.1.1 Translation

$$L^{-1}\left[e^{-bs} f(s)\right] = F(t-b)\,U(t-b),\ b > 0 \tag{A.1-1}$$

where U(t) is the Heaviside unit step function defined as

$$U(t) = \begin{matrix} 0\,,\ t < 0 \\ 1\,,\ t > 0 \end{matrix}$$

A.1.2 Linear Transformation

$$L^{-1}[f(s-a)] = e^{at} F(t) \tag{A.1-2}$$

A.1.3 Differentiation

$$L^{-1} sf(s) - F(+0) = F'(t) \tag{A.1-3a}$$

$$L^{-1}\ s^n f(s) - L^{-1}\ s^{n-1} F(+0) - L^{-1} s^{n-2}\ F'(+0) - \ldots - F^{(n-1)}(+0) = F^{(n)}(t) \tag{A.1-3b}$$

A.1.4 Convolution or Faltung

$$L^{-1}[f_1(s)\ \cdot\ f_2(s)] = \int_0^t F_1(t-\tau) F_2(\tau) = F_1 * F_2 \tag{A.1-4}$$

A.2 LAPLACE TRANSFORMS

f(s)	F(t)	
$\dfrac{e^{-a\sqrt{s}}}{s}$	$= \operatorname{erfc}\left(\dfrac{a}{2\sqrt{t}}\right)$	(A.2-1)
$\dfrac{e^{-a\sqrt{s}}}{\sqrt{s}}$	$= \dfrac{1}{\sqrt{\pi t}} \exp\left(-\dfrac{a^2}{4t}\right)$	(A.2-2)
$e^{-a\sqrt{s}}$	$= \dfrac{a}{2\sqrt{\pi t^3}} \exp\left(-\dfrac{a^2}{4t}\right)$	(A.2-3)
$\dfrac{1}{s^n}$, $n > 0$	$= \dfrac{t^{n-1}}{\Gamma(n)}$	(A.2-4)
$\dfrac{1}{s-ic}\cosh(bs^{1/2})\operatorname{sech}(as^{1/2})$	$= e^{ict}\cosh[b(ic)^{1/2}]\operatorname{sech}[a(ic)^{1/2}]$	
$a > b > 0$	$-2\pi \sum_{n=0}^{\infty} (-1)^n (n+1/2)[(n+1/2)^2 n^2 + ica^2]^{-1}$	
	$\cdot \cos[(n+1/2)\pi b/a]\exp[-(n+1/2)^2 n^2 t/a]$	(A.2-5)

A.3 LAPLACE INVERSION OF $s^{n+1/2}$

Because the inverse Laplace transform of $s^{n+1/2}$ for positive values of n is not reported in standard tables, the derivation of this may be useful to the reader. The gamma function (see Abramowitz and Stegun, 1972) defined as

$$\Gamma(z) = \int_0^{\infty} t^{z-1} e^{-t} dt \tag{A.3-1}$$

where z is the complex variable, is single valued and analytic over the entire complex plane with the exception of negative integers.

For positive values of the real part of z (i.e., x) Equation A.3-1 becomes

$$\Gamma(x) = \int_0^\infty t^{x-1} e^{-t} dt \tag{A.3-2}$$

and the characteristic equation is given by

$$\Gamma(x+1) = x\Gamma(x) \quad . \tag{A.3-3}$$

It may be easily shown that

$$\Gamma(-x) = \frac{\Gamma(1-x)}{(-x)}, x \neq 0,1,2,\ldots . \tag{A.3-4}$$

The Laplace transform of $t^{-n-3/2}$ may be written as

$$L\{t^{-n-3/2}\} = \int_0^\infty e^{-st} t^{-n-3/2} dt \quad . \tag{A.3-5}$$

Substitution of $s = u/t$ yields

$$L\{t^{-n-3/2}\} = \frac{1}{s^{-n-1/2}} \int_0^\infty u^{-n-3/2} e^{-u} du \quad . \tag{A.3-6}$$

Hence, from Equation A.3-2, we have

$$L^{-1} s^{n+1/2} = \frac{t^{-n-3/2}}{\Gamma(-n-1/2)} \tag{A.3-7}$$

Using the relation given by Equation A.3-4 and with the knowledge of $\Gamma(1/2) = \sqrt{\pi}$, we may derive $\Gamma(-n-1/2)$ through a recurrence formula. Thus it follows for

$n = 0$

$$\Gamma\left(-\frac{1}{2}\right) = -2\Gamma\left(\frac{1}{2}\right) = -2\sqrt{\pi} \tag{A.3-8a}$$

$n = 1$

$$\Gamma\left(-\frac{3}{2}\right) = -\left(\frac{2}{3}\right)\Gamma\left(-\frac{1}{2}\right) = (-1)^2\left(\frac{2}{3}\right)(2)\sqrt{\pi} = \frac{4}{3}\sqrt{\pi} \tag{A.3-8b}$$

$n = 2$

$$\Gamma\left(-\frac{5}{2}\right) = -\left(\frac{2}{5}\right)\Gamma\left(-\frac{3}{2}\right) = (-1)^3\left(\frac{2}{5}\right)\left(\frac{2}{3}\right)(2)\sqrt{\pi} = -\frac{8}{15}\sqrt{\pi} \tag{A.3-8c}$$

$n = p$

$$\Gamma\left(-p-\frac{1}{2}\right) = (-1)^{p+1}\left(\frac{2}{2p+1}\right)\left(\frac{2}{2p-1}\right)\cdots\left(\frac{2}{5}\right)\left(\frac{2}{3}\right)(2)\sqrt{\pi} \ . \tag{A.3-8d}$$

The above expressions may also be written as

$$\Gamma\left(-p-\frac{1}{2}\right) = (-1)^{p+1}\sqrt{\pi}\prod_{i=0}^{p}\left(\frac{2}{1+2i}\right) \ . \tag{A.3-9}$$

Hence Equation A.3-7 becomes

$$L^{-1}s^{n+1/2}(-1)^{n+1} = \frac{t^{-n-3/2}}{\sqrt{\pi}}\prod_{i=0}^{n}\left(\frac{1+2i}{2}\right) \ , \ n = 0, 1, 2, 3, \ldots \tag{A.3-10}$$

A.4 Nth DERIVATIVE OF ERROR FUNCTION

The Nth derivative of the error function (see Abramowitz and Stegun, 1972) is given by

$$\frac{d^{n+1}}{dz^{n+1}}\{\mathrm{erf}(z)\} = (-1)^n\frac{2}{\sqrt{\pi}}H_n(z)e^{-z^2} \ , \ n = 0, 1, 2, 3, \ldots \tag{A.4-1}$$

where H_n are the Hermite polynomials. A list of the first six polynomials is given hereafter.

$$H_0 = 1$$

$$H_1(z) = 2z$$

$$H_2(z) = 4z^2 - 2$$

$$H_3(z) = 8z^3 - 12z$$

$$H_4(z) = 16z^4 - 48z^2 + 12$$

$$H_5(z) = 32z^5 - 160z^3 + 120z$$

$$H_6(z) = 64z^6 - 480z^4 + 720z^2 - 120$$

The recurrence relation (see Schiff, 1950) is given by

$$H_{n+1}(z) = 2zH_n(z) - 2nH_{n-1}(z),\ n > 0 \quad .$$

References

Abramowitz, M., and I. A. Stegun, 1972. Handbook of Mathematical Functions, Dover Publications, Inc., New York, NY.

Schiff, L. I., 1950. Quantum Mechanics, McGraw-Hill, New York, NY.

APPENDIX B

QUADRATURE

The various solutions presented in this report require for the most part the evaluation of integrals. An exception is made in the case of the longitudinal dispersion-free solution associated with the single fracture case (Chapter 3) and the series-based solution for the parallel fracture case (Chapter 4). The integrals associated with the general solution of Equations 2-10 and 2-11 which emerge from the consideration of longitudinal dispersion effects or result from the numerical inversion of the Laplace transform show some similarity with respect to their limits (0, ∞). However, because of the distinct nature of their respective integrands the techniques used to approximate the integration over finite subintervals are quite different. Because of the remarkable convergence properties of the Gaussian integration formulas (see Stroud and Secrest, 1966), the Gauss-Legendre quadrature scheme has been adopted in this work.

B.1 TRANSFORMATION FOR INFINITE INTEGRAL ASSOCIATED WITH THE PRESENCE OF LONGITUDINAL DISPERSION

The integral of interest has the following form

$$I = \int_0^\infty f(x)dx \tag{B.1-1}$$

when the dependent variable of the integrand corresponds in our case to σ (see Equations 3-42, 3-44, 3-58, and 4-4). Hence by virtue of the properties inherent to the Heaviside function (see Equations 2-21), the lower limit, say σ_{min}, must meet the following criterion

$$t \geq R\chi \tag{B.1-2}$$

Substitution for χ given by Equation 3-22d. The potential lower limit may then be written as

$${}_1\sigma_{min} = \frac{x}{2}\left(\frac{R}{D_{xx}t}\right)^{1/2} . \tag{B.1-3}$$

The choice of the upper and lower limits of integration are also dictated by the condition that the maximum absolute value of the exponential argument appearing in Equation 3-22a written as

$$\psi(x,\sigma) = \frac{2}{\sqrt{\pi}} \exp\left[-\left(\sigma - \frac{y}{\sigma}\right)^2\right] \tag{B.1-4}$$

with

$$\gamma = \frac{ux}{4D_{xx}} \tag{B.1-5}$$

should always be less than or equal to the one allowed by the computer, say ARG. Hence equating the latter with the argument of the exponential form in Equation B.1-4, we obtain

$$\sigma^4 - (ARG + 2\gamma)\sigma^2 + \gamma^2 = 0 \tag{B.1-6}$$

where the roots of the above equation are given by

$$\sigma^2_{max} = \frac{(ARG + 2\gamma) + \left[(ARG + 2\gamma)^2 - 4\gamma^2\right]^{1/2}}{2} \tag{B.1-7}$$

$$_2\sigma^2_{min} = \frac{(ARG + 2\gamma) - \left[(ARG + 2\gamma)^2 - 4\gamma^2\right]^{1/2}}{2} \quad . \tag{B.1-8}$$

Note that both roots are positive. The potential values for the integration limits given by Equations B.1-7 and B.1-8 are now used to extract suitable upper (σ_{UL}) and lower limits (σ_{LL}). The integration domain is split over two finite intervals, i.e., $[\sigma_{LL}, \sigma_{IN}]$ and $[\sigma_{IN}, \sigma_{UL}]$, where σ_{IN} will correspond to the value of σ in Equation B.1-6 when function $\psi(x,\sigma)$ (see Equation 3-22a) is a maximum;

$$\sigma_{IN} = \gamma^{1/2}, \sigma_{LL} < \gamma^{1/2} < \sigma_{UL} \quad . \tag{B.1-9}$$

If the above condition is not satisfied, then

$$\sigma_{IN} = \frac{1}{2}(\sigma_{LL} + \sigma_{UL}), \gamma^{1/2} < \sigma_{LL} \text{ or } \gamma^{1/2} > \sigma_{UL} \tag{B.1-10}$$

where

$$\sigma_{LL} = MAX\,[_1\sigma_{min}, {}_2\sigma_{min}] \tag{B.1-11a}$$

$$\sigma_{UL} = MAX\,[_1\sigma_{min}, \sigma_{max}] \tag{B.1-11b}$$

Results yielded by this method proved to be very satisfactory, however, at the expense of an additional computational effort.

B.2 PARALLEL FRACTURE CASE

For the sake of simplicity, the discussion presented in this section is focused on the longitudinal dispersion-free form of the transport equation given by Equation 2-10. However, it may easily be extended to the general form of the transport equation.

The various integrands $G(\eta,t)$ associated with the solution of the parallel fracture case resulting from the the numerical inversion of the Laplace transform by means of contour integration may be looked upon as one corresponding to the product of two functions $g_1(\eta)$ and $g_2(\eta,t)$ written as

$$G = g_1(\eta) \cdot g_2(\eta,t) \tag{B.2-1}$$

where

$$g_1(\eta) = \exp(\beta_r)/\eta \text{ (Fracture, Mass Flux, and Cumulative Mass Flux)} \tag{B.2-2a}$$

$$g_1(\eta) = \sum_{m=1}^{2} \sum_{n=1}^{2} \frac{\exp(\bar{\beta}_r)}{\delta_1 \eta} \text{ (Rock Matrix)} \tag{B.2-2b}$$

and

$$g_2(\eta,t) = \sin(\bar{\gamma}'_\ell) + \sin(v - \bar{\gamma}'_\ell) \text{ (Fracture, Mass Flux)} \tag{B.2-3a}$$

$$g_2(\eta,t) = \sin(\bar{\gamma}'_\ell) + \sin(v - \bar{\gamma}'_\ell) \text{ (Rock Matrix)} \tag{B.2-3b}$$

$$g_2(\eta,t) = \sum_{k=1}^{2} I_k \text{ (Cumulative Mass Flux)} \tag{B.2-3c}$$

where I_1 and I_2 are given by Equations 5-30c and 5-31b.

Referring to Equations B.2-2 and B.2-3, these correspond to sets of smooth, exponentially decaying and quasi-sinusoidal functions, respectively, which generate rapidly oscillatory integrands (i.e., one with numerous local maxima and minima), however which decay over the range of integration. Figures B-1, B-2, and B-3 show some typical representative curves for $g_1(\eta)$ and $g_2(\eta,t)$ and the integrand G obtained for three different values of the variable x, all other parameters being kept constant.

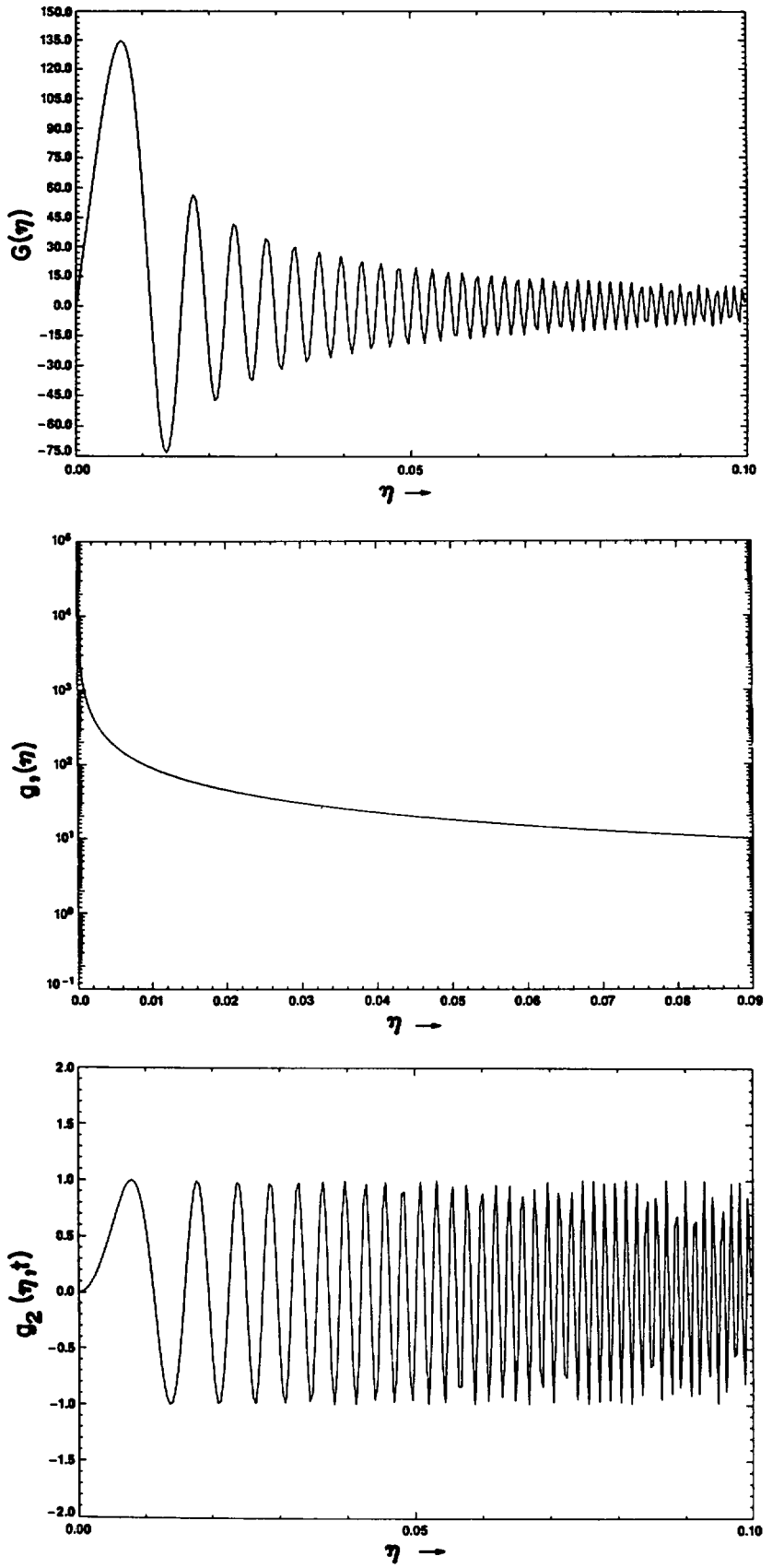

Figure B-1. Variations of Function $G(\eta)$, $g_1(\eta)$, and $g_2(\eta,t)$ for x=1 m

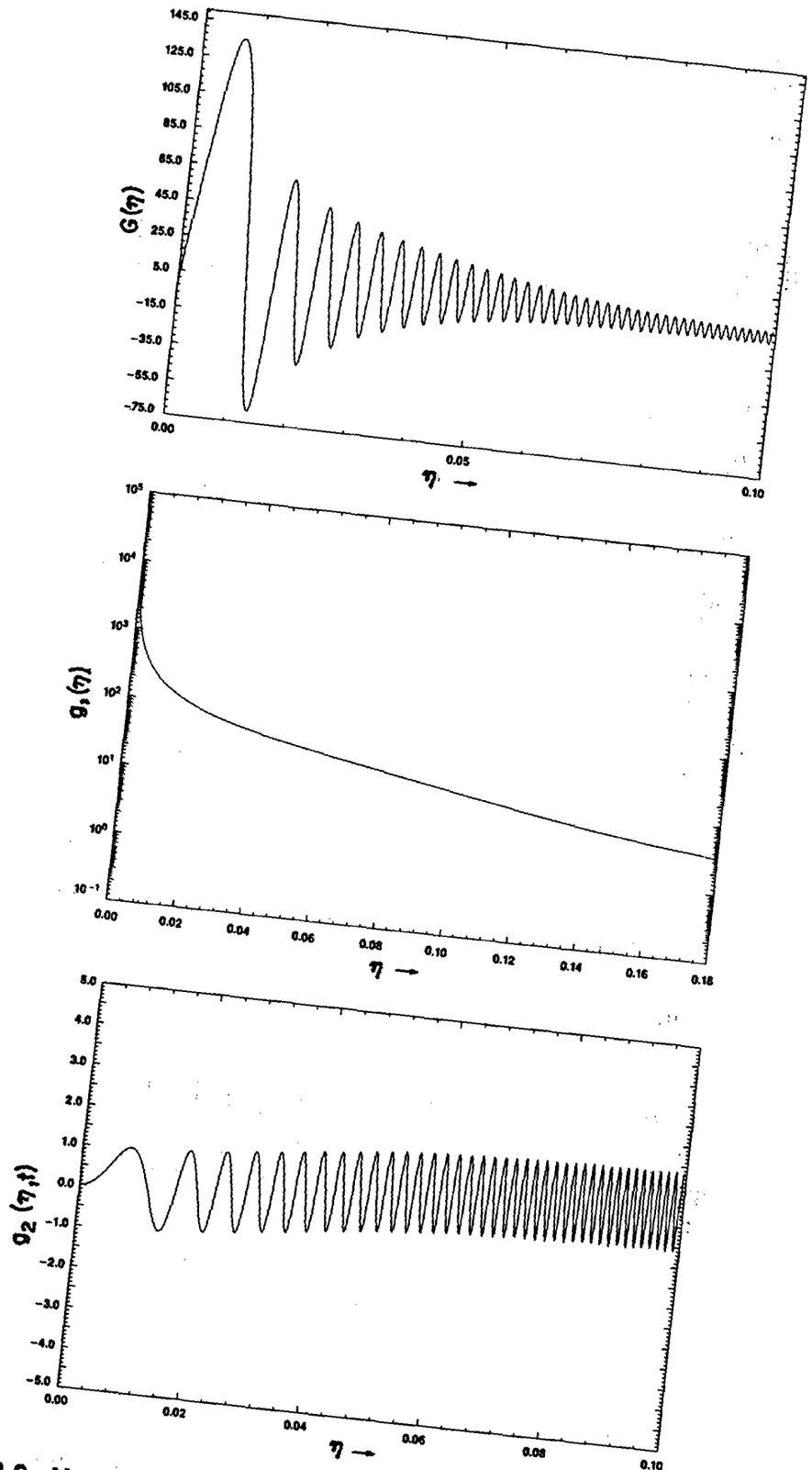

Figure B-2. Variations of Function $G(\eta)$, $g_1(\eta)$, and $g_2(\eta,t)$ for x=100 m

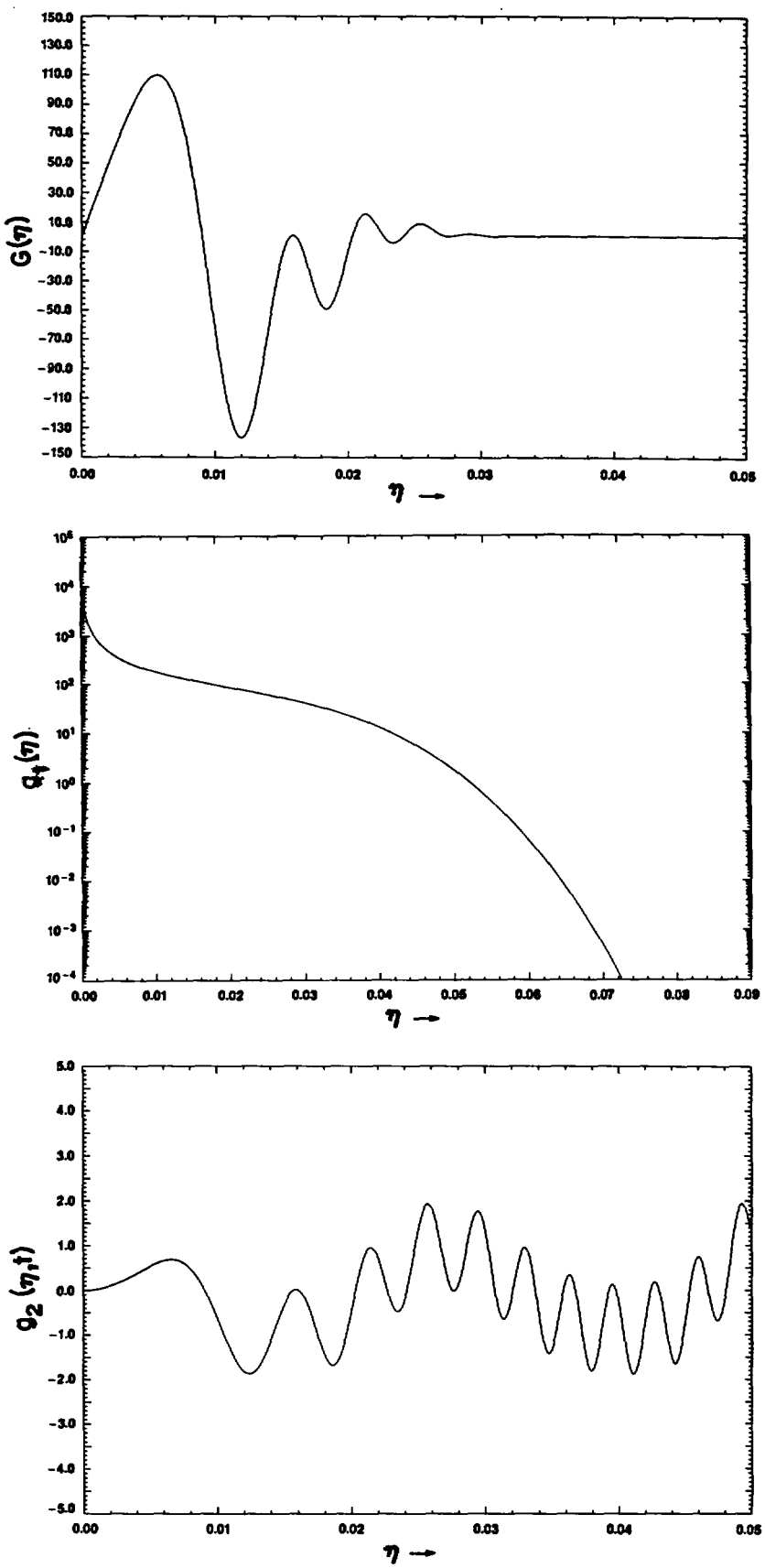

Figure B-3. Variations of Function $G(\eta)$, $g_1(\eta)$, and $g_2(\eta,t)$ for x=10,000 m

Table B-1. Parameters Used to Estimate $G(\eta)$, $g_1(\eta)$, and $g_2(\eta, t)$

x	1, 100, 10^4 m
L	0.32 m
b	0.005 m
u	10 m/yr
v	0 m/yr
D_{xx}	0 m^2/yr
D_{yy}	0 m^2/yr
D_e	0.01 m^2/yr
R	1.0
R'	100.0
ϕ	0.01
t	5×10^4 yr

Range of Integration

Reduction of the infinite interval to a finite interval became mandatory because an initial attempt to evaluate the integral using a Gauss-Legendre quadrature scheme failed to produce acceptable results. A potential upper limit (η_{UL}) for the range of integration is computed in our case after equating $g_1(\eta)$ to a small number (i.e., EPS)* and using the Newton-Raphson iteration formula. Subsequently, the segment $[0,\eta_{UL}]$ is subdivided into n unequal intervals (i.e., $[0,\eta_1]$, $[\eta_1, \eta_2]$, ... $[\eta_{n-1}, \eta_n]$) where the upper limit of each of these is computed using the following relation:

$$\eta_i = \eta_{UL} ab^{i-1} \ , \ i = 1,2,3,...n \tag{B.2-4}$$

with $b = \exp-[\ln(a)/n]$ and $a = 0.02$. This yields geometrically increasing intervals which would allow a highly accurate evaluation of the integrals in the region close to the origin using a modest number of integration points. Their contributions to the anticipated result may be quite significant under some circumstances. In order to optimize the convergence of the integral, a search for a tentative reduction of the integration domain is carried out after performing a quadrature which uses 60 integration points for each interval. Subsequently the contributions of successive intervals are summed up beginning from the last (i.e., nth) and, in the event the absolute ratio of this to the value of the integral is less than 1.E−06, η_{n-1} is then substituted for η_{UL}, where i denotes the current value of the summation index.

Because of the oscillatory nature of the aforementioned integrand, a composite iterative Gauss-Legendre quadrature scheme was adopted with (η_{-i1}, η_i) split initially into $m = 2$ subintervals and increased by a factor of 1.5 ($m \geq = 1000$) or 1.2 ($m > 1000$) at subsequent iterations, using at all times 20 Gaussian points. Note that care is taken to round off the value of m to the nearest integer whenever required. The convergence test is initiated at the end of the second iteration (see below). The selection of the initial value for m for subsequent intervals is taken to correspond to the one registered at the step of the iteration process prior to the last marking the convergence of the preceding interval. The maximum allowed value for m in the FRACFLO code corresponds to 750; when past this mark, iteration can no longer be performed. Note that in the case of the longitudinal dispersion free form of the transport equation the integration range is split into 25 intervals; however, due to the severe execution time constraint imposed by the solution of the general form of the transport equation, a maximum of 12 intervals was adopted in such an instance. In addition, the iterative quadrature scheme was

---

* EPS = 10^{-6} except in the case of the fracture, where it follows that for

$$.01 < \varepsilon/2\sqrt{t-R_X} < .1 \ , \ EPS = 0.01$$
$$\varepsilon/2\sqrt{t-R_X} < .01 \ , \ EPS = 0.02.$$

applied only when longitudinal dispersive effects are neglected. However, in the general case an adequate match with results yielded by the series solution was registered using 60 quadrature points for each subinterval.

The convergence criterion may be summarized as follows:

$$|(G_i)_n| = 1.E-15 \tag{B.2-5}$$

$$\left| (G_i)_n - (G_i)_{n-1} \right| = 1.E-04 \text{ (Absolute Error)} \tag{B.2-6a}$$

$$\left| \frac{(G_i)_n - (G_i)_{n-1}}{(G_i)_n} \right| = 1.E-03 \text{ (Relative Error)} \tag{B.2-6b}$$

where subscripts i and n refer to a typical integral and the iteration index, respectively. Note that for a particular integral, convergence is said to have been reached when either Equation B.2-5 or Equations B.2-6a and B.2-6b are satisfied. Convergence is normally witnessed at the end of the second iteration. Exceptions to this norm occur particularly when the integrand displays a high frequency of oscillation and its amplitude decreases very slowly with η. With the contribution of successive intervals summed up during the progress of the quadrature operation, a subsequent convergence test based on a criterion adopted for the series solution (see Equations 4-91 and 4-92) is performed past the 20th interval. This allows a further optimization of computer execution time.

Since the magnitude of parameter ε appearing in the expression of the exponential argument b_r in Equation B.2-1 (see also Equation 5-4a) controls the magnitude of the integration domain, and since parameter t controls the frequency of oscillations, numerical experiments such as the one reported in Table B-2 indicate that for a constant value of the Fourier number, the magnitude of the dimensionless number $\varepsilon/2\sqrt{t-R_X}$, which encompasses the two parameters of interest has a critical bearing on the convergence properties of the present quadrature scheme. It may be added that for a constant value of $\varepsilon/2\sqrt{t-R_X}$, convergence is almost independent of the Fourier number. Note for example that when 2,500 quadrature points are the minimum required to satisfy convergence in the case of the longitudinal dispersion free form of the transport equation, substantial increases are registered (i.e., 10,420 and 186,340 for Fo = 10; 12,250 and 168,320 for Fo = 408; and 10,120 and 169,420 for Fo = 1666 when the value of $\varepsilon/2\sqrt{t-R_X}$ drops to 0.1 and 0.005, respectively.

Table B-2. Quadrature Points Required for Selected Range of Values of Fo and $\varepsilon/2\sqrt{t-R_X}$ ($D_{xx} = 0$)

Fo	$\varepsilon/2\sqrt{t-R_X}$	Quadrature Points
10	1.0	2,200
10	0.1	10,420
10	0.005	186,340 (not converged)
408	1.0	2,500
408	0.1	12,250
408	0.005	168,320 (not converged)
1,666	1.0	3,080
1,666	0.1	10,120
1,666	0.005	169,420 (not converged)

B.3 GAUSS-LEGENDRE QUADRATURE

In the Gauss-Legendre quadrature scheme, the numerical approximation to a typical integral I is given by

$$I \approx \sum_{i=1}^{n} w_i f(x_i) \tag{B.3-1}$$

where w_i are the weighting functions and x_i are the integration points for an n-point Gaussian integration.

The evaluation of the integral may be described as follows. Consider the problem of evaluating

$$I \approx \int_a^b f(x)\,dx \tag{B.3-2}$$

By Gauss-Legendre quadrature, this is accomplished by making the change of variable from x to z given by

$$z = \frac{2x - a - b}{b - a} \tag{B.3-3}$$

$$x = \frac{1}{2}\,[(b - a)z + b + a] \tag{B.3-4}$$

which changes Equation B.3-2 to

$$\int_a^b f(x)\,dx = \frac{(b-a)}{2}\int_{-1}^{1} g(z)\,dz \tag{B.3-5}$$

with

$$g(z) = f\left[\frac{1}{2}(b-a)z + \frac{1}{2}(a+b)\right] \tag{B.3-6}$$

The value of the integral f(x) in the interval -1 and $+1$ is given by Equation B.3-1. It can be shown that an n-point Gaussian integration can evaluate exactly the integral of a $2n-1$ degree polynomial. Subroutine DGAUSS provides the user with values of roots of the Legendre polynomials as well as the corresponding weight factors for a number of integration points, i.e., 10, 20, 60, 104, and 256. [See Stroud and Secrest (1966), and Carnahan et al. (1969).]

Generally, the solution is sensitive to the number of integration points selected for the particular problem.

When the segment [a,b] is subdivided into m/2 intervals (m even), the integral is then approximated as

$$\int_a^b f(x)\,dx \approx \frac{(b-a)}{m}\sum_{j=0}^{(m/2)-1} f\left[a + \frac{(b-a)}{m}[1+z+2j]\right] \tag{B.3-7}$$

In the case of a double integral, Equation B.3-1 becomes

$$I \approx \sum_{j=1}^{m} w_j \sum_{i=1}^{m} v_{ij} f(x_i, y_{ij}) \tag{B.3-8}$$

where the double subscripts on the right reflect the fact that the abscissas and weights of the m-point rule must be adjusted for each value of j of the n-point rule. Note that the identity given by Equation B.3-8 is an mn-point rule for I.

References

Carnahan, B., H. A. Luther, and J. O. Wilkes, 1969. Applied Numerical Methods, John Wiley and Sons, Inc., New York, NY.

Stroud, A. H., and D. Secrest, 1966. Gaussian Quadrature Formulas, Prentice-Hall, Inc., Englewood Cliffs, NJ.

APPENDIX C

Nth DERIVATIVE OF A PRODUCT OF TWO FUNCTIONS

Let the two functions u and v be defined as

$$u = t^p \tag{C-1}$$

$$v = e^{a/t} \tag{C-2}$$

where a and p are constants.

The nth derivative of u with respect to t may be written as

$$\frac{d^n u}{dt^n} = t^{(p-n)} \prod_{i=1}^{n} (p-i+1) \tag{C-3}$$

and the nth derivative of v with respect to t (see Gradshteyn and Ryzhik, 1980, p. 19) is given by

$$\frac{d^n}{dt^n}(e^{a/t}) = (-1)^n \frac{1}{t^n} e^{a/t} \left[(\frac{a}{t})^n + (n-1)\binom{n}{1}(\frac{a}{t})^{n-1} + (n-1)(n-2)\binom{n}{2}(\frac{a}{t})^{n-2} \right.$$

$$\left. + (n-1)(n-2)(n-3)\binom{n}{3}(\frac{a}{t})^{n-3} + \ldots \right] \tag{C-4}$$

or symbolically,

$$\frac{d^n}{dt^n}(e^{a/t}) = (-1)^n \frac{1}{t^n} e^{a/t} \left[\sum_{m=1}^{n} \prod_{i=1}^{m-1} (n-i)\binom{n}{m-1}(\frac{a}{t})^{n-m+1} \right] . \tag{C-5}$$

Using Leibnitz's theorem for differentiation of a product (Abramowitz and Stegun, 1972, p. 12) given by

$$\frac{d^n(uv)}{dt^n} = \frac{d^n u^v}{dt^n} + \binom{n}{1}\frac{d^{n-1}u}{dt^{n-1}}\frac{dv}{dt} + \binom{n}{2}\frac{d^{n-2}u}{dt^{n-2}}\frac{d^2v}{dt^2} + \ldots + \binom{n}{r}\frac{d^{n-r}u}{dt^{n-r}}\frac{d^r v}{dt^r} + \ldots + u\frac{d^n v}{dt^n} \tag{C-6}$$

and substitution of Equations C-1, C-2, C-3, and C-4 in the above equation yields

$$\frac{d^n(t^p e^{a/t})}{dt^n} = t^{p-n} e^{a/t} \sum_{r=0}^{n} \binom{n}{r} \prod_{i=1}^{n-r} (p-i+1)(-1)^r \sum_{m=1}^{r} \prod_{j=1}^{m-1} (r-j)\binom{r}{m-1}(\frac{a}{t})^{r-m+1} . \tag{C-7}$$

References

Abramowitz, M., and I. A. Stegun, 1972. Handbook of Mathematical Functions, Dover Publications, Inc., New York, NY.

Gradshteyn, I. S., and M. Ryzhik, 1980. Table of Integrals, Series, and Products, Academic Press, New York, NY, 1160.pp.

APPENDIX D

A COMPLEX DEFINITE INTEGRAL

The following provides a proof of the integral relation

$$I(t) = \int_0^\infty \exp\left(-t^2 - \frac{z^2}{t^2}\right)dt = \frac{\sqrt{\pi}}{2}\exp(-2z) \tag{D-1}$$

when z is a complex quantity written as:

$$z = (c + id)^{\frac{1}{2}} \tag{D-2}$$

Noting that the function under the integral sign in Equation D-1 is an even function, substitution of z given by Equation D-2, yields

$$I = \int_0^\infty \exp\left(-t^2 - \frac{c}{t^2}\right)\exp\left(\frac{-id}{t^2}\right)dt \tag{D-3}$$

Using Euler's formula written as:

$$e^{i\theta} = \cos\theta + i\sin\theta \tag{D-4}$$

Equation D-3 becomes:

$$I = I_1 + I_2 \tag{D-5}$$

where

$$I_1 = \int_0^\infty \exp\left(-t^2 - \frac{c}{t^2}\right)\cos\left(\frac{d}{t^2}\right)dt \tag{D-6}$$

$$I_2 = -i\int_0^\infty \exp\left(-t^2 - \frac{c}{t^2}\right)\sin\left(\frac{d}{t^2}\right)dt \tag{D-7}$$

Recognizing the following integrals (see Gradshteyn and Ryzhik, 1980, p. 486)

$$\int_0^\infty \exp\left[-\left(p^2x^2 + \frac{q^2}{x^2}\right)\right]\cos\left(a^2x^2 + \frac{b^2}{x^2}\right)dx$$

$$= \frac{\sqrt{\pi}}{2r}\exp\left(-2rs\cos(A + B)\right)\cos\left(A + 2rs\sin(A + B)\right) \quad \text{for} \quad a^2 + p^2 > 0 \tag{D-8}$$

and

$$\int_0^\infty \exp\left[-\left(p^2x^2 + \frac{q^2}{x^2}\right)\right]\sin\left(a^2x^2 + \frac{b^2}{x^2}\right)dx$$

$$= \frac{\sqrt{\pi}}{2r}\exp\left(-2rs\cos(A + B)\right)\sin\left(A + 2rs\sin(A + B)\right) \quad \text{for} \quad a^2 + p^2 > 0 \tag{D-9}$$

where

$$r = (a^4 + p^4)^{\frac{1}{4}} \tag{D-10a}$$

$$s = (b^4 + q^4)^{\frac{1}{4}} \tag{D-10b}$$

$$A = \frac{1}{2}\,\text{arctg}\,\frac{a^2}{p^2} \tag{D-10c}$$

$$B = \frac{1}{2}\,\text{arctg}\,\frac{b^2}{q^2} \tag{D-10d}$$

the following relations are satisfied

$$p = 1 \qquad r = 1 \qquad q^2 = c \qquad s = (d^2 + c^2)^{\frac{1}{4}}$$

$$a = 0 \qquad A = 0 \qquad b^2 = d \qquad B = \frac{1}{2}\,\text{arctg}\,\frac{d}{c}$$

Then I_1 and I_2 are rewritten as

$$I_1 = \frac{\sqrt{\pi}}{2}\exp\left(-2\,(d^2 + c^2)^{\frac{1}{4}}\cos\left(\frac{1}{2}\,\text{arctg}\,\frac{d}{c}\right)\right)\cos\left(2\,(d^2 + c^2)^{\frac{1}{4}}\sin\left(\frac{1}{2}\,\text{arctg}\,\frac{d}{c}\right)\right) \tag{D-11}$$

$$I_2 = i\frac{\sqrt{\pi}}{2}\exp\left(-2\,(d^2+c^2)^{\frac{1}{4}}\cos\left(\frac{1}{2}\,\mathrm{arctg}\,\frac{d}{c}\right)\right)\sin\left(2\,(d^2+c^2)^{\frac{1}{4}}\sin\left(\frac{1}{2}\,\mathrm{arctg}\,\frac{d}{c}\right)\right) \quad . \tag{D-12}$$

Hence,

$$I = \frac{\sqrt{\pi}}{2}\exp(-x)\,[\cos y - i\sin y] = \frac{\sqrt{\pi}}{2}\exp[-(x+iy)] \tag{D-13}$$

where

$$x = 2\,(d^2+c^2)^{\frac{1}{4}}\cos\left(\frac{1}{2}\,\mathrm{arctg}\,\frac{d}{c}\right) \tag{D-14}$$

and

$$y = 2\,(d^2+c^2)^{\frac{1}{4}}\sin\left(\frac{1}{2}\,\mathrm{arctg}\,\frac{d}{c}\right) \quad . \tag{D-15}$$

Let

$$\mathrm{arctg}\,\frac{d}{c} = 2\theta \quad . \tag{D-16}$$

Using

$$\cos\theta = \frac{1}{\sqrt{2}}\,(\cos 2\theta + 1)^{\frac{1}{2}} \tag{D-17}$$

$$\cos\left(\frac{1}{2}\,\mathrm{arctg}\,\frac{d}{c}\right) = \cos\theta = \left[\frac{c + (c^2+d^2)}{2\,(c^2+d^2)}\right]^{\frac{1}{2}} \tag{D-18}$$

$$\sin\left(\frac{1}{2}\,\mathrm{arctg}\,\frac{d}{c}\right) = \sin\theta = \left[\frac{-c + (c^2+d^2)}{2\,(c^2+d^2)}\right]^{\frac{1}{2}} \tag{D-19}$$

Therefore, x and y given by Equations D-14 and D-15 become:

$$x = \sqrt{2}\,(c + (c^2+d^2)^{\frac{1}{2}})^{\frac{1}{2}} \tag{D-20}$$

$$y = \sqrt{2}\,(-c + (c^2+d^2)^{\frac{1}{2}})^{\frac{1}{2}} \quad . \tag{D-21}$$

Then I can be expressed as:

$$I = \frac{\sqrt{\pi}}{2} \exp\left[-2\left(\left(\frac{c + (c^2 + d^2)^{\frac{1}{2}}}{2}\right)^{\frac{1}{2}} + i\left(\frac{-c + (c^2 + d^2)^{\frac{1}{2}}}{2}\right)^{\frac{1}{2}}\right)\right] \quad . \tag{D-22}$$

Noting that the argument of the exponential function corresponds to the square root of the complex quantity (c + id) given by Equation D-2 (see Dwight, 1961, p. 17), hence the above equation can be written:

$$I = \frac{\sqrt{\pi}}{2} \exp\left(-2\,[c + id]^{\frac{1}{2}}\right) \tag{D-23}$$

and the required result is established.

References

Dwight, H. B., 1961. Table of Integrals and Other Mathematical Data, Fourth Edition, The Macmillan Company, New York, NY, 336 pp.

Gradshteyn, I. S., and I. M. Ryzhik, 1980. Table of Integrals, Series, and Products, Academic Press, New York, NY, 1160 pp.

APPENDIX E

NOTATIONS

Terms

a_L	longitudinal dispersivity
a_T	lateral dispersivity
A	concentration in the fracture
A^o	initial concentration of the species
b	half the fracture aperture width
B	concentration in the rock matrix
d	width of the finite line source at the origin
D	hydrodynamic dispersion tensor
D_d	molecular diffusion of nuclide in water
D_e	effective diffusivity in the rock matrix
D_p	pore diffusivity
D_{xx}, D_{yy}, D_{xy}	coefficients of hydrodynamic dispersion tensor in the fracture
Fo	Fourier number for rock matrix
F_x	mass flux in x-direction
F_y	mass flux in y-direction
J	diffusive rate of nuclide at surface of fracture per unit area of fracture surface
K_f	sorption distribution coefficient in the fracture
K_r	sorption distribution coefficient in the rock matrix
L	half the fracture spacing
Q	rate of production or removal of solute due to radioactive decay in the fracture
Q'	rate of production or removal of solute due to radioactive decay in the rock matrix
R	retardation factor in the fracture
R'	retardation factor in the rock matrix
S	concentration in the adsorbed phase in the fracture

S'	concentration in the adsorbed phase in the rock matrix
t	time
T	leaching time
$T_{1/2}$	half-life
u, v	x and y components of the fluid velocity vector in the fracture
V	average fluid velocity vector in the fracture
x, y	position vectors in the fracture
y_o	y coordinate of the center of the Gaussian source
y_1	y coordinate of the center of a typical finite patch source
z	position vector in the rock matrix
Γ	Gamma function
δ_d	constrictivity for diffusion
δ_{ij}	Kronecker delta
λ	first-order rate constant for decay
σ_y	standard deviation of Gaussian source at the origin
ρ_r	rock density
τ	tortuosity
ϕ	rock porosity
ϕ_r	volumetric fraction of the solid phase in the rock matrix

Abbreviated Forms

$$a_1 = \frac{\sigma_y^2 + 2p^2}{4p^2\sigma_y^2}$$

$$a_2 = -\frac{(y-g)\sigma_y^2 + 2y_\sigma p^2}{4p^2\sigma_y^2}$$

$$a_3 = \frac{(y-g)^2\sigma_y^2 + 2y_o^2 p^2}{4p^2\sigma_y^2}$$

Abbreviated Forms

$$c_f = \frac{\Phi}{b}(R'D_p)^{1/2}$$

$$c_r = (R'/D_p)^{1/2}$$

$$F_0 = \frac{D_p(t-R\chi)}{R'(L-b)^2} \; ; D_{xx} > 0; \chi \text{ becomes } \chi' \text{ for } D_{xx} = 0$$

$${}_x\overline{F}_1 = u - 2D_{xx}a_1(\sigma - a_1x) \; ; F_y = 0$$

$$F_1^* = uE_\Omega \; ; F_y \neq 0$$

$$F_1^* = u \; ; F_y = 0$$

$${}_xF_1 = uE_\Omega - D_{xx}[2a_1(\sigma - a_1x)E_\Omega + E_\Omega^x] - D_{xy}E_\Omega^y \; ; F_y \neq 0$$

$${}_yF_1 = vE_\Omega - D_{yx}[2a_1(\sigma - a_1x)E_\Omega + E_\Omega^x] - D_{yy}E_\Omega^y \; ; F_y \neq 0$$

$${}_iF_2 = \frac{\overline{\beta}c_f D_{ix}}{\sqrt{\pi}}E_\Omega \; ; i = x,y \; ; F_y \neq 0$$

$${}_x\overline{F}_2 = \frac{\overline{\beta}c_f D_{xx}}{\sqrt{\pi}} \; ; F_y = 0$$

$${}_iF_2^* = D_{ix}E_\Omega\overline{\beta} \; ; i = x,y$$

$$F_3 = \left[\left(uE_\Omega\right)^2 + \left(vE_\Omega - D_{yy}E_\Omega^y\right)^2\right]^{1/2} ; D_{xx} = D_{yx} = 0$$

$$g = \left(v - u\frac{D_{yx}}{D_{xx}}\right)\chi + \left(\frac{D_{yx}}{D_{xx}}\right)x$$

$$p = \left((D_{yy} - \frac{D_{yx}^2}{D_{xx}})\chi\right)^{1/2}$$

$$r_a = -R(s+\lambda) - c_f(s+\lambda)^{1/2}$$

$$r_b = -c_r(s+\lambda)^{1/2}$$

Abbreviated Forms

$$\alpha_1 = u/4D_{xx}\sigma$$

$$\beta = \left(\frac{R'}{D_p}\right)^{1/2}(L-b)$$

$$\bar{\beta} = x/2D_{xx}\sigma^2 \; ; \; D_{xx} > 0$$

$$\bar{\beta} = \frac{1}{u} \; ; D_{xx} = 0$$

$$\beta_r = -\frac{\varepsilon\eta}{2}\left[\frac{\sinh(\beta\eta) - \sin(\beta\eta)}{\cosh(\beta\eta) + \cos(\beta\eta)}\right]$$

$$\bar{\beta}_r = \beta_r + (-1)^{m+1}\frac{\beta\eta}{2} + (-1)^{n+1}\frac{\mu\eta}{2}$$

$$\bar{\beta}_\ell = \frac{\eta^2\tau}{2} - Y_\ell$$

$$\beta_\ell = \frac{\eta^2\tau}{2} - \bar{Y}_\ell$$

$$Y_\ell = \frac{\varepsilon\eta}{2}\left[\frac{\sinh(\beta\eta) + \sin(\beta\eta)}{\cosh(\beta\eta) + \cos(\beta\eta)}\right]$$

$$\bar{Y}_\ell = Y_\ell + (-1)^{m+1}\frac{\beta\eta}{2} - (-1)^{n+1}\frac{\mu\eta}{2}$$

$$\Gamma_\delta = (-1)^n \frac{4}{(2n+1)\pi}\cos(\delta\mu)$$

$$\delta = \frac{(2n+1)\pi}{2\beta}$$

$$\varepsilon = c_f X$$

$$\varepsilon' = c_f X' \; ; D_{xx} = 0$$

$$\bar{\varepsilon} = \frac{c_f X}{2}$$

Abbreviated Forms

$$\bar{\bar{\varepsilon}} = \frac{c_f X'}{2} \; ; \; D_{xx} = 0$$

$$\zeta_\ell = \gamma_\ell / \varepsilon$$

$$\zeta_r = \beta_r / \varepsilon$$

$$\mu = \left(\frac{R'}{D_p}\right)^{1/2} (L - z)$$

$$v = \frac{\eta^2}{2}\left(t - \frac{Rx^2}{4D_{xx}\sigma^2}\right)$$

$$v' = v(X') = \frac{\eta^2}{2}\left(t - \frac{Rx}{u}\right)$$

$$v_1 = v(\eta_1) = \frac{\eta^2}{2}(t - R_1\eta_1)$$

$$\bar{\xi}_k = k\beta + \bar{\varepsilon}$$

$$\bar{\bar{\xi}}_k = k\beta + \bar{\bar{\varepsilon}}$$

$$X = \frac{x^2}{4D_{xx}\sigma^2} \; ; \; D_{xx} > 0$$

$$X' = \frac{x}{u} \; ; \; D_{xx} = 0$$

APPENDIX F

MODEL PARAMETERS

CENT	Location of center of source 1 along y axis (IPATCH = 1)
DENSR	Rock matrix bulk density (M/L^3) (used if IDIST = 1)
DIFF	Molecular diffusion of species in water (L^2/T) (used if IDISP = 1)
DIFFR	Pore diffusivity (L^2/T)
DIMENS(I,J)	Dimensions used in the problem; each must be ≤ 12 characters in length DIMENS(1,J) = species name (2,J) = time (year) (3,J) = length (meter) (4,J) = L/T (meter/year) (5,J) = L^2/T (m^2/year) (6,J) = mass/volume (g/cc) (7,J) = volume/mass (cc/g) (8,J) = 1/time (1./year) (9,J) = activity (Ci)
DISPX	Longitudinal dispersivity/dispersion in the x direction (see IDISP)
DISPY	Lateral dispersivity/dispersion in the y direction (see IDISP)
EXMAX++	Largest allowed magnitude for exponential arguments
FDIST	Fracture separation distance (L) (used if IMULT = 1)
HALFL	Half-life of species (T)
IBAND	= 0 Step release at source = 1 Band release at source
ICONCF	= 0 Do not calculate fracture concentrations = 1 Do calculate fracture concentrations
ICONCR	= 0 Do not calculate rock concentrations = 1 Do calculate rock concentrations
ICUMF	= 0 Do not calculate cumulative mass flux = 1 Do calculate cumulative mass flux
IDISP	= 0 DISPX, DISPY correspond to dispersion coefficients = 1 DISPX, DISPY correspond to dispersivities
IDIST	= 0 RETARD_F,RETARD_R correspond to retardation factors = 1 RETARD_F,RETARD_R correspond to distribution coefficients

IFLUX	= 0 Do not calculate instantaneous mass flux = 1 Do calculate instantaneous mass flux
IGAUSL	= 0 Interval of integration constant = 1 Integration limits divided into INTERV intervals
IGRAPH	= 0 Graphics output disabled = 1 Graphics output enabled--formatted graphics data written to unit 30
IMULT	= 0 Single fracture plane (infinite diffusion field) = 1 Multiple fracture planes (finite diffusion field) series solution = 2 Multiple fracture planes (finite diffusion field) contour integration solution
INTERV	Number of subintervals x 2 for Gauss-Legendre integration (i.e., ≥ 4) (used if IGAUSL = 1)
IPATCH	= 0 Boundary condition corresponds to a Gaussian distributed source = 1 Boundary condition corresponds to a finite patch source
MSG1	≤ 72 characters, first line of graphics output
MSG2	≤ 72 characters, second line of graphics output
NMAX	Number of Gaussian points for Gauss-Legendre quadrature (it can only have the value of 4, 10, 20, 60, 104, or 256)
NRUNMAX	Number of data sets to be run
NT	≤ 50, number of time values to be evaluated
NUMBS	Number of patch sources (IPATCH = 1)
NX	≤ 50, number of positions to be evaluated in x direction
NY	≤ 50, number of positions to be evaluated in y direction
NZ	≤ 50, number of positions to be evaluated in z direction
PATCH	Width of finite source (i.e., IPATCH = 1) (L)
POROSR	Average porosity in rock matrix (L^3/L^3)
REFX(I)	x-position in space (L)
REFY(I)	y-position in space (L)
REFZ(I)	z-position in space (L)
RETARD_F	Retardation factor/distribution coefficient in the fracture (see IDIST)
RETARD_R	Retardation factor/distribution coefficient in the rock (see IDIST)
SPACING	Distance between consecutive waste packages (IPATCH = 1)

STD	Standard deviation (IPATCH = 0)
THICK	Fracture thickness (L)
TIME(I)	T-position in time (T)
TIML	Leach time (T) (used if IBAND = 1)
TITLE	2 lines, ≤80 characters per line, title of data set
TORT	Tortuosity (L/L) (used if IDIST = 1)
VELX	Average apparent velocity in the x-direction (L/T)
VELY	Average apparent velocity in the y-direction (L/T)
Y0	Location of the center of Gaussian source (IPATCH = 0)
+ +	Computer dependent.

DISTRIBUTION LIST

ABB Atom
Cnut Sundqvist
AB Statens anlaggningsprovning
Lars Dahlberg
Alberta Research Council
Stefan Bachu
ANDRA
Pascal Oustriere
Applied Decision Analysis, Inc.
L. Merkhofer
Arbetsmiljoinstitutet
Gunnela Westlander
Argonne National Laboratory
James C. Cunnane
John D. Ditmars
Anthony T. Dvorak
Christine Eddy
Philip F. Gustafson
Stan Niehoff
David Tomasko
Patrick Wilkey
Atkins Engineering Sciences
S. K. Liew
Tim Broyd
Atomic Energy Control Board
Peter A. Flavelle
Kenneth Bragg
Douglas Metcalfe
Atomic Energy of Canada Ltd
Tin Chan
Kenneth Dormuth
G. Moltyaner
J. A. Keith Reid
N. W. Scheier
Tjalle T. Vandergraaf
Battelle
Mick Apted (PNL)
Nino Aimo (PNL)
D. J. Bradley (PNL)
Kenneth Brog
H. C. Burkholder (PNL)
T. D. Chikalla (PNL)
Charles Cole (PNL)
Pam Doctor (PNL)
Mark Freshley (PNL)
Glendon Gee (PNL)
A. Berge Gureghian
Elizabeth Jacobson (PNL)
Kenneth Krupka (PNL, Wash., DC)
William Nelson
Walter E. Newcomb
R. J. Serne (PNL)
Michael Shea
John Smoot (PNL)
Abraham Van Luik (PNL, Wash., DC)
Bechtel Civil Inc.
Irene T. Findikakis
British Geological Survey
David Noy
Bundesamt fur Strahlenschutz (BfS)
H. Illi
H. Rothemeyer
Bundesanstält fur Geowissenschaften und Rohstoffe
Klaus Schelkes
Bureau de Recherches Géologiques et Minières
Jean-Paul Chilès
Jean-Pierre Sauty
CAE Support
Al Stephens
Center for Nuclear Waste Regulatory Analyses
Ron Green
Central Electricity Generating Board
J. O. Corbett
Central Research Institute of Electric Power Ind.
Motoi Kawanishi
CER Corporation
Edwin H. Price
Clay Technology AB
Lennart Borjesson
Clemson University
Robert A. Fjeld
Commissariat à l'Energie Atomique
Alain Cernes
Michel Durin
Joseph Lewi
Commission of the European Communities
B. Come
Sergio Finzi
S. Orlowski
Computer Soft Ware Development Co., Ltd.
Kenji Furuichi
Consultant
Erik Eriksson
David Gee
Jorma Miettinen
Robert F. Schurtz
Anne-Marie Thunberg
Cornell University Department of Agriculture
T. S. Steenhuis
J.-Y. Parlange

Cornell University Engineering Department
James A. Liggett
CTH
Jan-Olof Liljenzin
Dames and Moore
Michael Grant
Department of the Environment
Brian Thompson
Der Niedersachsische Umweltminister
Mr. Besenecker
Desert Research Institute
Scott Tyler
Dr. Stephen Wheatcraft
Deuel & Associates, Inc.
Robert W. Prindle
Ecole des Mines
Patrick Goblet
EG&G Idaho
Tom Clemo
E. I. du Pont de Nemours & Co., Inc.
France Sarl
E.N.R.E.S.A.
Carmen Bajos
Environmental Systems Engineering Department
Robert A. Fjeld
EWA, Inc.
C. B. Bennett
A. M. Djerrari
V. V. Nguyen
Federal Institute for Geosciences & Natural Resources
Lutz Liedtke
Federal Institute of Technology
A. Von Kanel
Geological Survey of Canada
Alexander Desbarats
Geostokos Limited
Isobel Clark
Gesellschaft fur Reaktorsicherheit
Peter Bogorinski
Golder Associates
Tom Doe
Ian Miller
Todd Schrauf
Charles V. Voss
Charles R. Wilson
GSF München
Georg Arens
Eckhard Fein
Peter Fritz
Richard Storck
Harwell Laboratory
David Lever
Peter Jackson
P. J. Sumner
Keith Winters
Hauptabt fur die Sicherheit der Kernanlagen
Johannes Vigfusson
Holcomb Research Institute
Aly I. El-Kadi
Osman A. Elnawawy
HydroGeologic, Inc.
Peter S. Huyakorn
Jan B. Kool
Industrial Power Company
Esko Peltonen
INTAKTA
Jacques Roman
Intera-ECL
David Hodgkinson
Neil Chapman
INTERA Technologies, Inc.
Robert W. Andrews
Andreas Haug
A. M. LaVenue
International Atomic Energy Agency
Shaheed Hossain
Y. Yurtsever
IT Corporation
Lowell Howlett
JAERI Div. of Environmental Safety Research
Hideo Kimura
Haruto Nakamura
Johanneum Research Association
Michal Stibitz
John Hopkins University
D. A. Sverjensky
Kemakta Consultants Co.
Magdalena Ericsson
Bertil Grundfelt
Alf Larsson
Tommy Nedbal
Karin Pers
Anders Rasmuson
Kristina Skagius
Kyoto University
Yuzo Onishi
L. Lehman & Associates, Inc.
Mark Larson
Linda L. Lehman
Lab. Géologie Appliquée
Ghislain de Marsily
Laboratory of Hydrology (Belgium)
F. DeSmedt
Lansstyrelsen i Blekinge lan
Camilla Odhnoff

Lawrence Berkeley Laboratory
Daniel Billaux
Kevin Coakley
Kevin Hestir
Deborah Hopkins
Satoshi Imamura
K. Karasaki
Jane C. S. Long
T. N. Narasimhan
Jahan Noorishad
Kasten Pruess
Chin-Fu Tsang
Yvonne Tsang
Joseph S. Y. Wang
Paul Witherspoon

Lawrence Livermore National Laboratory
Leslie Jardine
Wendell Johnson
Nai-hsien Mao
Lawrence Ramspott

Los Alamos National Laboratory
Steve Birdsell
Katherine Campbell
Sharad Kelkar
Donald T. Oakley
Edward Patera

Lucas Heights Research Laboratories
Peter Duerden
Cezary Golian

Massachusetts Institute of Technology
Jacob Bensabat
Lynn Gelhar
Danielle Veneziano

McMaster University
L. W. Shemilt
Grant Sheng

Michigan Technological University
Dae S. Young

Miljö- och energidepartementet
Ingvar Persson

Ministry of Trade and Industry
Sirkka Vilkamo

Mitsubishi Atomic Power Industries Inc. (MAPI)
Yutaka Nakahara

NAGRA
Peter Hufschmied
Charles McCombie
Stratis Vomvoris
Caroline Wittwer
Piet Zuidema

National Institute of Public Health and Environment Hygiene (RIVM)
Toon Leijnse

National Institute of Public Health and Environment Protection
Peter Glasbergen
Majid Hassanizadeh
Ton Slot

National Institute of Radiation Protection
Conny Hagg
Gunnar Johansson
Shelly Mobbs

National Radiological Protection Board
John P. Dais

National Tsing Hua University
Shi-Ping Teng

National Water Research Institute
Bobba Ghosh

New Mexico Environmental Evaluation Group
James K. Channell

New Mexico State University
Richard G. Hills

NIRAS/ONDRAF
E. Detilleux

NIREX Limited
Dennis George

Nuclear Engineering Laboratory
Seppo Vuori

Nuclear Research Institute
Jan Horyna

Oak Ridge National Laboratory
Allen G. Croff
E. M. Oblow
Brian Worley

OECD/Nuclear Energy Agency
Claes Thegerstrom

Ontario Hydro
Robert E. Allan

Paul Scherrer Institut
Jorg Hadermann
Andreas Jakob

PB-KBB, Inc.
Bruce T. Stanley

PNC
Kazoya Idemitsu
Minoru Yamakawa

Poly. Academy of Science (PAS)
Ewa Stepkowska

Power Reactor and Nuclear Fuel Development Corporation (PNC)
Hiroyuki Umeki

Princeton University
Michael Celia
Eric Wood

Raatihuoneenkatu 10
Risto Valkeapaa

Resource International
William V. Harper
RE/SPEC Inc.
Paul Gnirk
John Osnes
Joe Ratigan
Roy F. Weston, Inc.
Karen Albrecht
David Back
Levi Kroitoru
Clifford J. Noronha
Larry Rickertsen
Royal Institute of Technology
Ivars Neretnieks
Bjorn Dverstorp
Tryggve Eriksen
Luis Moreno
Ruder Boskovič Institute
Nikola Masič
Sandia National Laboratories
D. R. Anderson
R. Beauheim
E. J. Bonano
Paul A. Davis
Sharon Finley
R. J. Glass
Mike Goodrich
Elaine Gorham
Paul G. Kaplan
Jim McCord
Dave McTigue
Natalie Olague
Robert W. Prindle
C. A. Rautman
Brian Rutherford
Malcolm Siegel
Stephen W. Webb
Science Applications International Corporation
Dwayne Chesnut
Jim Danna
John H. Nelson
U Sun Park
Harry A. Perry
Dermot Ross-Brown
Jean L. Younker
SKB - Sweden
Harald Ahagen
SKI
Benny Sundstrom
Southwest Research Institute
Rachid Ababou
Budhi Sagar
Stanford University
Charles Fox
Roland N. Horne
Bob Johns
André G. Journel
State of Oregon
Ralph Patt
Statens Karnkraftinspektion
Torbjorn Carlsson
Statens stralskyddsinstitut
Lars Persson
Jan Olof Snihs
Statens vattenfallsverk
Goran Appelqvist
Nils Starfelt
Stone & Webster Engineering Corporation
Fonda L. Thompson
Studiecentrum voor Kernenergie
Arnold Bonne
Studsvik Nuclear AB
Leif Ericson
STUK
Esko Ruokola
Svensk Kärnbränslenamnd (SKN)
Soren Scherman
Swedish Board for Nuclear Fuel
Bjorn Cronhjort
Nils Rydell
Rolf Sjoblom
Swedish Geological Company
Kaj Ahlbom
Peter Andersson
Swedish Nuclear Fuel & Waste Management Company
Per Erik Ahlstrom
Tommy Hedman
Fred Karlsson
Nils A. Kjelbert
Tonis Papp
Anders Strom
Swedish Nuclear Power Inspectorate
Johan Andersson
Kjell Andersson
Lars Hogberg
Fritz Kautsky
Stig Wingefors
Technical Research Center of Finland
Seppo Vuori
Arto Ylinen
Technical Research Institute, Hazama-Gumi Ltd.
Akira Kobayashi
Ryo Yamashita
Technischer Uberwachungsverein Hannover e.V.
Mr. Wehmeyer

Tekniska Hogskolan i Lulea
Ove Stephansson
Texas Water Commission
Margaret Hart
TRW Inc.
Walter W. Matyskiela
David McNelis
Edward C. Taylor
U.K. Dept of the Environment
Nick Harrison
Universidad Politechnica de Cataluna
Jesus Carrera
Emilio Custodio
Javier Heredia
Agustin Medina
Javier Samper
University of Arizona
Stan Davis
Daniel D. Evans
Amado Guzman
Donald Myers
Shlomo Neuman
Todd Rasmussen
Michael Sully
Arthur W. Warrick
Peter Wierenga
T. C. Jim Yeh
University of British Columbia
R. A. Freeze
Leslie Smith
University of California Civil Engineering Department (Los Angeles)
W. W-G. Yeh
University of California at Davies
Don R. Nielsen
University of California Department of Nuclear Engineering
P. L. Chambré
W. W. Lee
T. H. Pigford
University of Florida
A. S. Donigian
P. S. C. Rao
University of Guelph
D. E. Elrick
University of Vermont
George F. Pinder
University of Washington
Richard Horner
University of Wisconsin
Kenneth R. Bardbury

U.S. Department of Energy
Donald Alexander
L. Barrett
Max Blanchard
Carl Cooley
Carl Gertz
T. H. Isaacs
A. J. Knepp
David Langstaff
Don Livingston
Karla J. Olson
S. Russo
Rich Schassburger
Ralph Stein
U.S. Department of Energy--Albuquerque Operations Office
Public Reading Room
U.S. Department of Energy Chicago Operations
Richard Baker
Anthony Bindokas
David Dashevsky
John D. Kasprowicz
Richard Lark
Public Reading Room
U.S. Department of Energy--Idaho Operations Office
James F. Leonard
Public Reading Room
U.S. Department of Energy--Nevada Operations Office
Jerry Boak
Russ Dyer
Bob Levich
Public Reading Room
U.S. Department of Energy--Oak Ridge Operations Office
Public Reading Room
U.S, Department of Energy--OTSI (250)
U.S. Department of Energy--Repository Technology & Transportation Division
Steven A. Silbergleid
U.S. Department of Energy--Richland Operations Office
D. H. Dahlem
Public Reading Room
U.S. Department of Energy--San Francisco Operations
Public Reading Room
U.S. Department of Energy --Savannah River Operations Office
Public Reading Room
U.S. Department of the Interior
F. L. Doyle

U.S. Environmental Protection Agency
Floyd L. Galpin
J. William Gunter
William F. Holcomb
Cheng Yeng Hung

U.S. Environmental Protection Agency--Region II
EPA Library

U.S. Geological Survey (Denver)
Alan Flint
Dwight Hoxie

U.S. Geological Survey--Nuclear Waste Program, Water Resources Division
George A. Dinwiddie

U.S. Geological Survey--Reston
L. F. Konikow
Debra Kopman
David B. Stewart
Newell J. Trask, Jr.
Clifford Voss

U.S. Nuclear Regulatory Commission
Eric Beckjord
George F. Birchard
David Brooks
Robert Browning
Ralph Cady
Donald Chery, Jr.
Richard Codell
Norman Eisenberg
William H. Ford
Daniel A. Galson
Philip Justus
Timothy McCartin
Keith McConnell
Thomas J. Nicholson
Mel Silberberg
John Starmer
Rex Wescott

U.S. Salinity Laboratory
M. Th. Van Genuchten

Verdandivagen 20
Ingmar Grenthe

Virginia Polytechnic Institute and State University
J. C. Parker

Westinghouse Hanford Company
Peter M. Clifton
Robert Hiergesell
George Jansen
Joyce Meints
Tom R. Thomas

Woodward-Clyde Consultants
Ram B. Kulkarni
Gordon R. Luster
Andrew Reisenauer
Atul M. Salhotra

☆U.S. GOVERNMENT PRINTING OFFICE:1990 -750 -860/29002

Item Description:	FRACFLO: Analytical Solutions for Two-Dimensional Transport of a Decaying Species in a Discrete Planar Fracture and Equidistant Multiple Parallel Fractures With Rock Matrix Diffusion
Availability:	X Publicly Available ☐ Non-Publicly Available
Sensitivity:	X Non-Sensitive ☐ Non-Sensitive–Copyright ☐ Sensitive ☐ Sensitive–Copyright
Electronic Media Type: (If applicable)	Microfiche
Contact:	US Nuclear Regulatory Commission Office of Nuclear Materials Safety and Safeguards Yucca Mountain Project Manager
Storage/File Location:	US Nuclear Regulatory Commission Office of Nuclear Materials Safety and Safeguards Two White Flint North Room T7- E34 11545 Rockville Pike Rockvillrl;Maryland 20852-2738

OWTD

Office of Waste Technology Development

BATTELLE Energy Systems Group